24

NASA CR-54467
MARTIN-CR-65-75

ADVANCED PRESSURIZATION SYSTEMS FOR CRYOGENIC PROPELLANTS

by

J. E. Anderson, O. L. Scott, and H. F. Brady

Prepared for

NATIONAL AERONAUTICS AND SPACE ADMINISTRATION

CONTRACT NAS 3-2574

MARTIN-MARIETTA CORPORATION
MARTIN COMPANY
Denver Division
Denver, Colorado

NASA CR-54467
MARTIN-CR-65-75

FINAL REPORT

ADVANCED PRESSURIZATION SYSTEMS FOR CRYOGENIC PROPELLANTS

by

J. E. Anderson, O. L. Scott, and H. F. Brady

prepared for

NATIONAL AERONAUTICS AND SPACE ADMINISTRATION

January 1967

CONTRACT NAS 3-2574

Technical Management
NASA Lewis Research Center
Cleveland, Ohio
Liquid Rocket Technology Branch
Donald L. Nored

MARTIN-MARIETTA CORPORATION
MARTIN COMPANY
Denver Division
Denver, Colorado

NOTICE

This report was prepared as an account of Government sponsored work. Neither the United States, nor the National Aeronautics and Space Administration (NASA), nor any person acting on behalf of NASA:

A.) Makes any warranty or representation, expressed or implied, with respect to the accuracy, completeness, or usefulness of the information contained in this report, or that the use of any information, apparatus, method, or process disclosed in this report may not infringe privately owned rights; or

B.) Assumes any liabilities with respect to the use of, or for damages resulting from the use of any information, apparatus, method or process disclosed in this report.

As used above, "person acting on behalf of NASA" includes any employee or contractor of NASA, or employee of such contractor, to the extent that such employee or contractor of NASA, or employee of such contractor prepares, disseminates, or provides access to, any information pursuant to his employment or contract with NASA, or his employment with such contractor.

Requests for copies of this report should be referred to

National Aeronautics and Space Administration
Office of Scientific and Technical Information
Attention: AFSS-A
Washington, D.C. 20546

FOREWORD

This report was prepared by the Denver Division of the Martin Company under Contract NAS3-2574, dated 20 November 1963. The contract was administered by the Lewis Research Center of the National Aeronautics Space Administration, Cleveland, Ohio. The NASA Project Manager for the contract was Mr. Donald L. Nored. This report is a final report for subject contract summarizing the technical work during the period 20 November 1963 to 25 June 1965.

The following personnel at the Martin Company contributed to the technical effort and preparation of this report:

C. D. Brown	J. E. Anderson	W. A. Gray
T. R. Heaton	D. N. Gorman	E. F. Wollam
S. C. Lukens	O. L. Scott	D. DiStefano
H. F. Brady	G. R. Page	P. Bingham

All personnel are employees at the Denver Division of the Martin Company except:

W. A. Gray
E. F. Wollam

who are with the Baltimore Division of the Martin Company.

ADVANCED PRESSURIZATION SYSTEMS

FOR CRYOGENIC PROPELLANTS

by

J. E. Anderson, O. L. Scott, and H. F. Brady

ABSTRACT

The purpose of this program was to select an optimized pressurization system for a vehicle using cryogenic propellants. Improvements in the method of analysis were also developed and incorporated in the program. The vehicle for study was an Apollo-type service module using liquid hydrogen and liquid oxygen as propellants. Systems of both pump-fed and pressure-fed engines were considered during the study with a final selection completed for the pump-fed engine system.

CONTENTS

Figure

Table

ADVANCED PRESSURIZATION SYSTEMS

FOR CRYOGENIC PROPELLANTS

by J. E. Anderson, O. L. Scott, and H. F. Brady

MARTIN-MARIETTA CORPORATION

SUMMARY

This program involved the analytical and experimental investigation of advanced pressurization systems for vehicles, using cryogenic propellants. The purpose of the program was to design a system for a specific vehicle and mission, the designed system to be ultimately built and tested to verify the analytical approach. The secondary objective of the program was to improve and check out the analytical computer program model that simulated the propellant tank and vehicle thermodynamics. The actual work completed involved only the development of the analytical design method and the selection of the most optimum system of a number of systems studied. The work completed was broken down into two major tasks.

Task I, "Analysis and Evaluation," was concerned with the selection of a number of representative pressurization system configurations for study and the development of an analytical model that could be used to select the optimum system. The systems selected were to meet the operating requirements of both pressure-fed and pump-fed propulsion systems for an Apollo-type vehicle and mission using cryogenic propellants. Two basic types of systems were considered: primary systems and advanced systems. Primary systems were defined as systems using helium gas as a pressurant, stored at liquid hydrogen temperature with subsequent expansion and heating prior to injection into the propellant tanks. This definition was applicable to only those systems used in conjunction with pressure-fed propulsion systems. In the case of primary pressurization systems used with pump-fed propulsion systems, the definition covered any system using state-of-the-art components and technology and was to be optimized primarily for high reliability.

Advanced pressurization systems for both pressure-fed and pump-fed propulsion systems were defined as systems requiring the use of advanced technology and were to be optimized for both high reliability and low weight. For the purpose of the study the following definition was used: system configurations using active heat sources for warming the pressurant prior to injection into the propellant tanks were considered to be advanced, pump-fed systems.

Initial studies were conducted on the primary and advanced systems for the pressure-fed propulsion systems. Using a simplified analytical technique, a group of systems was studied, and five each of the primary and advanced systems were selected as the most optimum from a weight standpoint. At this time, the analysis effort was started on the primary and advanced pressurization systems for pump-fed propulsion systems.

A group of both primary and advanced pressurization systems for pump-fed propellant systems was selected for study, and the preliminary screening was started. At this time, the study effort was concentrated on the primary systems. As the program continued and the analytical effort was expanded, using the more complex analytical models, the emphasis remained on the primary systems, and no further analysis was completed on the advanced systems. The preliminary screening was completed and resulted in continuing study of the five primary systems.

As a parallel effort, the systems analytical model was modified and checked out. At the time of the selection of the five primary systems, work had not been completed on the model, so a second level of analysis was made using an existing, less-sophisticated model with a simplified heat transfer technique. The five remaining systems were optimized for low weight, and a separate complexity analysis completed. From the results of these studies, two systems were selected representing wide differences in basic makeup. One system stored helium at liquid hydrogen temperature, then expanded the gas and warmed it, using a passive heat exchanger, prior to injection into the propellant tanks. The passive heat exchanger was located inside the liquid oxygen tank.

The second system stored helium gas at ambient temperature, then expanded the gas and injected it into the propellant tanks without heat exchange.

With the overall analytical model complete and checked out, the two remaining systems were analyzed again. At this time, the systems were not only compared on the basis of weight and complexity, but also for cost, leakage potential, zero-gravity operating capability, minimum pressurization time, and 20-day storage capability. The overall result of this comparison indicated that the system storing helium at ambient temperature was superior and was the best of the systems considered.

During the period when Task I was in progress, work was also in progress on Task II. Task II, "Problem Area Investigation," was concerned with experimental investigation of problems resulting from the Task I effort.

A test series was initiated to prove the feasibility of main tank injection (MTI) of liquid fluorine into the liquid hydrogen tank as a means of pressurization. Due to a delayed and unpredictable reaction in the hydrogen tank, feasibility was not proven, and this system was dropped from consideration. A gas generator to be used as an active heat source for a pressurant heat exchanger was designed, and a test model was built. The generator used hydrogen and oxygen as the fuel and oxidizer. A test series was initiated that included both cold flow testing and hot firing of the generator only. An exchanger was not included in this program since its design would depend on the system selected. The series was terminated after a successful 6-min, 10-sec firing of the unit. Shortly after the completion of the testing, active heat exchange was dropped from the program, and no further work was completed on this system.

A test series was initiated to compare the actual and analytical expansion of helium from a storage container. Adiabatic, isothermal, and polytropic runs were made, and it was found that the data correlated so closely with analytical data that no change was made to the analytical data.

Several general types of components were purchased and tested in the worst environments expected, in particular, at 37°R and 3000 psig. No problems were experienced during this test series that would drastically affect system configurations studied, although availability of components for operation at 37°R is definitely limited.

I. INTRODUCTION

In recent years, emphasis has not been placed on proper selection and optimization of the propellant pressurization systems for rocket vehicle stages. Generally, the propellant and engine systems were selected and matched, and then a pressurization system was designed to suit the need. One of the major problems was the lack of adequate analytical tools to produce an optimized design and to predict its performance. Since the ultimate purpose of any vehicle stage is to lift as much payload weight as possible, any saving in pressurization system weight becomes available as additional payload weight. With the pressurization system being, in many cases, a major contributor to total stage weight, the proper and efficient selection of this system is a major objective of vehicle design.

The purpose of this program was to investigate and evaluate different methods of propellant tank pressurization. From this evaluation, the most promising candidate pressurization systems were selected and optimized for a specific space vehicle and mission. In particular, the vehicle selected for study was an Apollo-type service module using liquid hydrogen and liquid oxygen as propellants. Systems for use with both pump-fed and pressure-fed engines were considered during the study with a final selection completed for the pump-fed system.

Work of a similar but more general nature was done by Aerojet-General Corporation under NASA contract NAS 7-169. However, this program is more specific in that it considers only the case of cryogenic propellants and is concerned more with the performance of the system than with the selection of specific component parts.

II. PROGRAM PLAN

To establish the optimum system, the plan shown schematically in Fig. 1 was used. It can be seen that feasibility of various component and system concepts were tested simultaneously with the overall system analysis. Continuous effort was also applied to improve the analytical model that analyzed the propellant tank thermodynamics.

Several screening steps were performed on the first system conceived. Since a complete analysis on all systems would have required a large amount of time, an elimination process was used. Using a simplified analysis, a large number of systems were compared. By selecting the most desirable systems on a basis of weight, the number of systems in the secondary and final screening were reduced. As the number of systems to be analyzed was reduced, the analysis was made more complete.

As two major systems were analyzed, the screening process was performed twice, once for pressure-fed engine systems and once for pump-fed engine systems. Each of these two types of systems was divided into primary and advanced classifications. Table 1 shows the extent of study for each type system considered.

Table 1 Pressurization System Study Sequence

Systems	Pressure-Fed Systems Evaluated or Selected			Pump-Fed Systems Evaluated or Selected					
	Initial Screening	Final Screening	Selection	Initial Screening	Selec-tion	Secondary Screening	Selec-tion	Final Screening	Selec-tion
Primary, Pressure-Fed	7	6	5						
Advanced, Pressure-Fed	14	7	5						
Primary, Pump-Fed				12	5	5	2	2	1
Advanced, Pump-Fed				5					

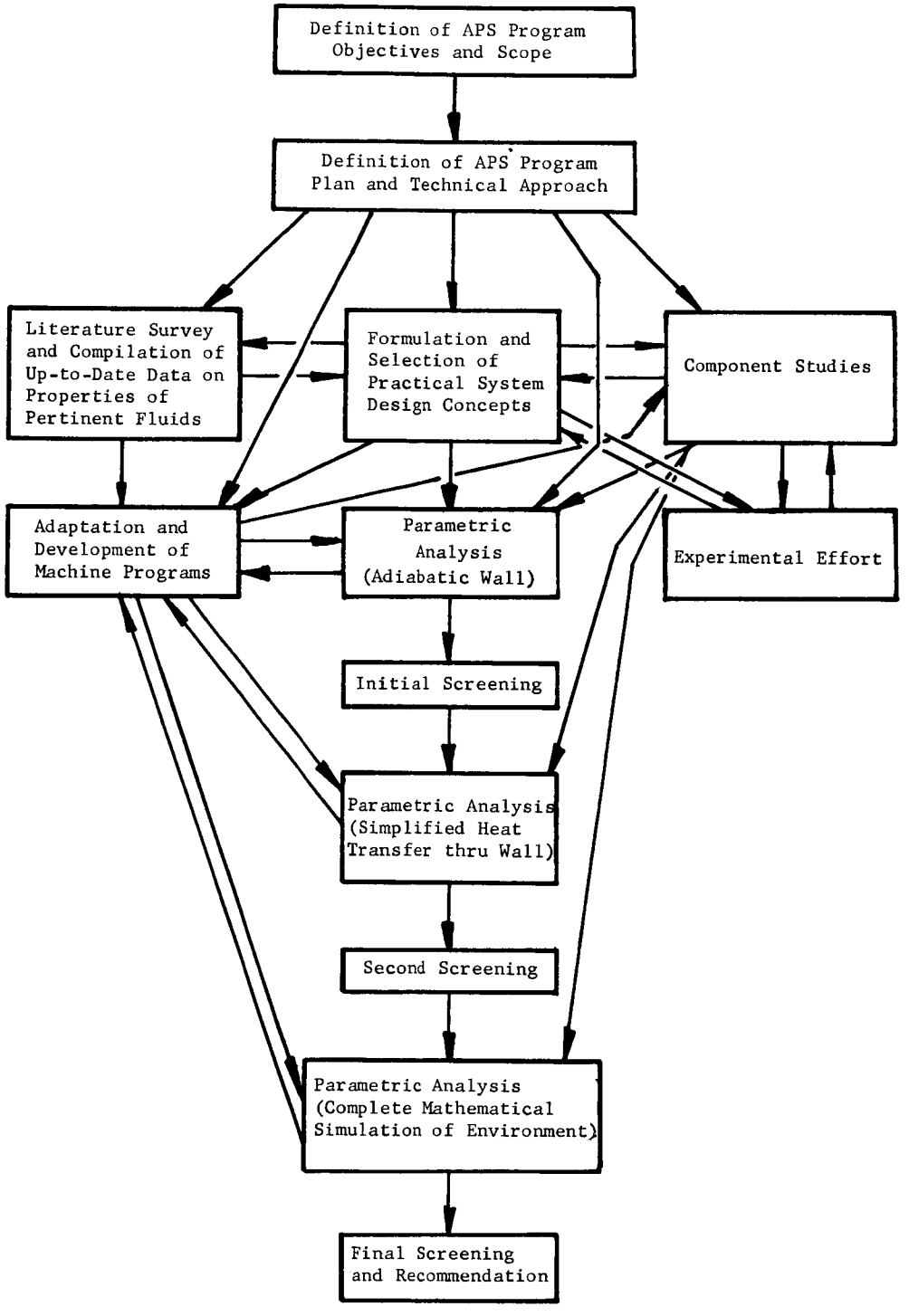

Figure 1 Pressurization System Program Plan

The mission employed in the analysis was the Apollo-type lunar mission. The propulsion stage, or module, used liquid hydrogen and oxygen as propellants rather than storable propellants. The vehicle requirements were as specified in Tables 2 and 3.

Table 2 Pressure-Fed Engine Vehicle Mission

Firing	Propellant Expelled (lb)	Firing Time (sec)	Time from Launch (hr)
1	980	18.7	26
2	980	18.7	48
3	18,280	349.0	78
4	980	18.7	126
5	6,576	125.5	138
6	233	4.45	158
7	233	4.45	186

Table 3 Pump-Fed Engine Vehicle Mission

Firing	Propellant Expelled (lb)	Firing Time (sec)	Time from Launch (hr)
1	1,641	47.1	26
2	381	10.9	48
3	19,705	564.9	78
4	935	26.8	126
5	6,232	178.7	138
6	337	9.7	158

Several vehicle tankage designs were used in the program. During the study of the pressure-fed engine system, the liquid hydrogen tank was a sphere and the liquid oxygen tank was a torus located below the liquid hydrogen tank. Two configurations were used in the pump-fed engine system. The spherical liquid hydrogen tank was positioned above the four, clustered, spherical, liquid oxygen tanks. In the initial screening of pump-fed systems, the liquid hydrogen tank was supported by two circular rings. However, during the secondary and final screening, the liquid hydrogen tank was supported by a single conical ring at tank centerline.

Propellant tankage design parameters used during the study are tabulated in Table 4.

Table 4 Propellant Tankage Design Parameters

Tank	Pressure Fed		Pump Fed	
	LO_2	LH_2	LO_2	LH_2
Ullage (% total tank volume)	3.0	5.0	3.0	5.0
Outage (% usable propellant)	2.0	4.0	0.5	1.0
Tank Pressure (psia)	170.0	170.0	-	-
Engine Net Positive Suction Pressure (psia)	-	-	15.0	8.0
Nominal Tank Volume (ft^3)	366	1300	360	1210

III. PRESSURIZATION SYSTEMS STUDIES

A. ANALYTICAL MODELS

One important aspect of the analytical portion of the program was the effort to perfect an analytical model that was used to optimize pressurization system weight. To allow the remainder of the program to proceed during the development period of the model, simplified analytical techniques were used to make preliminary system studies and selections.

A number of computer programs was used, some of which were existing and some of which were written specifically for this effort using both the IBM 1620 and the IBM 7094 computers. No effort will be made to describe the total computer effort; however, several specific programs will be discussed: IBM 1620 programs used to compute tank thermodynamics and pressurant usage, an IBM 7094 program designated as ØD041 used to compute tank thermodynamics, and the ØB014 program for the IBM 7094 that was considered to be the major analytical model.

1. Pressurant Usage Model

At the beginning of the program it was necessary to provide pressurant usage data to complete the preliminary screening of the pressure-fed systems. Since the larger IBM 7094 computer program that ultimately would supply this information was not ready for use, it was decided to develop a simplified 1620 program to obtain preliminary data. Two programs were developed because computer core limitations prevented developing a single program to analyze both coast and outflow phases of a mission. The first program was used to calculate coast period heat and mass balances for a final saturated equilibrium condition between vapor and liquid. Neither the heat capacity of the propellant container nor the external heat transfer into or out-of the propellant tank were considered in the heat and mass balances. The first program was also used to calculate the gas required to pressurize the propellant tank to normal operating pressure prior to propellant outflow. It was assumed that no mass transfer nor heat transfer occurred during the pressurization process. The second program calculated the tank pressurant required to maintain a constant pressure during propellant outflow. This program assumed zero external heat transfer to or from the propellant tank. Heat transfer was assumed to occur between the gas and the tank wall and

at the liquid-gas interface. The tank wall and the liquid were assumed to be at the same temperature during outflow so that no heat transfer occurred between the liquid and the wall. Propellant vaporization at the liquid-gas interface was assumed to occur.

These two programs were used alternately through the multiburn mission, described in Chapter III.C.5a to determine pressurant total usage as a function of the pressurant inlet temperature. When the more sophisticated IBM 7094 program became available for use, it was found that the predicted usage from the IBM 1620 program was conservative, being about twice that obtained from the IBM 7094 program. An investigation was made to determine the cause of the discrepancy. The major factor appeared to be the method of calculation of mass transfer (boiloff). In the IBM 1620 program, it was assumed that a thin layer of propellant at the ullage gas/propellant interface was at the propellant saturation temperature corresponding to the partial pressure of the propellant vapor in the ullage. A heat transfer rate from the ullage into the interface was then defined by the temperature difference between the ullage and the interface temperature. A similar heat transfer rate was defined between the interface and the propellant bulk temperatures. The difference between these two heat transfer rates, when divided by the heat of vaporization of the propellant, was the boiloff rate. The boiloff rate, in turn, entered the ullage at the bulk liquid temperature. This resulted in a reduction of ullage temperature and pressure, requiring addition of more helium to maintain the tank pressure at the required level. It was concluded that a more realistic approach in regard to boiloff would be to use the bulk enthalpy difference between the ullage gas temperature and the propellant temperature rather than the heat of vaporization. This method was employed in the IBM 7094 program.

The simplified IBM 1620 pressurant usage program was used in the initial studies of the pressure-fed systems only, although the usage data generated by this program are of larger magnitude than would actually be required. The systems selected as a result of this study were reevaluated using the more realistic approach to mass transfer. Although the system weights did change, the comparative relations of the systems remained the same.

2. Tank Pressurization Model

The ØD041 computer program is a propellant tank, thermodynamic model for launch and space vehicles. The program is designed to determine propellant and ullage gas temperatures and masses, the amount of ullage gas vented, and the amount of pressurant required. The computation for each propellant tank is done separately by inputting its properties for each case.

The model uses a lumped-system approach where each mass, such as the ullage gas, is taken at a single bulk temperature at any time; therefore, the properties of the propellant, ullage gas, and wall are a function of time, not configurations. The tank wall is considered as two separate segments, one in contact with the ullage gas and one in contact with the propellant.

The program is broken into three distinct sections: initialization, time rate, and equilibrium. A simplified flow diagram, shown in Fig. 2 and Table 5 indicates the input-output parameters of the program. The initialization section is used once to obtain the initial condition of each tank. The time rate section uses a forward difference method of calculation to determine thermodynamic changes such as heat transfer between the lumped masses, mass transfer at gas/liquid interface, vented ullage, and pressurant added. The addition of heat from external sources is also an option of the program. Another option allows for storage of pressurant in a sphere, using real gas relationships over a limited temperature range and an adiabatic expansion process.

In the equilibrium section, the propellant, ullage gas, and tank wall attain the same temperature with saturation conditions between the vapor and the liquid. The equilibrium calculation is not a transient solution, so it can be a time step of any amount. If heat flux to the tank wall exists, an integrated value of the flux is added to the system before equilibrium conditions are calculated.

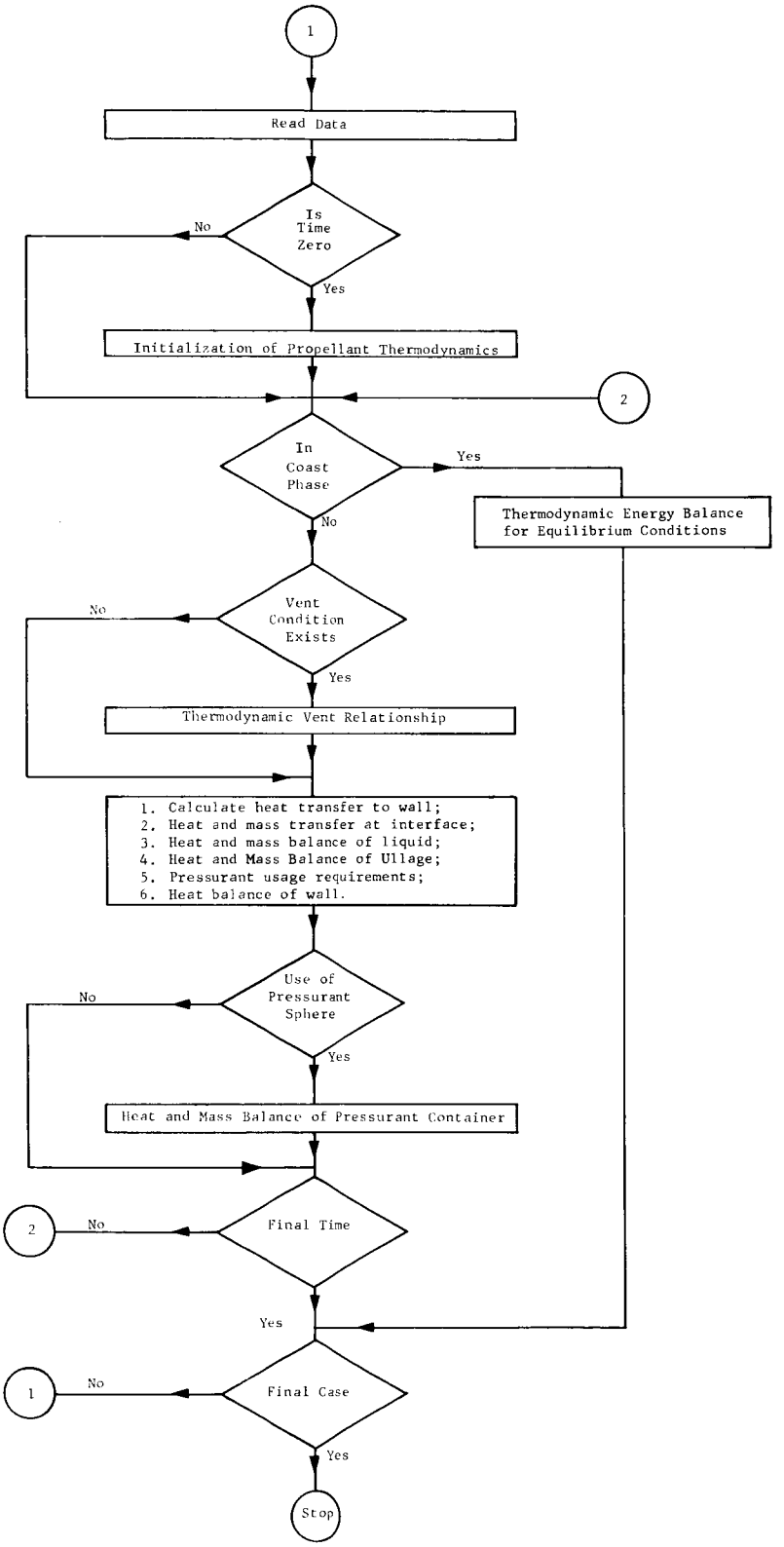

Fig. 2 Skeletonized Flow Diagram of Propellant Tank Computer Program

Table 5 ØD041 Input and Output Parameters

Input Data

Program Control Specification	Curves Defining Configuration	Propellant Properties	Pressurant Properties	Run Constants
External Heating	Gas-liquid Area versus Liquid Volume	Viscosity versus Temperature	Viscosity versus Temperature	Vent Parameters
Vapor Dissociation	Ullage Wall and Liquid Wall Area versus Liquid Volume	Thermal Conductivity versus Temperature	Thermal Conductivity versus Temperature	Regulator Settings
Type of Pressurant	Maximum Inflow Rate versus Time	Density versus Temperature	Specific Heat versus Temperature	Initial Volumes
Source of Pressurant	Propellant Outflow Rate versus Time	Vapor Pressure versus Temperature	Molecular Weight	Initial Temperatures
Outflow by Mass or Volume	Altitude versus Time	Heat of Vaporization versus Temperature	Critical Pressure	Initial Propellant Mass
Disposition of Heat Transfer at Liquid/Gas Interface	Atmosphere Pressure versus Time	Specific Heat versus Temperature	Critical Temperature	Initial Pressures
Venting Ability	Vehicle Velocity versus Time	Volumetric Expansion		Coefficients of Heat Transfer Equations
Subtraction of Pressurant Mass from Propellant	Specific Heat of Wall versus Temperature			Constants for Polynominal of Specific Heat of Vapor
Coast or Rate Section	Pressurant Inlet Temperature to Tank versus Time			Acceleration
				Weight of Tank Wall
				Percent of Pressurant Removed from Propellant
				Size of Pressurant Storage Sphere
				Constants for Ullage Compressibility
				Constants for Dissociation
				Heat Flux to External Wall
				Heat Source Inside Tank
				Run Time
				Print Time
				Compute Time

Output Data*

Temperatures	Pressures	Weight	Miscellaneous
Ullage	Ullage	Propellant	Time
Propellant	Sphere	Vapor	Ullage Volume
Sphere		Pressurant	Flow Rate of Pressurant
Wall Next to Ullage			
Wall Next to Liquid			

*Normal print. In a spill all values used in program are output, such as amount vented and heat transfer rates.

The options available in the program are:

1) Vapor dissociation may or may not be considered;

2) Heat transfer between the vehicle and its surroundings may be computed for any one of three conditions: stationary vehicle prior to flight, powered flight, and coast;

3) A pressurant regulator may or may not be used;

4) Propellant may be considered volatile or nonvolatile;

5) Pressurant may be considered condensible or noncondensible;

6) Venting may or may not be used;

7) Propellant quantity may be input by weight or by volume;

8) All heat transfer at the liquid/gas interface may be assumed to go into liquid boiloff or both boiloff and sensible heating may be considered.

3. Analysis of Propellants, Tankage, and Pressurization System Model

The ØB014 computer program has been written for the thermal and thermodynamic analysis of the propellant, tankage, and pressurization subsystems in spacecraft under transient conditions. It is designed to simultaneously consider all of the major heat transfer and thermodynamic processes occurring within the various fluids inside the vehicle and in the space between these fluids and the environment external to the vehicle. It permits consideration of a number of different propellants and pressurants and provides options for a rather wide variety of pressurization system configurations and control modes. Tables 6 and 7 summarize the available program control options and tabulate the significant input and output parameters. The program logic is organized as indicated in the skeleton flow diagrams of Fig. 3.

Table 6 ØB014 Input Data

Program Control Specifications	Curves Defining Configuration and Mission Profile	Material Properties for Structural Elements	Run Constants	Element Properties
Propellant type(s)	Gas/liquid interface area versus liquid volume	Material density	Relief valve cracking pressure	Element number
Pressurant type(s)	Ullage volume pressure regulator setting versus time	Thermal conductivity versus temperature	Relief valve reseat pressure	Element material identification
Ullage space pressure control schedule	Propellant outflow rate versus time	Emissivity versus temperature	Net pump suction head	Element type identification
Propellant outflow rate schedule	Multiplying factors defining solar, lunar, and earth radiation intensities versus time	Specific heat versus temperature	Regulator setting (if constant)	Orientation of each element relative to adjacent elements
Temperature schedule of pressurant entering tank	Pressurant storage vessel temperature versus time		Initial ullage volume	Specification of elements radiating to present element
Location of storage vessel for pressurants if pressurant in gaseous phase	Vehicle attitude versus time		Initial propellant volume	Element view factors, or multiple reflection parameters for radiation heat transfer
Independent variable of pressurant storage vessel, i.e., either volume or burnout pressure	Pressurant temperature into propellant tank versus time		Propellant outflow rate (if constant)	Emissivities of moon and earth
Atmosphere standard	Height of liquid in propellant tank versus volume		Initial propellant mass	Lengths of conduction paths
Initial pressurization option			Initial propellant temperature	Conduction areas
Tank purge option			Initial propellant density	Element volumes
Net pump suction head option			Temperature of pressurant entering tank (if constant)	Absorptivity to solar emission
Heat exchanger configuration			Coefficients of polynomial describing interface area versus liquid volume during zero-g	Height of wetted element above bottom of propellant tank
Disposition of heat transfer across gas/liquid interface			Gas side film coefficient gas liquid interface	
State of pressurant at its source			Gas side film coefficient for heat transfer between ullage gases and wall	
Pressurization system plumbing cooldown option			Initial atmospheric pressure	
Option defining heat transfer to pressurant storage vessel			Initial atmospheric temperature	
Computational interval definition at beginning of calculation			Environmental temperature of pressurant storage container	
Prepressurization of propellant tank with helium at engine start and then pressurization with propellant vapor			Storage vessel configuration parameters	
Type of pressurization at engine start during mission.			Initial pressure in pressurant storage vessel	
Possible selection of orifice for pressurant flow into propellant tank			Final pressure in storage vessel	
Disposition of basic heat transfer subroutine			Thermal properties of storage vessel wall material	
Subtraction of pressurant mass from propellant			Joule-Thompson coefficient	
Type of thermodynamic energy balance for coast conditions			Heat exchanger configuration parameters	
			Heat exchanger performance parameters	
			Thermal properties of heat exchanger fluids	
			Pressurization line configuration	
			Solar-, lunar-, and earth-emitted heat fluxes	
			Lunar and earth albedos	
			Run time specifications	
			Output data format options	
			Initial temperatures of tank and liquid elements	
			Iteration control constants	
			Iteration control constants	
			Run title and identification	
			Engine performance parameters	
			Vehicle performance characteristics	
			Engine operating times	
			Orifice areas at engine operation	
			Upstream pressure for orifice if pressurant is not helium	

Table 7 ØB014 Output Data

Temperature	Pressure	Mass	Heat	Volume
Temperature of ullage gases Propellant temperature Propellant boiling point temperature Temperature of pressurant entering ullage space Individual element temperatures	Ullage volume pressure Propellant vapor pressure Partial pressure of propellant vapors in ullage volume Relief valve cracking pressure Regulator setting	Total mass of gases and vapors in ullage space Mass of propellant vapor in ullage space Propellant outflow rate Propellant mass Evaporation (or condensation rate) Boiloff rate Total boiloff Total mass vented Mass of pressurant in ullage space Mass of propellant vapors vented Mass of pressurant vented Propellant density Pressurant rate of flow into tank	Heat transferred across gas/liquid interface Total heat exchange between mass in tank and its surrounding Same as 2. above for each computing interval Individual element enthalpies	Propellant volume Ullage volume Change in ullage volume over computer interval

Miscellaneous	Time	Storage	Heat Exchanger	Flight
Thermal mass Ratio of specific heats of mixture in ullage space Gas/liquid interface area for both positive and zero-g Iteration count Height of liquid in propellant tank Number of operating cycles of bang-bang valve Viscosity, conductivity buoyancy, and specific heat of propellant	Fligia time Engine firing time(s) Engine firing duration(s) Computing interval Burnout time	Temperature of pressurant Pressurent of pressurant Mass of pressurant Volume of vessel wall Surface area of vessel Volume of pressurant Increment of heat transferred to pressurant Compressibility factor of pressurant Temperature of pressurant tank wall	Temperature of hot gas entering and leaving evaporator Temperature of hot gas entering and leaving heat exchanger Temperature of pressurant entering and leaving evaporator Temperature of pressurant entering and leaving heat exchanger Transport properties of helium in oxidizer heat exchanger Transport properties of oxidizer used for oxidizer heat exchanger Overall heat transfer coefficient of heat exchanger Oxidizer heat exchanger geometric parameters Heat subtracted from propellant Pressurant tank heat transfer coefficient	Total mass of propellant consumed Total vehicle mass Mass fraction Vehicle velocity increment Total velocity change Vehicle acceleration

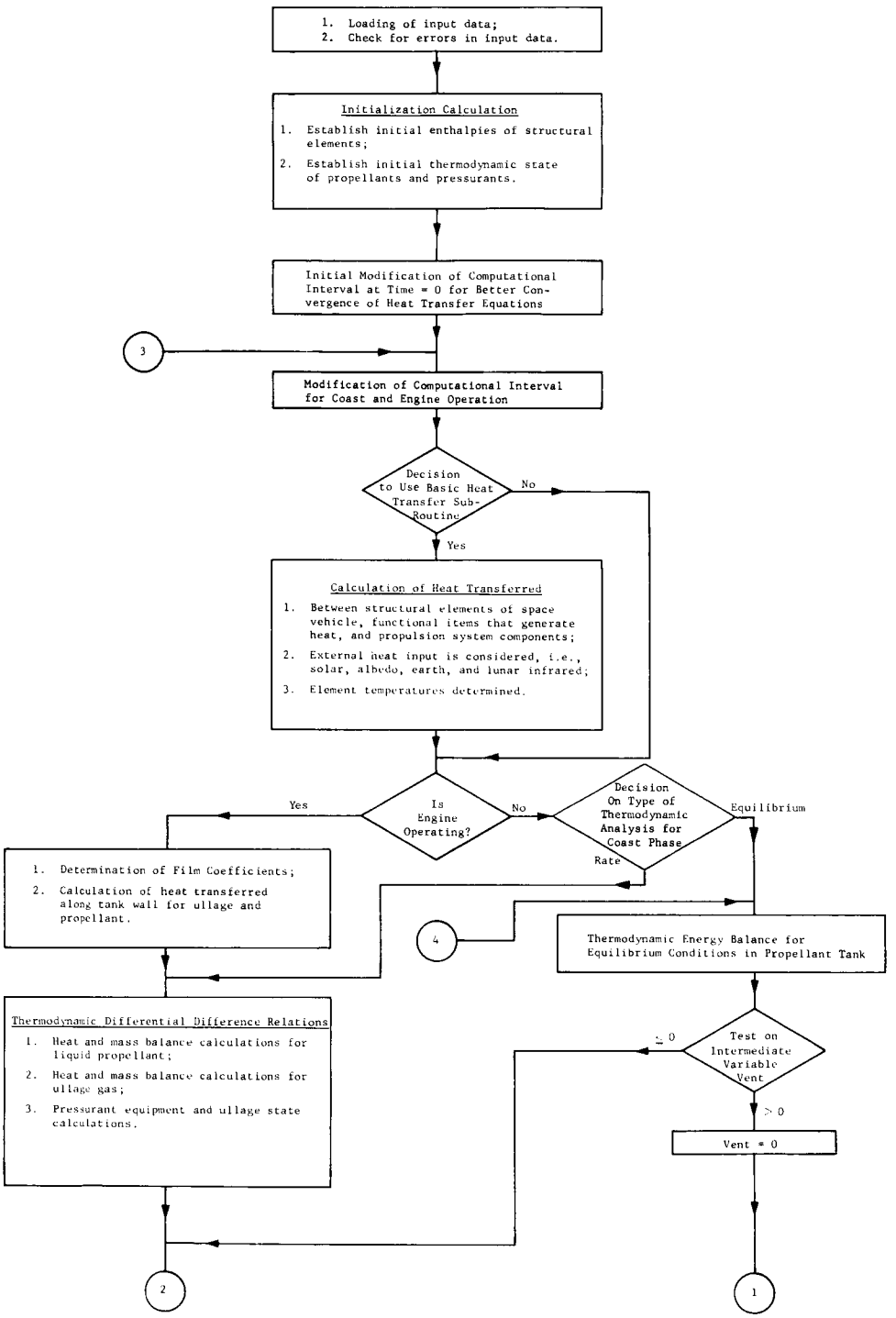

Fig. 3 Skeletonized Flow Diagram of Propellants Tankage Pressurization System Computer Program

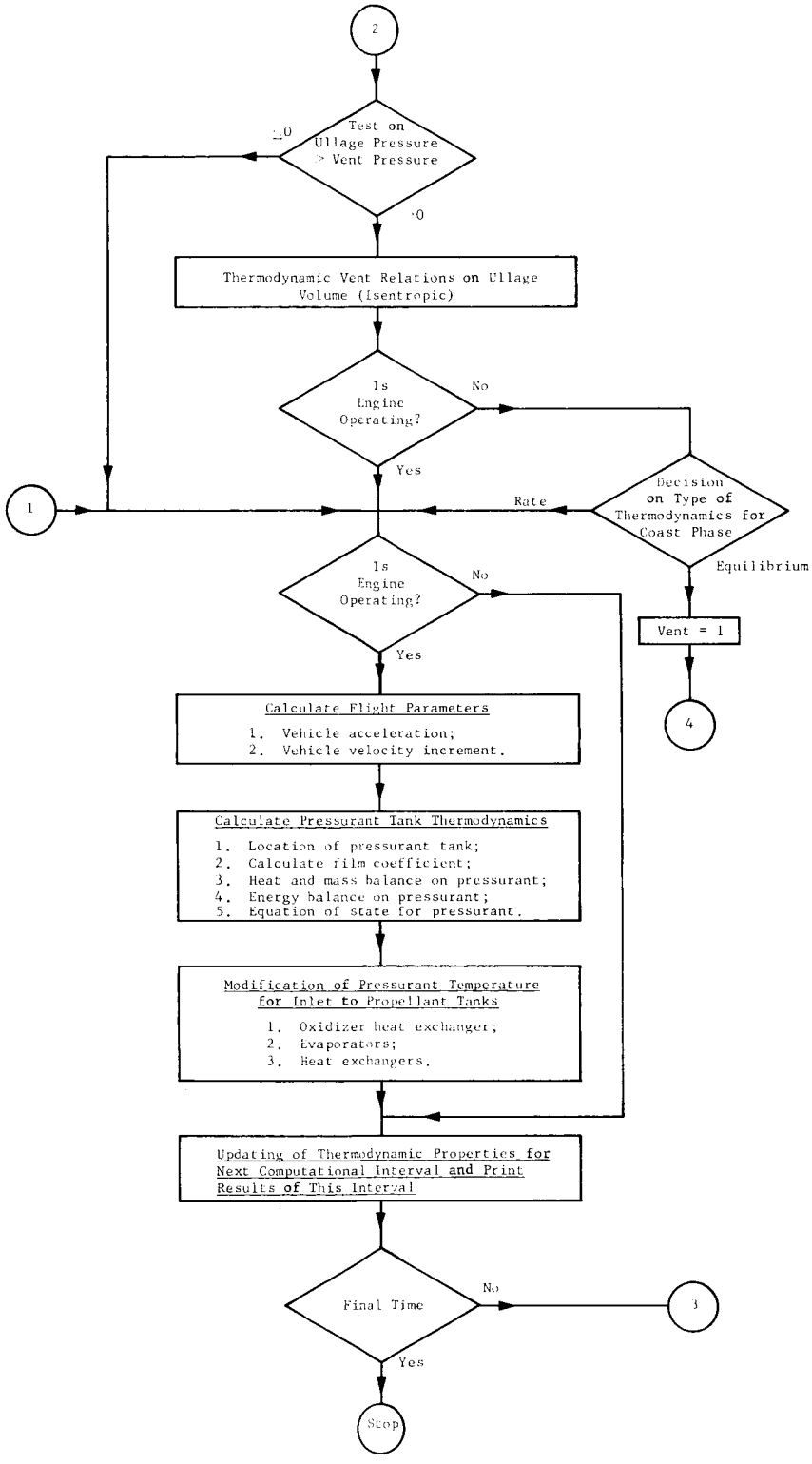
2
Test on Ullage Pressure > Vent Pressure
≤0
>0
Thermodynamic Vent Relations on Ullage Volume (Isentropic)
Is Engine Operating?
No
Yes
1
Rate
Decision on Type of Thermodynamics for Coast Phase
Equilibrium
Is Engine Operating?
No
Yes
Vent = 1
4
Calculate Flight Parameters
1. Vehicle acceleration;
2. Vehicle velocity increment.
Calculate Pressurant Tank Thermodynamics
1. Location of pressurant tank;
2. Calculate film coefficient;
3. Heat and mass balance on pressurant;
4. Energy balance on pressurant;
5. Equation of state for pressurant.
Modification of Pressurant Temperature for Inlet to Propellant Tanks
1. Oxidizer heat exchanger;
2. Evaporators;
3. Heat exchangers.
Updating of Thermodynamic Properties for Next Computational Interval and Print Results of This Interval
Final Time
No
3
Yes
Stop

Fig. 3 (concl)

The program uses the lumped-system approach in dealing with the various fluid masses involved (Ref 1). This approach treats the individual fluid masses as though their thermodynamic properties vary only as a function of time and not space. The program thus, in essence, works with the time-dependent, average properties of the fluids. The vehicle structure including the tank walls is treated as a distributed system, where temperatures are allowed to vary in both time and three-dimensional space.

The program is subdivided into three basic working sections, i.e., the initialization section, the heat transfer section, and the thermodynamics section. The computations performed in the initialization section are, for the most part, those that are required only once per run. These computations involve determination of the initial thermodynamic states of the propellant(s) and pressurant(s) and the selection of run constants and constant coefficients of the various equations employed in the heat transfer and thermodynamics sections. It is in this section that the raw input data are converted into the form best suited for subsequent use.

In the heat transfer section, a running three-dimensional energy balance is conducted on the significant structural elements of the system, and the three primary modes of heat transfer are considered. The convection processes occurring at the fluid-to-structure interfaces represent the link in the energy chain between the thermodynamic processes occurring within the fluid containers and the conduction and radiation processes occurring between the structure-to-structure and structure-to-environment interfaces. The procedure for conducting the energy balance involves the subdividing of the structure into discrete elements of known dimensions and mass. A differential-difference expression for the energy Equation [1] is written for each element, and the simultaneous solution of these equations is effected by numerical means. The differential-difference expression is implicit in temperature, and the solution for element temperatures involves iterative procedures for which convergence acceleration techniques are employed. The methods used for solving these implicit equations are inherently stable and converge to solutions that compare well with exact solutions in sample test cases.

The terms in the energy equation that treat radiation allow for consideration of solar radiation, earth and lunar albedo, earth and lunar infrared radiation, and infrared radiation exchange with multiple reflections between internal elements of the vehicle. The logic controlling the inputs to the energy equation

permits consideration of the effect of temperature on thermal conductivity, specific heat, and emissivity of the materials employed. An option is also provided for bypassing the heat transfer section of the program if it is desired to investigate only thermodynamic processes in a given problem. Mathematical methods employed in the heat transfer section of the program are described in more detail in Ref 2.

The thermodynamics section of the program is comprised of a number of different subsections through which a rather wide variety of paths may be taken depending on the system configuration and the options selected. In the analysis of a given configuration, the path taken depends on the phase of the mission in which the vehicle exists at a point in time and on tests made of various possible controlling parameters to determine if these parameters are within tolerance.

The heat balance equation employed in computer program ØB014 is:*

$$\frac{\rho V_E h_E}{t}_{Final} = \frac{\rho V_E h_E}{t}_{Initial} + \tfrac{1}{2}\Bigg[q_{int} + \sum_{i=1}^{i} q_{cond_i} + \sum_{j=1}^{m} q_{conv_j} + \sum_{k=1}^{n} q_{net_k} + q_{ray} - q_{rad_\infty} + q_{sol} + q_{earth} + q_{moon} + q_{pp} + q_{par}\Bigg]_{Initial} + \tfrac{1}{2}\Bigg[q_{int} + \sum_{i=1}^{m} q_{cond_i} + \sum_{j=1}^{n} q_{conv_j} + \sum_{k=1}^{p} q_{net_k} - q_{rad_\infty} + q_{ray} + q_{sol} + q_{earth} + q_{moon} + q_{pp} + q_{par}\Bigg]_{Final}, \quad [1]$$

*The sum of one-half the initial heating rate and one-half the final heating rate affects the average heating rate over the computing interval.

where

$\frac{\rho V_E h_{E_{Final}}}{t}$ and $\frac{\rho V_E h_{E_{Initial}}}{t}$ = Heat content of element at end and beginning of computing interval, respectively, divided by computing interval,

t = time (sec),

ρ = density $\left(lb_m/ft^3\right)$,

V_E = volume $\left(ft^3\right)$,

$h_{E_{Final}}$ = specific enthalpy (Btu/lb),

q_{int} = heating rate from internal source (Btu/sec),

$\sum_{i=1}^{i} q_{cond_i}$ = summation of conductive heating rates to and from other elements (Btu/sec),

$\sum_{j=1}^{m} q_{conv_j}$ = summation of convection heating rates to and from element in question (Btu/sec),

$\sum_{k=1}^{n} q_{net_k}$ = summation of radiation heating rates to and from elements in question as computed by net radiation exchange method (Btu/sec),

q_{ray} = summation of radiation heating rates to and from element in question as computed by ray tracing technique using multiple reflections (Btu/sec)

q_{rad_∞} = rate of radiation heat lost to space (Btu/sec),

q_{sol} = solar heating rate (Btu/sec),

q_{earth} = summation of earth-emitted and earth-reflected radiation rates (Btu/sec),

q_{moon} = summation of moon-emitted and moon-reflected radiation rates (Btu/sec),

q_{pp} = solar heat input by periodic equation (Btu/sec),

q_{par} = net rate of radiation exchange with infinite parallel plate (Btu/sec).

The basic flow of logic through the program when the propulsion system is operating, i.e., either when the system is being prepared for engine firing, or when the engine is firing, involves, in sequence:

1) An energy and mass balance at the gas-to-liquid interface to determine heat transfer and boiloff rate;

2) An energy and mass balance on the liquid propellant mass, where additional liquid is boiled off if required;

3) An energy and mass balance on the gases in the ullage space, where pressurant is either added or vented as required;

4) An energy balance on the pressurant and heat source fluid as they exchange heat across the walls of a heat exchanger;

5) An energy and mass balance on the pressurant storage subsystem.

During coasting flight, when the system is not operating, the option exists for computing either (a) the nonequilibrium thermodynamic states of the ullage gases and liquid propellant separately and the associated energy and mass transfer rates, or (b) the equilibrium thermodynamic state of the entire fluid mass within the tank including the mass of the tank wall that was the option used during this program. For either case, the tank is allowed to vent through a relief valve as required, and the logic allows for the venting of gases only. The heat transferred across the fluid-to-structure interfaces, as computed in the heat transfer section of the program, is considered in the thermodynamic energy balances conducted on the propellant masses, the ullage gases, and the stored pressurant.

The helium in the storage container is considered as a real gas, and the Beattie-Bridgeman equation of state is used. The constants used in this equation make the equation consistent with the latest National Bureau of Standards data on helium at high pressures and at LH_2 temperature.

B. SYSTEM DESCRIPTION

At the beginning of the program, one of the first objectives was to select a number of system configurations to study. Since the program was intended to cover the total range of possibilities to make the final system selection valid, a method was devised to ensure that as many combinations as practical were considered. The option chart shown in Fig. 4 was evolved to provide a completely general approach to system selection. The chart breaks up a pressurization system into two general subsystems: the pressurant storage subsystem and the heating subsystem. By beginning at the top of the chart, with consideration given to the vehicle or propellant system design and the mission under study, all possible options may be listed. In many cases, the mission and design constraints will eliminate some of the possible options.

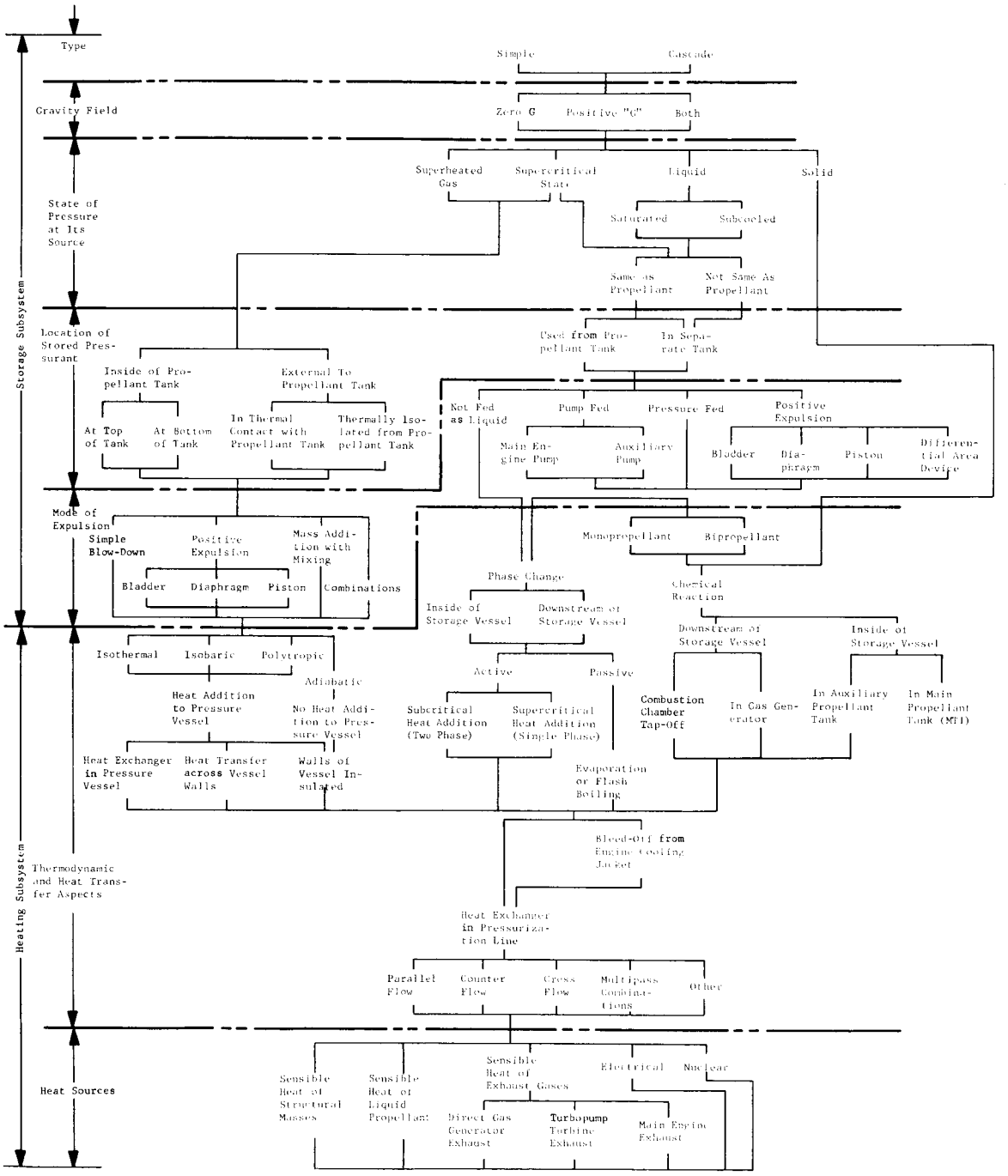

Fig. 4 System Configuration Option Chart

During the study phase of the program, four types of systems were selected for the optimization studies: primary and advanced systems for pressure-fed propellant systems and primary and advanced systems for pump-fed propellant systems, hereinafter referred to as primary and advanced pressure-fed and primary and advanced pump-fed systems. A different level of analysis was used for the two basic types of systems, i.e., pressure-fed systems and pump-fed systems. Since the study and preliminary selection of pressure-fed systems were taking place simultaneously with the development of the analysis methods, these systems were exposed to different levels of analysis than the pump-fed systems that were studied later in the program. Pressure-fed systems were exposed to simplified techniques in some cases, requiring hand calculations with no exposure to the final analytical model. Pump-fed systems, however, were exposed to an existing analytical model with a simplified heat transfer method and to the final analytical model.

During outflow, the pressurant expansion in the container may be isothermal, isentropic (adiabatic), isobaric, or combinations of these. The location of the pressurant container was not dictated by the vehicle configuration so that it could be mounted either inside or outside the liquid hydrogen propellant tank.

Since, in some cases, the pressurant was stored at cryogenic temperatures, yet injected into the propellant tanks at relatively high temperatures, some method of heating between storage and main tankage was required. The heat source subsystem consisted of the necessary gas generators and heat exchangers to preheat the helium prior to its use as a pressurant in the propellant tanks. The heat source subsystem also included the heat exchangers employed in maintaining the expansion process selected. The types of gas generators considered were liquid, solid, and hybrid.

The pressure control subsystem considered the use of single- and dual-stage pressure regulators and combinations of orifices, rapid-cycling valves, and pressure switches.

A major criterion employed in the design of the primary system was the use of current, state-of-the-art technology.

1. Primary Pressure-Fed Systems

The primary pressurization system for use with a pressure-fed propellant system was defined as a system storing helium at liquid hydrogen temperature with heating and expansion prior to injection into the propellant tanks. This system consisted of a pressurant storage container subsystem, a heat source subsystem, and a pressurant control subsystem and is shown schematically in Fig. 5. It was to be optimized primarily for reliability. The system studied, with the varied expansion processes used, is described as follows:

System 1 - Helium was stored at liquid hydrogen temperature with heating and expansion prior to use in the propellant tanks. The following expansion processes were used for the storage containers:

Isobaric, P = C;

Isothermal, T = C;

Isentropic, S = C;

Combination isobaric and isentropic, P = C, S = C;

Combination isentropic and isobaric, S = C, P = C;

Combination isobaric and isothermal, P = C, T = C;

Combination isothermal and isobaric, T = C, P = C.

2. Advanced Pressure-Fed Systems

Advanced pressurization systems for use in pressure-fed propellant systems were defined as those systems not constrained by state-of-the-art technology in either their design or operation. No constraints regarding pressurant type and pressurant storage location were imposed. Those systems were to be optimized for light weight and reliability. A variety of candidate systems was selected for evaluation and comparison during Task I of the contract. For the evaluation phase, 14 different systems were established. These systems are presented schematically in Fig. 6 and are described as follows:

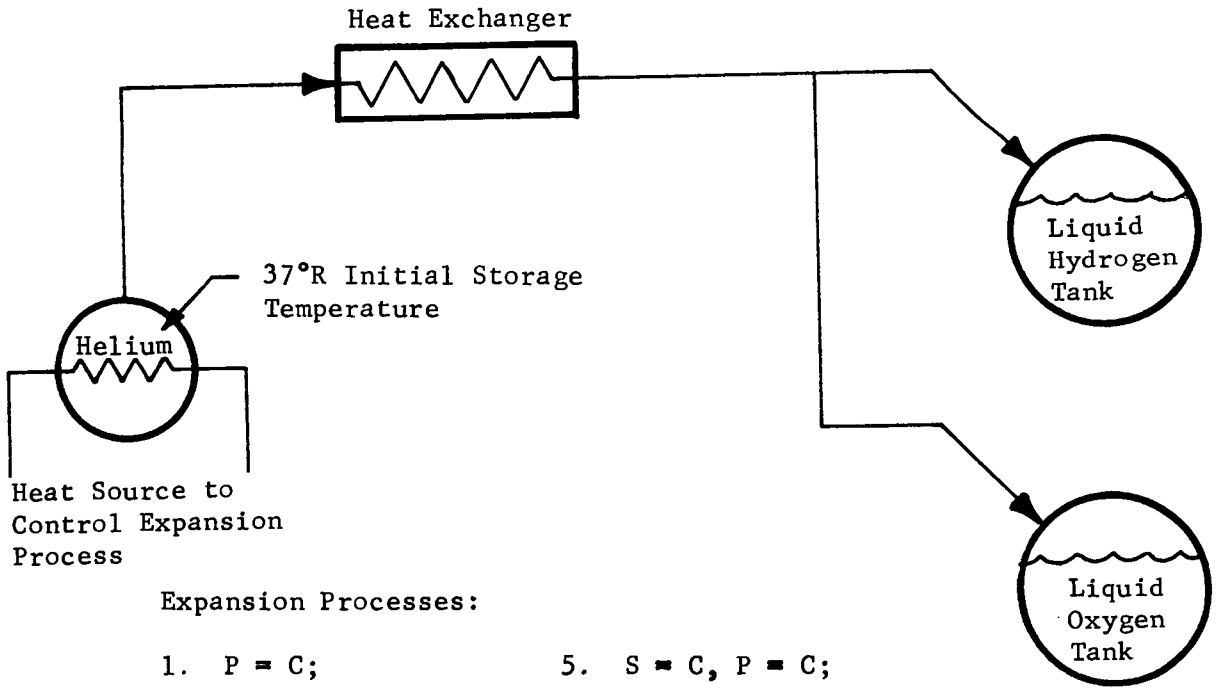

Expansion Processes:

1. P = C;
2. T = C;
3. S = C;
4. P = C, S = C;
5. S = C, P = C;
6. P = C, T = C;
7. T = C, P = C.

Fig. 5 Primary Pressurization System for Pressure-Fed Propellant System

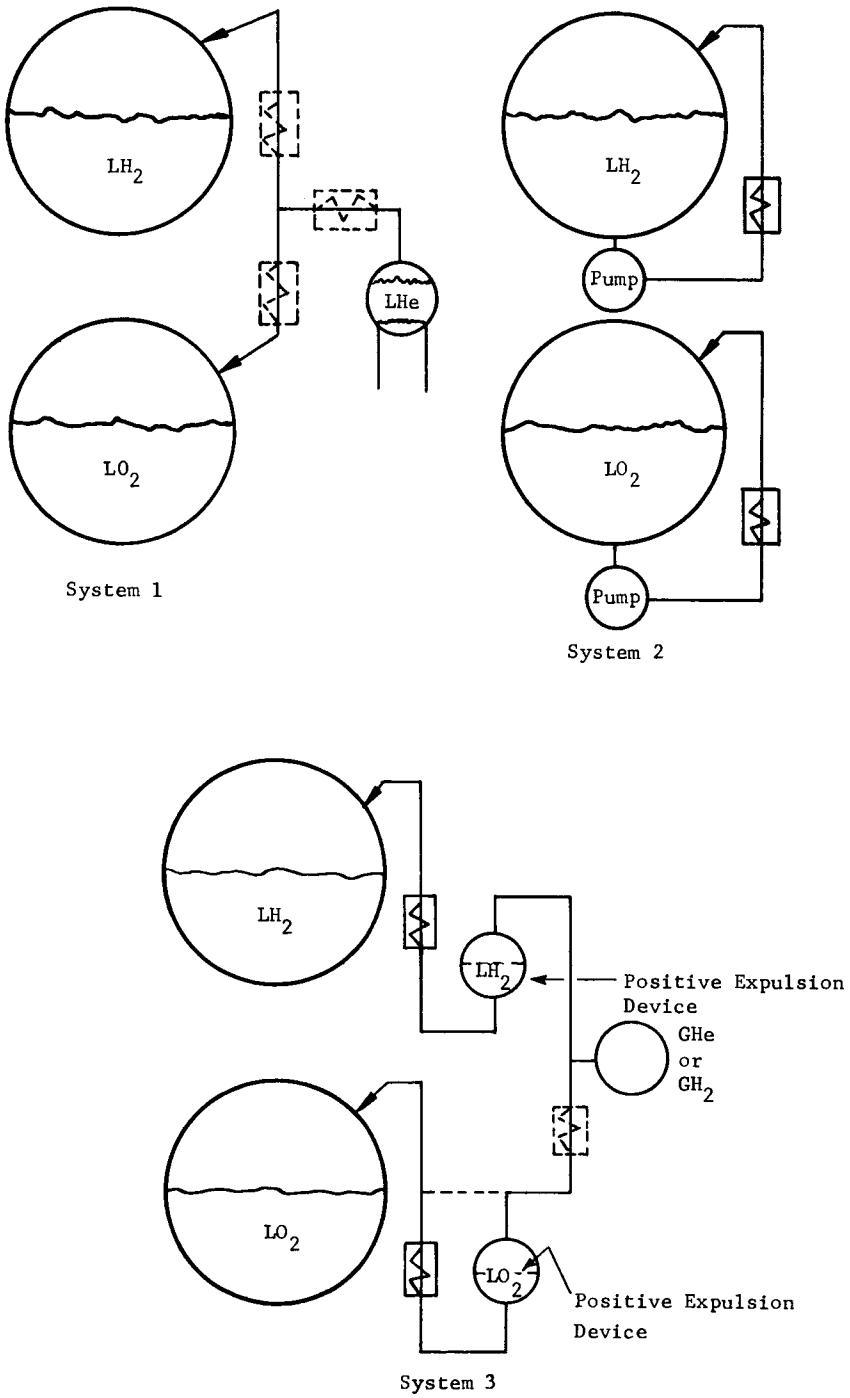

Fig. 6 Advanced Pressurization Systems for Pressure-Fed Propellant Systems

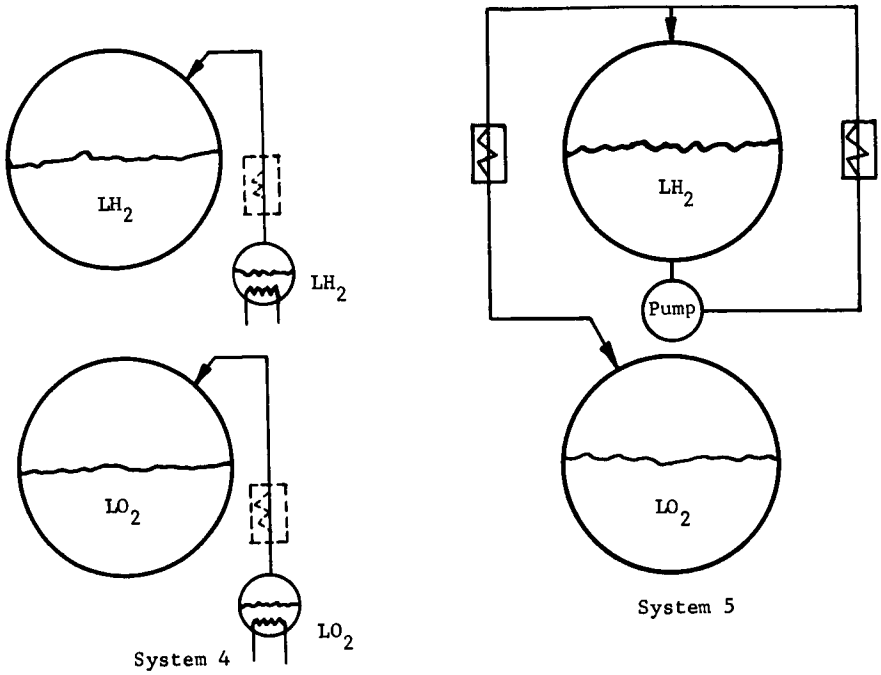
LH_2
LH_2
LO_2
LO_2
System 4
LH_2
Pump
LO_2
System 5

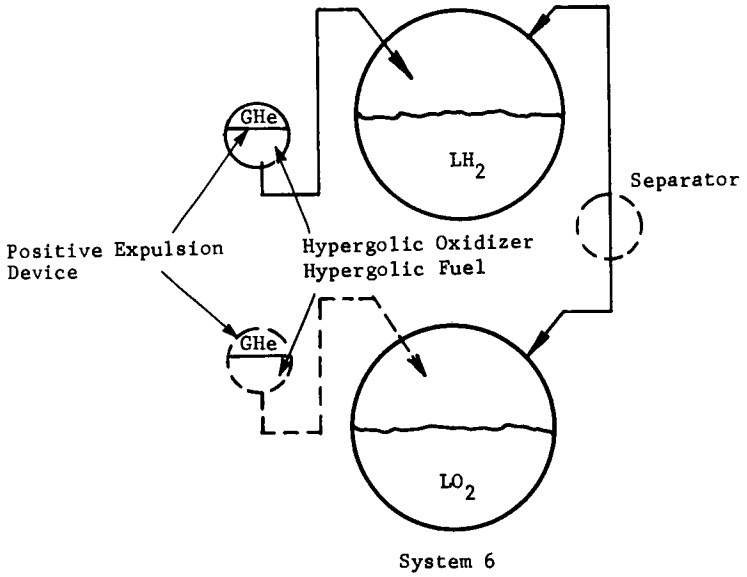
GHe
LH_2
Separator
Positive Expulsion Device
Hypergolic Oxidizer
Hypergolic Fuel
GHe
LO_2
System 6

Fig. 6 (cont)

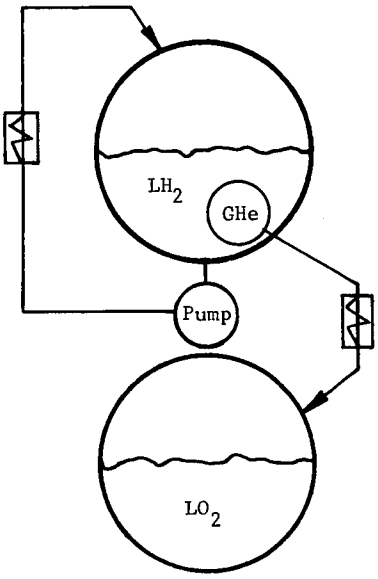

System 7

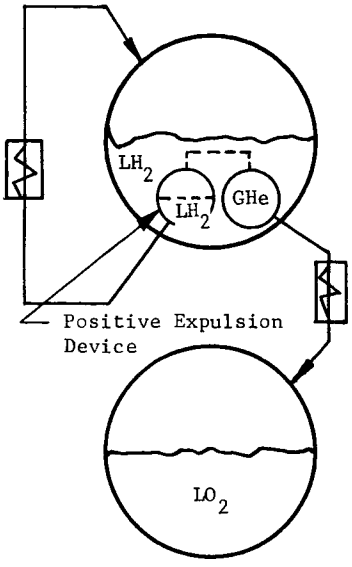

System 8

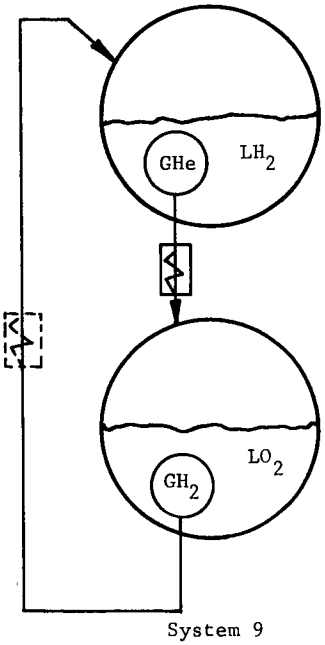

System 9

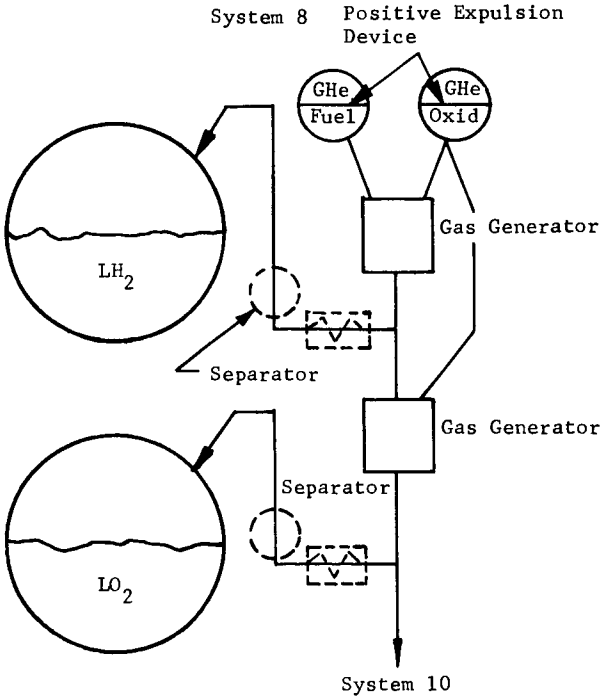

System 10

Fig. 6 (cont)

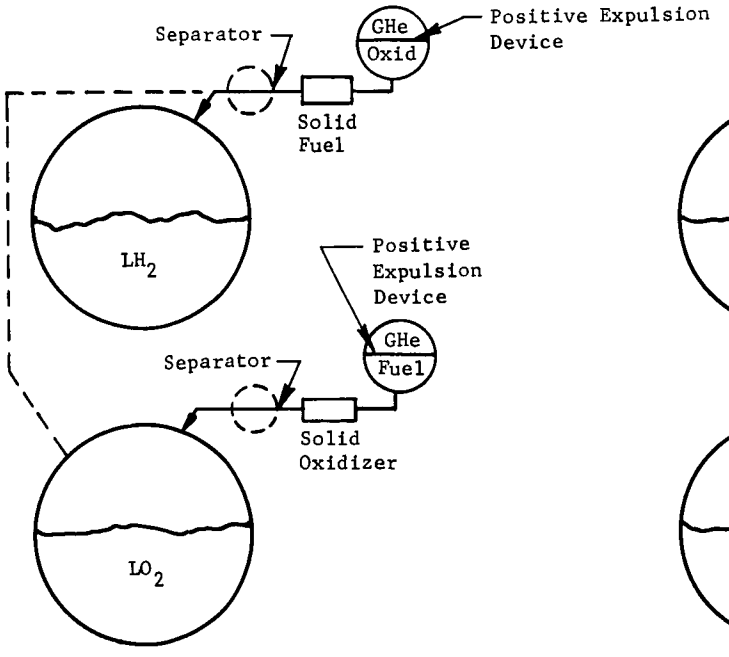

System 11

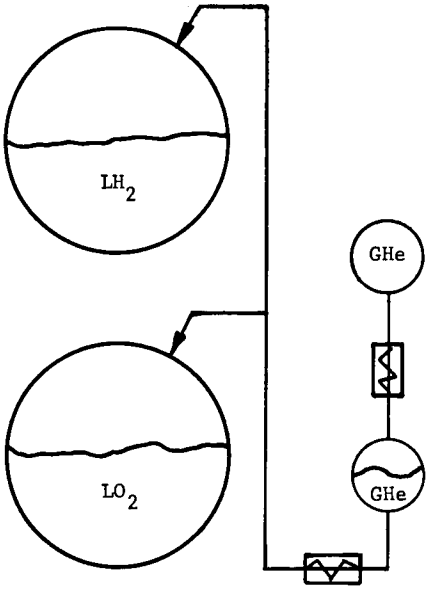

System 12

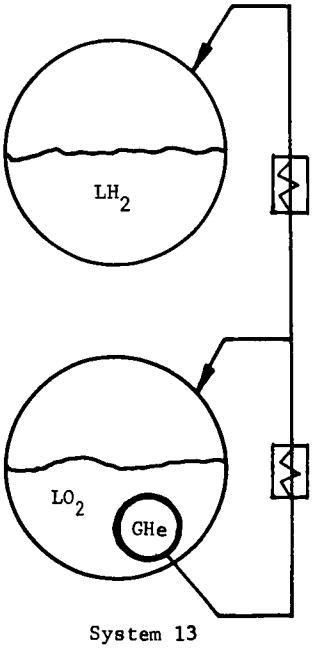

System 13

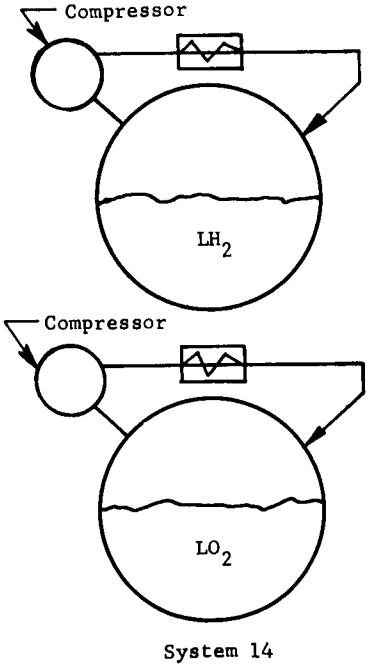

System 14

Fig. 6 (concl)

System 1 - Helium was initially stored as a liquid with subsequent vaporization and heating prior to use as a pressurant. The expansion process was to be isobaric.

System 2 - Autogenous pressurization was used employing pumped liquid propellants as pressurants.

System 3 - Autogenous pressurization was used, employing externally stored liquid propellants that were vaporized and heated prior to entering the propellant tanks. Expulsion of the pressurants was provided by stored helium gas and positive expulsion devices.

System 4 - Propellants were stored separately as liquids that were vaporized and heated to maintain an isobaric source of pressurant gases.

System 5 - An autogenous system converted liquid hydrogen fuel into a pressurant for both tanks using necessary pumps and heat sources.

System 6 - A main tank injection system employed the injection of a hypergolic liquid into the main propellant tank ullage to produce pressurizing gases. Alternatives were separate injection systems for each propellant tank or a single injection system on one tank with a line connecting the ullages of both tanks.

System 7 - This hybrid system employed both an autogenous system and a stored-gas system. The autogenous portion used a pump and heat exchanger to provide hydrogen pressurant in the fuel tank. The stored-gas system provides helium, by heating stored liquid hydrogen, as a pressurant for the oxidizer tank.

System 8 - This hybrid system was similar to System 7 except that the hydrogen source was a separate container mounted in the hydrogen tank and was pressurized by helium and a positive expulsion device.

System 9 - A stored-gas system supplied heated hydrogen to the fuel tank and heated helium to the oxidizer tank. Hydrogen was stored in a separate container in the liquid oxygen tank.

System 10 - This gas generator system used hydrogen and oxygen as reactants. The reactants were stored in separate containers. Hydrogen-rich exhaust was used to pressurize the hydrogen tank and oxygen-rich exhaust to pressurize the oxidizer tank. Separators were used to remove condensible gases.

System 11 - This system was similar to System 10 except that hybrid gas generators were used separately for each tank.

System 12 - A cascade system employed heated helium in both the primary and cascade-storage containers.

System 13 - Helium pressurant was stored at liquid oxygen temperature and heated prior to pressurizing the propellant tanks.

System 14 - Compressors recirculated ullage gases through the heat exchangers.

3. Primary Pump-Fed Systems

The primary pressurization systems for use with pump-fed propellant systems were defined as systems using state-of-the-art hardware and technology and were to be optimized primarily for reliability. No restriction was placed on the type of pressurant or the expansion process used. Passive-type heating of the pressurant was used in cases where the pressurant was stored at either liquid oxygen or liquid hydrogen temperature. Passive heating was defined as any heat exchange not involving a separate gas generator as a heat source.

Since the analysis of these systems followed the analysis for pressure-fed propellant systems, some of the undesirable systems considered during the previous study were not selected for study. For this reason, a smaller number of configurations was considered. The systems studied are shown in Fig. 7 and are described as follows:

System 1 - Helium was initially stored at liquid oxygen temperature in an insulated container using engine-bled hydrogen gas for heating. The hydrogen gas bleed entered the liquid hydrogen tank during burns. Helium was used in the liquid oxygen tank as the only pressurant and in the liquid hydrogen tank during prepressurization periods prior to each engine burn.

System 2 - Helium was stored initially at liquid hydrogen temperature for the liquid hydrogen tank and at liquid oxygen temperature for the liquid oxygen tank. Hydrogen gas from the engine bleed was used to heat the gas in both pressurant storage spheres before being used as a pressurant for the hydrogen tank during burn periods. Helium was used as a pressurant for the liquid hydrogen tank only during prepressurization periods prior to each engine burn.

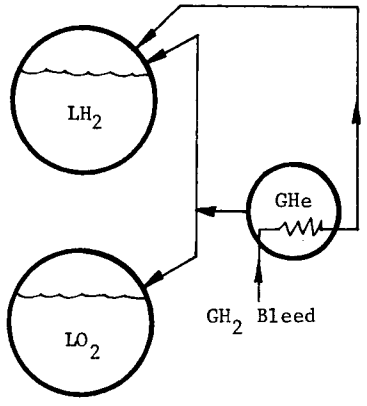

System 1

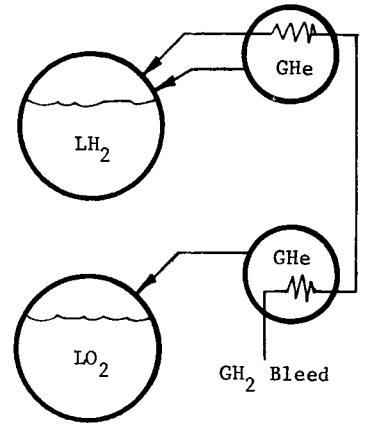

System 2

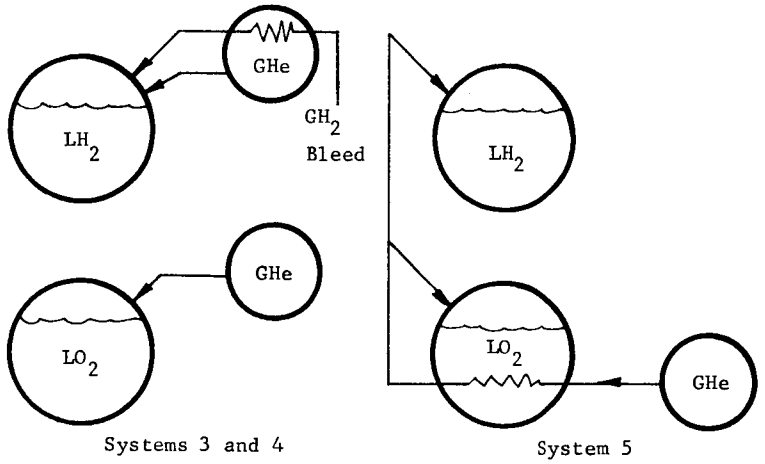

Systems 3 and 4

System 5

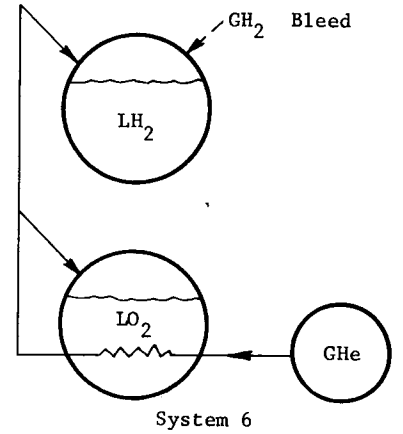

System 6

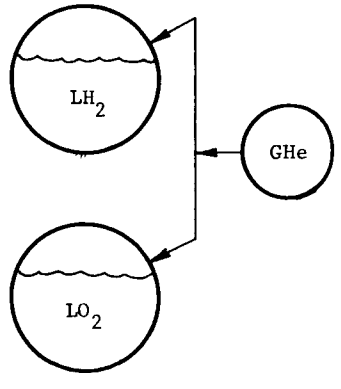

Systems 7, 9 and 11

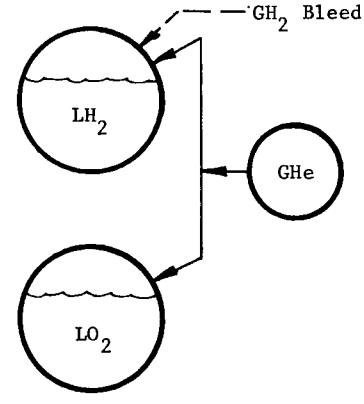

Systems 8, 10, and 12

Fig. 7 Primary Pressurization Systems for Pump-Fed Propellant Systems

System 3 - This was the same as System 2 except that only the helium storage container supplying the liquid hydrogen tank was heated by the engine bleed gas.

System 4 - This was the same as System 3 except that the initial helium temperature was at liquid oxygen temperature.

System 5 - Helium was stored initially at liquid hydrogen temperature, then heated in the liquid oxygen tank using a heat exchanger before entering the propellant tanks.

System 6 - This was the same as System 5 except that engine-bled hydrogen was added to the liquid hydrogen tank during burn periods.

System 7 - Helium was stored at ambient temperature and expanded adiabatically.

System 8 - This was the same as System 7 except that engine-bled hydrogen is added to the hydrogen tank.

System 9 - This was the same as System 7 except that the helium storage temperature was liquid oxygen temperature.

System 10 - This was the same as System 9 except that engine-bled hydrogen was added to the hydrogen tank.

System 11 - Helium was initially stored at liquid oxygen temperature and expanded polytropically.

System 12 - This was the same as System 11 except that engine-bled hydrogen was added to the hydrogen tank.

4. Advanced Pump-Fed Systems

The advanced pressurization systems for pump-fed propellant systems were defined as systems not constrained by state-of-the-art technology and were to be optimized for reliability and low weight. They were similar to the advanced systems for pressure-fed propellant systems although lower propellant tank pressures were required. Advanced systems, in general, used active heat sources to condition the pressurant in the storage container or after expansion, prior to injection into the propellant tanks. The advanced pump-fed systems that were studied are schematically shown in Fig. 8 and are described as follows:

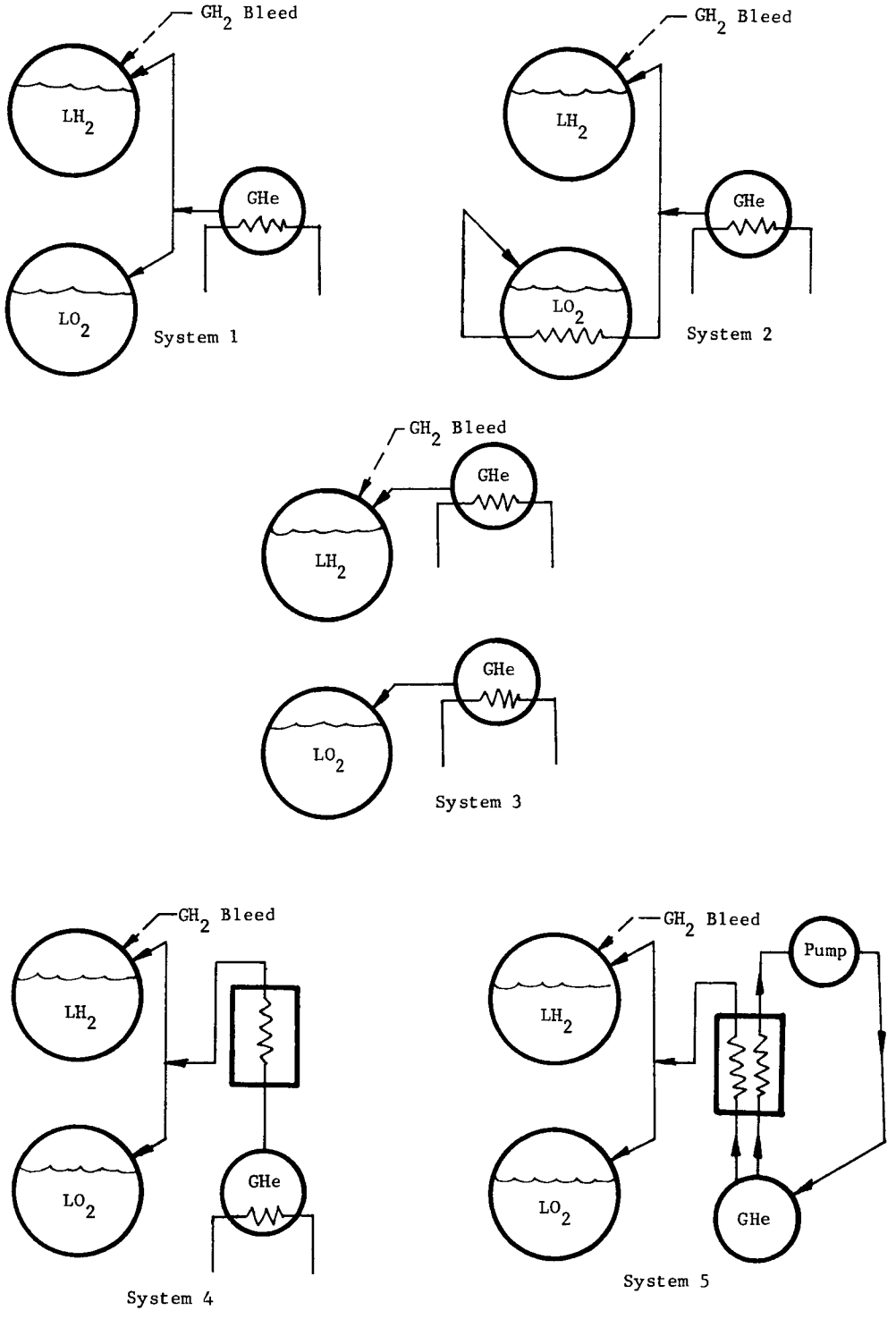

Fig. 8 Advanced Pressurization Systems for Pump-Fed Propellant Systems

System 1 - Helium at various initial storage temperatures was expanded isothermally by the addition of active heat to the storage sphere. Hydrogen-gas engine bleed may be added to the liquid hydrogen tank during burn periods.

System 2 - Helium stored at liquid hydrogen temperature was expanded isothermally by heat addition, using an active heat source, with the helium flow to the liquid oxygen tank subsequently being heated by the liquid oxygen before entering the ullage of the liquid oxygen tank. Hydrogen-gas engine bleed may be used in the liquid hydrogen tank during burn periods.

System 3 - Separate helium storage was used for each propellant tank with different initial storage temperatures. Isothermal expansion was used in each storage sphere. Gaseous hydrogen engine bleed may be added to the liquid hydrogen tank during burn periods.

System 4 - Helium was initially stored at liquid hydrogen temperature and expanded from a sphere, using varied heat addition to control the expansion process. It then received additional preheating before entering the propellant tanks. Gaseous hydrogen bleed may be used in the liquid hydrogen tank during burn periods.

System 5 - Helium was initially stored at liquid hydrogen temperature and expanded through an active heat exchanger before entering the propellant tanks. Some of the helium was recirculated by pumping the helium back into the storage sphere after being heated. Gaseous hydrogen bleed may also be used in the liquid hydrogen tank during burn periods.

C. SYSTEM ANALYSIS

1. Pressurant Selection

As a part of the process of selecting a group of pressurization systems to be studied, consideration of the pressurant to be used was an important factor. In addition to considering gases such as helium, hydrogen, nitrogen, oxygen, and carbon monoxide, the products of gas generator reactions and the injection of hypergolics into the propellant tanks were considered.

Gas generator exhaust products generally contain undesirable components that must be removed prior to tank injection. In the case of a hydrogen-oxygen gas generator, the undesirable product is water that must be removed by lowering the temperature of the exhaust gas to condense and freeze out the water. If a hydrocarbon were used as the gas generator fuel, excess carbon or carbon compounds would be formed. If other oxidizers were used with liquid hydrogen, the contaminants would be water, nitrogen, carbon dioxide, or one of the halogen compounds. In any case, the use of gas generator exhaust products is undesirable due to the contaminant removal requirement, with its associated equipment weight.

A study was made of main tank injection, wherein materials that are hypergolic with the propellants were injected directly into the propellant tanks. The resulting chemical reactions produced hot gases, made up of vaporized propellants and the products of the reaction. In the case of injection into liquid oxygen, the same problem occurred that caused rejection of gas generator exhaust pressurization, i.e., unwanted contaminants were produced and deposited in the tank. The liquid hydrogen, however, offered some hope since liquid fluorine, which is hypergolic with most materials, could be injected and would produce hydrogen gas and hydrogen fluoride. A test program was initiated to study the effects of fluorine injected into liquid hydrogen. A complete description of the test series is found in Chapter III.D.1 of this report. The results indicated that the reaction rate was unpredictable. In some cases, no apparent reaction took place until a significant quantity of fluorine was injected, at which time an explosion took place. For this reason no further consideration was given to MTI for application to this program.

With only stored gas systems remaining under consideration, a chart was set up to compare the critical properties of the gases considered. Comparison of the properties is shown in Table 8. A preliminary selection of the five gases listed was made, based primarily on their boiling points. A discussion of the pertinent factors of comparison for each gas is as follows:

Helium - This gas has the lowest boiling and freezing points of any of the gases considered. In addition, it is completely inert and would, therefore, have no chemical effect on the propellants or on the system components. It is less dense than any other gas considered except hydrogen and, although its heat of vaporization is extremely low (8.82 Btu/lb), its boiling point (8°R) is so much below the lowest temperatures expected in the propellant tanks (37°R) that this factor of comparison for helium was not considered. One factor that detracts from the qualities listed is the high cost and low availability.

Table 8 Pressurant Comparison

Comparison Category	Desired Properties	Helium	Hydrogen	Nitrogen	Oxygen	Carbon Monoxide
Density (lb/ft^3)*	Low	0.01114	0.0056	0.078	0.0892	0.074
Boiling Point (°R)	<37 for LH_2 <162.5 for LO_2	8	37	140	162.5	147
Freezing Point (°R)	<37 for LH_2 <162.5 for LO_2	--	26	114	99	123
Compatibility	Compatible with propellants and tank materials	--	Compat-ible	Compat-ible	Compat-ible	Compat-ible
Heat of Vaporiza-tion (Btu/lb)	High for usage Low for storage	8.82	192.7	85.7	91.6	91.8
Toxicity	Nontoxic	Nontoxic	Nontoxic	Nontoxic	Nontoxic	Toxic
*1 atm., 0°C.						

Hydrogen - The best property displayed by hydrogen is its low density, being only one-half that of helium. It is lower in density than the remaining gases considered by a factor of more than ten. It has low boiling and freezing points and a high heat of vaporization. Due to its high heat of vaporization, however, storage as a liquid causes a disadvantage since a large amount of heat must be added to vaporize the liquid prior to its use as a pressurant. It is not toxic. It is a reducing agent but is compatible with most materials. As a pressurant for liquid hydrogen, it is better than helium; however, as a pressurant for liquid oxygen, a major problem exists. In combination with oxygen over a mixture ratio range of 5 to 95%, it forms a combustible mixture. In addition, the energy level required to initiate combustion in the mixture is extremely low, being on the order of 2×10^{-3} joules, the equivalent of a weak static spark. For this reason, the pressurization of liquid oxygen with gaseous hydrogen and the reverse combination were not considered.

Nitrogen - This gas has a boiling point of 140°R that makes it unsuitable as a pressurant for liquid hydrogen due to the large amount of condensation that would take place in the propellant tank. As a pressurant for liquid oxygen, nitrogen at pressures greater than about 50 psia in the liquid oxygen tank will result in nitrogen condensation. It is approximately eight times as dense as helium and would have a significant effect on airborne pressurant system weight. It is inert and nontoxic although, as with hydrogen or helium, it will not support life. It is available in quantity at low cost. This is probably the only feature that makes it comparable with helium.

Oxygen - It cannot be used as a pressurant for liquid hydrogen for the reasons specified under the paragraph on hydrogen. It is an oxidant and the only gas considered that is both nontoxic and life supporting. It is over eight times as dense as helium and is readily available at low cost. It was considered as a self-pressurant for the liquid oxygen tank, using an autogenous configuration so that a separate pressurant storage system was not required.

Carbon Monoxide - This gas has a boiling point slightly higher than nitrogen but less than oxygen. It cannot be used in the liquid hydrogen tank for the same reason that nitrogen cannot be used, i.e., gross condensation and freezing at liquid hydrogen temperature. Its density is very close to that of nitrogen, and it is toxic. It will also condense in the liquid oxygen tank at pressures above 50 psia. It offers no advantage as a pressurant over other gases considered for either propellant.

Based on the foregoing comments, helium was the only pressurant considered for pressurization of both propellant tanks using a common pressurant system. Both hydrogen and oxygen were considered as pressurants for an autogenous system.

2. Storage System Weight Analysis

a. Method of Analysis

The pressurant storage system size is a function of the expansion process. A study to optimize the expansion process was carefully made, and the major results are covered in this section.

The pressure-fed storage system had a terminal pressure of 300 psia while the pump-fed storage systems usually had a terminal pressure of 150 psia. The study of the two systems overlapped, however, and some of the initial, pump-fed systems were studied with both terminal pressures. The major parameters of the expansion processes discussed in this report are tabulated below.

Expansion	Terminal Pressure (psia)	Thermodynamic System	Heat Transfer Considered from Environment
Ideal*	300	System included gas only	No
Ideal Isothermal	150	System included gas only	No
Polytropic	150	Gas and wall separate systems	Yes
Engine-Bleed Heating	150	Gas and wall lumped into one system	No
Cascade	300	Gas and wall separate systems	No
Recirculation	300	Gas and wall lumped into one system	No

*Isobaric, isothermal, isentropic, and combined expansions using two ideal expansions.

The pressurant storage container system is the heaviest of all the subsystems comprising a stored-gas pressurization system. The important parameters influencing the storage system weight are the initial and final gas conditions (mass, pressure, and temperature) and the container material density and working stress. The final gas temperatures and pressures, in turn, are functions of the expansion process that occurs in the container during outflow. To evaluate all the parameters and various expansion processes that might be followed, a method of analysis was established that consisted of calculating the ratio of the loaded storage container weight to the expelled gas weight. This ratio, referred to as the storage container weight ratio, is defined as follows:

$$\frac{W_L}{W_{GE}} = \frac{W_C + W_{GI}}{W_{GI} - W_{GF}}, \qquad [2]$$

where

W_L = loaded container weight,

W_{GE} = expelled gas weight,

W_C = container weight,

W_{GI} = initial loaded gas weight,

W_{GF} = final gas weight.

This equation was employed in the analysis of both ideal and actual expansion processes discussed in subsequent paragraphs. In the ideal expansion study, this equation was further expanded for a spherical container as follows:

$$\frac{W_L}{W_{GE}} = \frac{\dfrac{1.5\rho_m P_C R_G Z_{GI} T_{GI}}{P_{GI} S_W} + 1}{1 - \dfrac{Z_{GI}}{Z_{GF}} \dfrac{T_{GI}}{T_{GF}} \dfrac{P_{GF}}{P_{GI}}}, \qquad [3]$$

where

ρ_m = container material density $\left(lb_m / ft^3\right)$,

P_C = container design pressure $\left(lb_f / ft^2\right)$,

R_G = gas constant $\left(ft\text{-}lb_f / lb_m\text{-}°R\right)$,

Z_{GI} = initial gas compressibility factor,

T_{GI} = initial gas temperature (°R),

P_{GI} = initial gas pressure $\left(lb_f / ft^2\right)$,

S_W = container material working stress $\left(lb_f / ft^2\right)$,

Z_{GF} = final gas compressibility factor,

T_{GF} = final gas temperature (°R),

P_{GF} = final gas pressure $\left(lb_f / ft^2\right)$.

The derivation of this equation is given in Appendix A of this report. In applying this equation, note that the ratio of the design pressure, P_C, to the working stress S_W, determines the container wall thickness. Thus, the container is heaviest when this ratio is at maximum. For some expansion processes requiring heating of the gas in the container, the pressure-to-stress ratio may not be a maximum where the pressure is highest because of the temperature effect on material working stress. Therefore, it is necessary to determine where the maximum pressure-to-stress ratio occurs for each expansion to accurately apply the equation.

It is desirable that the storage container weight ratio be as low as possible. The limiting value that could theoretically be obtained is 1.0.

b. Ideal Expansion Study

The equation described in subsection a., preceding, was first employed in the analysis of various types of container gas expansion processes during the pressure-fed system study. The basic types of gas expansions considered were isobaric, isothermal, and isentropic processes. These processes were assumed to be ideal since no regard was given to the problem of supplying and controlling the heat flow required to maintain the process. Furthermore, heating effects of the environment or the heat capacity of the container wall were not considered.

Calculations for these expansions were made considering helium, hydrogen, and oxygen gases. Container materials used were titanium 6Aℓ-4V, aluminum 6061-T6, and stainless steel 304. A safety factor of 2.0 on the material ultimate strength was also used. A final storage container pressure of 300 psia was established to account for pressures losses in lines, valves, and heat exchangers between the storage container and the propellant tank inlets.

Typical results of this analysis for helium gas and a titanium container are plotted in Fig. 9 through 13. Figures 9, 10, and 11 present the data for isobaric expansions at initial temperatures of 10°, 37°, and 100°R, respectively. In these figures, the storage-container weight ratio is plotted as a function of final gas temperature for various pressures.

Figure 12 presents data for isothermal expansions. In this figure, the weight ratio is plotted as a function of the initial storage pressure. Finally, Figure 13 presents weight ratio data for isentropic expansions as a function of initial storage pressure and temperature. The isothermal and isentropic processes both exhibit a common characteristic in regard to initial storage temperature and optimum container weight ratio. This characteristic is illustrated in Fig. 12 and 13 by the dotted lines that connect the optimum weight ratio for each storage temperature. As the storage temperature is reduced, the optimum container weight ratio is also reduced until a minimum container weight ratio is reached. A further reduction in storage temperature results in an increase in container weight ratio. This transition results when the initial compressibility factor of the gas increases at a faster rate than does the working stress of the material.

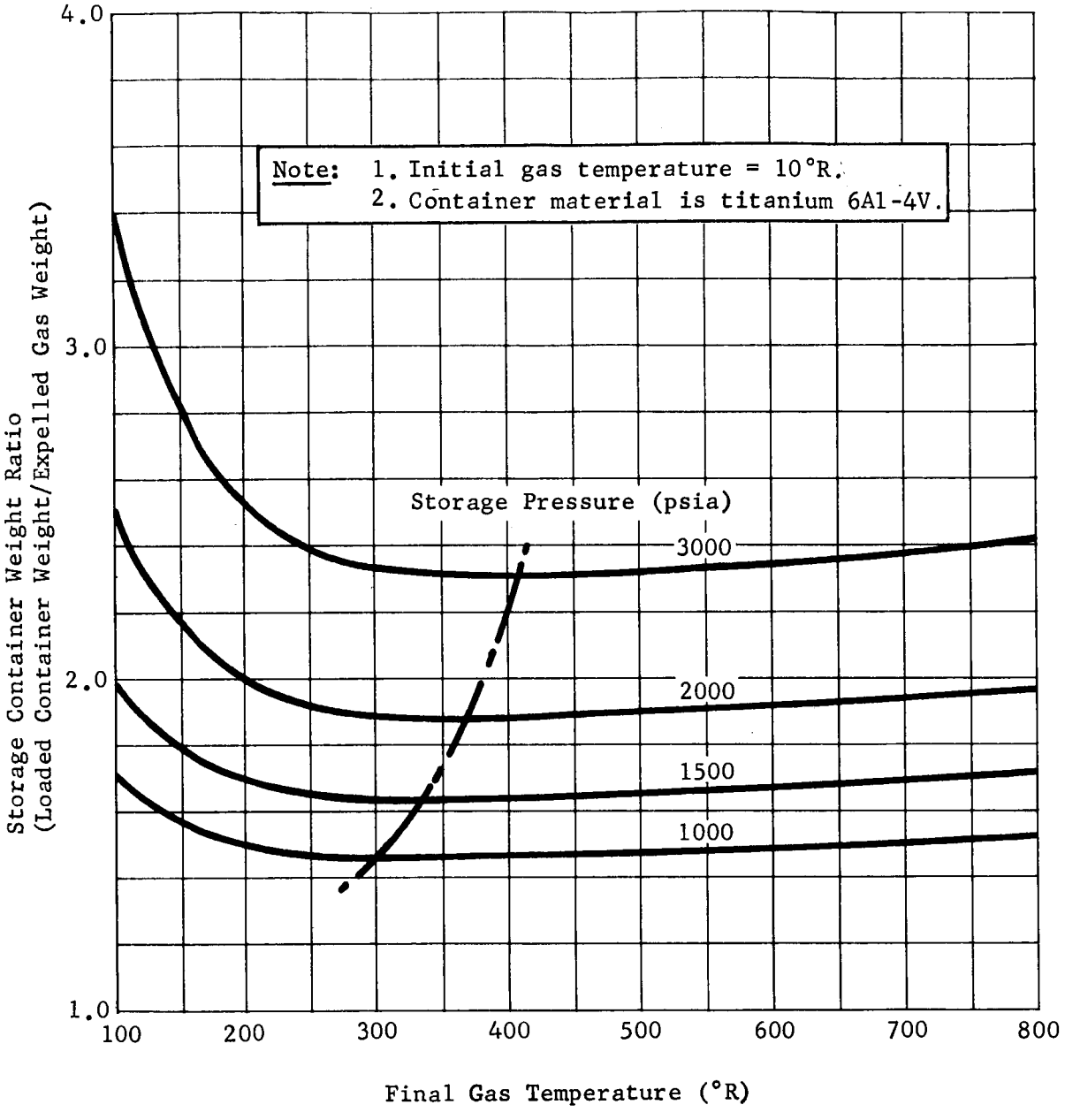

Fig. 9 Storage Container Weight Ratio for an Isobaric Expansion of Helium from a Spherical Container

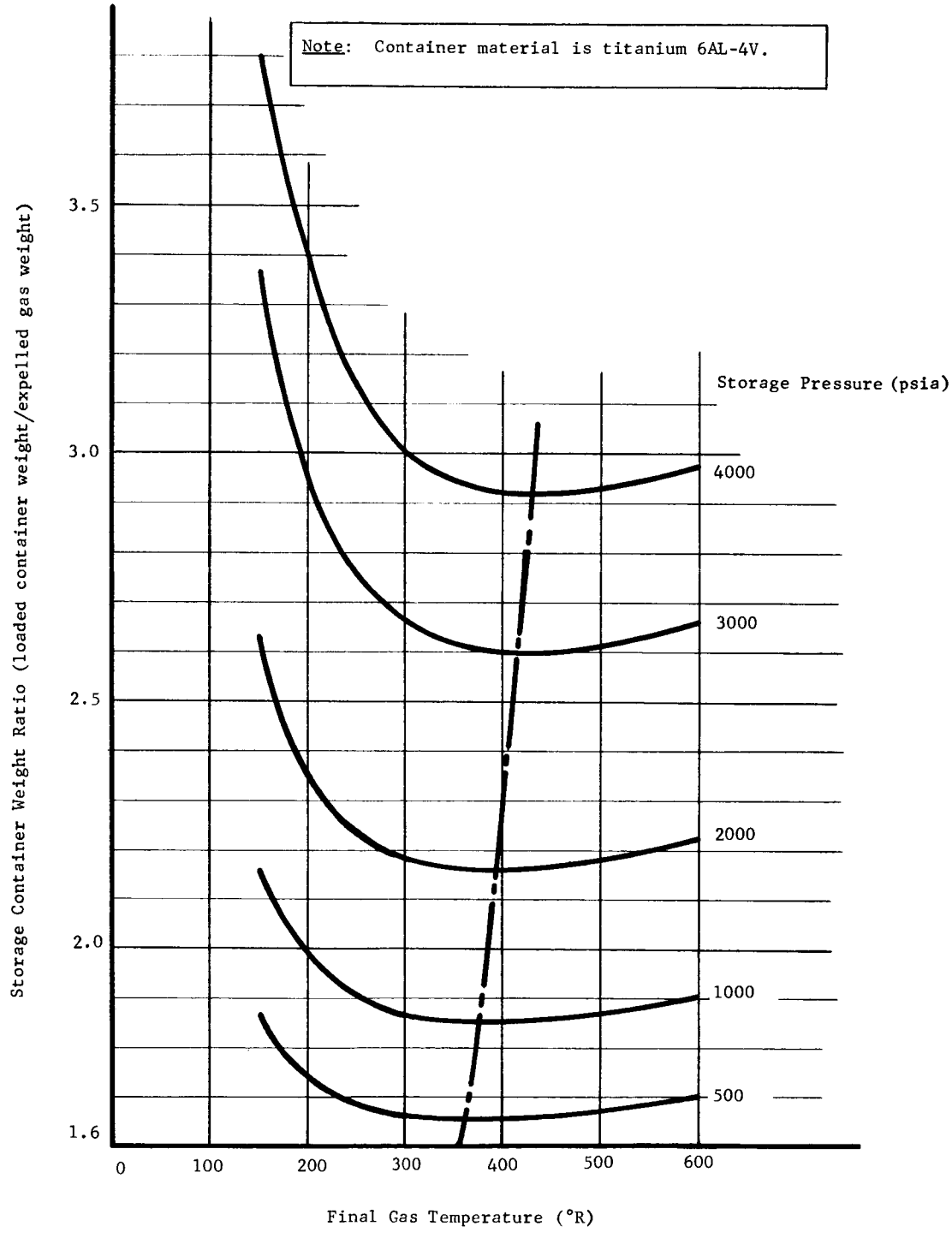

Fig. 10 Storage Container Weight Ratio for an Isobaric Expansion of Helium from a Spherical Container Initial Gas Temperature = 37°R.

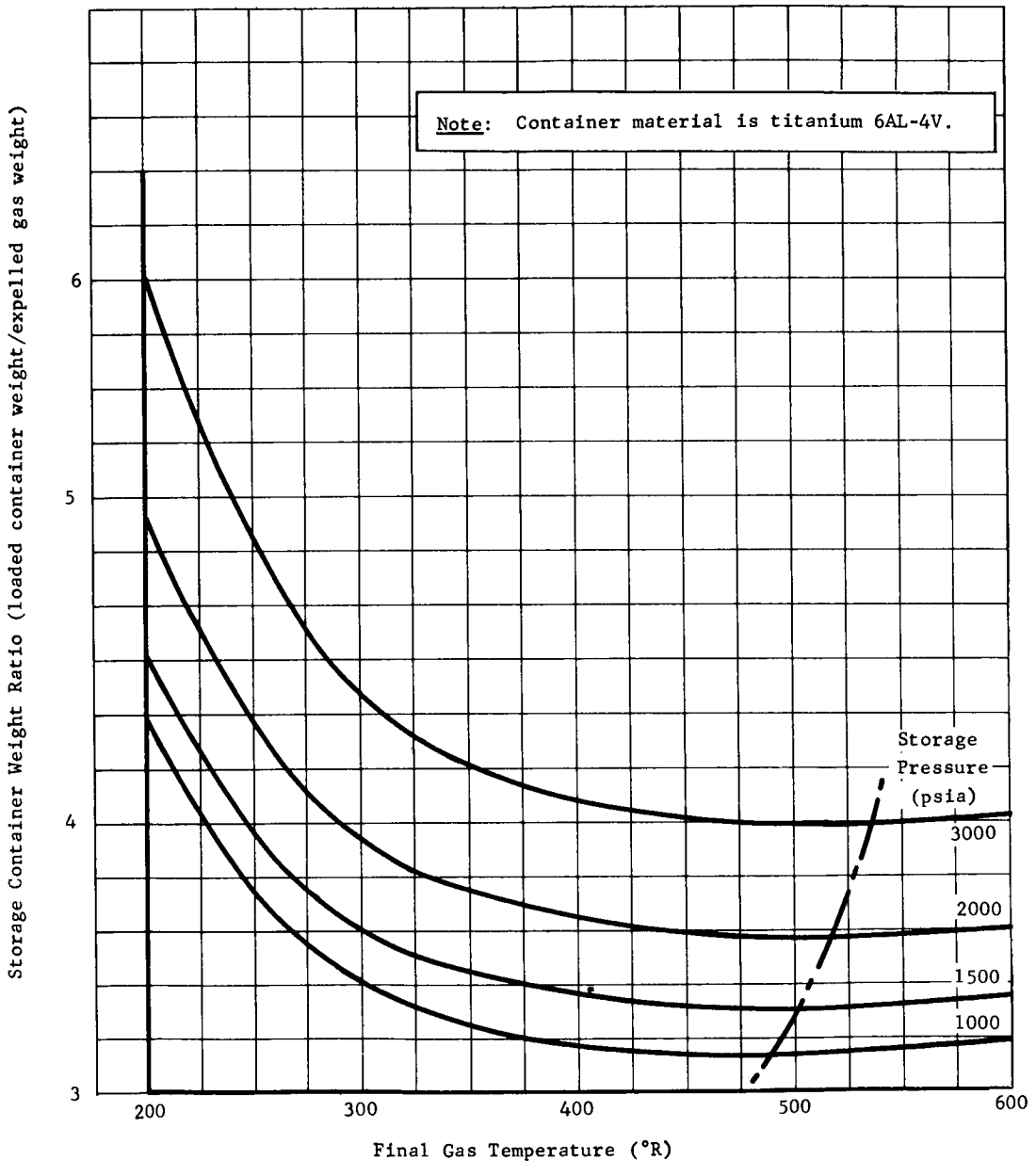

Fig. 11 Storage Container Weight Ratio for an Isobaric Expansion of Helium from a Spherical Container Initial Gas Temperature = 100°R.

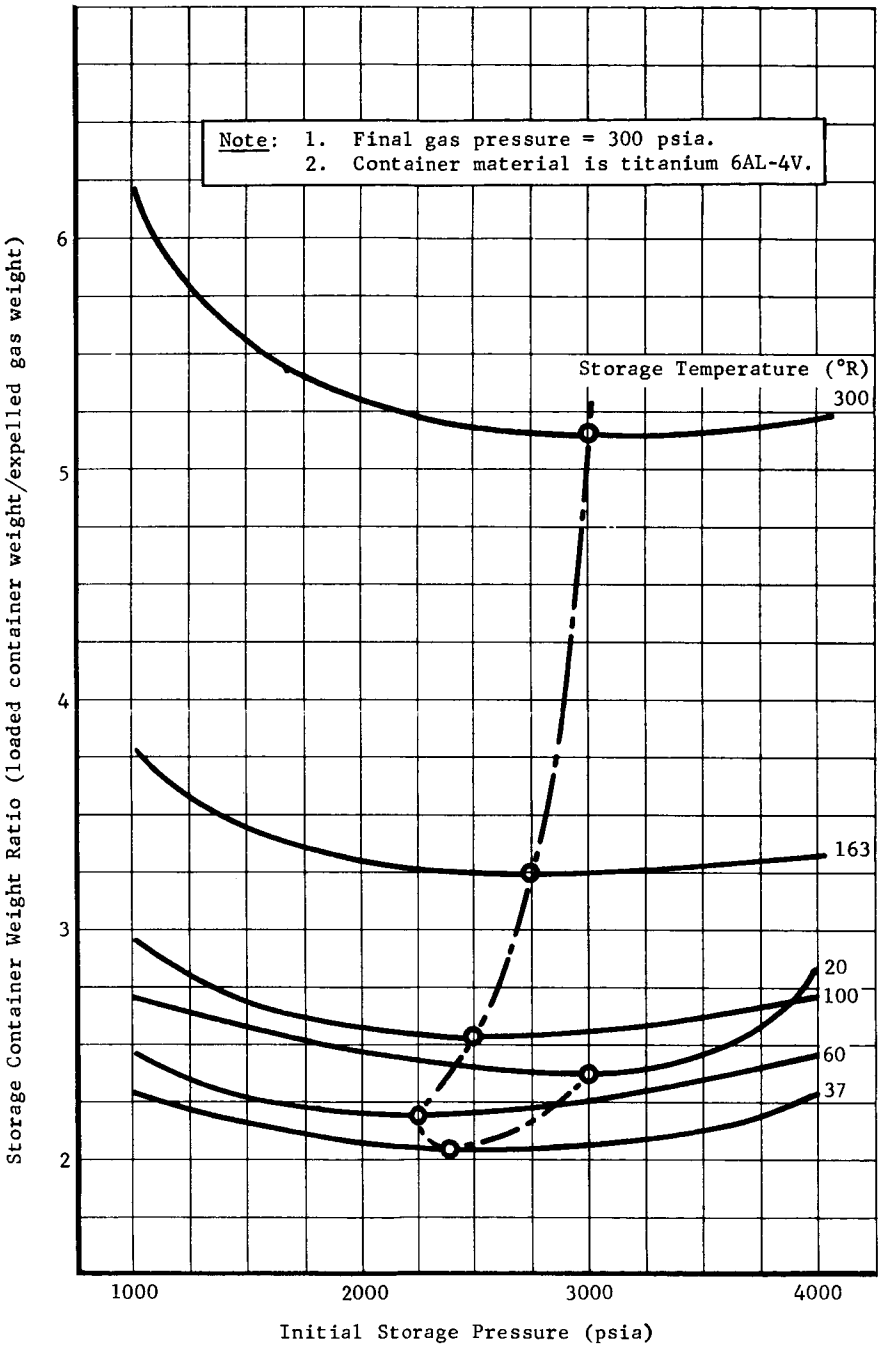

Fig. 12 Storage Container Weight Ratio for an Isothermal Expansion of Helium from a Spherical Container

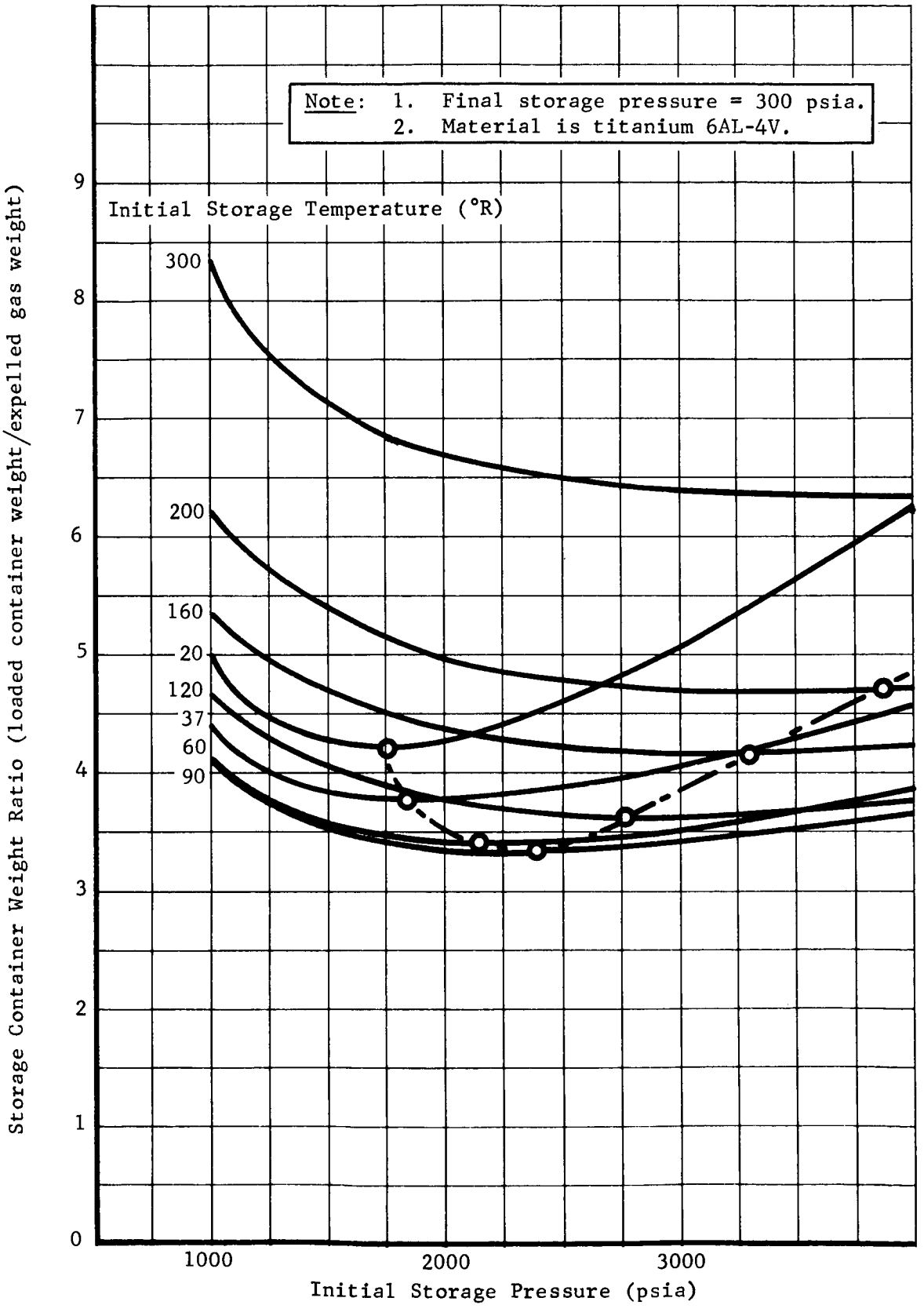

Fig. 13 Storage Container Weight Ratio for an Isentropic Expansion of Helium from a Spherical Container

Table 9 is a tabulation of the optimum container weight ratios for the three basic expansion processes and various combinations of gas, container material, initial storage temperature, and initial storage pressure. For the isothermal and isentropic expansions, the tabulated storage pressure is the optimum value corresponding to the optimum container weight ratio.

From Table 9, several conclusions can be made. First, for isobaric expansions, the container weight ratios decrease with decreasing storage pressure for all conditions of initial storage temperature, type of gas, and container material. Similarly, reducing initial storage temperature while maintaining the same storage pressure, type of gas, and container material also reduces the container weight ratio. Therefore, it may be concluded that, for isobaric processes, operation at low pressures and low initial temperatures is most desired.

As pointed out in a previous paragraph, the minimum container weight ratio for both isothermal and isentropic processes is a function of both initial pressure and temperature. This is illustrated by a dashed line in Fig. 12 and 13. For the isothermal expansion of helium from a titanium container to a final pressure of 300 psia, the optimum initial conditions are a 37°R temperature and a 2400-psia pressure. The isentropic process for the same operating conditions requires an initial temperature of 90°R and an initial pressure of 2400 psia. The corresponding container weight ratios are 2.05 and 3.3 for isothermal and isentropic processes, respectively. Thus, the isothermal process appears to be the more desirable.

The container material comparison indicates that the titanium alloy is the most desirable material from a weight standpoint because of its high strength-to-weight ratio. However, poor compatibility of this material with oxygen environments may seriously limit its application.

Table 9 Optimum Container Weight Ratios For Ideal Expansion Processes

Process	Gas	Container Material	Storage Temperature (°R)	Storage Pressure (psia)	Optimum Container Weight Ratio
Isobaric	Helium	Titanium 6Aℓ-4V	10	1000	1.45
				2000	1.86
				3000	2.3
			37	1000	1.86
				2000	2.16
				3000	2.6
			100	1000	3.15
				2000	3.58
				3000	4.0
		Stainless Steel 304	163	1000	9.45
				2000	10.8
				3000	11.95
	Hydrogen	Titanium 6Aℓ-4V	60	1000	1.7
				2000	2.4
				3000	3.05
			100	1000	2.45
				2000	3.0
				3000	3.65
		Stainless Steel 304	163	1000	14.7
				2000	16.45
				3000	19.6
	Oxygen	Stainless Steel 304	300	1000	2.18
				2000	2.2
				3000	2.48
Isothermal	Helium	Titanium 6Aℓ-4V	20	3000	2.38
			37	2400	2.05
			60	2250	2.2
			100	2500	2.52
			163	2750	3.25
			300	3000	5.15
		Aluminum 6061-T6	163	2000	6.45
		Stainless Steel 304	163	2100	5.0
	Hydrogen	Aluminum 6061-T6	163	2000	10.8
		Stainless Steel 304	163	2000	8.0
Isentropic	Helium	Titanium 6Aℓ-4V	20	1750	4.2
			37	1850	3.8
			60	2150	3.4
			90	2400	3.3
			120	2760	3.6
			160	3290	4.2
			200	3850	4.75
		Aluminum 6061-T6	163	3000	8.25
		Stainless Steel 304	163	3000	6.35
	Hydrogen	Titanium 6Aℓ-4V	163	1900	6.1
		Aluminum 6061-T6	163	1750	13.3
		Stainless Steel 304	163	1750	9.95

During the study of the basic expansions, it was found that, by combining the expansion processes, a significant reduction in weight ratio could be obtained. For example, the weight ratio for an expansion following an isobaric path initially and terminating in an isentropic (for an initial 1000-psia storage pressure and 37°R temperature) is 1.6. The weight ratio for the same initial conditions and a simple isobaric expansion is 1.85. The reduction is attributed to a lower container weight, resulting from a lower temperature at the end of the isobaric phase, and also lower gas residuals at the end of the isentropic phase, because of reduced final pressure. Four combined expansions that have been analyzed are:

Isobaric initial expansion with terminal isentropic expansion;

Isentropic initial expansion with terminal isobaric expansion;

Isobaric initial expansion with terminal isothermal expansion;

Isothermal expansion with terminal isobaric expansion.

All of these expansions considered helium gas at an initial temperature of 37°R. The container material employed in the analysis was titanium 6Aℓ-4V, and the final storage pressure was assumed to be 300 psia. The results of the analysis are plotted in Fig. 14 through 17. In these figures, the loaded container weight ratio is plotted as a function of the ratio of the expelled gas to initial gas weight. The expelled-gas to initial-gas ratio is the denominator of Equation [3] and is a most useful optimization parameter since it is a measure of weight utilization efficiency of the expansion process. Furthermore, the parameters used in analyzing the basic expansions (i.e., final temperature for isobaric processes and initial storage pressures for isothermal and isentropic processes) are not practical for use with combined expansions because neither pressure nor temperature were always constant during the expansion, nor were they related by any simple mathematical expression such as an isentropic relation. Therefore, it was more convenient to use the expelled- to initial-gas ratio as the optimization parameter for the combined expansions.

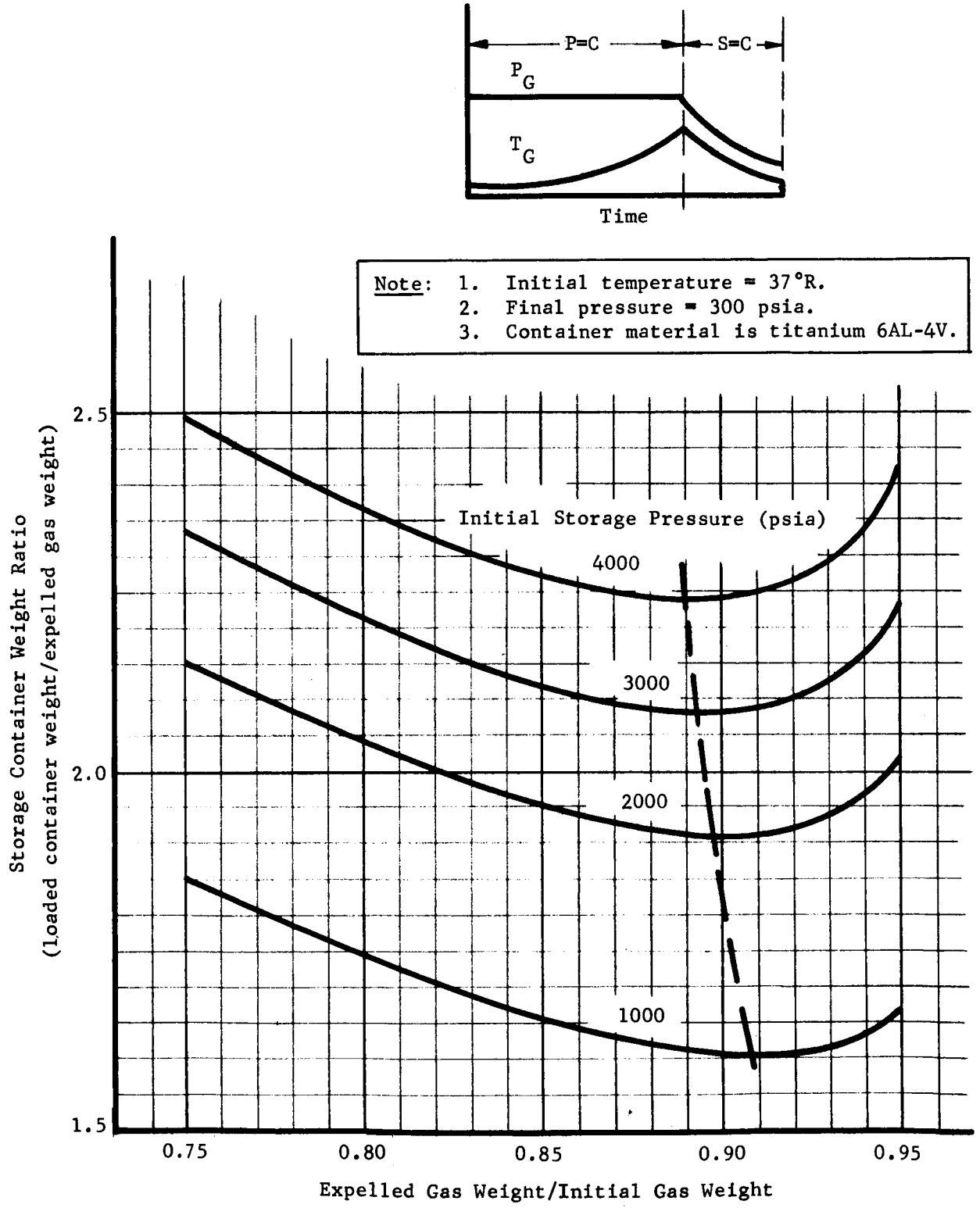

Fig. 14 Storage Container Weight Ratio for a Combined Isobaric/Isentropic Expansion of Helium from a Spherical Container

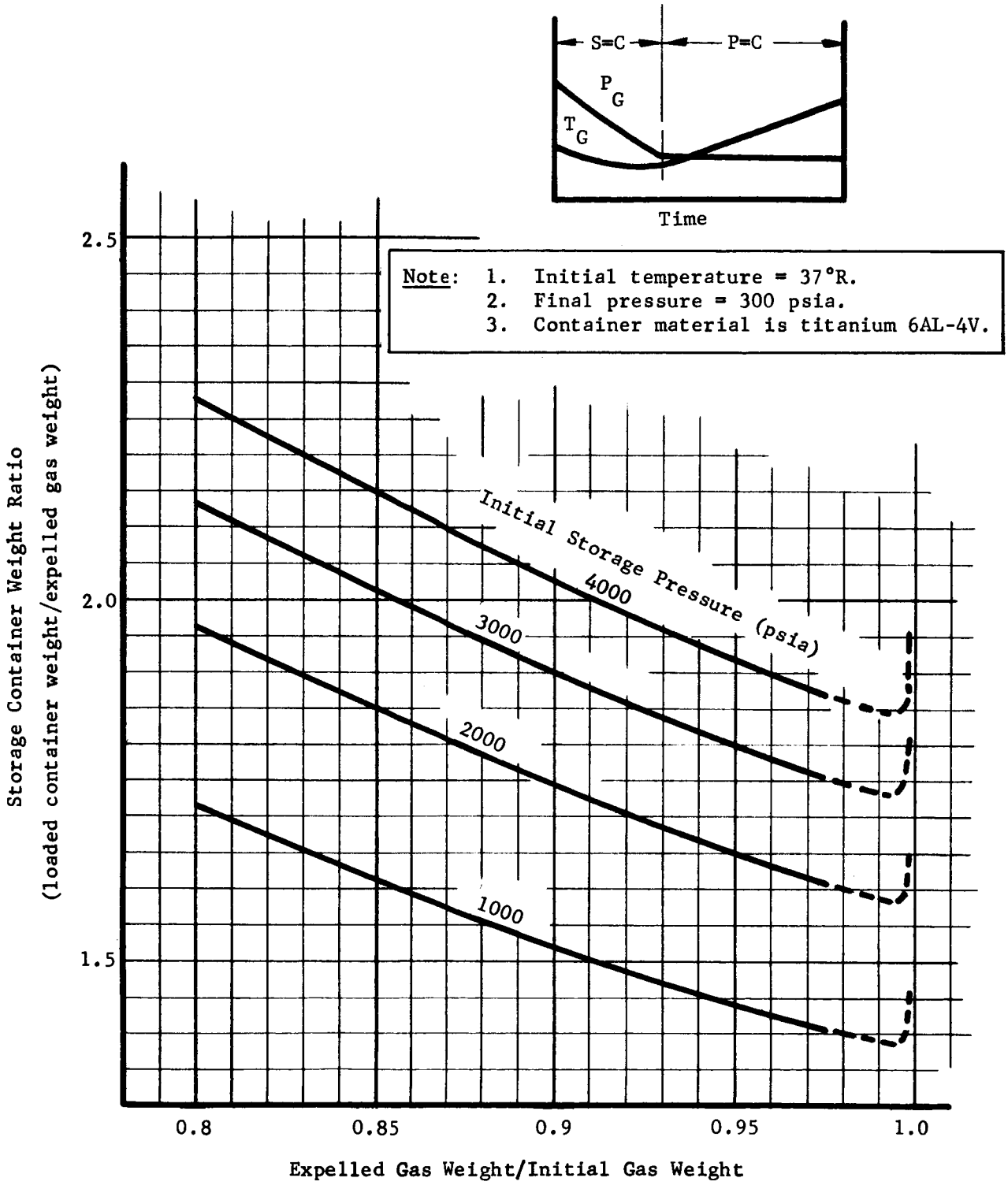

Fig. 15 Storage Container Weight Ratio for a Combined Isentropic/ Isobaric Expansion of Helium from a Spherical Container

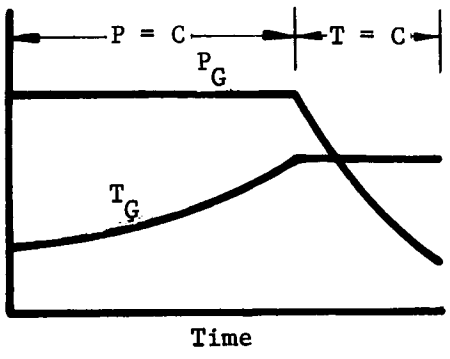

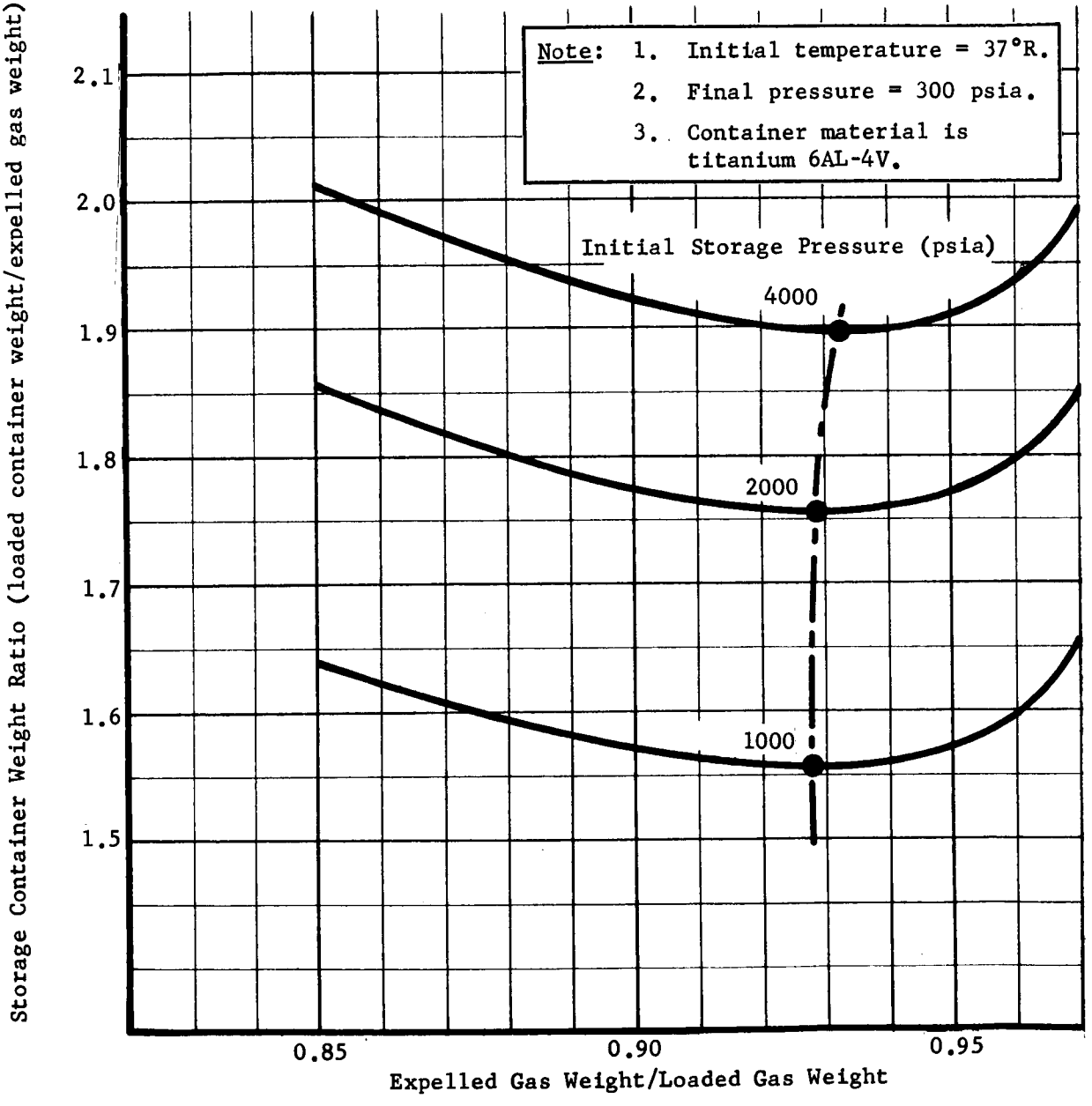

Fig. 16 Storage Container Weight Ratio for a Combined Isobaric/Isothermal Expansion of Helium from a Spherical Container

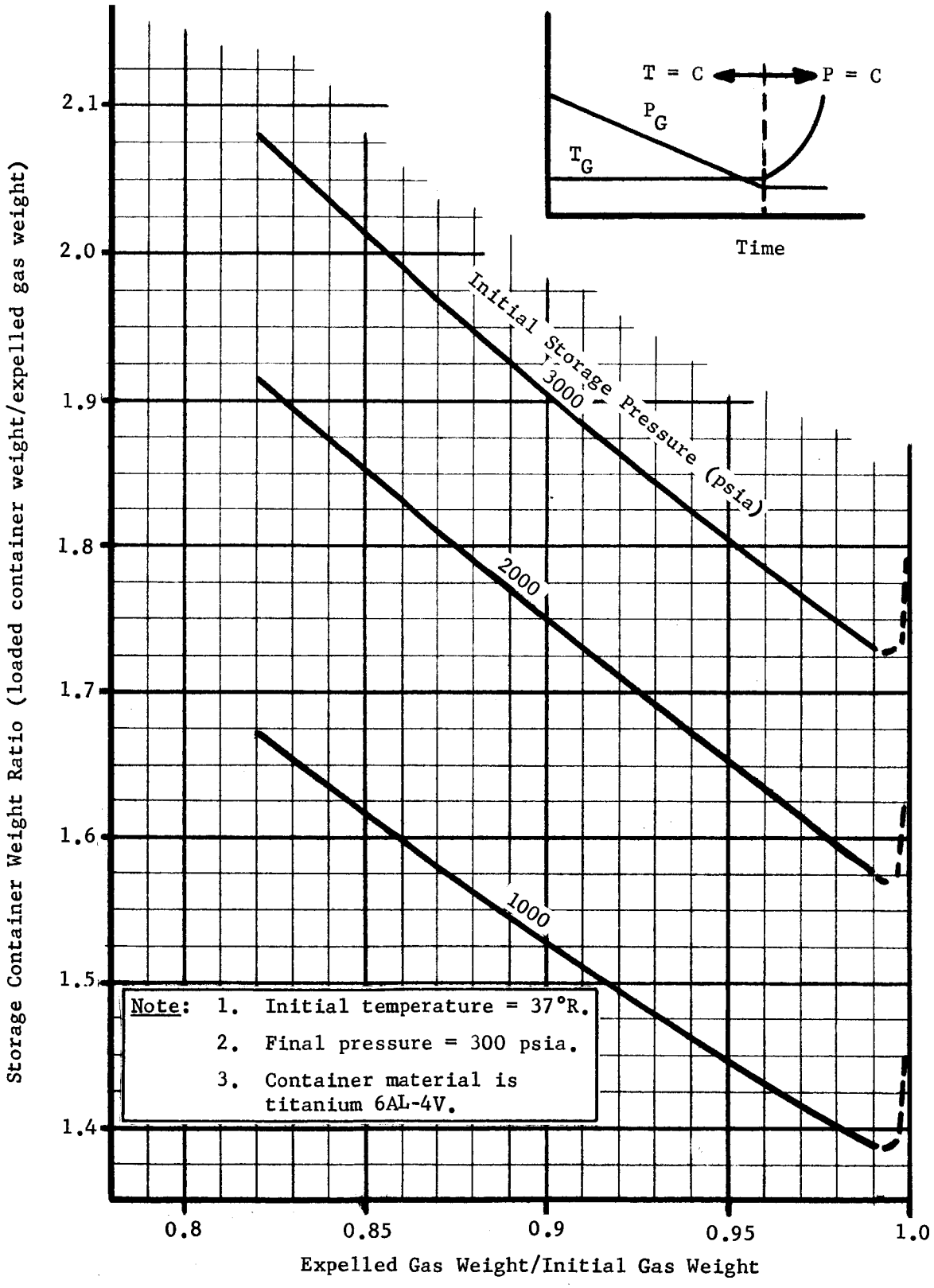

Fig. 17 Storage Container Weight Ratio for a Combined Isothermal/ Isobaric Expansion of Helium from a Spherical Container

When an isobaric expansion is the initial process in the combination, there is a definite minimum value of the weight ratio as illustrated in Fig. 14 and 16. However, when the isobaric process is the terminal process, the minimum, storage-container weight ratio occurs at an expelled- to initial-gas weight ratio very near 1.0 as illustrated by the dotted curves in Fig. 15 and 17. To reach this minimum, storage container weight ratio, high residual gas temperatures and heat transfer rates are required. To illustrate the maximum temperatures required, Table 10 has been prepared from Fig. 15 and 16 to compare isothermal-isobaric and isentropic-isobaric processes. The storage container weight ratios and the maximum temperatures required are presented for the processes as a function of expelled- to initial-gas ratio. It is evident from Table 10 that increasing the expelled- to initial-gas ratio from 0.95 to 0.99 results in a 4.0% reduction in container weight ratio. However, this reduction is accompanied by a fivefold increase in maximum temperature. The value of 0.99 for expelled- to initial-gas ratio still does not represent an optimum storage container weight ratio. The optimum value will be somewhere between 0.99 and 1.0. It is not considered practical to reach the optimum point because the high temperature and heat transfer rate place unreasonable demands on heat exchanger and gas generator design. Therefore, an expelled- to initial-gas weight ratio of 0.95 was selected as an attainable value for use in subsequent comparisons.

Table 11 was prepared to compare data for the four different combined processes. The container weight ratios presented are the optimum values for the isobaric-isothermal and isobaric-isentropic processes while the values for the isothermal-isobaric and isentropic-isobaric processes are based on an expelled- to initial-gas weight ratio of 0.95. The maximum gas temperature for each process is also included in the table. All the expansion processes were analyzed assuming the total expulsion duration was 540 sec. At some point during this time period, the initial expansion process terminates, and the final expansion process begins. The time at which this change of process occurs, as measured from the start of pressurant outflow, is called the time of transition and is included in the table. The criterion that determines the time of transition is that the terminal pressure at the end of the final expansion process must be 300 psia.

Table 10 Effect of Expelled- to Initial-Gas Weight Ratio on Container Weight Ratio and Maximum Gas Temperature for Isothermal-Isobaric and Isentropic-Isobaric Processes

Process	Initial Storage Pressure (psia)	Expelled- to Initial-Gas Weight Ratio	Container Loaded Weight to Expelled-Gas Weight Ratio	Maximum Gas Temperature (°R)
Isothermal-Isobaric	1000	0.95	1.45	295
	2000	0.95	1.65	228
	3000	0.95	1.81	188
	1000	0.99	1.39	1462
	2000	0.99	1.58	1128
	3000	0.99	1.73	936
Isentropic-Isobaric	1000	0.95	1.44	288
	2000	0.95	1.65	226
	3000	0.95	1.8	188
	1000	0.99	1.38	1466
	2000	0.99	1.58	1128
	3000	0.99	1.73	936

Table 11 Comparison of Combined Expansion Processes

Process	Initial Pressure (psia)	Expelled-to Initial-Gas Ratio	Optimum Container Weight Ratio	Maximum Gas Temperature (°R)	Time of Transition (sec)
Isobaric-Isentropic	1000	0.908	1.6	248	485
	2000	0.896	1.9	230	435
	3000	0.893	2.08	206	390
Isobaric-Isothermal	1000	0.927	1.56	195	450
	2000	0.928	1.76	158	355
	3000	0.933	1.89	144	300
Isentropic-Isobaric	1000	0.95	1.44	295	340
	2000	0.95	1.65	228	390
	3000	0.95	1.8	188	420
Isothermal-Isobaric	1000	0.95	1.45	288	185
	2000	0.95	1.65	226	155
	3000	0.95	1.81	188	178

Comparison of data in Tables 9 and 11 indicates the advantage of combining the expansion processes. Isobaric-isentropic or isobaric-isothermal expansions provide reductions in container weight ratio of 12 to 28% depending on the initial pressures. The isobaric-isothermal process container weight ratios are somewhat lower than the isobaric-isentropic combination because the terminal temperature is higher resulting in a lower residual gas mass.

Reversing the process combination (i.e., employing the isobaric expansion as a terminal process) results in an even greater reduction in container weight ratio. Comparing the container weight ratios in Table 11 for isobaric-isentropic and isentropic-isobaric expansions for a 1000-psia initial storage pressure indicates a reduction from 1.6 to 1.44. This reduction also occurs at the higher pressures.

In general, the following conclusions were reached during the study of ideal expansion processes. On the basis of lowest container weight ratios, and, neglecting the complexity of gas generators and heat exchangers, the isobaric expansion is the most desirable of the basic or simple expansion processes. The isothermal process provides the next-lowest, container weight ratios and the isentropic process provides the highest values. By combining the above expansion processes, a significant reduction in container weight ratio, below that of the simple isobaric process, can be obtained. Furthermore, in the combination of processes, it is more beneficial to use an isobaric expansion as a terminal process.

While the results from this analysis indicate an advantage in the use of combined expansion processes, they were not ultimately considered in the final analysis and selection of a pressurization system. They were eliminated because they require active heat sources that were also eliminated from the study.

c. Actual Expansion Study

In the ideal expansion study discussed previously, it was assumed, as a first approximation, that isentropic and isothermal expansion processes could be obtained by either insulating the container or by immersing the container in the propellant tanks. Later during the program, a more

realistic evaluation of each of these processes was made by means of analytical models that were generally based on Equation [4] below. The derivation of this equation is found in Appendix B and was based on an energy balance of an open system. The system considered is the gas volume and did not include the container.

$$\dot{T} = \frac{\dot{Q} - \left[\left(\frac{\partial P}{\partial T}\right)_V \left(\frac{VT}{m}\right)\left(\frac{\dot{m}}{778}\right)\right]}{mC_v}, \qquad [4]$$

where

T = time rate of change of gas temperature (°R/sec),

$\dot{Q}$ = heat-transfer rate into the system (Btu/sec),

P = instantaneous gas pressure $\left(lb_f/ft^2\right)$,

T = instantaneous gas temperature (°R),

V = container volume $\left(ft^3\right)$,

m = instantaneous system mass $\left(lb_m\right)$,

$\dot{m}$ = gas-outflow rate $\left(lb_m/sec\right)$,

C_v = gas specific heat at constant volume $\left(Btu/lb_m/°R\right)$.

The above temperature-change equation was applied to the study of various types of expansion processes that are discussed in subsequent paragraphs.

1) Adiabatic Expansion

Adiabatic expansion was defined in this study as one in which no heat transferred into the system from the environment. Such a condition would be approximated by a storage container insulated by the vacuum of space. To evaluate the container weight ratios for this process, an analytical model was established and programed on the IBM 1620 digital computer. The system considered included both the gas and the container. Modification of the temperature change Equation [4] was necessary for the new system. The first modification was to account for the heat capacity of the wall by replacing mC_v by $\left(mC_v + m_c C_c\right)$. This assumed that the wall temperature and gas temperature were always the same.

The second modification of Equation [4] was to set $\dot{Q}$ equal to zero, since this represents the heat transfer into the system (i.e., heat transfer to the container from the environment, which would have to be zero for an adiabatic system). The resulting equation is as follows:

$$\dot{T} = - \frac{\left(\frac{\partial P}{\partial T}\right)_V \left[\left(\frac{VT}{m_g}\right)\left(\frac{\dot{m}_g}{778}\right)\right]}{\left(m_g C_{vg} + m_c C_c\right)}, \qquad [5]$$

where

m_g = instantaneous gas mass $\left(lb_m\right)$,

$\dot{m}_g$ = gas outflow rate $\left(lb_m/sec\right)$,

m_c = container mass $\left(lb_m\right)$,

C_{vg} = gas specific heat at constant volume $\left(Btu/lb_m/°R\right)$,

C_c = container specific heat $\left(Btu/lb_m/°R\right)$,

and all other terms are as previously defined.

The analysis was carried out for a pump-fed system with the mission profile listed in the program plan. The initial storage pressure and temperature, pressurization gas flow requirements, pressurization and burn-period time durations, and the container volume and weight were supplied as input. Several runs were made for each initial, pressure-temperature combination, varying the container volume and weight until the final container pressure was 150 $\pm$ 5 psia. The container weight, initial gas weight, and final gas weight were then used in Equation [2] to compute the loaded container weight ratio.

Figure 18 presents the storage container weight ratio for an adiabatic expansion of helium as a function of the initial helium storage pressure. The initial helium storage temperature is 37°R. Also included in Fig. 18 for comparison are data for an isentropic expansion process occurring between the same initial and final pressures. It can be seen that, if isentropic conditions are assumed, the storage container system weights are higher than those for the more-realistic, adiabatic process. This difference is attributed to lower terminal temperatures and, therefore, higher gas residual masses in the isentropic expansion. The higher temperatures in the adiabatic expansion case are due in part to the fact that the heat capacity of the container wall was included in computing temperature change rates. In the isentropic case, the gas temperature was a function of gas pressure only.

2) Polytropic Expansion

When a pressurant storage container was mounted in a propellant tank or jacketed in some manner with propellant, it was assumed that the expansion process would be isothermal in nature. Later in the study, it was decided to further investigate the heat transfer occurring in order to determine whether isothermal conditions could actually be attained during the expansion. An analytical model was developed which considered both outflow and coast phases of a specified, six-burn mission. The burn phase of the model considered heat transfer from the propellant into the gas by means of free convection during outflow. The coast phase was concerned with heating of the container gas by conduction when no outflow was occurring. An IBM 1620 computer program was developed to carry out the analysis. A description of the analytical methods employed in the program are described in the following paragraphs.

a) Outflow

The outflow portion of the program was based upon the energy balance Equation [4] discussed previously, the equation of state for helium (Ref 3), and heat-transfer equations for free convection.

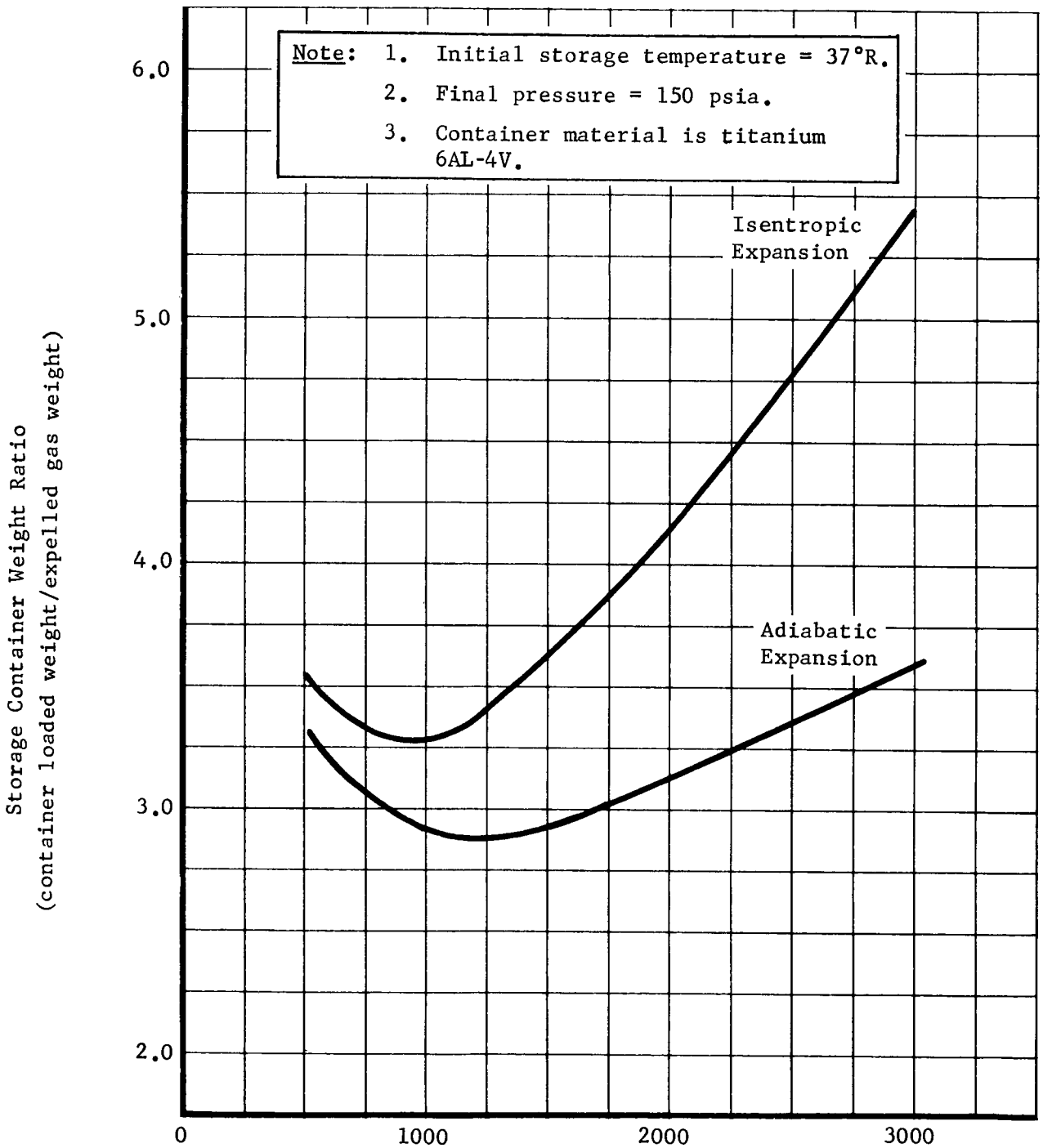

Fig. 18 Storage Container Weight Ratio Comparison for Isentropic and Adiabatic Expansions of Helium from a Spherical Container

The heat-transfer equation employed for free convection on both the helium side and the propellant side of the container is stated as follows (Ref 4):

$$h = 0.13K_f \left[\frac{\rho_f^2 \beta_f C_p g \Delta T}{\mu_f K_f}\right]^{1/3}, \qquad [6]$$

where

h = heat-transfer coefficient $\left(\text{Btu/sec/ft}^2/^\circ\text{R}\right)$,

K_f = film thermal conductivity (Btu/sec/ft/°R),

ρ_f = film density $\left(\text{lb}_m/\text{ft}^3\right)$,

C_p = specific heat at constant pressure (Btu/lb_m/°R),

g = acceleration $\left(\text{ft/sec}^2\right)$,

ΔT = temperature difference across the film (°R),

β_f = coefficient of thermal expansion $\left(^\circ\text{R}^{-1}\right)$,

μ_f = film viscosity $\left(\text{lb}_m/\text{ft/sec}\right)$.

The heat transfer rate, $\dot{Q}$, in the energy balance equation was based on the helium film coefficient and the helium-wall temperature difference. The wall temperature was not assumed constant but allowed to vary between the helium and the propellant temperatures, since the storage container was mounted in the propellant tank. The following equation was used to compute the wall temperature:

$$T_w = \frac{\left(\frac{C_l}{C_g}\right)^{0.75} T_l + T_g}{1 + \left(\frac{C_l}{C_g}\right)^{0.75}}, \qquad [7]$$

where

T_w = wall temperature (°R),

T_l = propellant temperature (°R),

T_g = gas temperature (°R),

C_l and C_g = parameters derived from the film coefficients for the propellant and the gas, respectively, as explained below.

The wall temperature equation was derived by assuming that the heat transfer from the liquid to the wall is equal to that transferred from the wall to the gas. That is:

$$\dot{Q}_g = \dot{Q}_l, \qquad [8]$$

where

$\dot{Q}_g$ = heat transferred from the wall to the gas (Btu/sec),

$\dot{Q}_l$ = heat transferred from the liquid to the wall (Btu/sec).

For free convection:

$$h_g A_g (T_w - T_g) = h_l A_l (T_l - T_w), \qquad [9]$$

where

h_g and h_l = free convection film coefficients $(\text{Btu/sec/ft}^2/°\text{R})$,

A_g and A_l = wall surface area (ft^2),

T_w, T_g and T_l = wall, gas, and liquid temperatures, respectively (°R).

The film coefficient equation for both liquid and gas side can be written as:

$$h = C(\Delta T)^{1/3}, \qquad [10]$$

where

$$C = 0.13K_f \left[\frac{\rho_f^2 C_p \beta_f g}{\mu_f K_f}\right]^{1/3},$$

Substituting into [9] and cancelling area terms (since the container inside and outside areas are approximately the same):

$$\left.\begin{aligned} &C_g(T_w - T_g)^{1/3}(T_w - T_g) = C_l(T_l - T_w)^{1/3}(T_l - T_w), \\ &\text{or} \\ &C_g(T_w - T_g)^{4/3} = C_l(T_l - T_w)^{4/3}, \end{aligned}\right\} [11]$$

where C_g and C_l are defined by [10] for gas and liquid, respectively. Solving [11] yields [7] for T_w:

$$T_w = \frac{\left(\frac{C_l}{C_g}\right)^{0.75} T_l + T_g}{1 + \left(\frac{C_l}{C_g}\right)^{0.75}}. \qquad [7]$$

The derivation of [7] neglects the temperature gradient across the wall since the thermal conductivity of the wall is high compared to the gas and liquid heat transfer coefficients.

b) Coast

The calculation of the helium temperature at the end of coast was based upon theory for transient conduction in a solid sphere, initially at a uniform temperature and whose surface is suddenly changed and maintained at a different temperature. From this theory, data for the central temperature history of a sphere were obtained from Fig. 10-8 of Ref 5. This figure presents a temperature ratio

$$\frac{T_o - T_s}{T_i - T_s},$$

as a function of

$$\frac{\alpha\theta}{R^2},$$

where

T_o = central temperature (°R),

T_i = the initial sphere temperature (°R),

T_s = surface temperature (°R),

α = thermal diffusivity of the sphere $\left(ft^2/sec\right)$,

θ = time after suddenly changing the surface temperature (sec),

R = radius of the sphere (ft).

It is not known whether this theory can be strictly applied to gas in the same manner as solids. However, there are now no known, proven theories applicable for heat transfer to and within a gas in a zero-gravity environment.

The application of this theory in the computer program will now be described. The gas temperature at the end of the burn cycle of the program is assumed to be uniform throughout the sphere and is taken as T_i in the temperature ratio described above. The surface temperature, T_s, is assumed to be the liquid hydrogen temperature. This assumption neglects the heat capacity of the container wall that is reasonable in light of the low wall specific heat and high thermal conductivity. The time, θ, is an input constant equal to the assumed duration of the coast period. The computer then assumes a central temperature. To determine mean properties to be used in calculation of thermal diffusivity, α, the mean bulk gas temperature is assumed to be the arithmetic mean of the central temperature and the wall temperature. The value $\alpha\theta/R^2$ is then computed to obtain a temperature ratio. From the temperature ratio, a central temperature is computed and compared with the assumed value. The calculations are repeated until the absolute difference of the assumed and calculated central temperatures is within 0.01°R. The mean gas temperature is supplied as the initial temperature for the next burn cycle.

c) Results

The computer program was employed to analyze helium storage containers mounted in both the liquid oxygen and liquid hydrogen tanks. A six-burn, five-coast mission profile was employed. The results of the analysis are presented in Fig. 19. The container material employed in the liquid hydrogen tank installation was Titanium 6Aℓ-4V. However, for the liquid oxygen tank application, Aluminum 2219-T87 was specified to be compatible with the liquid oxygen.

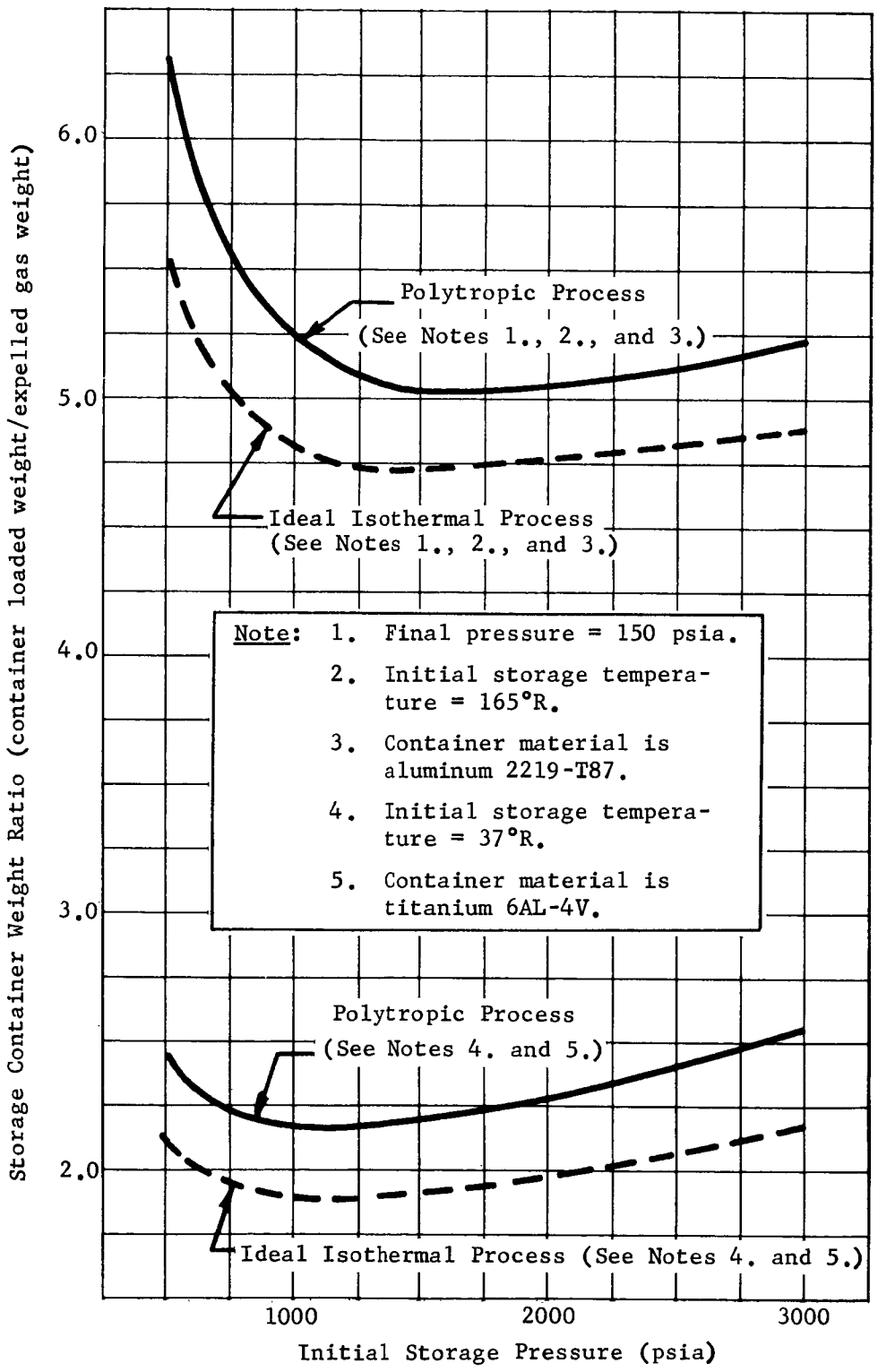

Fig. 19 Storage Container Weight Ratios for a Polytropic Expansion of Helium in a Spherical Container Mounted in the Propellant Tanks

Also shown in Fig. 19 are the ideal isothermal curves for each installation. It can be seen that the ideal curves are somewhat lower than the more-realistic, polytropic expansion curve. This difference is attributed to the polytropic terminal temperature being lower than the surrounding propellant temperature so that the residual gas mass is higher for the same terminal pressure of 150 psia. This analysis was performed for a single spherical container. However, if the total gas volume was divided into several smaller spherical containers, the effective heat transfer surface would be increased so that the temperature profile during outflow would be more nearly constant. The use of several containers does create a more complex installation problem and, for that reason, was not considered in the analysis.

A comparison of the optimum storage container weight ratios for the adiabatic process and the polytropic process from Fig. 18 and 19 (for an initial storage temperature of 37°R) indicates that approximately a 30% reduction in container system weight can be achieved if the polytropic process is employed. This reduction is the result of the reduced-pressurant residual associated with higher gas terminal temperatures. It is of interest to note, however, that the optimum storage pressure in either case is approximately 1200 psia.

This program was developed after the pressure-fed systems were being studied; therefore, no expansion with 300-psia final pressure was calculated with this program.

3) Engine-Bleed Heating

During ideal expansion studies, it was shown that reduction of container residual gas and a subsequent reduction in container weight ratio could be obtained by heating the gas in the container during outflow. During the evaluation of the pump-fed pressurization system, an investigation into the usage of an engine, hot-hydrogen bleed as a heat medium to reduce container residual gas was made.

An analytical model was developed that employed the temperature change Equation [4], the helium equation of state from National Bureau of Standards Technical Note 154, and the six-burn mission profile. An assumption made in the analysis was that the only heat transfer into the helium came from the hydrogen bleed, i.e., no external heating. Furthermore, it was assumed that a tubular heat exchanger was mounted internal to the helium tank. In this configuration, the helium was heated by free convection over the outer tube surface while the hydrogen bleed flowed through the tube providing the heat source by forced convection.

The computation of the instantaneous value of Q into the helium and the resulting hydrogen temperature drop through the heat exchanger was based on the following heat-transfer equations (Ref 4).

a) Helium side-free convection over a horizontal tube

$$h_c = 0.53 \frac{K_c}{D_o} \left[\frac{D_o^3 \rho_c^2 \beta_c g \Delta TC_{pc}}{\mu_c K_c} \right]^{1/4}, \qquad [12]$$

where

h_c = helium heat-transfer coefficient $\left(\text{Btu}/\text{sec-ft}^2\text{-}^\circ\text{R}\right)$,

K_c = helium thermal conductivity (Btu/sec/ft/°R),

μ_c = helium viscosity $\left(\text{lb}_m/\text{ft-sec}\right)$,

β_c = helium thermal-expansion coefficient $\left(^\circ\text{R}^{-1}\right)$,

C_{pc} = helium specific heat at constant pressure $\left(\text{Btu}/\text{lb}_m\text{-}^\circ\text{R}\right)$,

g = accleration $\left(\text{ft-sec}^2\right)$,

ΔT = temperature difference between helium-bulk temperature and tube-surface temperature (°R),

D_o = tube outer diameter (ft),

ρ_c = helium density $\left(lb_m/ft^3\right)$.

b) Hydrogen side-forced convection

$$h_H = 0.02 \left(\frac{K_H}{D_i}\right) Re^{0.8} Pr^{1/3} \left(\frac{T_b}{T_s}\right)^{0.15}, \qquad [13]$$

where

h_H = hydrogen heat-transfer coefficient $(Btu/sec\text{-}ft^2\text{-}°R)$,

K_H = hydrogen thermal conductivity (Btu/sec-ft-°R),

D_i = tube inside diameter (ft),

Re = Reynolds' Number,

Pr = Prandtl's Number,

T_b = hydrogen-bulk temperature (°R),

T_s = tube-surface temperature (°R).

To compute the instantaneous value of $\dot{Q}$ to use in the energy-balance equation, a calculation process that iterated on both hydrogen outlet temperature and heat exchanger surface temperature was employed.

For given values of hydrogen mass flow and inlet temperature, a value is assumed for the outlet temperature. The bulk temperature of the hydrogen is calculated as the arithmetic mean of the inlet and outlet temperatures. A first-trial value for heat-exchanger surface temperature is calculated as the arithmetic mean of the hydrogen-bulk temperature and helium temperature. The hydrogen and

helium heat-transfer coefficients are next calculated from the equations discussed above. The heat-exchanger surface temperature is calculated from the following expression:

$$T_s = \frac{h_H T_H + h_c T_c}{h_H + h_c}, \qquad [14]$$

where

T_s = surface temperature (°R),

T_H = hydrogen-bulk temperature (°R),

T_c = helium temperature (°R),

h_H = hydrogen heat-transfer coefficient $\left(\text{Btu/sec-ft}^2\text{-°R}\right)$,

h_c = helium heat-transfer coefficient $\left(\text{Btu/sec-ft}^2\text{-°R}\right)$.

The above equation was obtained by equating the heat-transfer rate from hydrogen into the wall and the heat-transfer rate from the wall into the helium as follows:

$$Q = h_H A_H \left(T_H - T_s\right) = h_c A_c \left(T_s - T_c\right). \qquad [15]$$

In this relation, the heat capacity of the wall and the temperature gradient across the wall are assumed negligible. Solving Equation [15] for T_s, and assuming that the hydrogen and helium surface areas are equal, yields the desired expression, Equation [14].

The calculated surface temperature is compared with the initial trial value. If the difference between the calculated value and trial value is greater than the assigned tolerance of 5°R, the calculated value becomes the trial value. The heat-transfer coefficients are recalculated and, subsequently, a new calculated surface temperature

is obtained. When the difference between calculated and trial values is within the tolerance, the heat transfer rate, $\dot{Q}$, is calculated based on the helium side-heat-transfer coefficient. The hydrogen-outlet temperature is then calculated from the following relation:

$$\dot{Q} = \dot{m}_H C_{PH} (T_{HI} - T_{HO}), \qquad [16]$$

where

$\dot{m}_H$ = hydrogen flow rate, (lb_m/sec);

C_{PH} = mean specific heat of the hydrogen $(Btu/lb_m\text{-}°R)$;

T_{HO} = hydrogen-outlet temperature (°R);

T_{HI} = hydrogen-inlet temperature (°R).

The calculated value of hydrogen-outlet temperature is compared with the value originally assumed. If the difference between the two values is greater than the assigned limit of 5°R, the entire $\dot{Q}$-calculation procedure is repeated with the assumed hydrogen-outlet temperature replaced by the value just calculated. When the difference is within the assigned limit, the calculated value of $\dot{Q}$ is employed in the energy balance equation to calculate $\dot{T}$.

Two different storage conditions were evaluated. The first consisted of the helium initially at liquid-oxygen temperature in an aluminum container. The second condition considered the helium to be initially at liquid-hydrogen temperature and stored in a titanium container. The different container materials were selected to be compatible with the propellants used. The hydrogen bleed from the engine entered the heat exchanger at 280 psia and 280°R. The flow rate assumed in the analysis was 0.055 lb_m/sec. The hydrogen heat exchanger outlet temperature varied from 200 to 240°R for the case initially at liquid-oxygen temperature. For the case initially at liquid-hydrogen temperature, the

outlet temperature varied from 245 to 270°R. The heat-exchanger configuration consisted of a 1.0-in. diameter tube whose length was 80 ft for the initial liquid-oxygen temperature and 10 ft for the initial liquid-hydrogen temperature. These heat-exchanger lengths were selected to limit heat flow into the container so that overpressurization of the container during outflow did not occur. The minimum pressure at the end of expansion was 150 psia in all cases.

The results of the analysis are plotted in Fig. 20. The container weight ratios presented do include the weight of the heat-exchanger tubes as part of the container weight. By comparing Fig. 20 with Fig. 19 for the polytropic expansions, it is apparent that the container weight ratios for both processes are very nearly the same. Therefore, there appears to be no particular container-weight advantage in heating the container gas by engine-bleed hydrogen rather than mounting the container inside the propellant tanks and allowing free convection and conduction heat-transfer processes to heat the gas. A disadvantage in engine-bleed heating is associated with the installation of the heat exchanger in the gas storage container. At least one and possibly two extra pierce points would be required in the container surface for the heat-exchanger inlet and outlet. The extra fittings associated with these points increase the possibility of external helium leakage.

4) Cascade Expansion Study

A rather unique, pressurant-storage system investigated during the study was called the Cascade, Pressurant-Storage System. This system is described schematically in Fig. 21. Operation of this system involves an initial adiabatic expansion of the pressurant from the primary container into the propellant tanks until a minimum pressure occurs in the primary container. Cascade storage gas is then heated and permitted to flow into the primary container, maintaining primary storage pressure at a minimum required level with a positive-expulsion device (e.g., bladder). Heat may be supplied to the cascade gas by a gas-generator heat exchanger to minimize the quantity of cascade gas required.

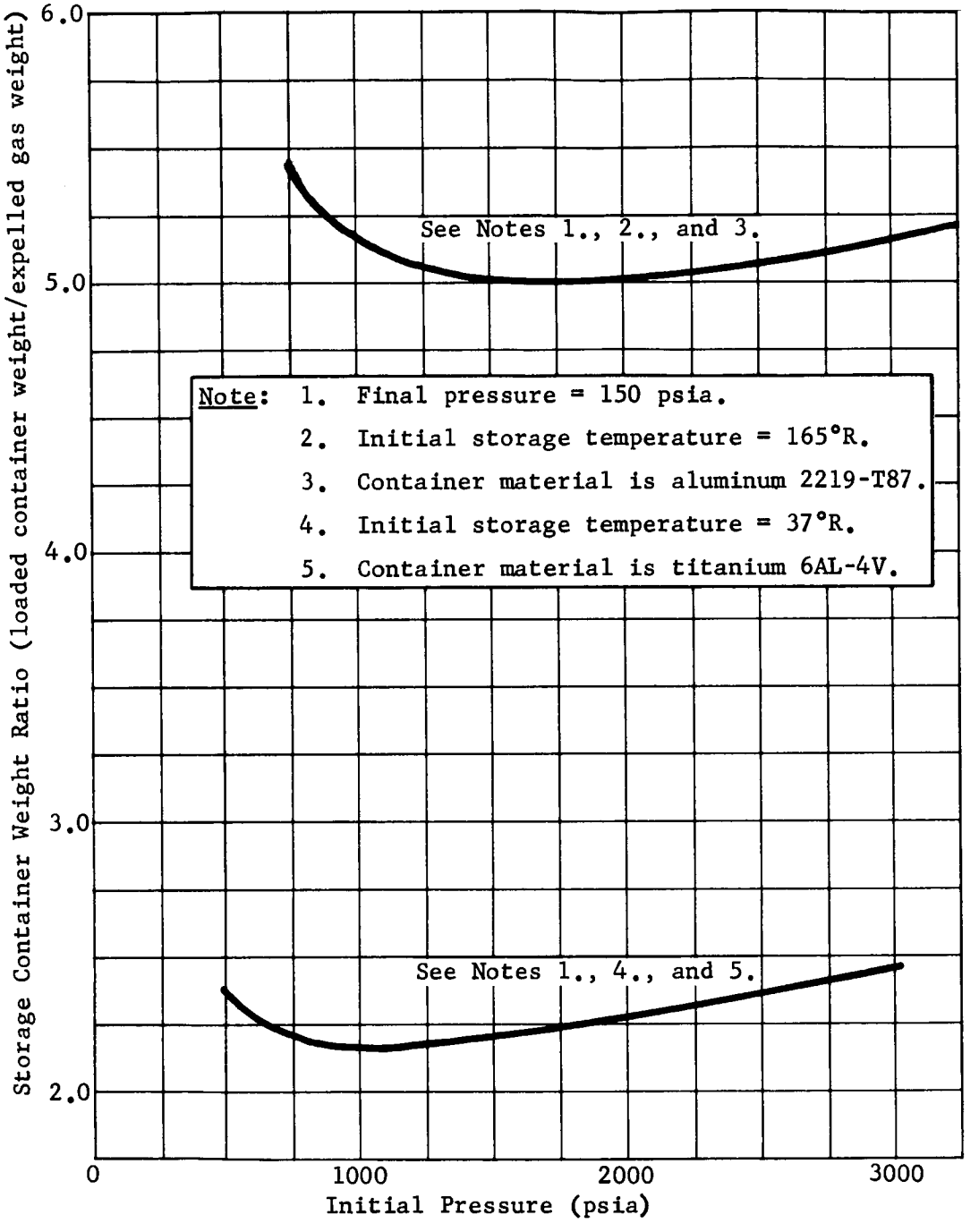

Fig. 20 Storage Container Weight Ratio for Helium Expanding from a Spherical Container with Heating by an Engine Hydrogen Bleed

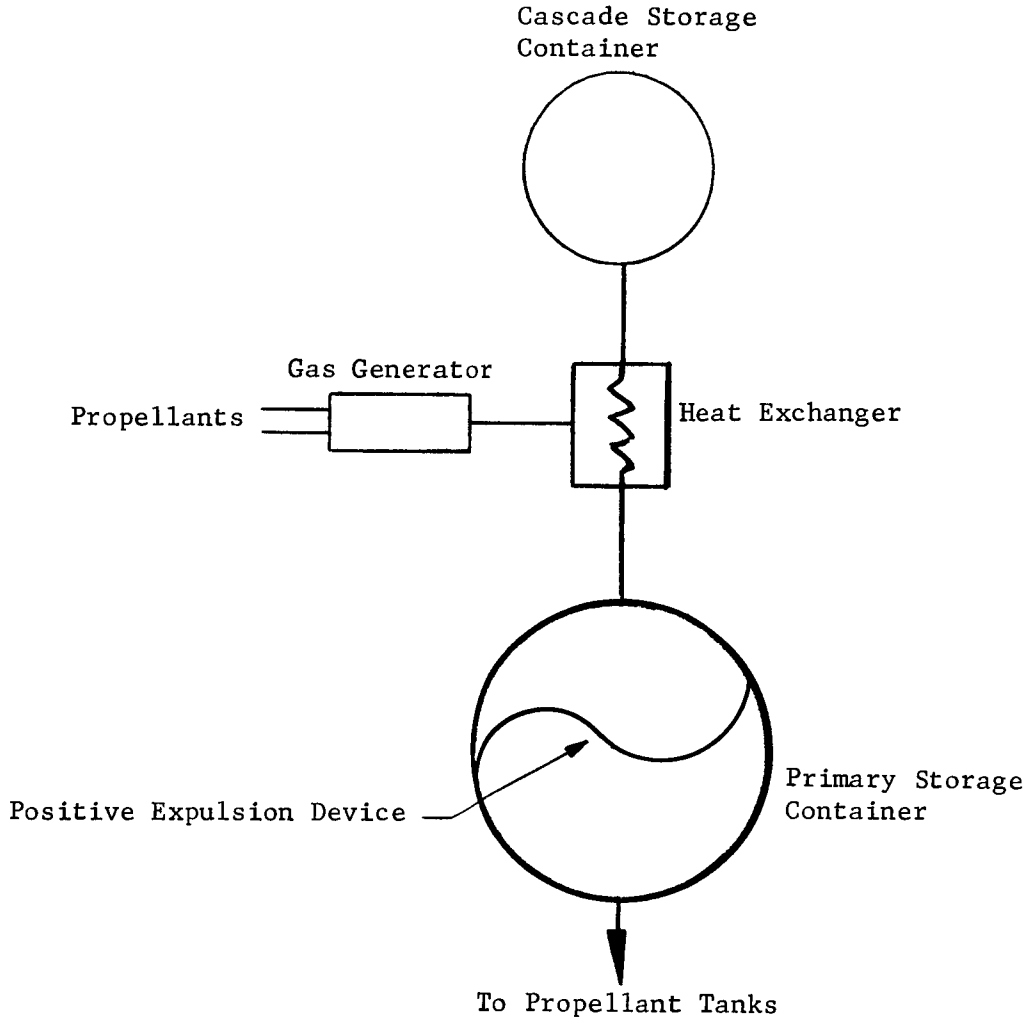

Fig. 21 Cascade Pressurant Storage System

An analysis of this system was completed to determine and compare container expansion ratios with other processes. The container conditions assumed in the analysis are tabulated as follows:

Cascade storage container,

Isothermal expansion (assumed installed in liquid-hydrogen tank),

Storage temperature = 37°R,

Initial pressure = 2500 psia,

Final pressure = 400 psia;

Primary Storage Container,

Initial pressure = 1000 psia,

Final pressure = 300 psia,

Initial and final temperatures are in Table 12.

The primary tank was sized so that the loaded helium mass was equal to the helium pressurant required in the propellant tanks. The weight of cascade gas that flowed into the primary tank was equal to the gas residual weight.

The initial storage pressure for the cascade container was obtained from the ideal analysis for isothermal processes. The primary storage pressure was arbitrarily selected considering both container weight and volume. Helium gas was considered as both primary and cascade fluids.

An analytical model was developed and programed on the IBM 1620 computer to evaluate the cascade pressurization-system requirements. The whole computation process was carried out in three distinct phases. The first phase consisted of a simple, adiabatic expansion of the primary container gas from 1000- to 300-psia pressures. After 300 psia was reached, the second or cascade phase of the expansion process was initiated. In this phase, the model computed the quantity of cascade gas necessary to maintain 300 psia in the primary container during pressurant expulsion.

Table 12 Cascade Storage-Container Weight-Ratio Study

Container Initial Temperature (°R)	Primary Gas Weight (lb_m)	Container Weight (lb_m)	Gas Final Temperature (°R)	Cascade Gas Weight (lb_m)	Cascade Container Weight (lb_m)	Cascade Heat-System Weight (lb_m)	Total System Weight (lb_m)	Storage Container Weight Ratio (total system weight/primary-gas weight expelled)
15	370	115.0	315	17.3	10.3	35.4	548.0	1.48
25	370	137.0	374	17.4	10.3	37.8	572.5	1.54
37	370	172.0	426	19.0	11.2	43.2	615.4	1.66

Note: 1. Gas-inlet temperature from cascade container = 1000°R.
2. Cascade heat system includes gas generator, heat exchanger, and propellants.

During the cascade process, heat transfer between the primary-container wall and both primary- and cascade-gas masses was considered. However, no external heating from the environment was assumed. Heat transfer between the cascade- and primary-gas masses across the positive-expulsion device was also calculated. Mass and energy balances were employed on both primary and cascade masses to determine cascade-mass inflow and temperature histories of both gas masses.

The third phase of the computation was associated with coast periods during which no primary gas outflow was required. At the end of each coast period, the primary and cascade gas and the primary-container wall temperatures were assumed to be equal. This equilibrium temperature was calculated with an energy balance between the primary gas, cascade gas, and container wall with no external heat transfer considered.

The mission profile used in the analysis was for the pressure-fed systems as listed in the program plan.

An oxygen-hydrogen gas generator was assumed as the heat source. The gas-generator and heat-exchanger required weights were calculated with 1620 computer models, developed during the study and discussed in other sections of this report.

Only one analysis was performed on the cascade system to determine if there was an optimum operating condition. A study was performed on the effect of cascade-inlet temperature into the primary container. The inlet temperature from the cascade container was varied from 800 to 1200°R, and it was found that essentially no change in system weight occurred. A temperature of 1000°R was assumed for the remaining study. No other system parameters (i.e., pressure) were optimized.

Three, initial, primary storage temperatures of 15, 25 and 37°R were assumed in the study. At each storage temperature, four cases of different helium outflow were studied. From the results in Table 12 it can be seen that the colder storage temperature lowers the storage-container weight ratio. Different pressurant requirements did not affect the storage-container expansion ratio. The primary-container weight is proportional to the expelled gas weight and affects the expansion similarly in each size system.

The cascade expansion produced one of the lowest helium storage-system weights.

5) Recirculation Expansion

During the expansion study, another process involving recirculation and heating of the helium pressurant was investigated. The purpose of the recirculation was to make up the energy removed by the helium pressurant so that specified expansions (i.e., isobaric, isothermal, or combinations) could be maintained in the container. The proposed system is illustrated as follows.

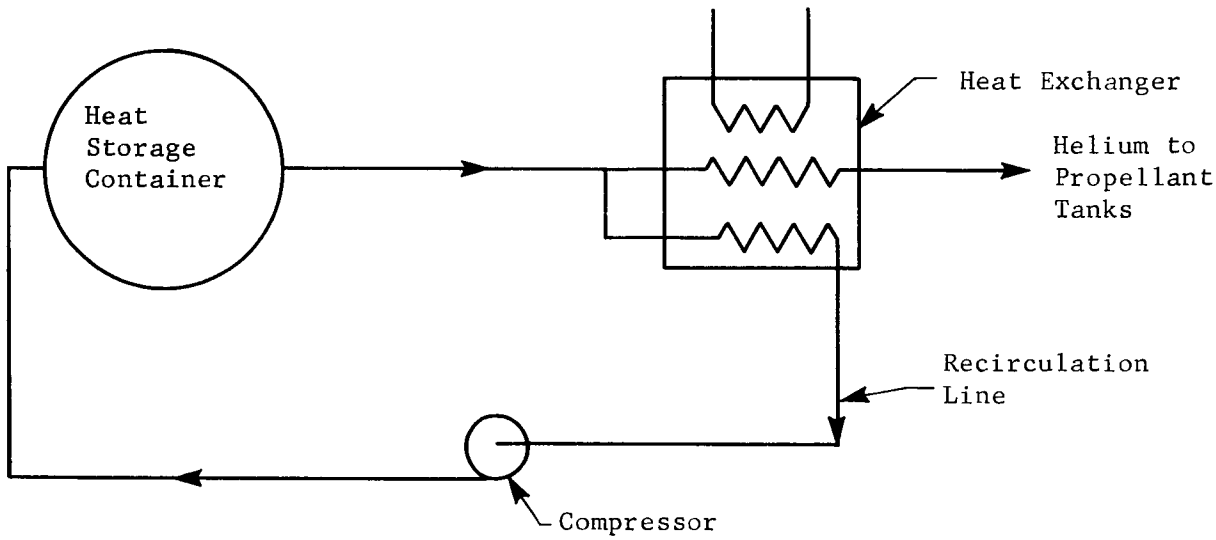

The driving force for the recirculation fluid is supplied by the compressor. One major advantage of this system is that the heating process may be carried out under zero-gravity conditions since the recirculating fluid is heated by forced rather than free convection.

An analysis was performed to determine feasibility of the recirculation process. An energy balance was performed on the pressurant-storage container to determine the recirculation temperature and flow rates to maintain a constant-pressure process in the container. The derivation of this energy balance is given below.

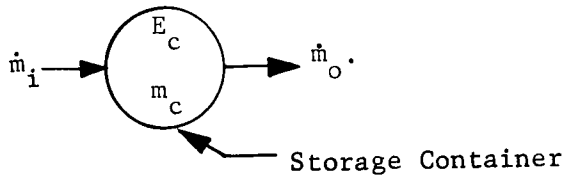

Let

E_c = total internal energy of the container at any instant (Btu),

m_c = the mass of gas present in the container at any instant (lb_m),

$\dot{m}_i$ = gas flow rate, in (lb_m/sec),

$\dot{m}_o$ = gas flow rate, out (lb_m/sec).

Assuming complete mixing of the inlet gas and no heat transfer from the container wall, the energy balance is:

$$\dot{E}_c = \dot{m}_i h_i - \dot{m}_o h_c, \qquad [17]$$

where

h_i = specific enthalpy of gas entering container (Btu/lb_m),

h_c = specific enthalpy of gas leaving container (Btu/lb_m).

Now,

$$\dot{m}_o = \dot{m}_g + \dot{m}_i, \qquad [18]$$

where

$\dot{m}_g$ = gas flow rate required to pressurize propellant tanks (assumed constant) (lb_m/sec).

Substituting [18] into [17] and simplifying, the steady-state relation becomes:

$$\dot{E}_c = \dot{m}_i (h_i - h_c) - \dot{m}_g h_c. \qquad [19]$$

Now,

$$\dot{E}_c = \dot{m}_c e_c + m_c \dot{e}_c, \qquad [20]$$

where

e_c = specific internal energy of container gas $\left(\text{Btu}/\text{lb}_m\right)$;

$\dot{m}_c$ = container-gas-mass rate of change $\left(\text{lb}_m/\text{sec}\right)$ =

$$= \dot{m}_i - \dot{m}_o = \dot{m}_i - \dot{m}_g - \dot{m}_i = -\dot{m}_g. \qquad [21]$$

Equation [20] now becomes:

$$\dot{E}_c = \dot{m}_g e_c + m_c \dot{e}_c. \qquad [22]$$

Combining Equations [19] and [22] and simplifying,

$$\dot{m}_g \left(h_c - e_c\right) + m_c \dot{e}_c = \dot{m}_i \left(h_i - h_c\right). \qquad [23]$$

From the definition of enthalpy,

$$h_c - e_c = p_c v_c = \frac{P_c V_c}{m_c}. \qquad [24]$$

Substituting [24] into [23] and rearranging,

$$\dot{m}_i = \frac{\dot{m}_g P_c V_c + m_c^2 \dot{e}_c}{m_c \left(h_i - h_c\right)}. \qquad [25]$$

Equation [25] was applied to determine the required recirculation flow rate as a function of recirculation temperature. Figure 22 presents typical data generated by Equation [25] for the pump-fed systems using the mission profile as shown in the program plan. In the isobaric-polytropic expansion, the recirculation flow rate was increased to maintain an isobaric condition up to a point at which it was held constant for the remaining outflow. The maximum flow rate presented in Fig. 22 was used to determine the size of compressors, motors, and batteries required to recirculate the helium. Sizing of the above components was accomplished in the following manner. First, the power requirements to pump the recirculation fluid were calculated from the following expression:

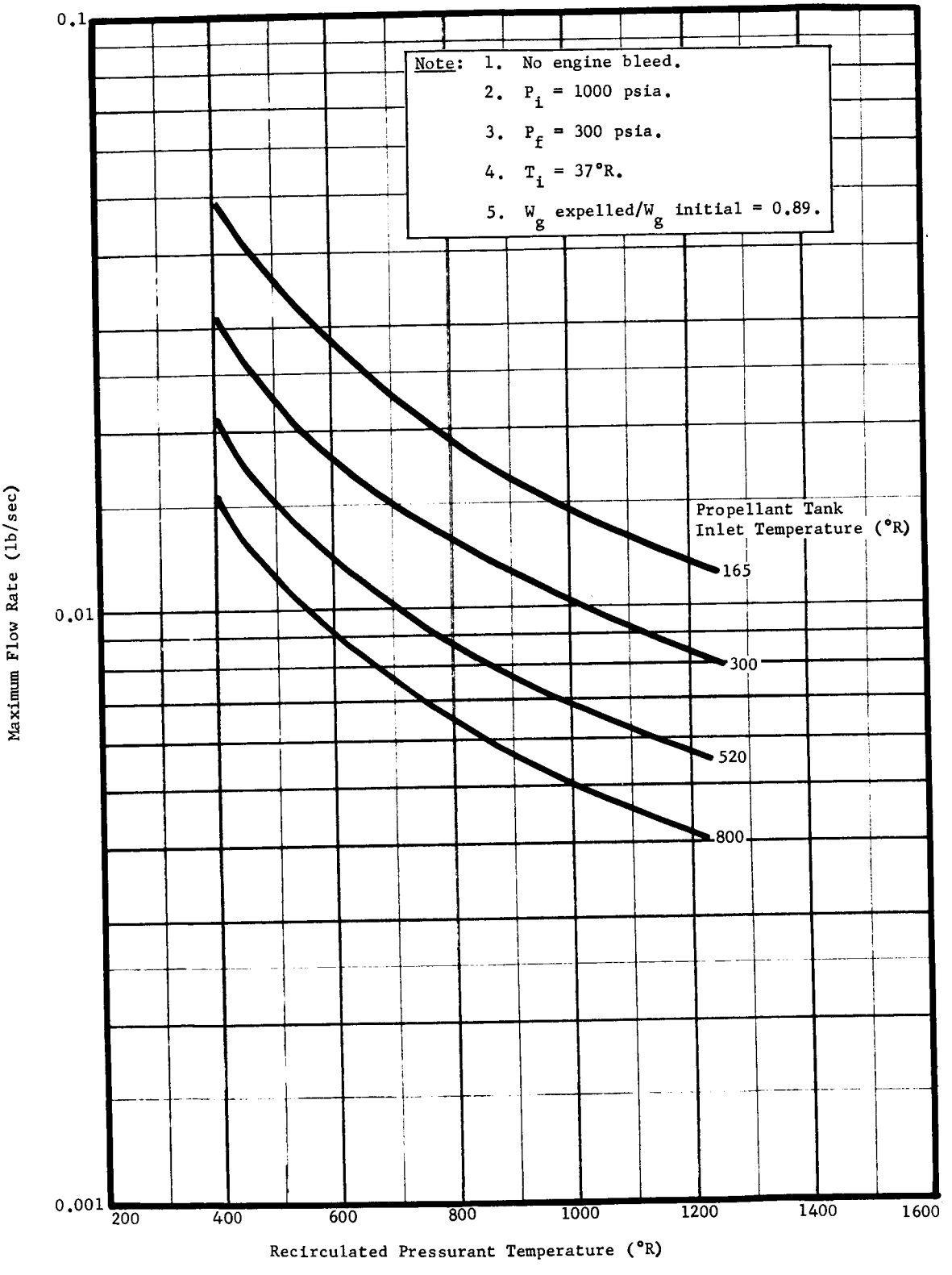

Fig. 22 Recirculated Pressurant Flow Rate, Helium Gas Isobaric Polytropic Expansion

$$P = \frac{\dot{m}\Delta P}{550\rho}, \qquad [26]$$

where

P = power required (hp),

$\dot{m}$ = recirculation flow $\left(lb_m/sec\right)$,

ΔP = pressure rise across pump $\left(lb_f/ft^2\right)$,

ρ = density of fluid, $\left(lb_m/ft^3\right)$.

A pressure rise of 50 psi was assumed in this analysis.

When the pump power required for each flow rate was obtained, the pump, motor, and battery weights were obtained from Fig. 23, 24, and 25,* respectively. Figures 23 and 24 were obtained by plotting various manufacturers' catalog data for flight-weight type components.

Since the heat capacity of the storage container is extremely small at cryogenic temperatures, the container was assumed to be at the same temperature as the gas. No heat from the environment was considered; hence, coast periods did not affect the expansion.

Estimates of gas-generator, heat-exchanger, and gas-generator propellant weights were made for each condition of recirculation flow and temperature. The recirculation subsystem included the gas generators, gas-generator propellants, heat exchanger, pump motor, and battery. The recirculation sybsystem optimized with a recirculation temperature of 650 to 750 °R for all various outflows.

*Machine Design. 11 April 1963.

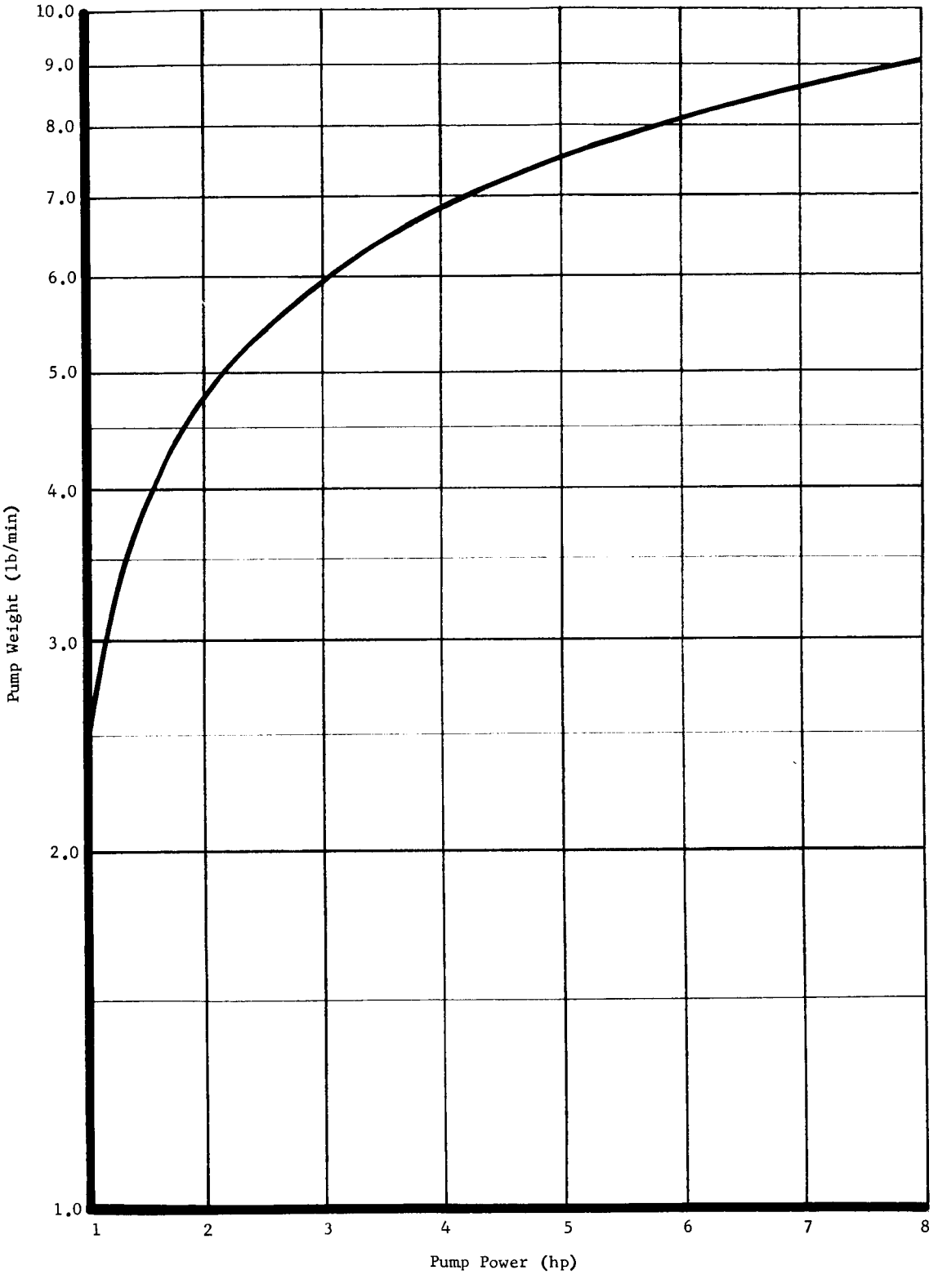

Fig. 23 Recirculation Subsystem Centrifugal Pump Sizing

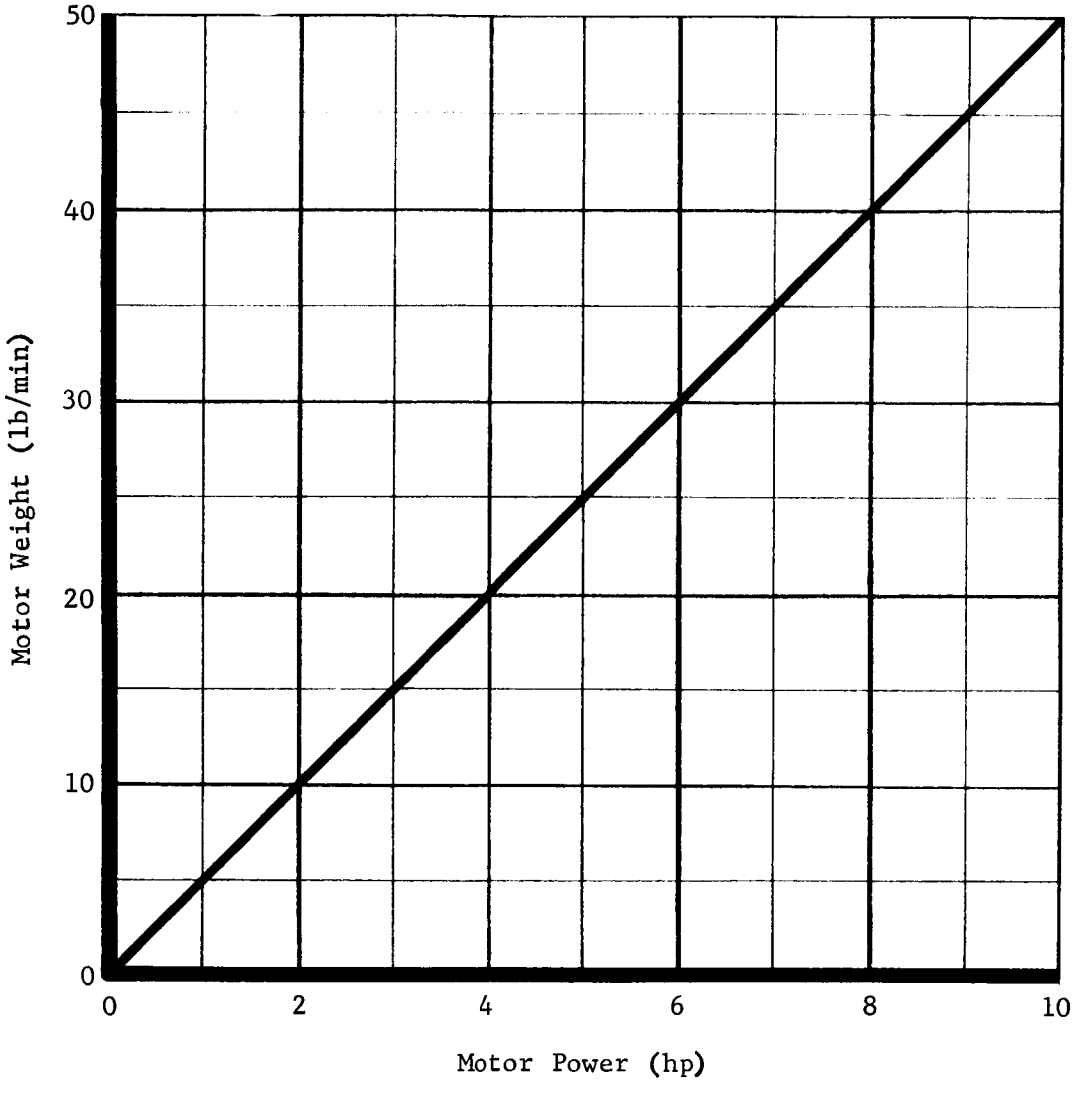

Fig. 24 Recirculation Subsystem Pump Drive Motor Sizing

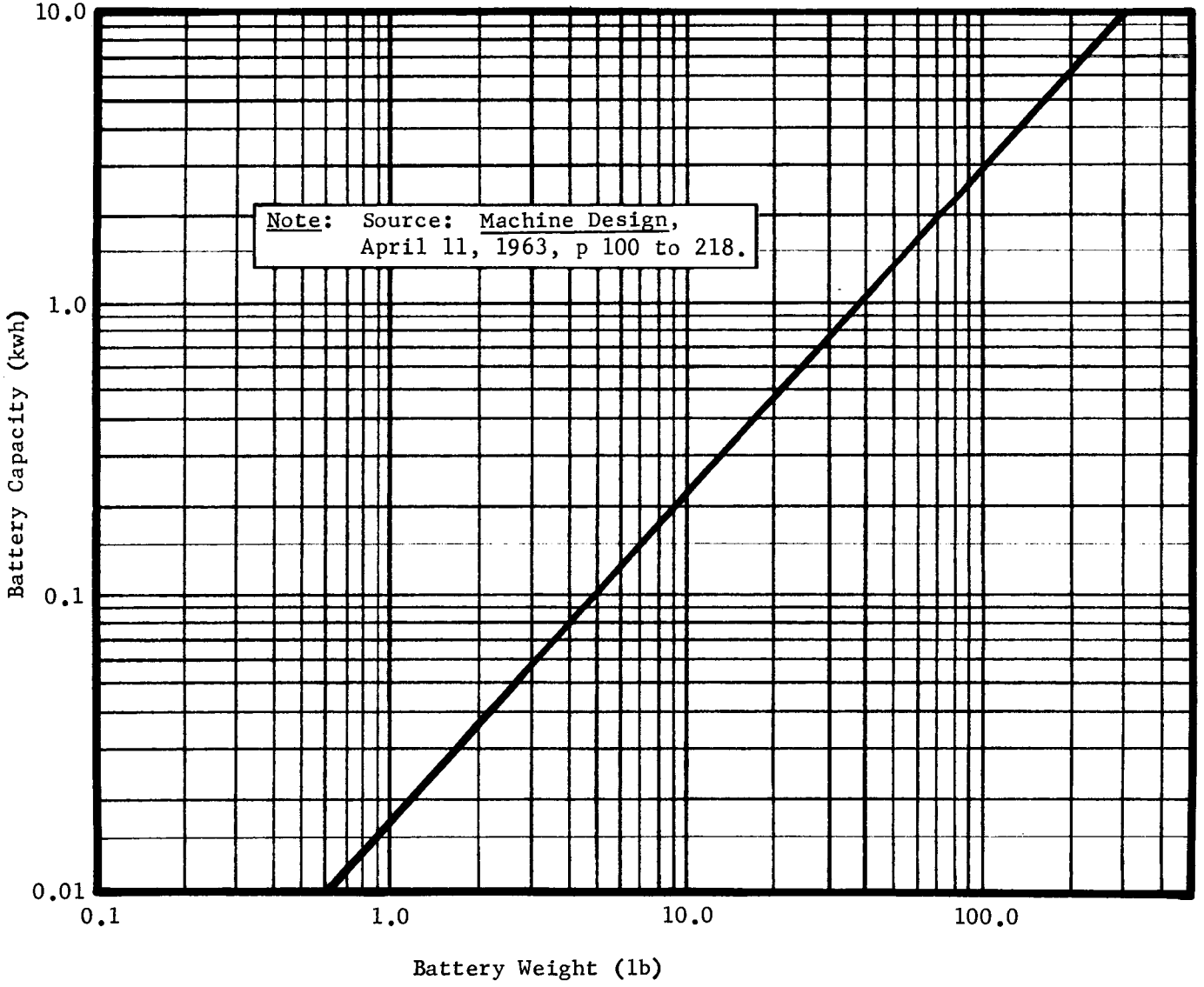

Fig. 25 Battery Sizing, 28-vdc, Silver-Zinc, Sealed, Airborne Type

The loaded-container weight ratios were computed for the recirculation system used in a pump-fed pressurization system. Both hydrogen bleed and no bleed were used. The results are tabulated in Table 13 and include the storage-container weight, pressurant gas, and recirculation-subsystem weight. The expansion in the storage container is an isobaric-polytropic combination. The initial storage pressure and temperature are 1000 psia and 37°R, respectively. A final pressure of 300 psia was used. The container material was titanium. A total time of 900 sec was used to size the battery.

From Table 13, the loaded-container weight ratios appear to be 25 to 30% higher than the values for the cascade system. However, when compared with the polytropic expansion, the recirculation systems appear to be favorable. Furthermore, the recirculation system possesses a capability of heating the storage container by forced convection under zero-gravity conditions. Since only one storage-container pressure was considered in the analysis, additional work is necessary to determine if there is an optimum initial-storage pressure that would result in even lighter system weights.

6) Conclusions

Numerous conclusions have been drawn throughout this section, so those below are of a more general nature. To compare and optimize the pressurant-storage subsystem, the ratio of the total storage-system weight and the expelled-gas weight was calculated. This ratio is called the storage-container weight ratio.

In all expansion systems studied, except for the recirculation system, the storage-container weight ratio remained essentially constant for all pressurant requirements at a given initial storage condition. The recirculation system was more optimum as the pressurant requirement increased. It was found that the

Table 13 Container Weight Ratios for a Recirculation Expansion (Isobaric-Polytropic Expansion)

	No Engine Bleed				With Engine Bleed			
Recirculation-Subsystem Optimization Temperature (°R)	750	730	700	680	730	690	670	650
Propellant-Tank Inlet Temperature (°R)	165	300	520	800	165	300	520	800
Initial Gas Weight (lb_m)	212	142.1	95.1	69.6	123.6	79.9	53.5	39.1
Container Weight (lb_m)	102	77.4	44.5	32.4	59.4	37.2	25.1	19.7
Optimum Recirculation-Subsystem Weight (lb_m)	33	28.8	25.9	24.4	27.6	25.0	23.6	23.0
Expelled-Gas Weight (lb_m)	189	126.5	84.6	62.0	110.0	71.1	47.6	34.8
Container Weight Ratio (total-system weight/ gas-expelled weight)	1.84	1.88	1.96	2.04	1.92	2.00	2.15	2.35

Note: 1. Weight expelled = 0.89 loaded-gas weight.
2. Final temperature (all cases) = 137°R.
3. Initial pressure = 1000 psia.
4. Initial temperature = 37°R.

more-desirable systems all required the addition of heat to the container. A cross section of systems is presented in the following tabulation.

Process	Initial Pressure (psia)	Final Pressure (psia)	Storage-Container Weight Ratio
Isentropic	1850	300	3.80
Isothermal	2400	300	2.05
Isothermal	1100	150	1.92
Isobaric	1000	300	1.86
Isothermal-Isobaric	1000	300	1.45
Polytropic	1100	150	2.15
Engine-Bleed Heat	1100	150	2.15
Recirculation	1000	300	1.96
Cascade	1000	300	1.66

Note: 1. Initial temperature = 37°R.
2. Container material titanium 6Aℓ-4V.

The initial pressure is lowered as the final pressure is also lowered. Some systems optimized below 1000-psia initial pressure, but the lower pressures were not considered since the size of the container would become too large. The size of the system could be reduced if heat was added at the end of the expansion process. The added heat reduces the residual-gas weight.

The first five systems listed above (which are ideal) do not include the weight of the heating system.

3. Heat Source Subsystem

a. Heat-Exchanger Studies

1) Active Pressurant Heating

a) Parallel Flow

The first active heat-exchanger program was developed for use during the initial screening of the pressure-fed systems. It was used primarily to obtain heat-exchanger weights to be included in the total system weights. The design point for the heat exchanger was the maximum load condition of each system.

To account for variation of the specific heats of both fluids and the variation of the overall heat-transfer coefficient the classical method of mean temperature difference (i.e., log-mean) was ruled out. The instantaneous temperature difference between the two fluids is calculated for only a small increment of the heat-exchanger surface. This procedure is repeated until the specified outlet temperature is reached. The total area of the heat exchanger is equal to the summed increments.

The model used parallel-flow design. The design parameters of the heat exchanger were as follows:

Types of fluids;

Inlet and outlet temperature of the cold fluid;

Flow rate of the cold fluid;

Inlet and outlet temperature of the hot fluid.

Incremental Area Calculations - By using these design parameters, the program calculated the flow rate of the heating fluid and the size of the heat exchanger. Assuming a flow rate of the hot fluid and an incremental temperature drop of the hot fluid, the incremental area was calculated as follows. Using the properties of the

hot fluid and the assumed temperature change, the heat transferred was calculated by:

$$\dot{Q}_h = \dot{W}_h \, C_{ph} \, \Delta T_h . \qquad [27]$$

Since the heat lost by the hot fluid was the same as the heat gained by the cold fluid, the temperature change of the cold fluid was calculated:

$$\Delta T_c = \frac{\dot{Q}_c}{\dot{W}_c \, C_{pc}} = \frac{\dot{Q}_h}{\dot{W}_c \, C_{pc}} . \qquad [28]$$

The heat-transfer coefficients for both the hot and cold fluids were determined from the average temperature of each fluid by use of the general term; (Stanton No.)(Prandtl No.)$^{2/3}$ = g (Reynolds' No.). The values of g (Reynolds' No.) were obtained from figures presented in Ref 6.

Ignoring the resistance of the tube wall, the overall heat transfer coefficient was evaluated:

$$U = \frac{1}{\frac{1}{h_h} + \frac{1}{h_c}} . \qquad [29]$$

The area required for the increment was calculated by:

$$A = \frac{Q_h}{U \, \Delta T_{h\text{-}c}} , \qquad [30]$$

where

$\dot{W}$ = flow rate (lb/sec),

Q = heat transferred (Btu),

C_p = specific heat at constant pressure (Btu/lb-°R),

ΔT = temperature difference (°R),

h = heat-transfer coefficient $\left(Btu/ft^2\text{-sec-°R}\right)$,

U = overall heat-transfer coefficient $\left(Btu/ft^2\text{-sec-°R}\right)$,

A = area $\left(ft^2\right)$;

Subscripts:

h = hot,

c = cold.

This calculation was repeated over successive increments until the desired outlet temperature of the cold fluid was reached. The total area was obtained by summing the incremental areas.

If the outlet temperature of the hot fluid was not equal to the stipulated value, the assumed flow rate of the hot fluid was modified and the calculation redone. Modification of the hot-fluid flow rate was continued until the calculated outlet temperature was equal to the desired value.

b) Cross Flow

The second active heat-exchanger program was developed to provide greater detail of information about the heat exchanger than was obtained in the first program. It was still needed to obtain heat-exchanger weights but could also calculate additional data that would assist in the event pressure losses of both fluids used in the heat exchanger were calculated.

To account for various configurations of flow and physical arrangement, the average temperature of each fluid was considered. The number-of-heat-transfer-units (NTU) method was used to calculate the performance of the heat exchanger.

The program calculation initially assumed a one-cubic-foot size heat exchanger. From this assumed size, flow properties were evaluated and a heat-exchanger size was calculated. The assumed size was adjusted until it agreed with the calculated size.

The design parameters of the heat exchanger were:

Number of heat transfer units;

Types of fluid;

Inlet and outlet temperatures of the cold fluid;

Flow rate of the cold fluid;

Inlet and outlet temperatures of the hot fluid.

The heat exchanger dimensions and the flow rate of the hot fluid were obtained from the above design parameters. The pressure losses of both fluids were calculated, and the Mach number at all inlet and outlet points was determined. The following sequence was used in the program.

By using a simple arithmetic mean between the inlet and outlet temperatures, the thermal and transport properties of both fluids were evaluated. Assuming all heat lost by the hot fluid was equal to the heat gained by the cold fluid, the flow rate of the hot fluid was calculated by:

$$\dot{W}_h = \frac{\dot{W}_c \, C_{pc} \, \Delta T_c}{C_{ph} \, \Delta T_h} . \qquad [31]$$

For both fluids the Mach numbers were calculated at the inlet and outlet points:

$$M = \frac{V}{\sqrt{\gamma \, RT_g}} . \qquad [32]$$

The heat-transfer coefficients for both the hot and cold fluids were determined from the average temperature of each fluid by the use of the general term; (Stanton No.)(Prandtl No.)$^{2/3}$ = g (Reynolds' No.). The value of g (Reynolds' No.) was obtained from Ref 6.

The overall heat-transfer coefficient was calculated by assuming that a zero heat resistance was offered by the wall:

$$U = \frac{1}{\frac{1}{h_h} + \frac{1}{h_c}} . \qquad [33]$$

The area required was calculated by:

$$A = \frac{(NTU)\ \dot{W}_h\ C_{ph}}{U} . \qquad [34]$$

The values of NTU can be evaluated by using one of Figures 2 thru 13 of Ref 6. Explanations of terms are:

$\dot{W}$ = flow rate (lb/sec);

C_p = specific heat constant pressure;

T = temperature difference (°R);

M = Mach number;

V = velocity (ft/sec);

γ = ratio of specific heats;

R = gas constant $(ft\text{-}lb_f) / (lb_m\text{-}°R)$;

T = temperature (°R);

U = overall heat-transfer coefficient $(Btu/ft^2\text{-}sec\text{-}°R)$;

h = heat-transfer coefficient $\left(\text{Btu}/\text{ft}^2\text{-sec-}^\circ\text{R}\right)$;

NTU = number of heat transfer units;

A = area $\left(\text{ft}^2\right)$;

Subscripts:

c = cold;

h = hot.

This calculation loop was recycled until the assumed initial size agreed with the calculated size. After agreement was accomplished, the pressure losses of both fluids were calculated by accounting for friction losses:

$$\Delta P = \frac{\rho V^2 f L}{772 D_H}, \qquad [35]$$

where

P = pressure loss (psi),

ρ = density $\left(\text{lb}/\text{ft}^3\right)$,

V = velocity (ft/sec),

f = drag friction coefficient,

L = characteristic length (ft),

D_H = hydraulic diameter (in.).

2) Passive Pressurant Heating

A passive, circular, finned-tube heat exchanger mounted in the liquid oxygen tank was evaluated during the pump-fed system study. The helium was assumed to be stored at liquid-hydrogen temperature and was heated by forced convection while flowing through the tube. The liquid oxygen supplied the heat by free convection over the tube and fin surface.

An analytical model, employing a conventional log-mean temperature difference method, was established to calculate heat-exchanger performance. A double iteration, involving both heat exchanger wall and gas outlet temperature, was employed in the calculation procedure. The analytical model was initially programmed on the IBM 1620 computer. Later, the model was incorporated in the Propellant-Tankage and Pressurization System program.

As input, the computer program required the helium-inlet pressure, temperature, and flow rate, the heat-exchanger geometry (tube diameter, fin diameter, fin spacing, tube length, tube material), and the vehicle acceleration. The computer program calculated the helium-outlet pressure and temperature. In the following paragraphs, the steps and techniques employed in the calculation procedure will be briefly discussed.

The first step in the calculation is the assumption of the helium temperature leaving the heat exchanger. This value was arbitrarily made 20% greater than the inlet temperature. The mean helium temperature through the heat exchanger to be used for determination of properties was calculated by the following relation:

$$T_{gm} = T_L - \Delta T_{LM} = T_L - \frac{T_{g2} - T_{g1}}{\ell n \frac{T_L - T_{g1}}{T_L - T_{g2}}}, \qquad [36]$$

where

T_{gm} = mean gas temperature (°R),

T_L = liquid bulk temperature (°R),

ΔT_{LM} = log mean temperature difference (°R),

T_{g2} = helium-outlet temperature (°R),

T_{g1} = helium-inlet temperature (°R).

As first guess in the wall temperature iteration, the wall temperature was assumed to be the arithmetic mean of the liquid temperature, T_L, and the mean gas temperature, T_{gm}. The next step was the calculation of the gas heat-transfer coefficient from the following equation (Ref 4):

$$h_g = 0.02 \frac{K_g}{D_{TI}} (Re)^{0.8} (Pr)^{1/3} \left(\frac{T_{gm}}{T_W}\right)^{0.575}, \qquad [37]$$

where

h_g = gas heat-transfer coefficient (Btu/sec-ft^2-°R),

K_g = gas thermal conductivity (Btu/sec-ft-°R),

D_{TI} = tube inside diameter (ft),

Re = Reynolds' number,

Pr = Prandtl number.

All gas properties in [37] were evaluated at the mean gas temperature, T_{gm}.

The next calculation was the determination of the liquid heat-transfer coefficient. Since the liquid side area consists of both vertical-plane and horizontal-tube surfaces, a mean film coefficient was used that was based on the two types of surfaces and relative area of each. The expression for the mean film coefficient, h_L, was obtained in the following manner.

The heat transfer on the liquid side of the heat exchanger was:

$$\dot{Q} = h_L A_L (T_L - T_W), \qquad [38]$$

where

$\dot{Q}$ = heat transfer rate (Btu/sec),

h_L = mean heat-transfer coefficient $(Btu/sec\text{-}ft^2\text{-}°R)$,

A_L = total heat-transfer surface (ft^2).

The heat transfer rate, $\dot{Q}$, was made up of two parts as follows:

$$\dot{Q} = \dot{Q}_F + \dot{Q}_T, \qquad [39]$$

where

$\dot{Q}_F$ = heat-transfer rate from fin surface (Btu/sec),

$\dot{Q}_T$ = heat-transfer rate from tube surface (Btu/sec).

Now, assuming the wall temperature was constant over both tube and finned surfaces,

$$\dot{Q}_F = h_F A_F (T_L - T_W), \qquad [40]$$

and

$$\dot{Q}_T = h_T A_T (T_L - T_W), \qquad [41]$$

where

h_F = heat-transfer coefficient on fin surface $(Btu/sec/ft^2/°R)$,

h_T = heat-transfer coefficient on tube surface $(Btu/sec/ft^2/°R)$,

A_F = fin surface area (ft^2),

A_T = tube surface area (ft^2).

Combining expressions for $\dot{Q}$, $\dot{Q}_F$, and $\dot{Q}_T$,

$$h_L A_L (T_L - T_W) = h_F A_F (T_L - T_W) + \\ + h_T A_T (T_L - T_W). \quad [42]$$

Simplifying,

$$h_L A_L = h_F A_F + h_T A_T. \quad [43]$$

Solving for h_L,

$$h_L = (h_F A_F + h_T A_T)/A_L. \quad [44]$$

Now, $A_F = A_L - A_T$, so that h_L became:

$$h_L = \frac{(h_T - h_F) A_T}{A_L} + h_F. \quad [45]$$

This expression was employed in the program to compute the film coefficient on the liquid side of the heat exchanger.

For calculation of h_T, the tube-surface coefficient, the following expression from Ref 4 was employed:

$$h_T = 0.53 \frac{K_L}{D_{TO}} [Gr\ Pr]^{1/4}, \quad [46]$$

where

K_L = liquid thermal conductivity (Btu/ft-sec-°R),

D_{TO} = tube diameter (ft),

Gr = Grashof number,

Pr = Prandtl number.

The characteristic dimension used in the Grashof number was the tube diameter, D_{TO}.

The equation used for the finned surface (vertical plane) was also obtained from Ref 4. The equation was as follows:

$$h_F = 0.508 \frac{K_L}{D_F} \left[\frac{Pr}{0.952 + Pr} Gr\ Pr \right]^{1/4}, \qquad [47]$$

where

D_F = fin diameter (ft).

The characteristic dimension used in the Grashof number in this case was fin diameter, D_F, which was an arbitrary assumption.

The next item calculated in the program was the finned-surface efficiency. This value was computed from the following expression:

$$\eta_L = 1 - \frac{A_F}{A_L} (1 - \eta_F), \qquad [48]$$

where

η_L = surface efficiency,

A_F = fin area (ft^2),

A_L = total surface area, liquid side (ft^2),

η_F = fin efficiency.

To obtain the fin efficiency, η_F, a method presented in Ref 5 was employed. In this method, the fin efficiency for a straight rectangular fin was first calculated based on the circular fin thickness and height. The following relations were used:

$$\eta_{SF} = \frac{1}{\sqrt{2X}} \tanh \sqrt{2X} \qquad [49]$$

and

$$X = \left(\frac{D_F - D_{TO}}{2}\right)^{3/2} \sqrt{\frac{2h_L}{K_W\, t_F\, (D_F - D_{TO})}}, \qquad [50]$$

where

η_{SF} = fin efficiency for a straight rectangular fin,

D_F = fin diameter (ft),

D_{TO} = tube diameter (ft),

h_L = mean heat-transfer coefficient (Btu/ft^2-sec-°R),

K_W = thermal conductivity of fin material (Btu/ft-sec-°R),

t_F = fin thickness (ft).

A correction factor to convert the straight-fin efficiency to a value for a circular fin was then applied by the following expression:

$$\eta_{CF} = \eta_{SF} + \Delta\eta, \qquad [51]$$

where

η_{CF} = circular-fin efficiency,

$\Delta\eta$ = correction factor to convert from straight fin to circular fin.

To determine $\Delta\eta$, Fig. 4-11 of Ref 5 was employed. An expression for $\Delta\eta$ in terms of fin and tube diameters and straight-fin efficiency was derived assuming the efficiency lines in the figure were straight lines. The resulting expression was:

$$\Delta\eta = \left[\frac{D_{TO}}{D_F} - 1\right]\left[-0.031 + 0.756\ \eta_{SF} - 0.725\ \eta^2_{SF}\right]. \quad [52]$$

The next major step in the calculation was the verification of the assumed-wall temperature. It was assumed that the wall temperature was uniform throughout and that all the heat transferred from the liquid to the wall was transferred from the wall to the gas. An energy balance performed on the wall yielded the following expressions:

$$\dot{Q}_g = \dot{Q}_L \quad [53]$$

or

$$h_g A_g (T_W - T_{gm}) = \eta_L h_L A_L (T_L - T_W), \quad [54]$$

where

$\dot{Q}_g$ = heat transfer rate from wall to gas (Btu/sec),

$\dot{Q}_L$ = heat transfer rate from liquid to wall (Btu/sec),

h_g = gas heat transfer coefficient $\left(Btu/sec\text{-}ft^2\text{-}°R\right)$,

A_g = gas side-heat-transfer area (ft^2),

T_W = wall temperature (°R),

T_{gm} = mean gas temperature (°R),

η_L = liquid side-heat-transfer surface efficiency,

h_L = liquid heat-transfer coefficient $\left(\text{Btu}/\text{sec-ft}^2\text{-°R}\right)$,

A_L = liquid side-heat-transfer area $\left(\text{ft}^2\right)$,

T_L = liquid temperature (°R).

Solving for T_W:

$$T_W = \frac{h_g T_{gm} + \left(A_L/A_g\right) \eta_L h_L T_L}{h_g + \left(A_L/A_g\right) \eta_L h_L} . \qquad [55]$$

The value of T_W computed from this expression was compared with the original assumed value. If the difference between the assumed and calculated value was less than 0.5°R, the computation proceeded to the next step. If the difference was greater than 0.5°R, the assumed value was made the calculated value, and a new computation cycle was started by transferring back to the place where the gas heat-transfer coefficient was calculated.

After the wall-temperature iteration was completed, the overall heat-transfer coefficient based on the liquid-side surface area was calculated as follows:

$$U_L = \frac{1}{\frac{A_L}{A_g h_g} + \frac{1}{\eta_L h_L}} , \qquad [56]$$

where

U_L = overall heat-transfer coefficient.

This heat-transfer coefficient was used in the calculation of the gas-outlet temperature from a relation based on heat-exchanger effectiveness. This relation was derived from the following general expressions for heat-exchanger effectiveness presented on pages 453 and 454 of Ref 4:

$$\epsilon = \frac{C_c}{C_{min}} \frac{(T_{co} - T_{ci})}{(T_{hi} - T_{ci})} , \qquad [57]$$

and

$$\epsilon = \frac{1 - e^{-\left[1+(C_{min}/C_{max})\right]UA/C_{min}}}{1 + (C_{min}/C_{max})} , \qquad [58]$$

where

ϵ = effectiveness,

C_c = capacity rate for cold-side fluid = $\dot{m}_c C_{pc}$ (Btu/sec-°R),

C_{min} = smaller capacity rate of hot and cold fluids (Btu/sec-°R),

C_{max} = larger capacity rate of hot and cold fluids (Btu/sec-°R),

T_{co} = cold-fluid outlet temperature (°R),

T_{ci} = cold-fluid inlet temperature (°R),

T_{hi} = hot-fluid inlet temperature (°R),

A = heat-transfer area (ft^2),

U = overall heat-transfer coefficient based on A (Btu/ft^2-sec-°R).

Since the liquid temperature was assumed to remain constant, the liquid capacity rate was, by definition, equal to infinity (see page 455, Ref 4). Therefore, the ratio C_{min}/C_{max} was equal to zero, and C_{min} was equal to C_c that has a finite value of $\dot{m}_g C_{pg}$. The above equations for ϵ can be rewritten as follows:

$$\epsilon = \frac{T_{g2} - T_{g1}}{T_L - T_{g1}} \qquad [59]$$

and

$$\epsilon = 1 - e^{-U_L A_L / \dot{m}_g C_{pg}}, \qquad [60]$$

where

$\dot{m}_g$ = gas flow rate $\left(lb_m/sec\right)$,

C_{pg} = gas specific heat $\left(Btu/lb_m\text{-}°R\right)$.

These two equations for ϵ were combined and the resulting expression solved for T_{g2} as follows:

$$T_{g2} = T_L - \left(T_L - T_{g1}\right)e^{-\left[U_L A_L / \left(\dot{m}_g C_{pg}\right)\right]}. \qquad [61]$$

This equation was employed in the program to calculate the outlet-gas temperature. The calculated value was compared with the assumed value. If the difference between the two values was 0.2°R (an arbitrary assumed value), the computation cycle moved on to calculate the pressure loss. If the difference was greater than 0.2°R, the assumed value was replaced by the calculated value and the entire computation, including the wall-temperature iteration, was started over.

The pressure-drop analysis was based on a simplified equation taken from Ref 6. The equation employed was as follows:

$$\Delta P = \frac{G^2}{2_{gc}} v_1 \left[2\left(\frac{v_2}{v_1} - 1\right) + \frac{f\ L}{D_{TI}} \frac{v_m}{v_1} \right], \qquad [62]$$

where

ΔP = pressure loss $\left(lb_f/ft^2\right)$,

G = mass velocity and flow rate/flow area $\left(lb_m/sec\text{-}ft^2\right)$,

g_c = mass-conversion factor $\left[32.2(lb_m/lb_f)(ft/sec^2)\right]$,

v_1 = gas-inlet specific volume $\left(ft^3/lb_m\right)$,

v_2 = gas-outlet specific volume $\left(ft^3/lb_m\right)$,

v_m = mean specific volume (assumed to be the arithmetic mean of v_1 and v_2)$\left(ft^3/lb_m\right)$,

f = friction factor,

L = tube length (ft),

D_{TI} = tube inside diameter (ft).

This equation is simplified in that the entrance and exit pressure-loss factors in the original equation have been eliminated.

An expression for the friction factor, f, was developed from a curve fit of Fig. 29 in Ref 6. The expression is based on the curve for a L/D ratio equal to infinity and Reynolds' numbers greater than 10,000. The temperature-ratio factor has been assumed as unity since the exponent is very small. The resulting expression for f follows:

$$f = 0.04499\ Re^{-0.1927}, \qquad [63]$$

where

Re = Reynolds' Number.

An iteration process was again employed. The gas-outlet pressure was initially assumed to be 0.98 of the inlet pressure. The calculated outlet pressure was then compared with the assumed value. If the absolute difference between the assumed and calculated pressure was greater than 1.0 psi (an arbitrary selection), a new assumed value was calculated as follows:

$$P_{g2n} = P_{g2p} + (P_{g2c} - P_{g2p})/2, \qquad [64]$$

where

P_{g2n} = new assumed value,

P_{g2p} = previous assumed value,

P_{g2c} = calculated value.

The calculation was repeated until the limit of 1 psi was reached.

In establishing a desirable heat-exchanger geometry, various aspects were considered. First, it was necessary to estimate the maximum length of tubing that could be installed in the liquid oxygen (lox) tanks. It was required that the heat exchanger be mounted so as to be completely submerged in the liquid oxygen at the beginning of the last burn in the mission profile. The length estimate was based on the following assumptions:

Four individual lox tanks were used,

Each lox tank radius was 33.4 in.,

Lox level was 7.5 in. above tank bottom at the beginning of the last burn,

Tubes were staggered so that lox free-convection flow over each tube was independent of adjacent tubes,

Tubes were installed in coil fashion in tank bottom.

The estimated maximum length as a function of fin diameter is tabulated as follows:

Fin Diameter (in.)	Maximum Tube Length (ft/tank)
2	32.2
3	21.9
4	14.2

Another factor considered in the selection of heat-exchanger geometry was the fin spacing. Theoretically, it is desirable to reduce fin spacing to a minimum so that the maximum number of fins and, therefore, maximum surface area may be provided. However, since the heat exchanger must operate under very low gravity fields, liquid surface-tension forces could exceed buoyant forces in the propellant so that no convective flow would occur if the fins were too close together. A review of studies concerning fluid behavior in reduced-gravity fields (such as Ref 7) indicated that the buoyant forces should exceed the capillary forces by at least a factor of 4.0. This ratio is defined as the Bond number. This Bond number limit was established for simple capillary tubes that had no similarity to the proposed heat-exchanger configuration. However, in the absence of any better data, the Bond number of 4.0 was established as a design parameter. To determine the minimum fin spacing, the following expression was derived (Appendix C):

$$b = \frac{Bo\ (D_F - D_T)}{0.00545\ (\rho/\sigma)\ g\ \left(D_F^2 - D_T^2\right) - Bo}, \qquad [65]$$

where

b = fin spacing (in.),

D_F = fin diameter (in.),

D_T = tube diameter (in.),

ρ = liquid density $\left(lb_m/ft^3\right)$,

σ = surface tension $\left(lb_m/ft^3\right)$,

g = acceleration (g),

Bo = Bond number (dimensionless).

Final heat-exchanger sizing was accomplished by a series of runs on the computer. Since there are a large number of variables affecting the heat-exchanger design, certain parameters were fixed to reduce the time and effort on the computer. The following data were assumed constant:

Helium-inlet pressure = 280 psia,

Helium-inlet temperature = 40°R,

Lox temperature = 160°R,

Vehicle acceleration = 0.01 g,

Bond number = 4.0.

It was also assumed that the heat-exchanger material was aluminum. A minimum wall temperature of 110°R was also established as part of the heat-exchanger design criteria to prevent lox freezing on the tube and fin surfaces.

Fin diameters of 2, 3, and 4 in., in combination with tube diameters of 1.5, 2.0, 2.5, and 3.0 in., were evaluated. Helium flow rates from 0.25 to 1.0 $lb_m/$ sec were also investigated. Fin thicknesses considered in the evaluation varied from 0.01 to 0.15 in. The number of fins per unit length of tube for each heat-exchanger configuration was calculated by the following expression:

$$N_F = \frac{1}{b + t_f} \qquad [66]$$

where

N_F = number of fins per unit length,

b = fin spacing,

t_f = fin thickness.

Conclusions - Several conclusions were reached from the analysis. It was found that large tube diameters (3-in. as opposed to 1.0-in.) were necessary to pass the helium and prevent freezing the lox during pressurization periods. It is during the pressurization periods that the helium flow rate is the highest. Smaller tubes could be used with a reduced flow rate; however, longer durations of pressurization would be required resulting in a heavier settling subsystem. The tradeoff between settling subsystem weight and pressurization time is further discussed in Chapter III.C.5, Total System Weight Analysis.

Another conclusion reached was that a series-flow heat exchanger, in which helium flows through each lox tank, produced higher helium-outlet temperature than if the helium flow was divided in fourths and allowed to flow through individual or parallel heat exchangers.

The final heat exchanger selected for use in System 6 of the pump-fed systems consisted of a 3-in. diameter tube with 4-in. diameter fins. The total length of the heat exchanger was 60 ft. It was divided into four 15-ft segments in each lox tank. Series flow was used, and the total weight was 121 lb_m. The number of fins used per inch was 3.21, and the fin thickness was 0.05 in. The fin spacing was 0.307 in.

3) Pressurant Container Heating

During the ideal expansion study, various processes such as the isobaric process, were considered that required heating of the pressurant in the container. Various methods of supplying heat from external gas generators were considered.

a) Internal Heating

For internal heating of the pressurant in the container, a circular, finned tube mounted inside the container was considered. The pressurant was heated on the external surface of the heat exchanger by free convection with lox-hydrogen, gas generator exhaust passing through the tube and providing the heat source. A 1620 computer program was established to calculate the heat-exchanger size and weight for a specified, pressurant flow rate and the required heat transfer rate. The program calculation procedure employed an overall heat-transfer coefficient based on the log-mean temperature difference and the pressurant side area of the heat exchanger. To simplify the analysis, the temperature drop across the tube wall was neglected so that the overall heat-transfer equation was expressed as follows (Ref 4):

$$U = \frac{1}{\frac{A_C}{A_H}\frac{1}{h_H} + \frac{1}{\eta_C h_C}}, \qquad [67]$$

where

U = overall heat-transfer coefficient $\left(\text{Btu}/\text{sec-ft}^2\text{-}^\circ\text{R}\right)$,

A_C = cold-side area of the heat exchanger $\left(\text{ft}^2\right)$,

A_H = hot side of the heat exchanger $\left(\text{ft}^2\right)$,

h_H = hot-side heat-transfer coefficient $(Btu/sec\text{-}ft^2\text{-}°R)$,

h_C = cold-side heat-transfer coefficient $(Btu/sec\text{-}ft^2\text{-}°R)$,

η_C = surface efficiency of the cold-side heat-transfer area (finned surface).

The hot-side heat-transfer coefficient was based on the forced-convection equation of Sieder-Tate as presented in Ref 4. This equation was employed in the following form:

$$h_H = 0.02 \frac{K}{D} (Re)^{0.8} (Pr)^{1/3} \left(\frac{T_b}{T_s}\right)^{0.15}, \qquad [68]$$

where

K = thermal conductivity of the gas (Btu/sec-ft-°R),

D = tube diameter (ft),

Re = Reynolds' number,

Pr = Prandtl's number,

T_b = bulk temperature of the gas (°R),

T_s = heat-exchanger surface temperature (°R).

All hot-gas properties in the above equation were based on the bulk temperature, T_b, that is defined as follows:

$$T_b = T_C + \Delta T_{LM}, \qquad [69]$$

where

T_C = container-pressurant temperature,

ΔT_{LM} = log-mean temperature difference.

The log-mean temperature difference is defined as follows:

$$\Delta T_{LM} = \frac{T_{H1} - T_{H2}}{\ell n \left[\frac{T_{H1} - T_C}{T_{H2} - T_C} \right]}, \qquad [70]$$

where

T_{H1} = hot-gas inlet temperature (°R),

T_{H2} = hot-gas exit temperature (°R).

The heat-transfer coefficient on the pressurant (cold) side, h_C, was based on a heat-transfer correlation for free convection over a horizontal tube presented in Ref 4. The equation is stated as follows:

$$h_C = 0.53 \frac{K}{D_o} \left[Gr_D \, Pr \right]^{1/4}, \qquad [71]$$

where

K = thermal conductivity (Btu/sec-ft-°R),

D_o = outer tube diameter (ft),

Gr_D = Grashof number, based on the tube diameter,

Pr = Prandtl number.

The properties of the pressurant in this equation were based on the arithmetic mean of the pressurant bulk temperature, T_C, and the surface temperature T_s.

The surface efficiency, η_C, was calculated by the following expression:

$$\eta_C = 1 - \frac{A_F}{A_C}(1 - \eta_F), \qquad [72]$$

where

A_F = fin area (ft^2),

A_C = total cold-side heat-transfer area (ft^2),

η_F = fin efficiency.

The fin efficiency was calculated by a procedure outlined on page 84 of Ref 5. This procedure calculates the efficiency for a straight rectangular fin of the circular fin height and thickness and then applies a correction factor to account for the fact that the fin is circular rather than straight.

The actual heat-exchanger calculation process was carried out as follows. First, the following data were supplied as input:

Hot-gas inlet pressure and inlet and outlet temperature,

Pressurant-bulk temperature and required heat-transfer rate,

Tube inside and outside diameter, fin diameter, fin thickness, and number of fins per inch.

The wall temperature (initial trial) is calculated as the arithmetic mean of the hot-gas and pressurant-bulk temperatures. The total cold-side heat-transfer area required is then calculated with the heat-transfer equations previously discussed. With the heat-transfer area just calculated, a new value for wall temperature is calculated and compared with the previous assumed value. If the calculated and assumed wall temperatures are within 1°R, the required heat-exchanger tube length, weight, volume, and outlet pressure are calculated. If the temperature difference is greater than 1°R, the assumed temperature is replaced by the calculated value, and the computation is started over.

The analytical model was employed to calculate heat-exchanger weights and volume for all expansions employing an isobaric process. The heat source employed was an oxygen-hydrogen gas generator with exhaust products entering the heat exchanger at 100 psia and 1800°R temperature. The outlet temperature was arbitrarily assumed to be 1300°R to maintain the heat-exchanger wall temperature above the freezing point of water in the gas-generator exhaust. The heat-exchanger tube diameters were chosen so as to limit the inlet Mach number of the exhaust gas to a value of 0.2. As a result, the required tube diameters for the cases considered were in the order of 1.0 to 1.5-in. The Mach-number limitation was selected to minimize compressibility effects in calculating pressure losses and also to maintain the Reynolds' number at a value of 10,000 or greater, so as to stay within the range of application of the heat-transfer equation.

The fin geometry employed consisted of fin diameters of 2.0 in. The number of fins per inch was varied between 10 and 15, and the fin thicknesses varied between 0.01 and 0.02 in. depending on the magnitude of the heat-transfer rate. The heat-exchanger material employed was Allegheny-Ludlum A-286 steel to withstand the high gas temperatures.

b) External Heating of Helium Storage Sphere

An analytical inquiry was made into the feasibility of heating the helium in the storage vessel by a hot gas stream over the outside of the sphere as follows:

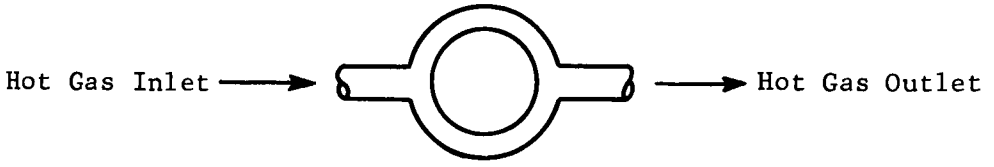

The hot-gas flow was to be contained in the annular space between the helium storage vessel and an outer vessel (both are spheres). The proposed source of hot gas was a lox-hydrogen gas generator.

Typical, expected flow conditions in the annulus were studied to determine flow velocities and Reynolds' numbers. Flow in the hot-gas inlet pipe (assumed 1-in. inside diameter) was that corresponding to a Mach number of 0.1 or less. The radial distance between the spheres was assumed as 1 in. Storage vessel diameter was assumed as 6 ft.

Based on a hot-gas composition of 86% H_2, 14% H_2O vapor (typical for an oxygen-hydrogen gas generator) and an initial temperature of 1800°R, flow velocities were found to vary from 526 ft/sec at the inlet to the sphere to a low value of 4.1 ft/sec at a point on the great circle midway between hot-gas inlet and exit. Calculations were based on a modified form of the continuity equation that reflected a drop of 800°R in the hot gas as it flowed from inlet to exit.

Examination of the available literature on calculation procedures for convective heat transfer contained little information for such a spherical, annular passage. Therefore, it was necessary to use a series of empirical relations obtained for geometries of a somewhat similar nature to calculate a value for the convective film coefficient on the outside of the storage sphere. Seven

independent calculations were made to solve for this coefficient: three were referenced to free fluid flow around a sphere; one for flow in an annular, cylindrical passage; one for flow in a very narrow, spherical annulus; and two for flow between two adjacent flat plates.

Values of the heat-transfer coefficient, as calculated from the seven different relations, varied from 0.8 to 18.4 $Btu/hr\text{-}ft^2\text{-}°R$. It was concluded that, because of the wide variation in heat-transfer coefficients, additional experimental work was necessary before a completely rigorous evaluation of this method of heating could be completed.

b. Gas Generator

A variety of gas generator fuels and oxidizers was considered to determine which combination would require the lowest system weight and be compatible with the propellants if the gas generator products were used directly in the propellant tanks.

A performance comparison of liquid propellants for the gas generator was achieved by using the products in a simple heat exchanger. The heat exchanger considered in the comparison is shown below:

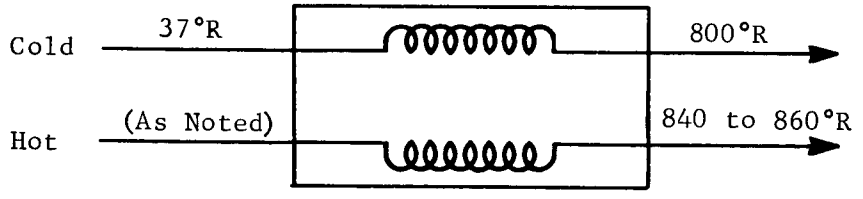

Table 14 Heat-Exchanger Results Obtained for the Pressure-fed Systems

Gas-Generator Propellants	Hot-Gas Inlet Temperature (°R)	Required Hot-Gas Flow Rate (lb/sec)
Hydrogen/oxygen	1800	0.55
50% N_2H_4-50% UDMH and N_2O_4	2060	1.02
N_2H_4 Decomposition	2460	0.82
N_2H_4 Decomposition	2060	1.09
50% N_2H_4-50% UDMH and H_2O_2	1822	1.26

Note: For a helium-flow rate of 0.95 lb/sec.

Combustion products from an H_2O_2 gas generator operating below 2000°R contains 80 to 85% hydrogen gas, the remainder being water. It was relatively higher in heat capacity than other products due to the hydrogen gas, and, therefore, had a lesser flow-rate requirement. The integrated gas-generator propellants for the oxygen-hydrogen combination was lower than for other propellants.

The weight of an oxygen-hydrogen gas generator was scaled from units manufactured by Sundstrand Aviation of Denver (Ref 8). The following empirical expression was derived:

$$W_{gg} = 8\sqrt{\frac{\dot{m}}{0.0417}}, \qquad [73]$$

where

W_{gg} = weight of gas generator (lb),

$\dot{m}$ = flow rate through gas generator (lb/sec).

4. Vehicle Thermal Analysis

To design a pressurization system for optimum operation in any vehicle, external environmental effects must be carefully considered. Gas temperatures and pressures resulting from convective heat inputs along with radiative heat inputs have a direct bearing on system performance. In this study, vehicle and system operations were considered under space vacuum conditions only; i.e., in earth orbit, in earth-to-lunar transfer orbit and in lunar orbit. Under these conditions, then, only radiative heat inputs to the vehicle are considered. The vehicle thermal analysis was performed to evaluate the effect of space heating on pressurization system weight and propellant boiloff. The following values had to be determined:

1) Space radiation flux to the vehicle,

2) Geometric view factors of the vehicle internal surfaces,

3) Equivalent conductances for radiation,

4) Vehicle heat transfer with heat leak into propellant tanks.

These four steps are schematically shown in Fig. 26 for the studies during the secondary and final screening of the pump-fed systems only.

The radiation flux to the external skin of the vehicle was determined by a computer program, "Radiation Flux to an Orbiting Satellite" (Martin PD016), which accounted for solar, reflected, and emitted radiation.

To evaluate internal vehicle radiation, the geometric view factors and the equivalent conductances had to be determined. A geometric view factor is the fraction of the total radiation emitted from one surface that is intercepted by another. By using the surface areas, surface characteristics, and geometric view factors, the equivalent conductances are determined.

The vehicle heat transfer during the secondary screening was determined by using the "Aerodynamic and Structural Heat Transfer," computer program (Martin FD018). In the final screening, the vehicle heat transfer was evaluated by the "Propellant, Tankage, and Pressurization System," computer program (Martin ØB014).

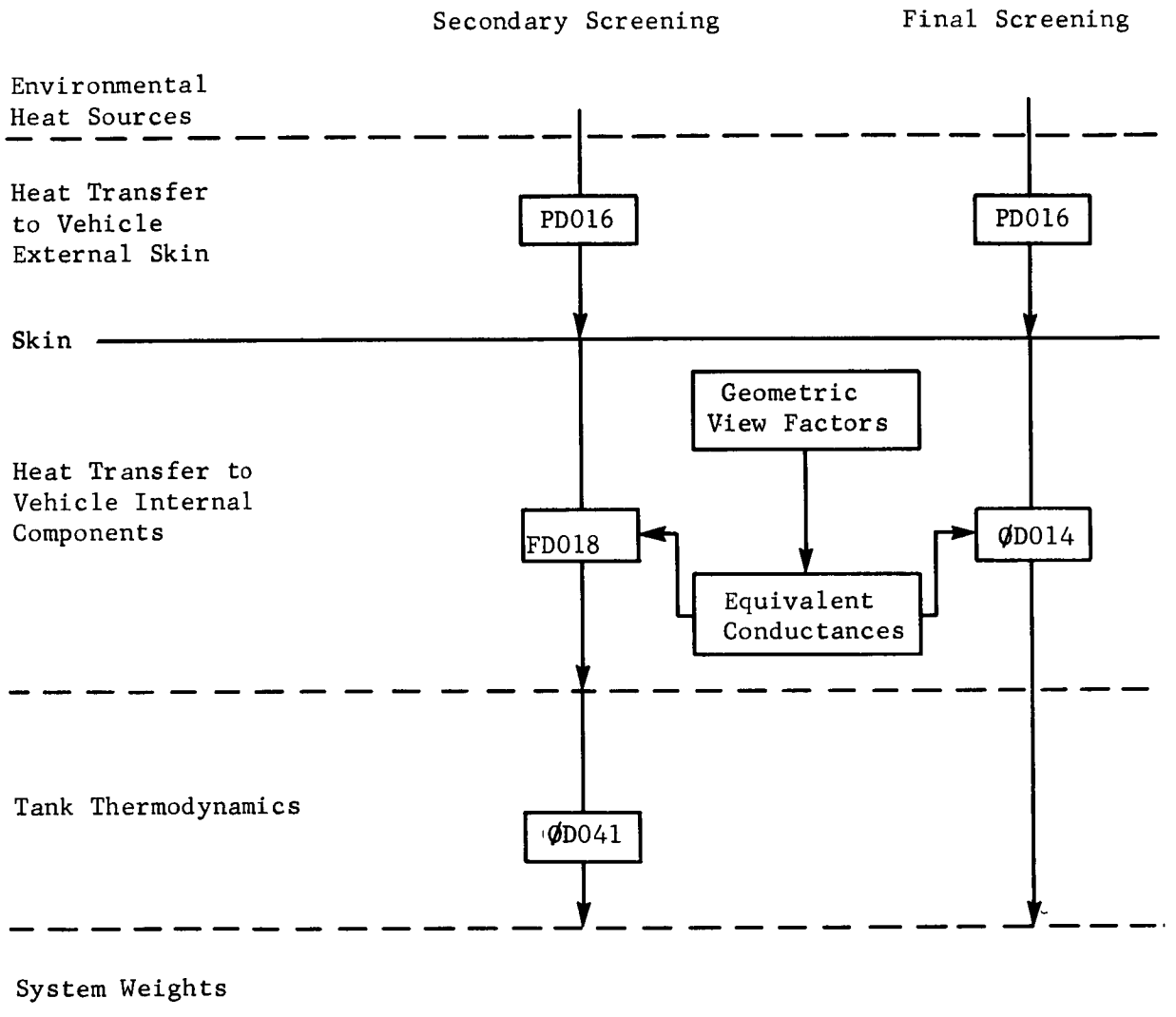

Fig. 26 Computer Programs Used for Vehicle Thermal Analysis

a. Space Heat Flux

Computer program PD016 computes the major space thermal radiation flux to a specified surface of a space vehicle in an elliptical orbit. Radiation sources considered are:

Direct solar radiation,

Solar radiation reflected from the earth,

Direct earth low-temperature radiation,

Solar radiation reflected from the moon,

Direct lunar radiation.

The only space radiation source neglected was galactic radiation which is extremely small (equivalent to a 20°R black body).

The program computes and lists the vehicle position and the radiation fluxes absorbed by the specified surface at time intervals until the vehicle again reaches its original position. The program allows the option of assuming the vehicle has a fixed orientation with respect to either the earth or the sun.

The program inputs used for this study were:

Earth orbit - 110 miles, no eccentricity, 88 min;

Lunar orbit - 30 miles, no eccentricity, 115 min;

Transfer orbit approximated by an elliptical orbit - perigee of 110 miles, eccentricity of 0.967;

Solar absorptivity of 0.25;

Low temperature absorptivity of 0.13;

Vehicle is sun oriented.

The external surface was considered to be painted to reduce the heat absorption and, thereby, reduce the heat leak into the propellant tanks. A silicone base titanium oxide pigment paint, which is stable under ultraviolet radiation and impingement, will have these absorption values.

The heat flux into the external skin of the vehicle is shown in Fig. 27, 28, and 29.

b. Internal Radiation

Several vehicle internal configurations were considered. Figure 30 shows the vehicle configuration used during the secondary screening. Figures 31 and 32 represent vehicle configurations used during the final screening for primary pump-fed Systems 6 and 8, respectively.

To determine the internal radiation heat transfer, geometric view factors were determined. The values were computed by use of the "Form Factometer".

The Form Factometer is a parabolic mirror approximately 1 in. in diameter which has been subdivided into 40 zones. Each zone is worth 1/40 or 0.025 of the total view factor of the mirror. The local view factor, F_{i-j}, from a point on surface i to all of surface j, is computed by proportioning the area of the mirror encompassed by the image of surface j. The mirror is viewed along its parabolic axis, and the image is either recorded by sketch, using a form as shown by Fig. 33, or by photograph. In using the mirror, readings were taken systematically at various positions on the given surface. The local view factors obtained were then plotted as a function of angular position of the mirror and are shown by Fig. 34.

Only certain view factors had to be determined through the use of the Form Factometer. The remaining view factors were determined by the following relationships:

$$A_i F_{i-j} = A_j F_{j-1} \quad \text{(Reciprocity rule)} \qquad [74]$$

$$\sum_{j=1}^{n} F_{i-j} = 1.0. \qquad [75]$$

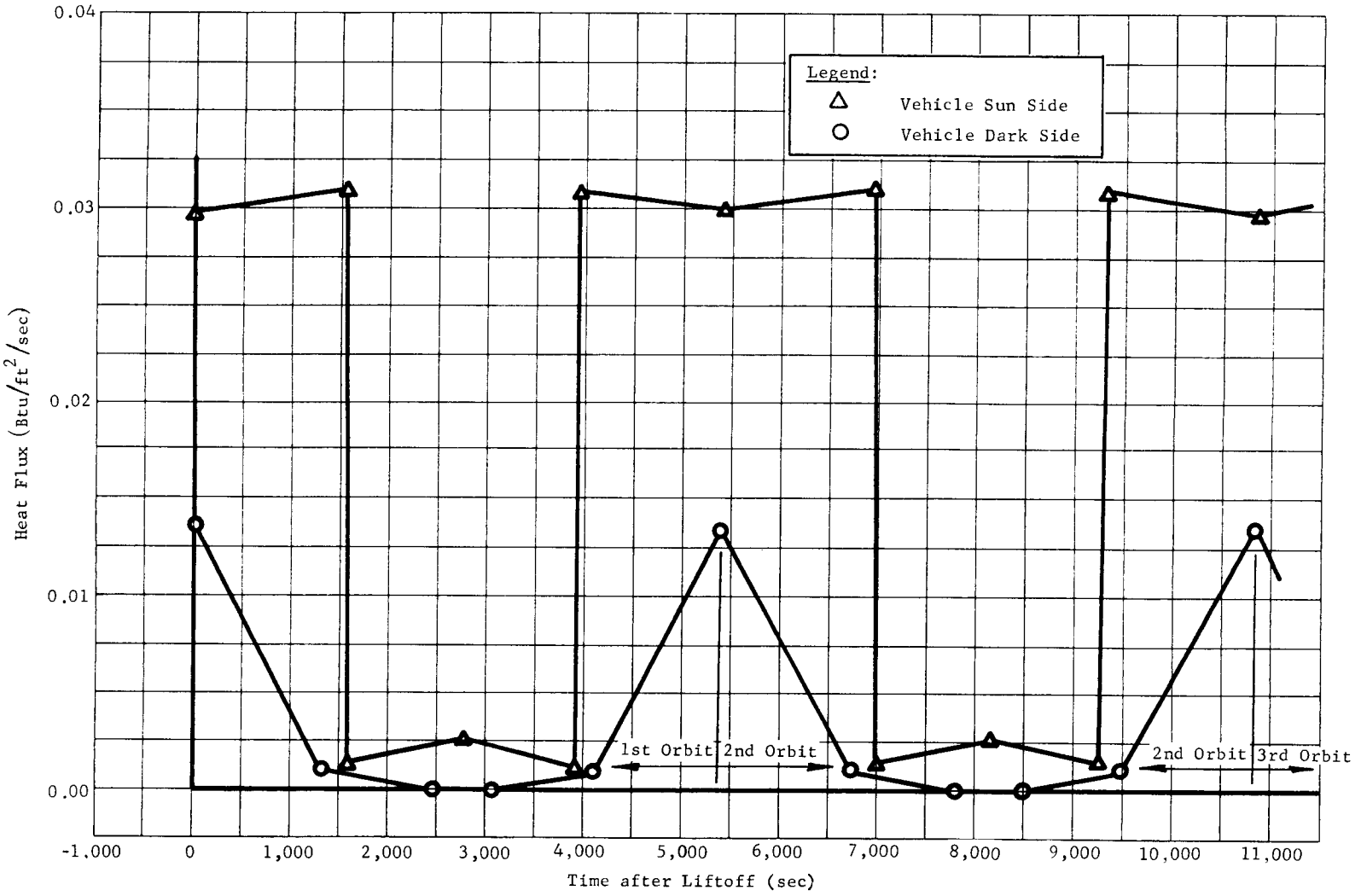

Fig. 27 Solar Heat Flux Curves for Earth Orbits

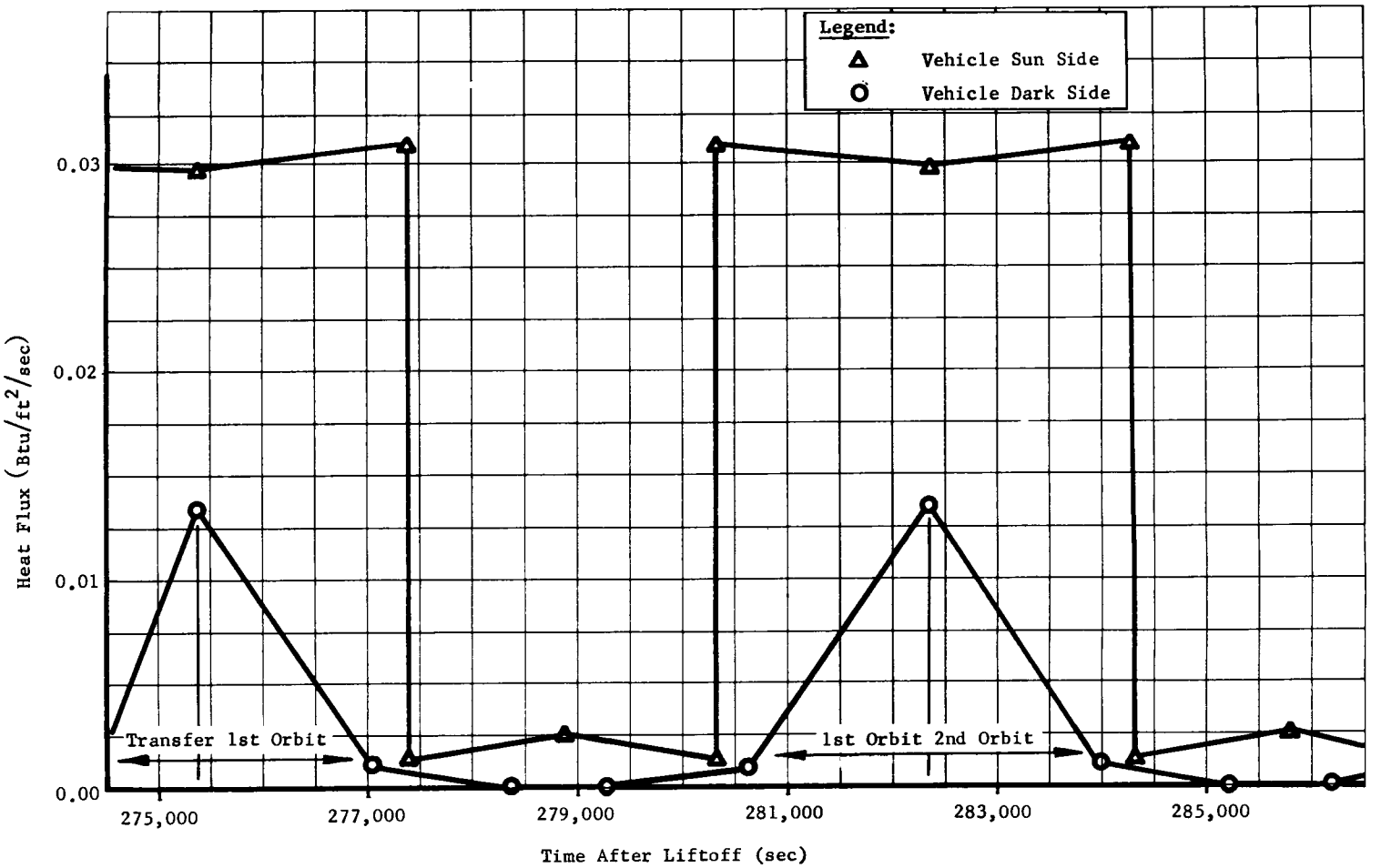

Fig. 28 Solar Heat Flux Curves for Lunar Orbit

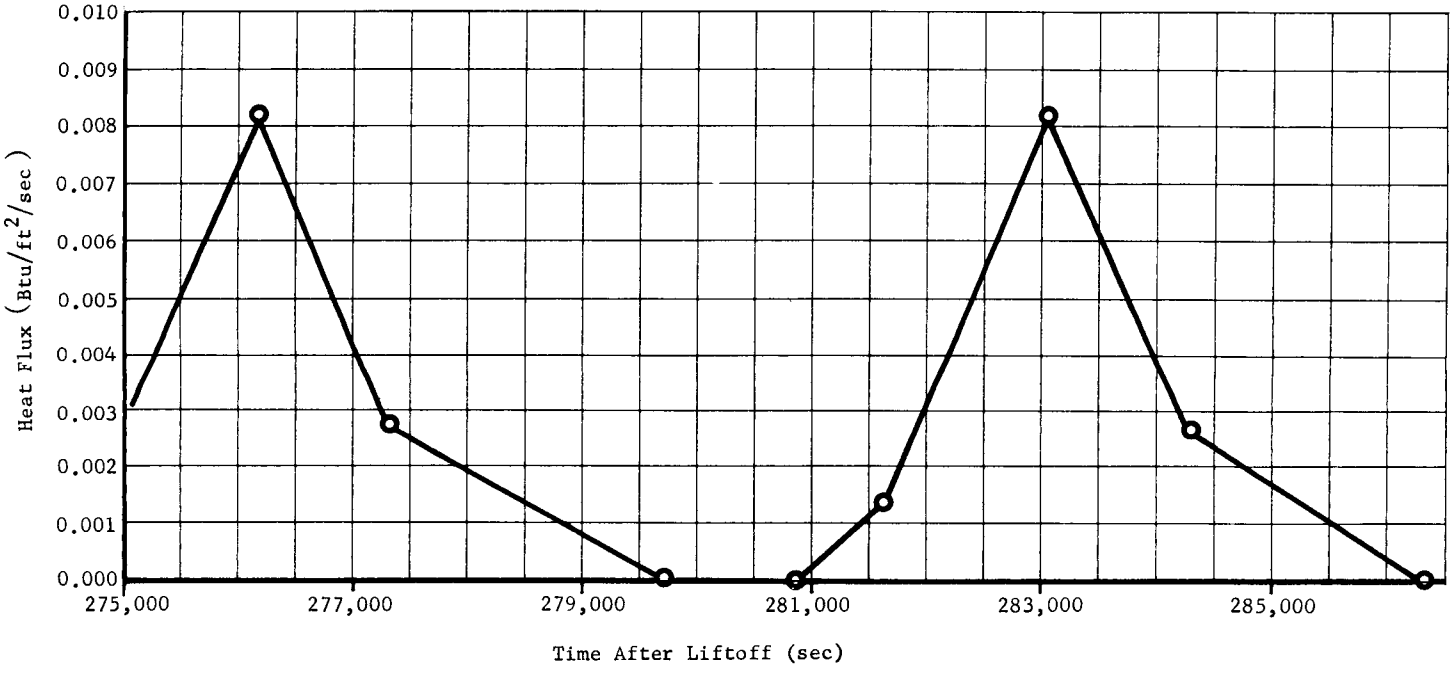

Fig. 29 Solar Heat Flux Curves for Lunar Orbit, Aft End of Vehicle

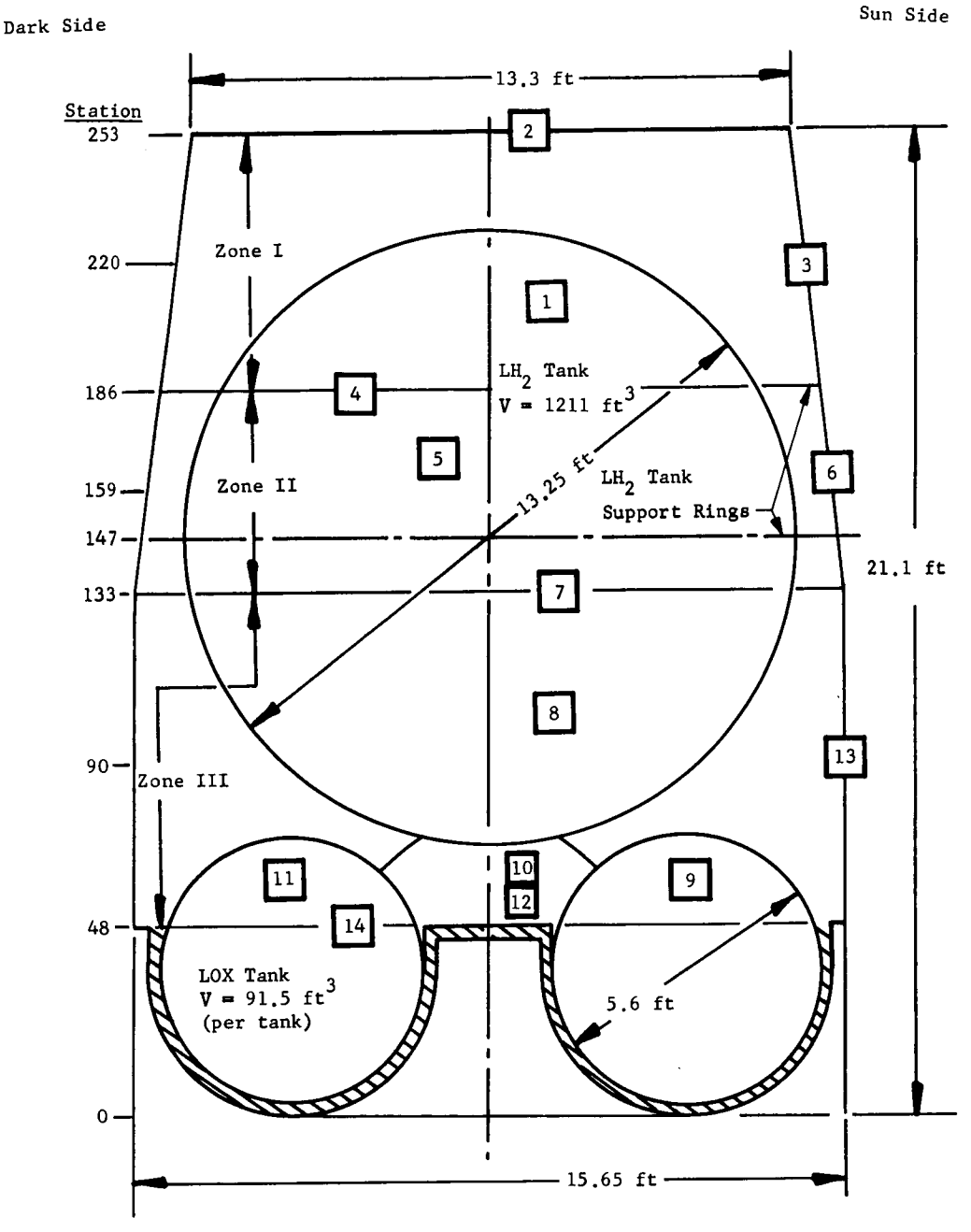

Fig. 30 Tank Configuration for Radiation Heat Transfer Analysis, Secondary Screening

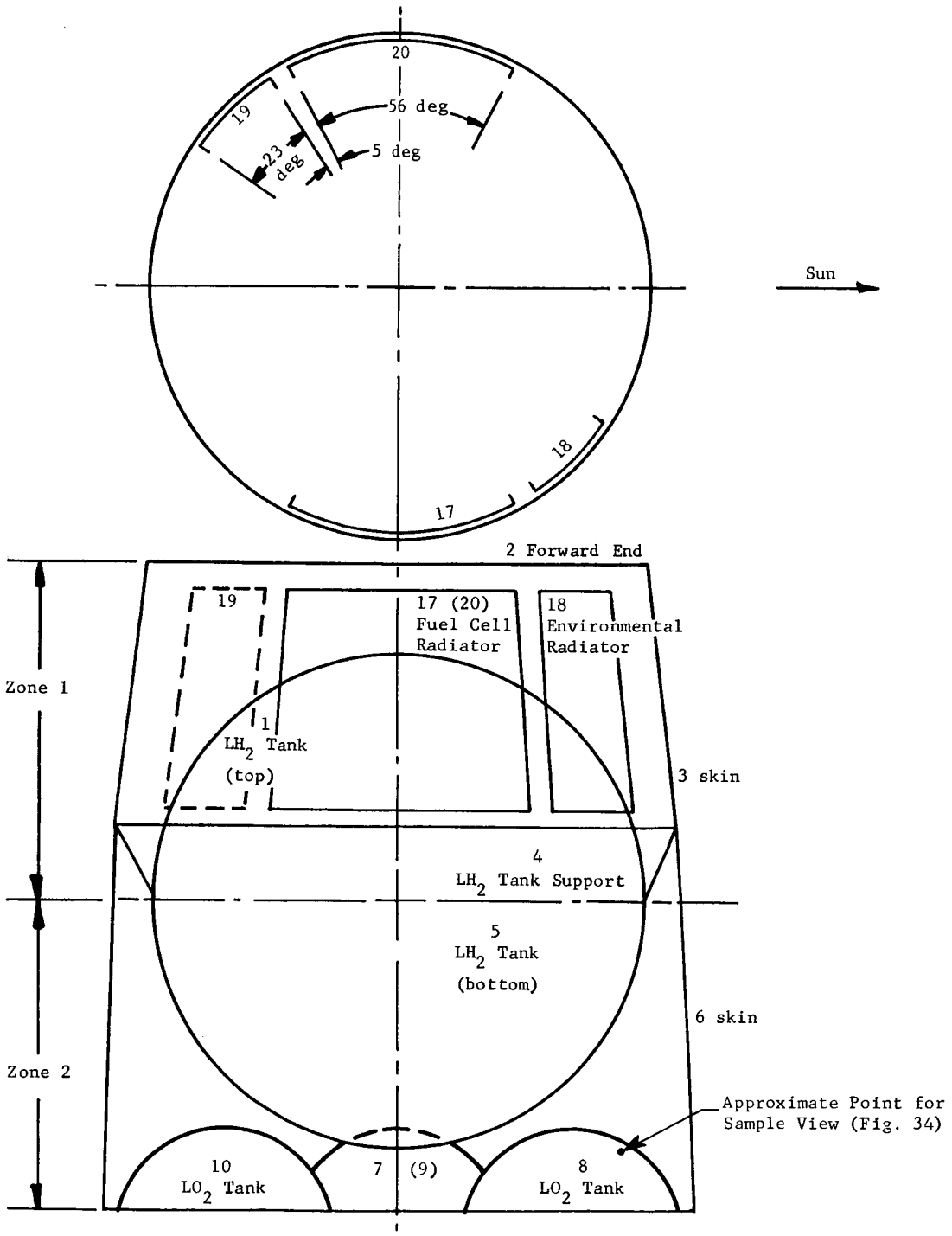

Fig. 31 Vehicle Configuration for Radiation Heat Transfer Model for System 6, Final Screening

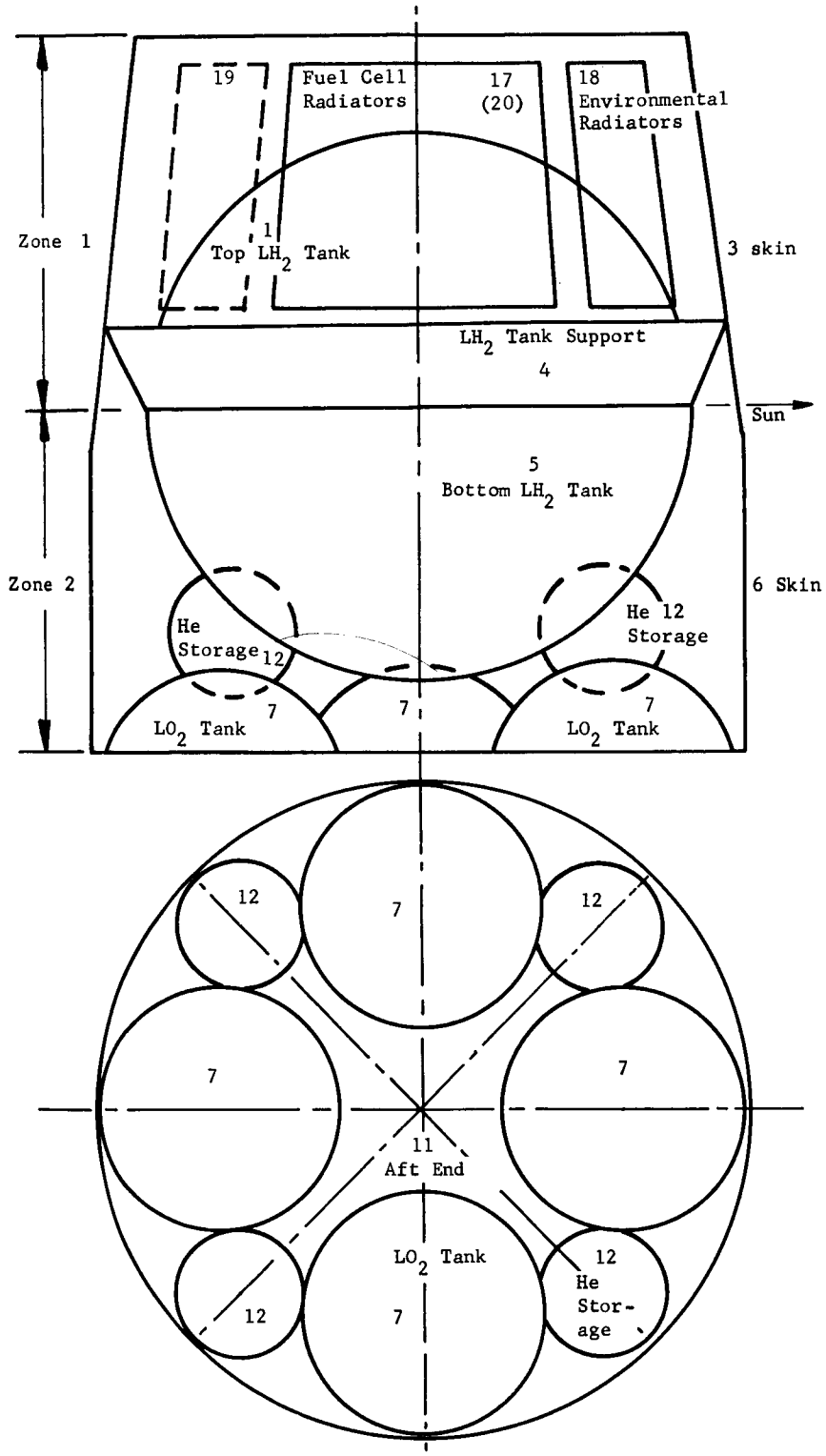

Fig. 32 Vehicle Configuration for Radiation Heat Transfer Model for System 8, Final Screening

Note: 1. Mirror on body No. 8 LO_2 Tank at position θ = 30 deg and φ = 30 deg.
2. θ = longitudinal position with θ = 0 at the plane of symmetry between surfaces 8 and 5. φ = latitudinal position with φ = 0 at north pole of surface 8.

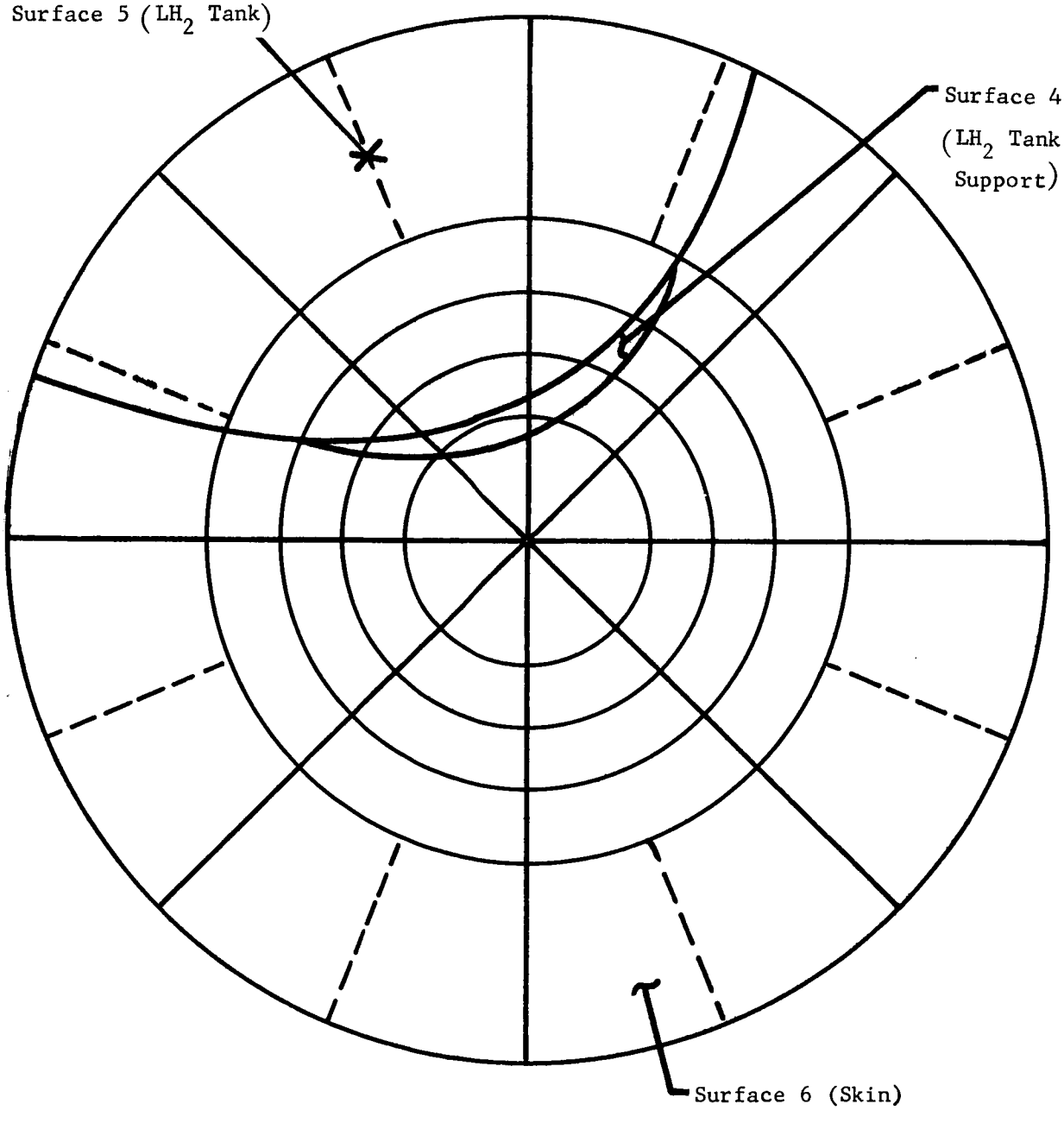

Fig. 33 Form Factometer Sample View Sheet for System 6

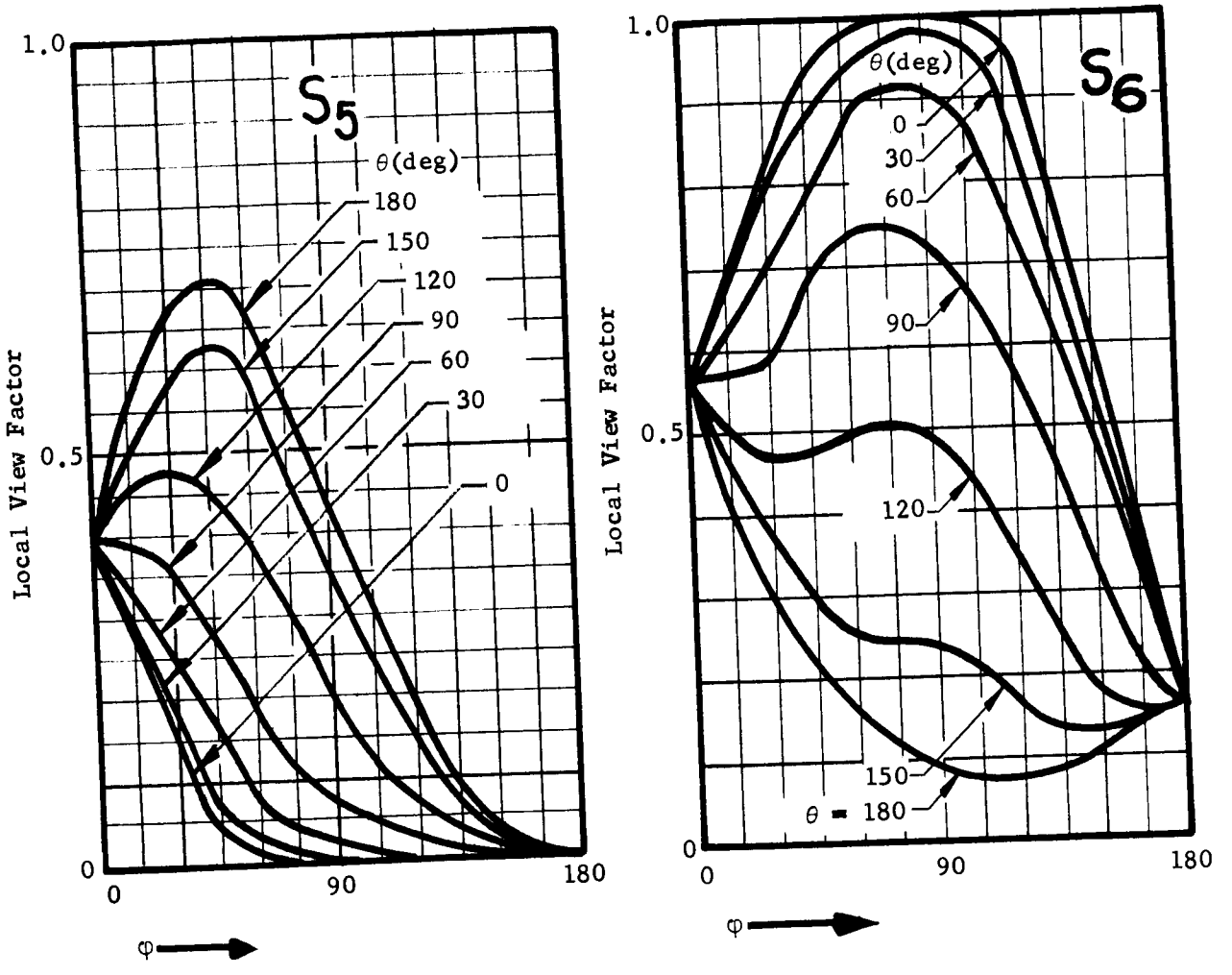

Fig. 34 Sample Local View Factors of Surfaces 5 and 6, As Seen From Surface 8

Some of the geometric view factors for surfaces of simple shape were checked by hand calculations, and good agreement was obtained with the results of the Form Factometer.

The equation for the total view factor between surfaces i and j may be written as

$$F_{i-j} = \frac{1}{A_i} \int_{A_i} F_{i-j} \, dA_i, \qquad [76]$$

where A_i is the total area of surface i. Thus, by measuring the local view factor at various points on surface i, the total view factor can be computed. Since the equation is normally solved by numerical means, it is more appropriately written as

$$F_{i-j} = \frac{1}{A_i} \sum_{n=1}^{m} F_{i-j,n} \, \Delta A_{i,n}, \qquad [77]$$

where m equals the number of data points (i.e., the number of values of F_{i-j}) measured on surface i.

When dividing a surface into incremental areas, the method and size is arbitrary. In a flat surface, a grid division could be used. In a sphere, longitudinal and latitudinal position can be used for division. For the analysis of this vehicle, the liquid hydrogen and oxygen tanks were divided into longitudinal and latitudinal position. As an arbitrary reference point on the liquid oxygen tank, the top or north pole of the sphere was taken as $\varphi = 0$. For a longitudinal position, $\theta = 0$ was taken on a plane of symmetry between the two propellant tanks. Figure 33 is a typical view sheet made from the Form Factometer. Figure 34 shows the results plotted from the view sheets.

The numerical integrations of summations were performed on the IBM 1620 computer using Simpson's Rule. For cases where surface i was either spherical in shape or the frustum of a right-circular cone, Equation [76] was modified so that F_{i-j} was expressed in terms of parameters describing the position of the Form Factometer mirror on surface i.

The net heat transfer between surfaces was calculated by obtaining the equivalent conductances. The internal surface of the external skin was considered to be polished aluminum, and the insulation was considered to be covered with aluminum foil to reduce the heat transfer to the propellant tanks.

The equivalent conductances were calculated from the geometric view factors and the emissivity of the various surfaces by using an equivalent electrical network:

$$\left.\begin{aligned} J &= \rho G + \epsilon E_B, \\ q_{net} &= A(J - G) = A \frac{\epsilon}{\rho} (E_B - J), \\ q_{i-k} &= A_i F_{i-k} (J_i - J_k), \\ q_{i-k} &= A_i \mathcal{F}_{i-k} (E_{Bi} - E_{Bk}), \end{aligned}\right\} \qquad [78]$$

where

J = radiosity (the rate of radiation emitted, reflected, and transmitted from a surface per unit area),

G = irradiation (the rate or radiation incident on a surface per unit area),

E_B = black body emissive power,

ρ = reflectivity,

ϵ = emissivity,

A = area,

F = geometric view factor,

$\mathcal{F}$ = gray body view factor.

A typical equivalent electrical network for radiation between two nodes is illustrated as follows:

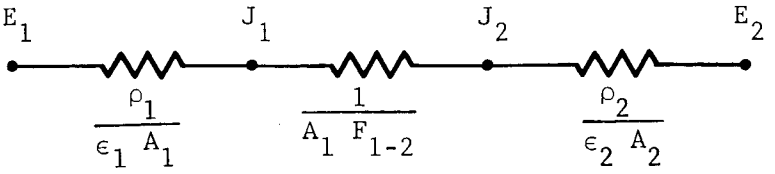

By taking values of $E_1 = 1.0$ and $E_2 = 0.0$, the current flow from J_2 to E_2 would represent the value of $A_1 \mathcal{F}_{1-2}$ which is the equivalent conductance. The values of emissivity and reflectivity were taken at the average vehicle temperatures of each surface. The total heat transfer between two surfaces would be

$$Q_{1-2} = \sigma A_1 \mathcal{F}_{1-2} \left(T_2^4 - T_1^4\right), \qquad [79]$$

where

σ = Stefan-Boltzmann constant,

T = temperature,

Q = total heat flux,

$A_1 \mathcal{F}_{1-2}$ = equivalent conductance.

The values obtained for geometric view factors for internal radiation of the vehicle as shown in Fig. 30 are listed in Appendix D. For the equivalent conductances, the vehicle was divided into two sections by passing a plane through the vertical axis. One section was sun oriented and the other section was considered to be the dark side facing away from the sun. The surfaces were designated dark and light side by the letters D and L. The view factors between the light and dark sides are small and are taken as zero.

c. Vehicle Analysis During Secondary Screening

The vehicle configuration shown in Fig. 30 was used in this study phase. The liquid hydrogen tank is supported by two rings at Stations 133 and 186. The radiation calculations for the interior of the vehicle were considered in three zones established by the tank support rings.

By using the "Aerodynamic and Structural Heat Transfer", computer program, the heat transfer by radiation and conduction in the vehicle was determined. This heat transfer included the heat leaks into the propellant tanks. The program used a thermal nodal (lumped) system to approximate the vehicle. The nodal system used is shown in Appendix D. The heat transfer into the tanks was then used as input into the tank pressurization computer program.

The following conditions were used in the thermal model:

The engine is a conduction heat source at a constant temperature of 350°R;

The forward surface of the module is at a constant temperature of 520°R;

An integrated value of 5.22×10^{-4} Btu in./hr-ft^2-°R was used for the super-insulation thermal conductivity;

The vehicle external skin is 0.1-in. thick aluminum;

The super insulation is covered with aluminum foil

The inside of the external skin is polished aluminum;

The heat flux to the external skin is obtained from the PD016 computer program;

The tank walls and propellants are infinite heat sinks at constant temperatures of 40°R for the liquid hydrogen tank and 163°R for lox tanks;

The tank supports are made of titanium;

Aluminum vent and suction lines were used and are detailed as follows;

Tank	Line	Inside Dia (in.)	Length (in.)	Material Cross Section ($in.^2$)
Liquid Hydrogen	Suction	2 1/2	24	5.14
Liquid Hydrogen	Vent	2 5/8	54	0.13
Liquid Oxygen	Suction	1	78	0.885
Liquid Oxygen	Vent	3/4	142	0.037

The mission plan was approximated by using as an average;

One 90-minute earth orbit,

The first two hours of transfer orbit,

Two 115-minute lunar orbits,

The first two hours of return orbit.

Using one-half in. of insulation, the heat flow into each of the four lox tanks was 70% through conduction and 30% through radiation. For the liquid hydrogen tank, using the same thickness of insulation, 30% of the heat flux into the tank was by conduction and 70% by radiation. The average heat flux (Btu/sec units for 1/2 in. of insulation) into each propellant tank is:

	Liquid Oxygen	Liquid Hydrogen
Earth Orbit	0.0086874	0.07828
Transfer	0.0086972	0.07731
Lunar Orbit	0.0082096	0.07568

As noted in the preceding paragraph, 1/2 in. of insulation was used. This was based on the results of a parametric study of the thickness of insulation versus total system weight. The study indicated that the optimum thickness of insulation was approximately 1/2 in. for five systems studied (see Chapter III.C.5). The systems studied varied from ambient to liquid oxygen pressurant gas temperature at the inlet to the propellant tanks. The results indicated that the insulation thickness will not vary for changes of pressure or temperature in the pressurant storage subsystem. However, propellant tank configuration and the temperature of the propellants will dictate insulation thickness, so that this particular optimum insulation will not be valid for all vehicles.

d. Vehicle Analysis During Final Screening

Two vehicle configurations were used in this analysis as shown in Fig. 31 and 32. One system contained the pressurant storage inside the liquid hydrogen tank, and the other system contained four spherical pressurant storage spheres between the propellant tanks. These pressurant storage spheres were at ambient temperatures initially. The liquid hydrogen tank was supported by one conical ring at tank centerline. This placement divided the internal radiation analysis into two zones. The heat loads of four radiators were also included in the analysis.

The heat leaks into the propellant tanks were obtained by using a thermal nodal system shown in Appendix D and the heat leaks were evaluated by the "Propellant, Tankage, and Pressurization System," computer program. This program also evaluated the total vehicle thermodynamics.

The following values were used to describe the vehicle configurations:

The engine is a conduction node at a constant temperature of 350°R;

Plume radiation from the engine to the aft end of the vehicle is considered during engine firing;

The forward surface of the module is a constant temperature of 520°R;

The vehicle external skin is 0.01-in. thick aluminum;

Tank insulation is covered with aluminum foil;

The inside of the external skin is polished;

The heat flux to the external skin is obtained from the "Radiation Flux to an Orbiting Satellite" computer program;

Tank supports are made of titanium;

The thermal conductivity values of the super insulation are;

Earth to moon (both tanks) - 7×10^{-4} Btu-in./ hr-ft^2-°R,

LH_2 tank (moon to earth) - 2.5×10^{-4} Btu-in./ hr-ft^2-°R,

LO_2 tank (moon to earth) - 3.2×10^{-4} Btu-in./ hr-ft^2-°R,

Note: The insulation thermal conductivity on the earth-to-moon trajectory was higher than on the return trip because all the air in the insulation had not been pumped out. The difference between the thermal conductivities on the tanks during the return trip was attributed to the different propellant tank surface temperatures.

Density - 10 lb/ft^3,

Aluminum vent and suction lines are used and are described as follows;

Tank	Line	Inside Dia (in.)	Length (in.)	Material Cross Section (in.^{2})
Liquid Hydrogen	Suction	2 1/2	24	5.14
Liquid Hydrogen	Vent	2 5/8	54	0.13
Liquid Oxygen	Suction	1	78	0.885
Liquid Oxygen	Vent	3/4	142	0.037

Radiators were located in the surface of the vehicle skin with only heat transfer by radiation being considered. There were two environmental radiators (16.5 sq ft each) with a heat load of 109.5 Btu/ft^2-hr each and two fuel cell radiators (40 sq ft each) with a heat load of 351.5 Btu/ft^2-hr each;

Insulation thicknesses and locations were:

Super Insulation -

0.5 in. covering the ambient storage spheres,

0.5 in. covering the liquid hydrogen tank,

0.5 in. covering the liquid oxygen tank,

0.2 in. next to the forward end of the vehicle,

0.6 in. on the inboard side of the environmental radiators,

1.0 in. on the inboard side of the fuel cell radiators;

Polyurethane Foam -

1.0 in. covering the bottom of the liquid oxygen tanks on the outside of the super insulation,

1.0 in. on the aft end of the vehicle between the liquid oxygen tanks.

The nodal system used in the final screening is discussed in Appendix D. Nodes 35, 36, and 37 were used in the ambient stored pressurant system only. When the pressurant storage sphere was located in the liquid hydrogen tanks, the heat transfer to the sphere was from the liquid hydrogen and was considered in the tank thermodynamics. In the ambient system, the heat loss by conduction and radiation from the pressurant sphere has a direct effect on system weight since the larger the heat loss the greater the residual gas density. To reduce the number of nodes used, the four lox tanks were lumped and considered as a single tank containing a single total mass of liquid.

The heat leaks into the propellant tanks are 64,161 Btus into the liquid hydrogen tank and 23,546 Btus into the four lox tanks for the total mission time of 158 hr.

The vehicle thermal analysis computes the heat leak into the propellant tanks which determines propellant temperatures and the amount of propellant boiloff and vapor vented. The exact expansion of the ambient pressurant sphere is also determined. The vehicle analysis is peculiar to its design, although the method employed would be valid for any configuration.

e. Conclusions

A major problem with a space vehicle using cryogenic propellants, is to limit propellant boiloff due to space radiation. An optimum insulation thickness for the propellant tanks exists which results from a minimum vehicle weight. This optimization thickness is a function of vehicle design insulation weight and flight mission. The size and location of the pressurization system has virtually no effect on the heat transferred into the propellant tanks. For the vehicles in this study, the optimized insulation thickness of the propellant tanks was 1/2 in.

Radiation heat transfer inside a vehicle using cryogenic propellants is important because of the significant temperature difference of surfaces. It is necessary to condition all surfaces of the vehicle, internally and externally, to reduce the radiation heat transfer from space to the propellant tanks.

5. Total System Weight Analysis

Since one of the main criteria for system selection was weight, a detailed system weight total was computed for each system. The calculation methods of total system weights were improved as the study progressed. As an example, external heating of the propellant tanks was not considered in the initial studies but was subsequently included in the later analyses.

Although heating to the external surface of the propellant tanks was not considered in the initial studies, the ranking of the systems would be the same if external heating had been considered.

Total system weights were computed for various tank inlet temperatures, since tank inlet temperature has a weight effect on all components of the system. The total system weights were compiled using optimized components; i.e., using the optimum pressurant storage vessel for the particular expansion process used. Therefore, the optimum weight of each system studied included the optimization of each portion of that system.

To determine the minimum weight of each system, the total system weights were determined as a function of pressurant tank inlet temperature. Figure 35 is a typical example of such data. Items used in the system weights were obtained where possible from generalized data, such as the example shown in Fig. 36. In this case, the gas and vapor weights in the liquid hydrogen tank are independent of the type of pressurant storage system used. These weights are only a function of the temperature entering the hydrogen tank and, therefore, are applicable to all systems studied that use helium as a pressurant.

a. Initial Screening, Pressure-Fed Systems

For the initial screening of pressurization systems for pressure-fed engines, the total system weights were obtained by the use of an IBM 1620 computer program which calculated the quantities of pressurant required and propellant boiloff. The heat exchangers needed to provide the required tank inlet temperatures were sized by the use of another IBM 1620 computer program. Hand calculations were used to determine pressurant storage system weights for various expansion processes.

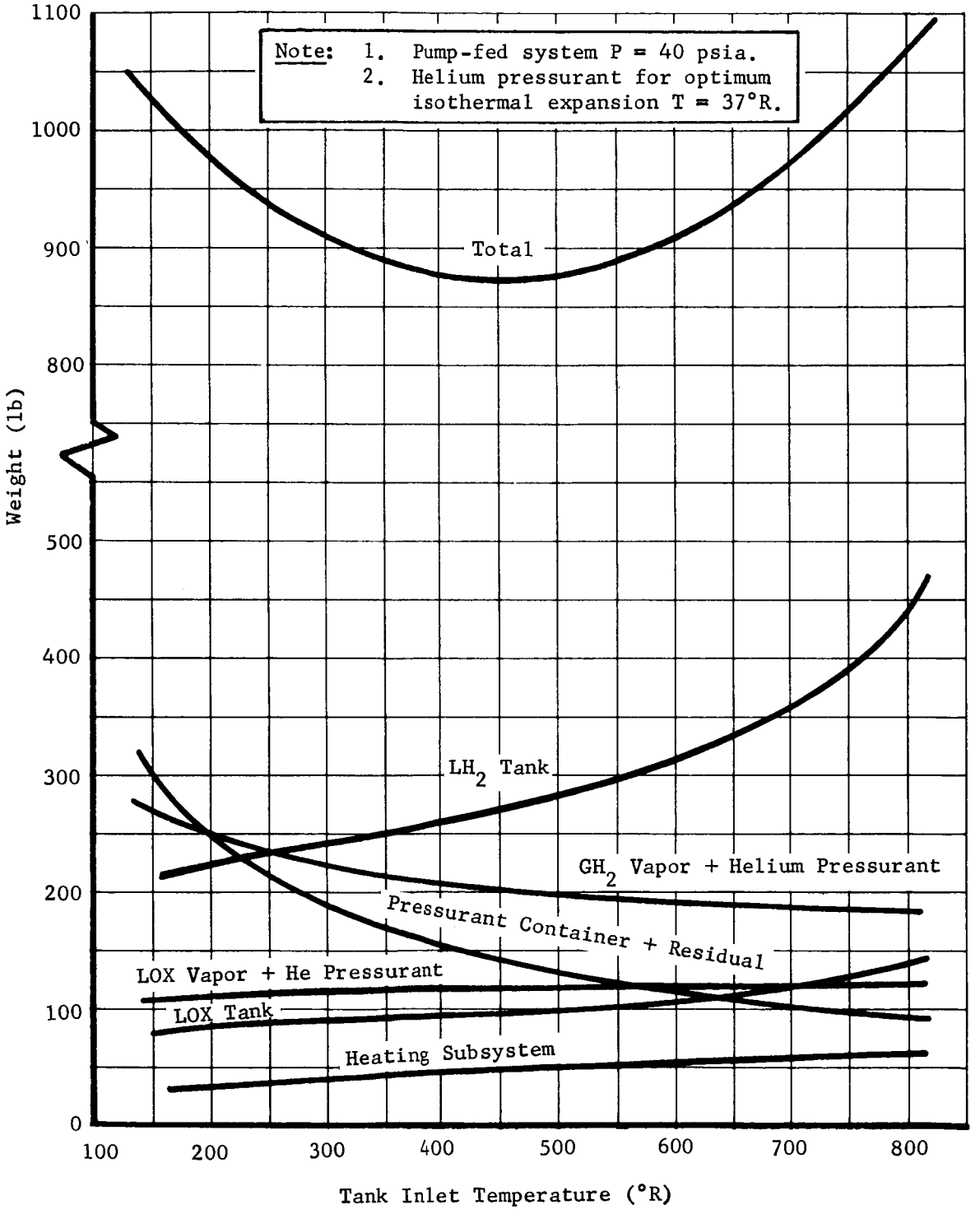

Fig. 35 Total System Weight

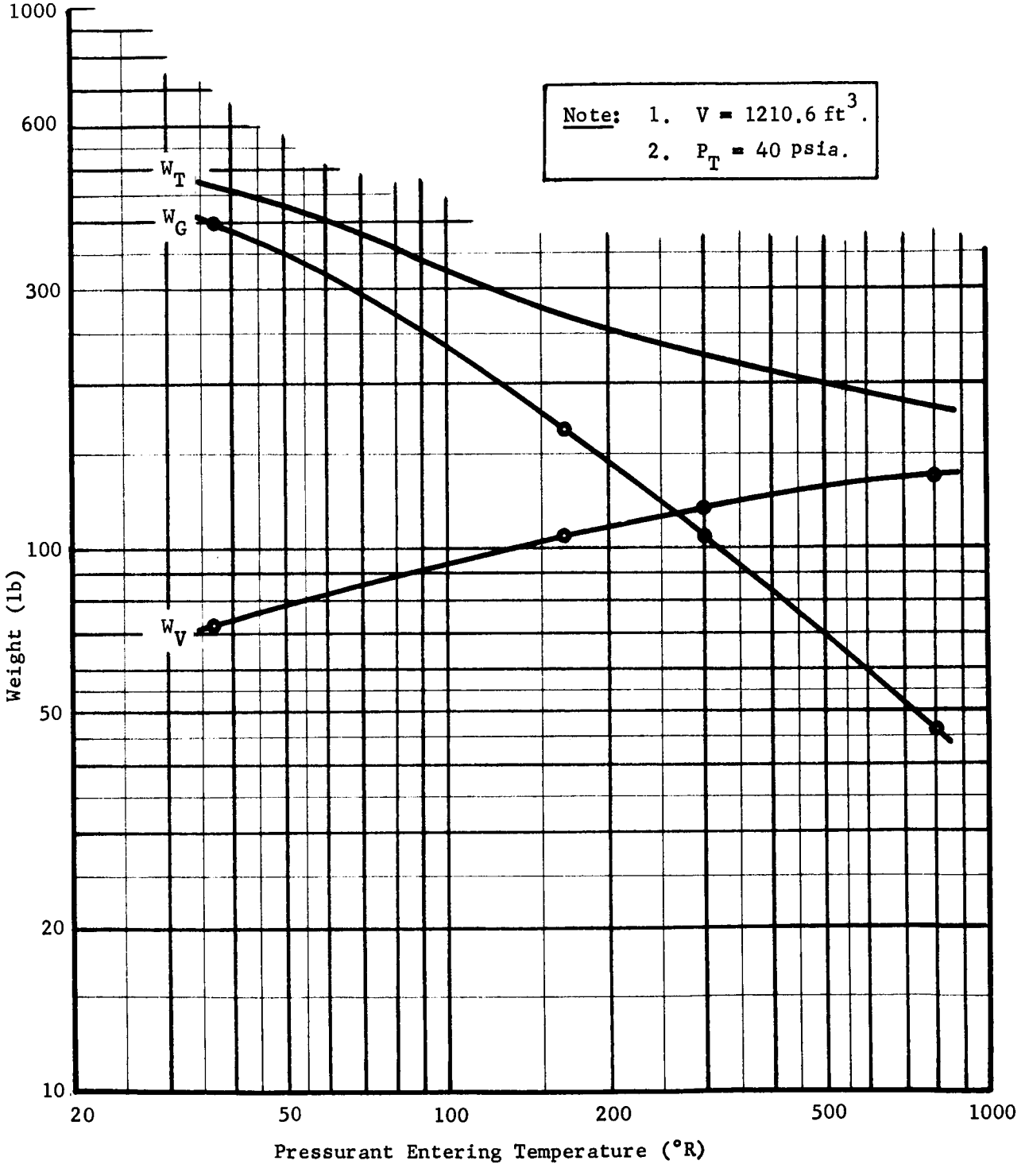

Fig. 36 Helium and Vapor Weights for Liquid Hydrogen Tank

The factors considered during this phase of the study were:

Items included in system weight, as necessary;

Liquid hydrogen tank (spherical),

Liquid oxygen tank (toroidal),

Hydrogen vapor,

Oxygen vapor,

Pressurant,

Pressurant container and residual,

Gas generators,

Heat exchangers,

Propellants for gas generator,

Pumps,

Heat transfer was not considered to or from the external walls of the propellant tanks to simplify the analysis;

Heat capacity of the storage sphere wall was not considered in the expansion process;

For sizing purposes, the spherical liquid hydrogen tank was assumed to have an ullage of 5% and an outage of 4%. The working stress used for the 6Aℓ-4V titanium skin was 120,000 psi (Ref 9);

For sizing purposes, the toroidal lox tank was assumed to have an ullage of 3% and an outage of 2%. The working stress used for 2219-T87 aluminum skin was 53,300 psi (Ref 10) and was based on liquid oxygen temperature;

Tank pressures during burn periods were 170 psia with an initial loaded pressure of one atmosphere;

The mission profile studied was;

Firing	Propellant Expelled (lb)	Firing Time (sec)	Time from Launch (hr)
1	980	18.7	26
2	980	18.7	48
3	18,280	349.0	78
4	980	18.7	126
5	6,576	125.5	138
6	233	4.45	158
7	233	4.45	186

Note: An engine mixture ratio of 5 to 1 was used.

The final or lowest pressure allowed in the storage sphere was 300 psia which provided 130 psi for valve and line losses;

The gas generator weights were determined from an empirical expression described in Chapter III.C.3;

Propellant quantities required for the gas generator and the heat exchanger size were determined by using an IBM 1620 heat exchanger program which is also described in Chapter III.C.3;

Wall thickness of the propellant tanks and storage spheres was determined by hoop stress requirements using the following formulas;

$$\text{Sphere-} \quad t = \frac{PR}{2\sigma_W}$$

$$\text{Torus-} \quad t = \left[1 + \frac{a}{a - R}\right] \frac{PR}{2\sigma_W}, \text{ (Ref 11)} \qquad [80]$$

where

t = wall thickness (in.),

P = maximum pressure $\left(lb_f/in.^2\right)$,

R = tank radius (small radius of torus) (in.),

a = large radius of torus (in.),

σ_W = working stress $\left(lb_f/in.^2\right)$;

The working stress used for the pressurant sphere was the lesser of ultimate strength/2.0 or yield strength/1.67 (Ref 12). The maximum allowable working stress of titanium was taken as 120,000 psi;

The working stress for the propellant tanks was the minimum of ultimate strength/1.4 or yield strength/1.1 (Ref 13).

The primary systems were defined as systems using helium as a storage pressurant at 37°R. The pressurant was to be expanded and heated before entering the propellant tanks. In addition, the system detail design was to be limited to the use of state-of-the-art technology. Figure 5 is a simple schematic of the primary system.

The total system weights computed for the primary systems are shown in Table 15.

The advanced systems were simply defined as systems not constrained by state-of-the-art technology.

Of the advanced pressure-fed systems considered (see Fig. 6), several were eliminated from consideration before the weight analysis.

Hydrogen pressurant used to pressurize the lox tank (System 5) was eliminated because of the low energy required to initiate a catastrophic explosion as described under Chapter III.

System 6, which involved injection of hypergolic reagents into the propellant tanks, was eliminated from consideration because testing did not prove its feasibility. The tests performed and results obtained are described elsewhere in this report.

System 10 required a separator to remove solid and condensible combustion products. Separators would lower the pressurant temperature and thus increase the size and weight of the gas generator and would also increase the required pressurant weight. The complexity of the system was also quite high. For these reasons, the system was eliminated.

Table 15 Pressure-Fed Primary System Selection, Weight, and Temperature Summary

System Description	Storage		Optimum		
	Temperature (°R)	Pressure (psia)	Weight (lb_m)	TGE (°R)	Systems Selected
Primary					
GH_e, P = C	37	1000	3400	750	
	37	2000	3560	850	
	37	3000	3780	900	
	37	4000	3940	900	
GH_e, T = C	37	2350	3490	750	
S = C, Ext	37	2100	4320	860	
Int	37	2100	4440	880	
GH_e, P = C/S = C	37	1000	3030	1000	x
	37	2000	3150	900	
	37	3000	3230	860	
GH_e, S = C/P = C	37	1000	2990	840	x
	37	2000	3090	840	
	37	3000	3170	800	
GH_e, P = C/T = C	37	1000	3030	800	x
	37	2000	3130	800	
	37	3000	3200	800	
GH_e, T = C/P = C, Int	37	1000	3010	900	
Ext	37	1000	2980	850	x
Int	37	2000	3100	900	
Ext	37	2000	3080	850	
Int	37	3000	3170	1000	
Ext	37	3000	3140	900	x

Legend:

P = C (Isobaric)

T = C (Isothermal)

S = C (Isentropic)

Int = Helium Stored Inside LH_2 Tank

Ext = Helium Stored Outside LH_2 Tank

System 11 also required a separator and so had the same disadvantages of System 10. As described in Chapter III.C.1, solid fuel and oxidizer increases system weight more than a system using liquid fuel and oxidizer.

System 14 was eliminated because of its high degree of complexity. To maintain pressure in the ullage, the recirculated gas would have to be heated to a high temperature as the ullage volume increased. The only additional source of gas would be from liquid vaporization which would be small. The complexity of installing an inlet and an outlet for the recirculating gas to heat the total ullage also made the system undesirable.

The total system weights of the advanced system are listed in Table 16.

b. Final Screening, Pressure-Fed Systems

The second and final screening of pressurization systems for pressure-fed engines used the "Tank Pressurization" computer program which calculated more accurate values of propellant boiloff and pressurant requirements than the IBM 1620 program. All of the system weights were recalculated to obtain a good comparison except for those systems eliminated by the initial screening.

The strengths of the propellant tanks were taken at the maximum temperature each would experience; i.e., pressurant inlet temperature. All other factors were the same as the initial screening. This resulted in a much lower optimum inlet gas temperature than experienced in the initial screening.

The system weights computed during this phase are listed in Tables 17 and 18 for the primary and advanced systems, respectively.

c. Initial Screening, Pump-Fed Systems

For the analysis and selection of the lightest weight pressurization systems for pump-fed engines, the "Tank Pressurization" computer program was used to calculate pressurant usage and propellant boiloff for each system considered. A description of the "Tank Pressurization" computer program is found in Chapter III.A.2. Pressurant storage expansion processes and heat exchanger performances were calculated by IBM 1620 computer programs which were previously described.

Table 16 Advanced Pressure-Fed System Selection, Weight, and Temperature Summary

System No.	System Description	Storage		Optimum		System Selected
		Temperature (°R)	Pressure (psia)	Weight (lb_m)	TGE (°R)	
	Advance					
1	GH_e, P = C	10	1000	3120	700	
		10	2000	3350	800	
		10	3000	3580	800	
		20	1000	3210	700	
		20	2000	3450	750	
		20	3000	3660	850	
		163	1000	6700	1000	
		163	2000	7200	1000	
		163	3000	7700	1000	
2	LO_2, LH_2, Pumped			2950	1000	x
3	LO_2, LH_2, GH_e, T = C	37	2350	3550	920	
3	LO_2, LH_2, GH_e, S = C	37	2100	3640	900	
4	GO_2, P = C, GH_2, P = C	300, 600	1000	3950	1000	
		300, 600	2000	3920	1000	
		300, 600	3000	4450	1000	
		300, 100	1000	4050	1000	
		300, 100	2000	4000	1000	
		300, 100	3000	4550	1000	
		300, 163	1000	5150	1000	
		300, 163	2000	5180	1000	
		300, 163	3000	5950	1000	
7	LH_2, Pumped, GH_e, T = C	37	2350	2620	700	x
7	LH_2, Pumped, GH_e, S = C	37	2100	2800	700	x
8	LH_2, GH_e, T = C	37	2350	2980	800	x
8	LH_2, GH_e, S = C	37	2100	3240	800	
9	GH_2, T = C, GH_e, T = C	163, 370	1800, 2350	3380	900	
9	GH_2, S = C, GH_e, S = C	163, 370	1725, 2100	3790	900	
12	Cascade*	37	1000	3110	680	x
13	GH_e, T = C	163	2300	4950	900	
13	GH_e, S = C	163	3200	5450	1000	

*Initial storage conditions of the cascade sphere were 37°R and 2500 psia. Inlet temperature to the primary sphere from the cascade was 1000°R.

Table 17 Pressure-Fed Primary Systems

Expansion	Optimum Entering Temperature (°R)	Weight (lb)
Isobaric P_i = 1000 T_i = 37	450	3040
Isothermal P_i = 2350 T_i = 37	450	3020
Isobaric Isentropic P_i = 1000 T_i = 37	420	2860
Isobaric Isothermal P_i = 1000 T_i = 37	410	2815
Isothermal Isobaric P_i = 1000 T_i = 37	415	2755
Isentropic Isobaric P_i = 1000 T_i = 37	410	2790

Table 18 Pressure-Fed Advanced Systems

System No.	Expansion	Optimum Entering Temperature (°R)	Optimum Weight (lb)
1 (Isobaric)	P_i = 1000 T_i = 10	400	2795
1 (Isobaric)	P_i = 1000 T_i = 20	425	2835
2 (Pumped)	--	200	2930
7 (Isothermal)	P_i = 1000 T_i = 37	200	2300
7 (Isentropic)	P_i = 1000 T_i = 37	200	2500
8 (Isothermal)	P_i = 1000 T_i = 37	400	2660
12 (Cascade)	P_i = 1000 T_i = 37	400	2790
12 (Cascade)	P_i = 1000 T_i = 25	430	2735
12 (Cascade)	P_i = 1000 T_i = 15	420	2705

During this phase of the study, the systems shown in Fig. 7 and 8, and described in Chapter III were analyzed, and total system weights were calculated.

The factors considered during this phase were:

Items included in system weights, as necessary;

Liquid hydrogen tank (spherical),

Liquid oxygen tank (spherical),

Hydrogen vapor,

Oxygen vapor,

Pressurant,

Pressurant container and residual,

Gas generators,

Heat exchangers,

Propellants for gas generator,

Pump, motor, and battery,

No external heat transfer was considered to or from the propellant tank walls; however, the heat capacity of the tank walls was considered (i.e., heat transfer between the ullage gas and the tank wall was considered);

No heat transfer was considered to or from the external wall in the pressurant expansion process. The heat capacity of the wall was considered;

Hydrogen gas bleed from the engine was at 280°R and 280 psia;

The spherical liquid hydrogen tank was sized for an ullage of 5% and an outage of 1%. The working stress of the 2219-T87 aluminum wall was based on the maximum temperature to which it was exposed (i.e., the pressurant inlet temperature). Minimum wall thickness was limited to no less than 0.020 in.;

The four equal spherical lox tanks were sized for an ullage of 3% and an outage of 0.5%. The working stress of the 2219-T87 aluminum wall was based on the maximum temperature it was exposed to;

The allowable working stress used for the design of the propellant tanks was ultimate/1.4 or yield/1.1. The temperature stress curves of 2219-T87 aluminum are shown in Fig. 37;

Tank pressures during burn periods were 40 psia with an initial lockup of 17.0 psia;

The mission profile studied was;

Firing	Propellant Expelled (lb)	Firing Time (sec)	Time from Launch (hr)
1	1,641	47.1	26
2	381	10.9	48
3	19,705	564.9	78
4	935	26.8	126
5	6,232	178.7	138
6	337	9.7	158

Note: An engine mixture ratio of 5 to 1 was used.

The final or lowest storage pressure was 300 psia;

The gas generator weights were determined from an empirical expression (Ref 8) derived from H_2O_2 gas generators manufactured by Sundstrand Aviation of Denver, Colorado;

Wall thicknesses of the propellant tank and of the storage sphere were determined using Ref 11,

$$t = \frac{PR}{2\sigma_W} \qquad [81]$$

where

t = wall thickness (in.),

P = maximum pressure ($lb_f/in.^2$),

R = tank radius (in.),

σ_W = working stress ($lb_f/in.^2$);

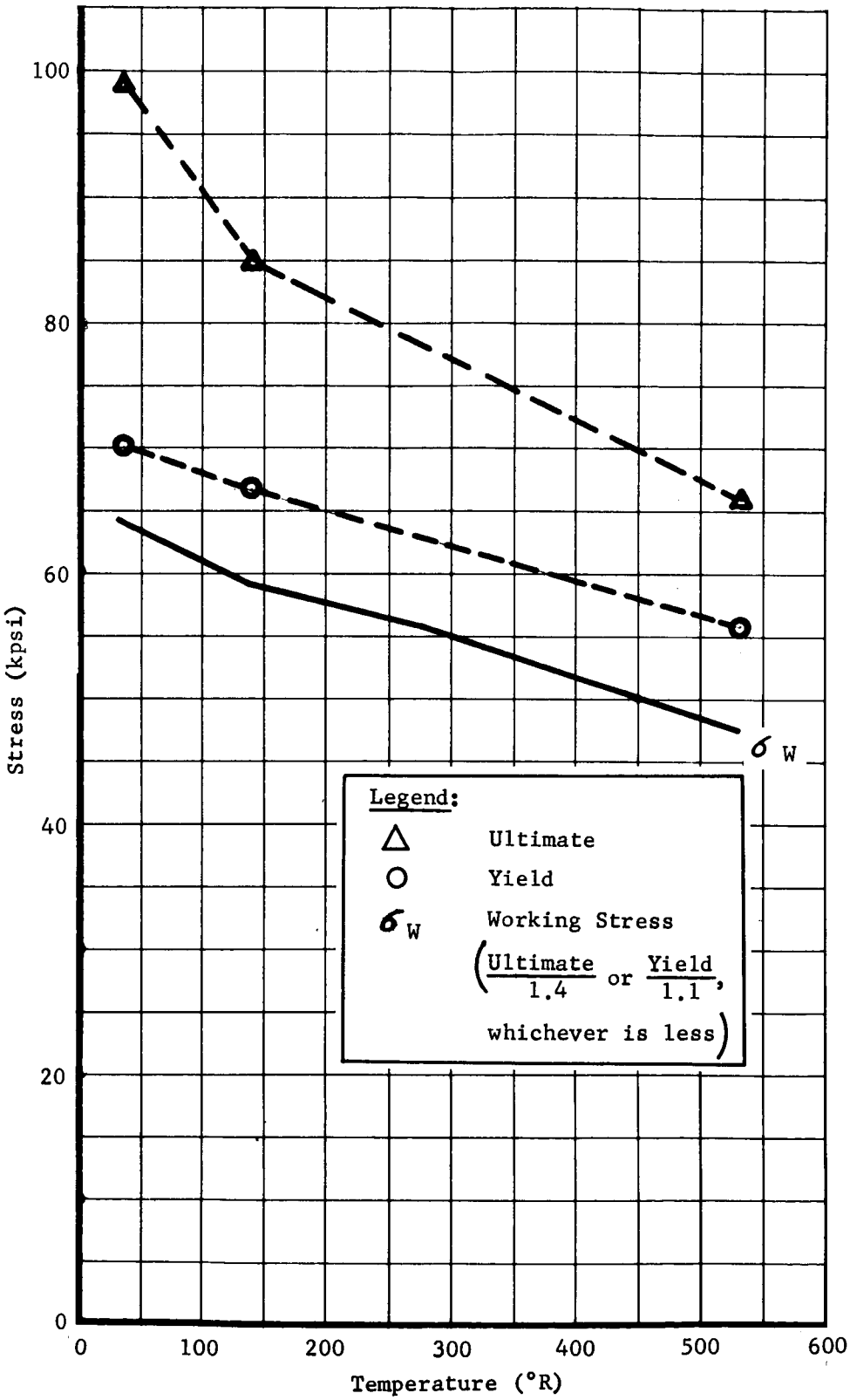

Fig. 37 Stress versus Temperature, Aluminum Alloy 2219-T87

The gas generator was controlled to prevent an excess of products being dumped overboard;

Pressurant storage container material was 6Aℓ-4V titanium with a maximum working stress of 120,000 psi. The working stress is the minimum of ultimate strength/2 or yield strength/1.67 (Ref 12);

The NPSH requirements for the engine were 8 and 15 psia for the liquid hydrogen and liquid oxygen, respectively.

The total system weights for the initial screening of the pressurization system for pump-fed engines are shown in Tables 19 and 20 for the primary and advanced systems, respectively.

d. Secondary Screening, Pump-Fed Systems

The systems studied during the secondary screening of the primary pump-fed systems phase were the five systems selected from the initial screening described in Chapter III.C.5.c. Figures 38 thru 43 depict the five systems studied.

A study was conducted to determine the optimized insulation thickness for the propellant tanks. The "Tank Pressurization" computer program was again used for propellant tank thermodynamics. The heat flux into the propellant tanks was calculated from an analytical model of the vehicle as described in Chapter III.C.4. The analytical model represents the structural portion of the space module for heat transfer. Heat leaks into the propellant tanks were calculated for various insulation thicknesses and used as inputs to the "Tank Pressurization" computer program. Figure 44 shows that the optimum thickness of propellant tank insulation was approximately 1/2 in. Although this figure was for System 8, all five system studies produced the same results. The optimum insulation thickness study was performed using a non-venting scheme with an equilibrium condition existing during coast periods.

Table 19 Total System Weight, Primary Pump-Fed Engines

System	Tank Inlet Conditions (°R)	Storage Conditions	Weight (lb)	System Selected
1	GHe: LH_2 Tank, 165 to 85 LO_2 Tank, 165 to 85 GH_2: LH_2 Tank, 180	165 to 85°R, 3000 to 300 psia Common Storage GH_2 Heating Container	1179	x
2	GHe: LH_2 Tank, 37 to 28 LO_2 Tank, 165 to 170 GH_2: LH_2 Tank, 80	37 to 28°R, 2200 to 300 psia 165 to 170°R, 2500 to 300 psia GH_2 Heating Both Containers	1323	
3	GHe: LH_2 Tank, 37 to 35 LO_2 Tank, 165 to 70 GH_2: LH_2 Tank, 80	37 to 35°R, 2000 to 300 psia 165 to 70°R, 3000 to 300 psia GH_2 Heating Container for LH_2 Tank	1238	
4	GHe: LH_2 Tank, 165 to 95 LO_2 Tank, 165 to 70 GH_2: LH_2 Tank, 180	165 to 95°R, 3000 to 300 psia 165 to 70°R, 3000 to 300 psia GH_2 Heating Container for LH_2 Tank	1178	
5	GHe: LH_2 Tank, 165 LO_2 Tank, 165	37 to 25°R, 2000 to 300 psia Common Storage	1107	x
6	GHe: LH_2 Tank, 165 LO_2 Tank, 165 GH_2: LH_2 Tank, 280	37 to 25°R, 2000 to 300 psia Common Storage	914	x
7	GHe: LH_2 Tank, 520 LO_2 Tank, 520	520°R, 3300 to 300 psia Common Storage	1555	
8	GHe: LH_2 Tank, 520 LO_2 Tank, 520 GH_2: LH_2 Tank, 280	520°R, 3300 to 300 psia Common Storage	1130	x
9	GHe: LH_2 Tank, 165 LO_2 Tank, 165	165°R, 3000 to 300 psia Common Storage	1208	
10	GHe: LH_2 Tank, 165 LO_2 Tank, 165 GH_2: LH_2 Tank, 280	165°R, 3000 to 300 psia Common Storage	960+	x
11	GHe: LH_2 Tank, 165 to 76 LO_2 Tank, 165 to 76	165 to 76°R, 3000 to 300 psia Common Storage	1560	
12	GHe: LH_2 Tank, 165 to 76 LO_2 Tank, 165 to 76 GH_2: LH_2 Tank, 280	165 to 76°R, 3000 to 300 psia Common Storage	1216	

Table 20 Total System Weight, Advanced Pump-Fed Engines

System	Tank Inlet Temperatures, (°R) LH_2 Tank	LO_2 Tank	Engine Bleed	Storage Container Process	Weight (lb_m)
1	450	450		T = C, T = 37°R	870
1	380	380	280	T = C, T = 37°R	785
2	37	165		T = C, T = 37°R	1500
2	37	165	280	T = C, T = 37°R	1230
3	37	165		T = C, T = 37°R, T = 165°R	1535
3	37	165	280	T = C, T - 37°R, T = 165°R	1260
4	440	440		Adiabatic/Isobaric, T_i = 37°R	785
4	345	345	280	Adiabatic/Isobaric, T_i = 37°R	745
4	375	375		Isobaric/Adiabatic, T_i = 37°R	810
4	360	360	280	Isobaric/Adiabatic, T_i = 37°R	740
5	400	400		Isobaric/Recirculative T = 730°R	795
5	375	385	280	Isobaric/Recirculative T = 675°R	745

Since the exact conditions of the fluids in the propellant tanks during a zero-gravity period were not known, doubt existed whether equilibrium would be achieved. A conservative approach was, therefore, taken in which all the heat into the propellant tanks was assumed to go into propellant boiloff. No condensation was allowed, so a nonequilibrium condition existed. Under these conditions, with no venting allowed, the tank pressures rose to 198.3 and 113.1 psia in the liquid oxygen and liquid hydrogen tanks, respectively. This pressure rise resulted in an approximate 700-lb increase in tank weights over that required for burn periods.

To provide the lightest possible system, a venting analysis was performed. The four vent schemes investigated were:

Vent scheme 1 which consisted of using three vent periods during each coast period. The vent periods occurred immediately after a burn, at the middle of the coast period, and just prior to pressurization. One-step equilibrium calculations were performed between vent periods;

Legend:

(1)	LO_2 Tank	(11)	LH_2 Pressurization Control Valve
(2)	LO_2 Vent Valve	(12)	LH_2 Pressurization Control Switch
(3)	LO_2 Vent Pressurization Switch	(13)	LH_2 Prevalve
(4)	LO_2 Pressurization Control Valve	(14)	LH_2 Pump
(5)	LO_2 Pressurization Control Switch	(15)	He Tank (Shrouded)
(6)	LO_2 Prevalve	(16)	He Fill and Drain Valve
(7)	LO_2 Pump	(17)	Heat Exchanger
(8)	LH_2 Tank	(18)	LO_2 Fill and Drain Valve
(9)	LH_2 Vent Valve	(19)	LH_2 Fill and Drain Valve
(10)	LH_2 Vent Pressurization Switch	(20)	He Fill and Drain Pressurization Switch

Note: 1. Helium stored at liquid oxygen temperature is heated by gaseous hydrogen engine bleed during burn periods.
2. Augmentation by gaseous hydrogen engine bleed is used in the liquid hydrogen tank.

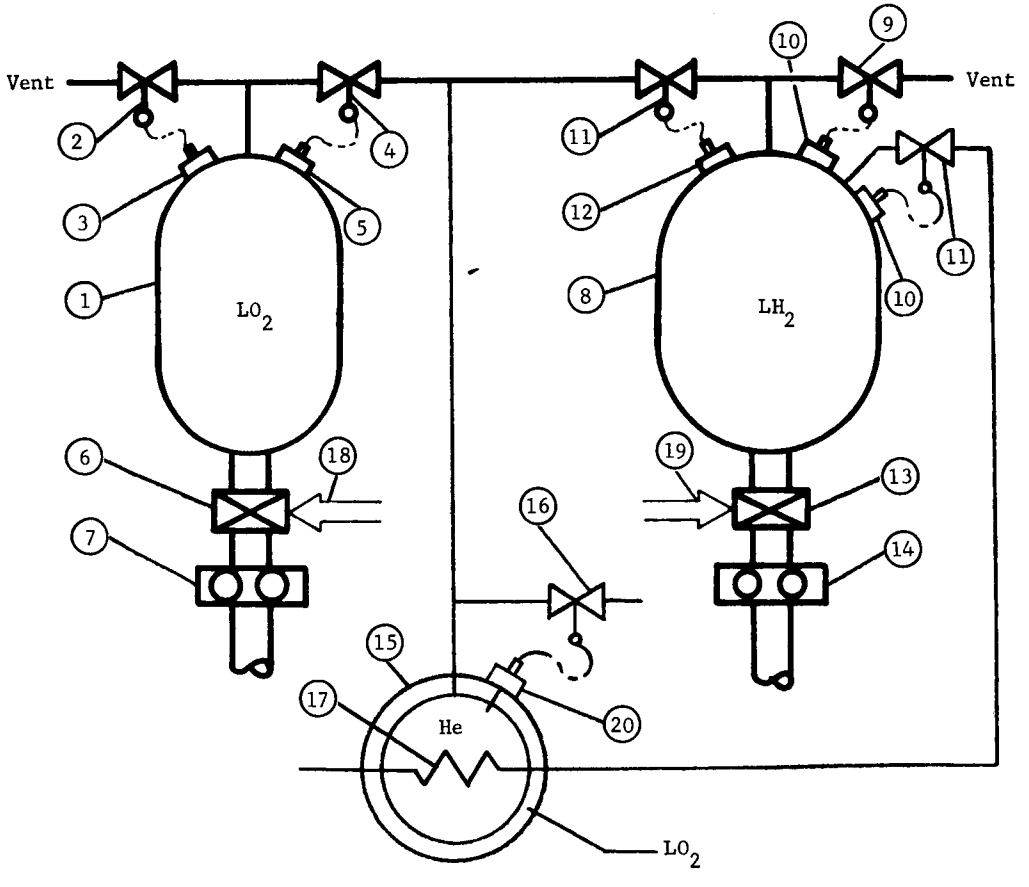

Fig. 38 System 1

Legend:

(1)	LO_2 Tank	(11)	LH_2 Tank Pressurization Valve
(2)	LO_2 Tank Vent Valve	(12)	LH_2 Tank Pressurization Switch
(3)	LO_2 Tank Vent Pressurization Switch	(13)	LH_2 Prevalve
(4)	LO_2 Tank Pressurization Valve	(14)	LH_2 Pump
(5)	LO_2 Tank Pressurization Switch	(15)	He Tank
(6)	LO_2 Prevalve	(16)	He Fill and Drain Valve
(7)	LO_2 Pump	(17)	Heat Exchanger
(8)	LH_2 Tank	(18)	LO_2 Fill and Drain Valve
(9)	LH_2 Tank Vent Valve	(19)	LH_2 Fill and Drain Valve
(10)	LH_2 Tank Vent Pressurization Switch	(20)	He Fill and Drain Pressurization Switch

Note: Helium stored at liquid hydrogen temperature with an adiabatic expansion, then heated by the liquid oxygen.

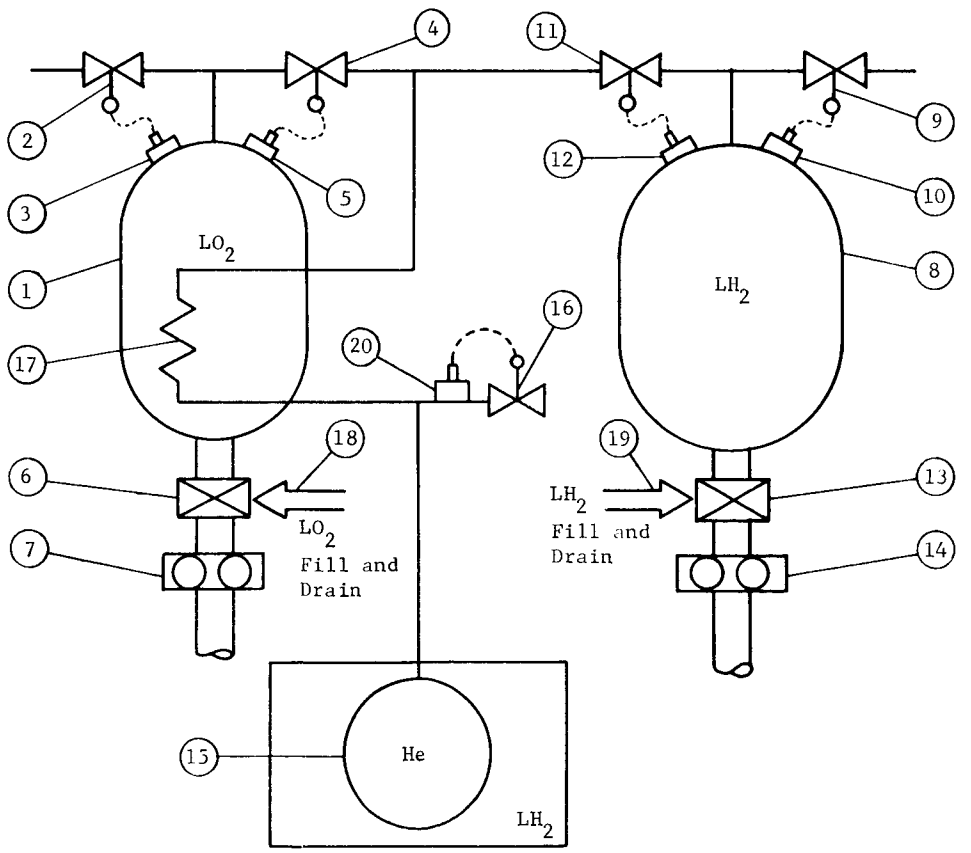

Fig. 39 System 5

Legend:

1. LO_2 Tank
2. LO_2 Tank Vent Valve
3. LO_2 Tank Vent Pressurization Switch
4. LO_2 Tank Pressurization Valve
5. LO_2 Tank Pressurization Switch
6. LO_2 Prevalve
7. LO_2 Pump
8. LH_2 Tank
9. LH_2 Tank Vent Valve
10. LH_2 Tank Vent Pressurization Switch
11. LH_2 Tank Pressurization Valve
12. LH_2 Tank Pressurization Switch
13. LH_2 Prevalve
14. LH_2 Pump
15. He Tank
16. He Fill and Drain Valve
17. Heat Exchanger
18. LO_2 Fill and Drain Valve
19. He Fill and Drain Pressurization Switch
20. LH_2 Fill and Drain Valve

Note: 1. Helium stored at liquid hydrogen temperature with polytropic expansion, then heated by the liquid oxygen.
2. Augmentation by gaseous hydrogen engine bleed is used in the liquid hydrogen tank.

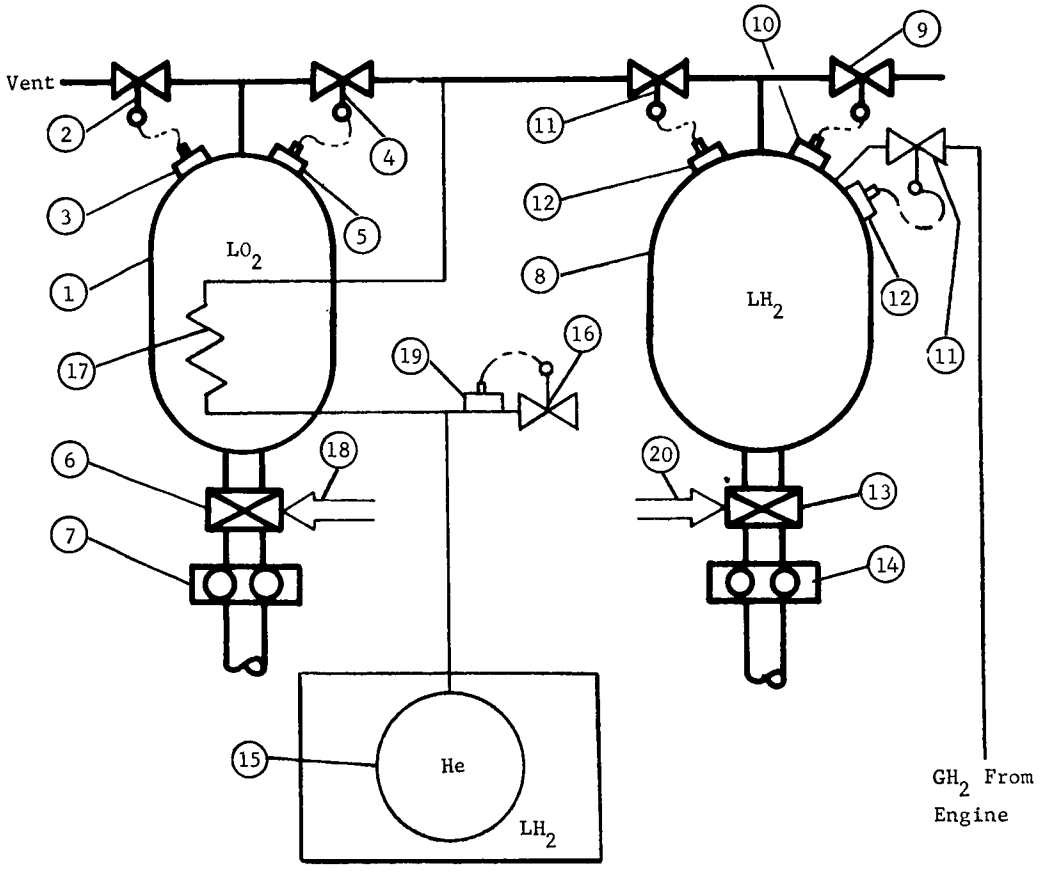

Fig. 40 System 6

Legend:

(1)	LO_2 Tank	(11)	LH_2 Tank Pressurization Valve
(2)	LO_2 Tank Vent Valve	(12)	LH_2 Tank Pressurization Switch
(3)	LO_2 Tank Vent Pressurization Switch	(13)	LH_2 Prevalve
(4)	LO_2 Tank Pressurization Valve	(14)	LH_2 Pump
(5)	LO_2 Tank Pressurization Switch	(15)	He Tank
(6)	LO_2 Prevalve	(16)	He Fill and Drain Valve
(7)	LO_2 Pump	(17)	Heat Exchanger
(8)	LH_2 Tank	(18)	LO_2 Fill and Drain Valve
(9)	LH_2 Tank Vent Valve	(19)	He Fill and Drain Pressurization Switch
(10)	LH_2 Tank Vent Pressurization Switch	(20)	LH_2 Fill and Drain Valve

Note: 1. Helium stored at liquid hydrogen temperature is heated by gaseous hydrogen engine bleed during burn periods, then heated by the liquid oxygen.
2. Augmentation by gaseous hydrogen engine bleed is used in the liquid hydrogen tank.

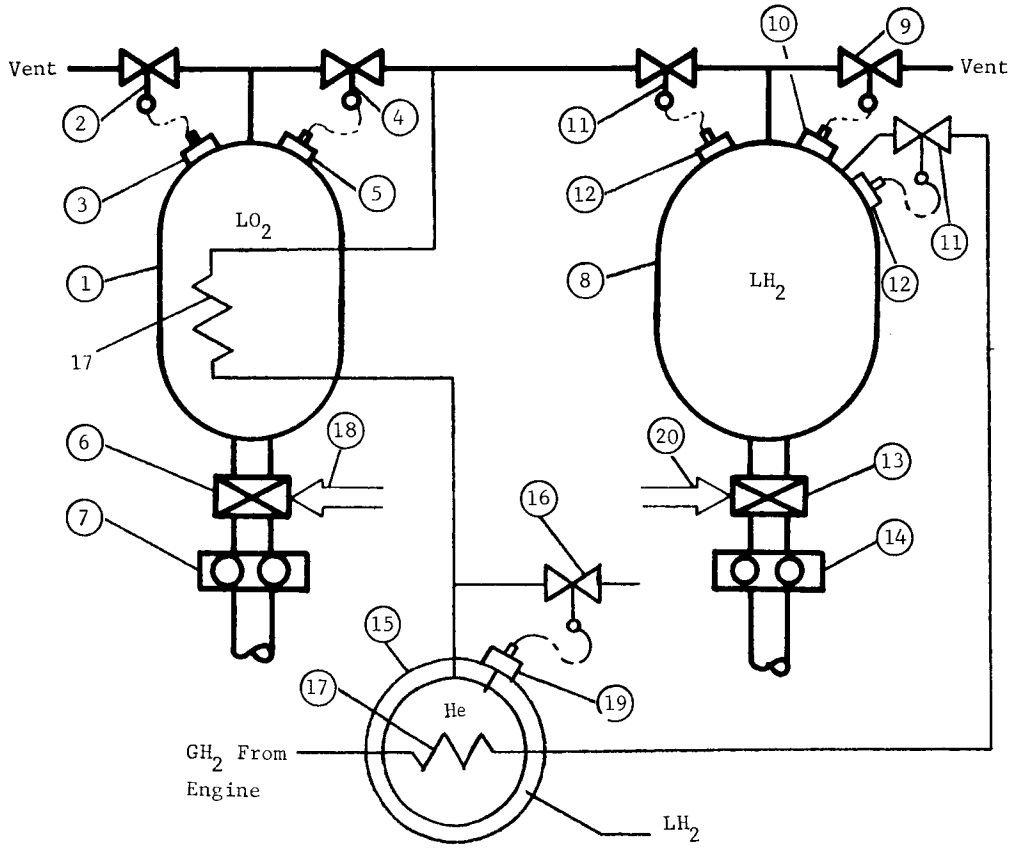

Fig. 41 System 6 (modified)

Legend:

1. LO_2 Tank
2. LO_2 Vent Valve
3. LO_2 Vent Pressurization Switch
4. LO_2 Pressurization Control Valve
5. LO_2 Pressurization Control Switch
6. LO_2 Prevalve
7. LO_2 Pump
8. LH_2 Tank
9. LH_2 Vent Valve
10. LH_2 Vent Pressurization Switch
11. LH_2 Pressurization Control Valve
12. LH_2 Pressurization Control Switch
13. LH_2 Prevalve
14. LH_2 Pump
15. He Tank
16. He Fill and Drain Valve
17. LO_2 Fill and Drain Valve
18. LH_2 Fill and Drain Valve
19. He Fill and Drain Pressurization Switch

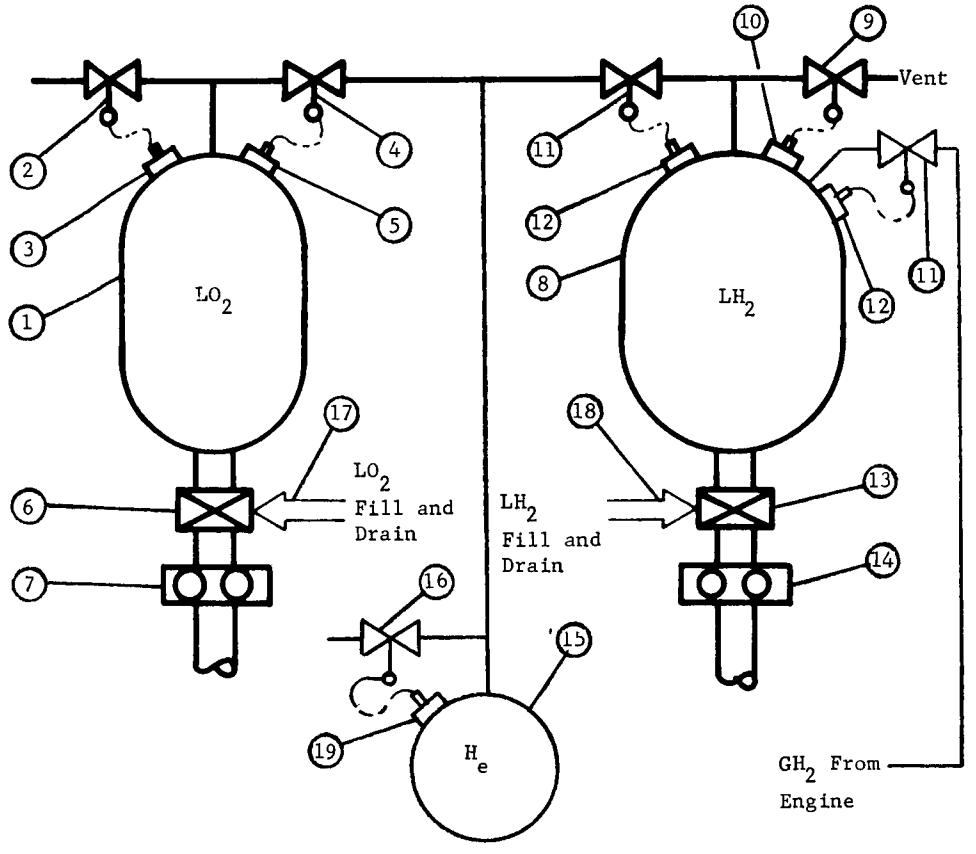

Note: 1. Ambient stored helium with an adiabatic expansion.
2. Augmentation by gaseous hydrogen engine bleed is used in the liquid hydrogen tank.

Fig. 42 System 8

Legend:

(1) LO_2 Tank	(11) LH_2 Vent Pressurization Switch
(2) LO_2 Vent Valve	(12) LH_2 Pressurization Control Valve
(3) LO_2 Vent Pressurization Switch	(13) LH_2 Pressurization Control Switch
(4) LO_2 Pressurization Control Valve	(14) LO_2 Fill Valve
(5) LO_2 Pressurization Control Switch	(15) LH_2 Fill Valve
(6) LO_2 Prevalve	(16) LH_2 Prevalve
(7) He Fill Pressurization Switch	(17) LH_2 Pump
(8) LO_2 Pump	(18) He Tank
(9) LH_2 Tank	(19) He Fill and Drain Valve
(10) LH_2 Vent Valve	(20) Heat Exchanger

Note: 1. Helium is stored in the liquid oxygen tank then heated by the liquid oxygen.
2. Augmentation by gaseous hydrogen engine bleed is used in the liquid hydrogen tank.

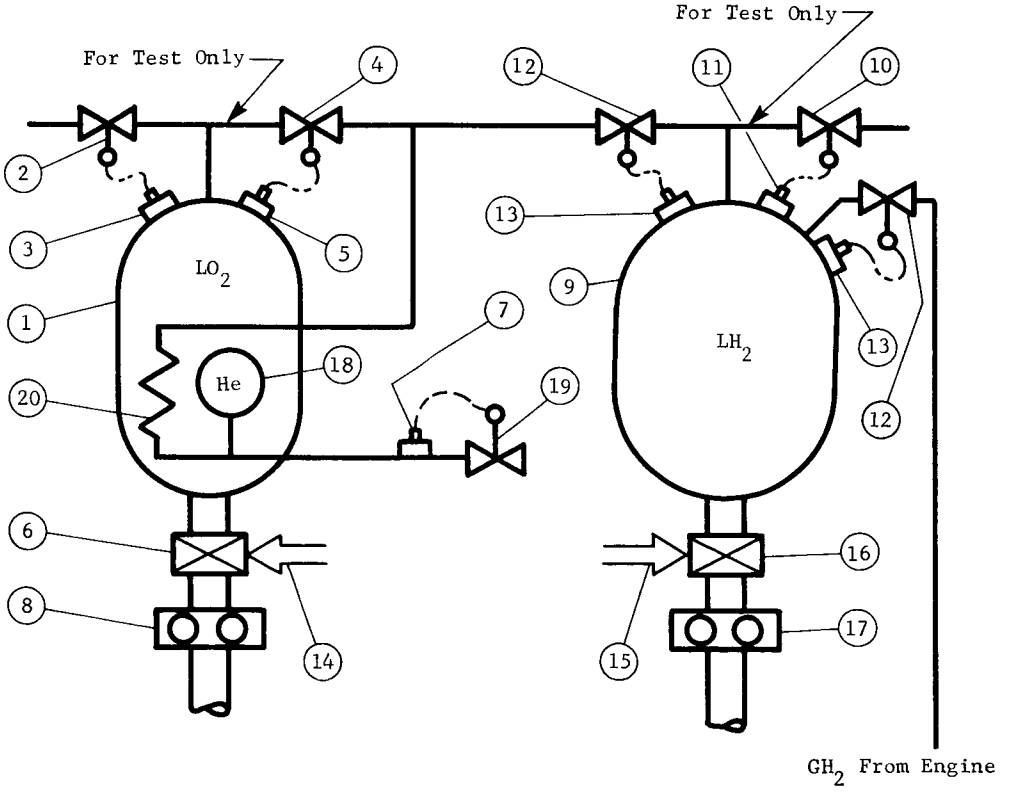

Fig. 43 System 10

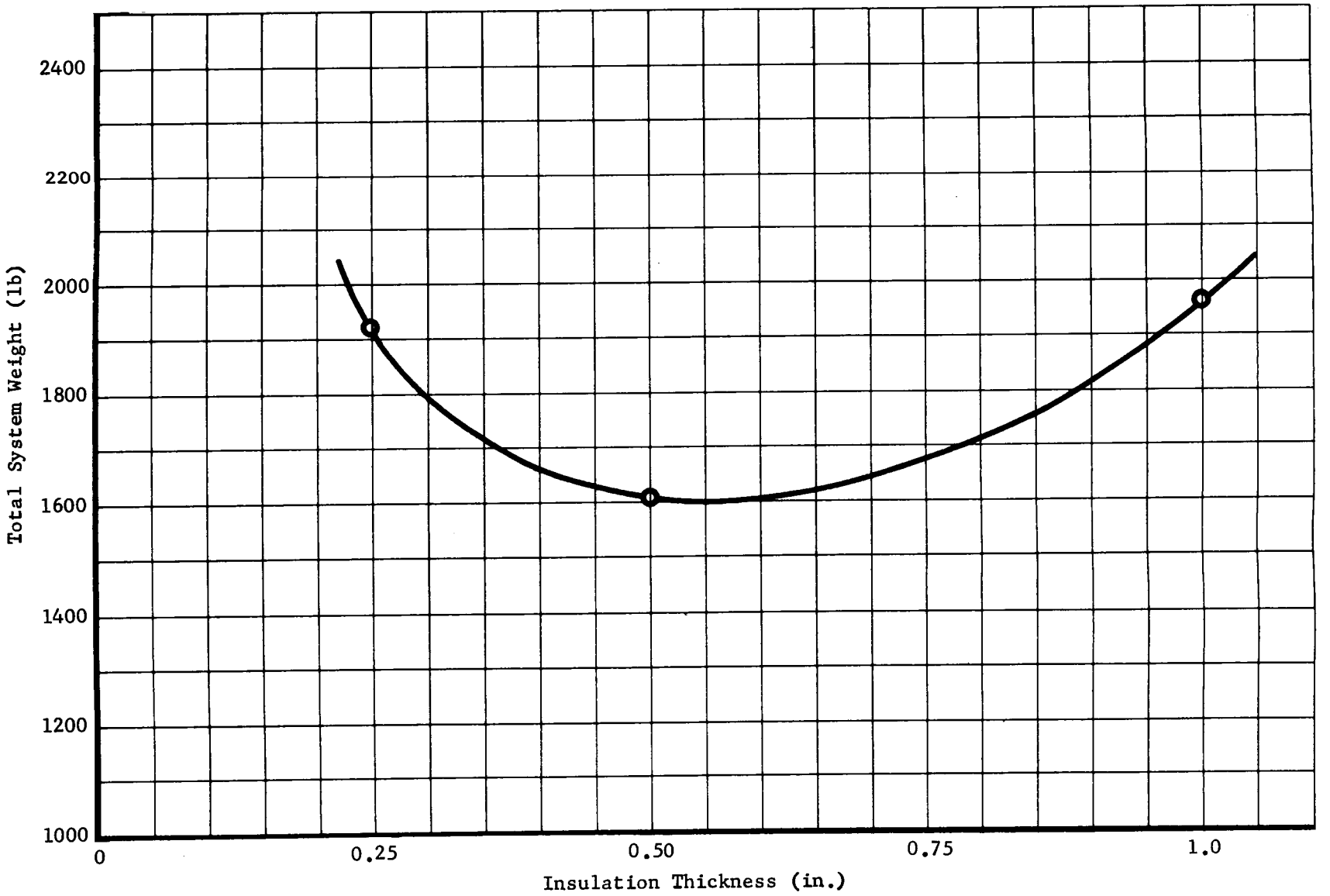

Fig. 44 Total System Weight and Insulation Thickness Parameters, Pump-Fed System 8

Vent scheme 2 was to vent once, just prior to pressurization. One-step equilibrium was used from the end of a burn to the vent period;

Vent scheme 3a assumed that equilibrium occurred after each burn followed by a slow vent to a tank pressure of 17.5 psia and continuous venting for the remainder of the coast period. All heat into the propellant tank went into propellant boiloff;

Vent scheme 3b was identical to 3a except that the tanks were rapidly vented down to 17.5 psia after each burn, and then continuous venting occurred through the remainder of the coast period. All the heat into the propellant tank went into propellant boiloff.

These four vent schemes are shown schematically in Fig. 45. A system weight comparison of the four vent schemes and a no-vent scheme with equilibrium during coast periods is shown in Table 21 for Systems 6 and 10. Table 21 indicates weight differences between the vent schemes of up to approximately 100 lb with a potential weight savings over the no-vent case of at least 350 lb. Vent scheme 1 was used for the remaining portion of the secondary screening study.

The conditions used for this phase of the study were:

Items included in the total system weight;

LH_2 tank,

LO_2 tank,

H_2 vapor,

O_2 vapor,

Pressurant,

Pressurant container and residual,

Heat exchangers,

LH_2 tank insulation,

LO_2 tank insulation,

Technique

Note: 1. Equilibrium calculations.
2. Three vents per coast period: one after engine burn, one in middle of coast, one just prior to pressurization.

(a) Scheme 1

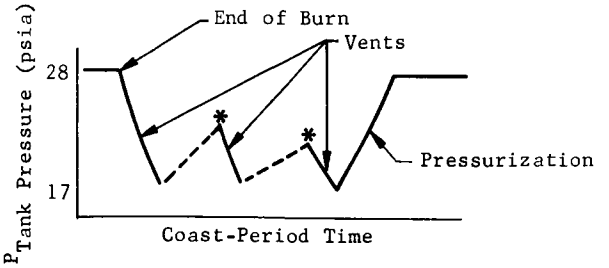

Note: 1. Equilibrium calculation.
2. One vent per coast period just prior to pressurization.

(b) Scheme 2

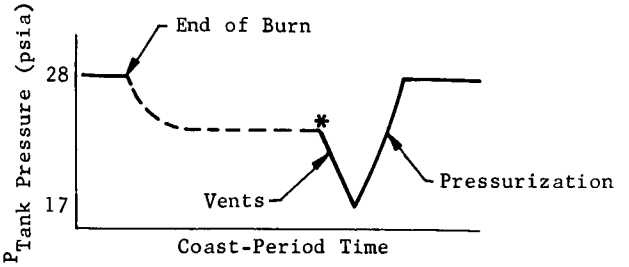

Note: 1. All incident radiative heat into propellant boiloff during coast.
2. Vent to 17 psia and hold at 17 psia - slow initial vent.

(c) Scheme 3a

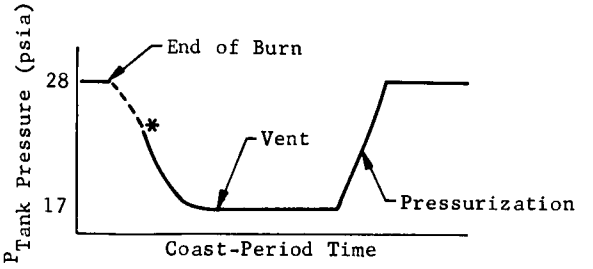

Note: 1. All incident radiative heat into propellant boiloff during coast.
2. Vent to 17 psia and hold at 17 psia - rapid initial vent.

(d) Scheme 3b

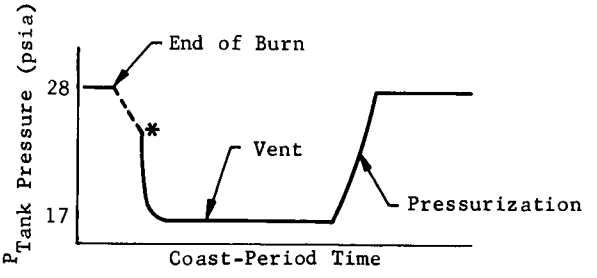

Legend:
* Conditions at End of Equilibrium Calculations
——— Actual Process
– – – Assumed Process During Equilibrium

Fig. 45 Advanced Pressurization Systems Vent Scheme Definition (H_2 Tank)

Table 21 Venting Scheme Comparison, Pump-Fed Pressurization Systems

	System 10				System 6			
	Vent 1	Vent 2	Vent 3a	Vent 3b	Vent 1	Vent 2	Vent 3a	Vent 3b
Tank Pressures								
LH_2 Tank	28.0	28.0	28.0	28.0	28.0	28.0	28.0	28.0
LO_2 Tank	34.0	34.0	34.0	34.0	34.0	34.0	34.0	34.0
Helium Used								
LH_2 Tank Residual	47.69	45.19	42.96	43.58	47.69	45.19	42.96	43.58
LO_2 Tank Residual	18.76	21.56	20.28	19.92	18.76	21.56	20.28	19.92
LH_2 Tank Vented	20.60	15.90	16.40	17.20	20.6	15.9	16.40	17.20
LO_2 Tank Vented	34.80	29.08	36.56	37.24	34.8	29.08	36.56	37.24
Storage Container Residual	27.7	25.38	26.39	26.73	107.96	99.0	102.8	104.4
Storage Container Propellant Vapor	468.0	428.5	446.0	452.6	121.11	110.9	115.2	117.0
LH_2 Tank Residual	98.13	112.82	116.41	113.82	98.13	112.82	116.41	113.82
LO_2 Tank Residual	55.48	30.72	46.92	48.24	55.48	30.72	46.92	48.24
LH_2 Tank Vented	154.0	167.00	166.00	174.00	154.0	167.0	166.00	174.00
LO_2 Tank Vented	283.6	232.40	270.40	266.40	285.6	232.4	270.40	266.40
Propellant Tankage								
LH_2 Tank	168.0	169.5	169.5	169.5	168.0	169.5	169.5	169.5
LO_2 Tank	84.5	84.4	84.4	84.4	84.5	84.4	84.4	84.4
Insulation								
LH_2 Tank	232.9	234.0	234.0	234.0	232.9	234.0	234.0	234.0
LO_2 Tank	162.7	162.3	162.5	162.5	162.7	162.3	162.5	162.5
Heat Exchanger	20.0	20.0	20.0	20.0	20.0	20.0	20.0	20.0
Total Weight With Venting	1876.86	1778.75	1867.52	1870.13	1610.27	1534.8	1604.33	1612.2
Total Weight Without Venting	2225	2225	2225	2225	2035	2035	2035	2035
Weight Saved By Using Vent Program	348.14	446.25	357.48	354.87	424.73	500.2	430.67	422.8

Note: All values are in lb.

Space heat flux to external skin was calculated by the PD016 computer program;

Heat flux into propellant tanks through the vehicle structure was obtained from the Aerodynamic and Structural Heat Transfer computer program;

Heat transfer was not considered from the environment for helium expansion when the container was not immersed in either propellant tank. Heat transfer was considered from the environment for helium expansion when the container was immersed in the propellant tank. The heat capacity of the walls was included in all expansions;

Specifications of the propellant tanks are;

	Oxygen	Hydrogen
Type	Four-spherical	One-spherical
Ullage	3%	5%
Outage	0.5%	1%
Minimum Wall Thickness (in.)	0.015	0.020
Nominal Size (ft^3)	90 (each)	1210

(Wall strength was based on maximum temperature of pressurant gas.)

Hydrogen bleed gas from the engine was at 280°R and 280 psia;

The working stress of the propellant tanks was the minimum of ultimate strength/1.4 or yield strength/1.1 (Ref 13). The strength curve of 2219-T87 aluminum is shown in Fig. 37;

The NPSH requirements for the engine were 8 and 15 psia for the liquid hydrogen and oxygen tanks, respectively. When venting procedures were used, tank pressures were 28.0 and 34.0 psia for the liquid hydrogen and oxygen tanks, respectively. Venting procedures hold the liquid vapor pressures at approximately the lockup pressure of 17.0 psia;

The mission profile was the same as that used for the initial pump-fed study;

The final or lowest storage pressure allowed was 150 psia which provided 115-psi line and valve losses;

Wall thickness of the propellant tanks and the pressurant sphere was based on hoop stress;

Pressurant storage container material was 6Aℓ-4V titanium;

Assumed accelerations were 0.01g during prepressurization periods and 0.2g during burn periods.

The system weights for this portion of the study (Table 22) were based on the use of vent scheme 1 and the optimum propellant tank insulation thickness shown in Fig. 44.

The analysis resulted in the selection of two systems from the five systems studied. The selection of the two systems, primary pump-fed Systems 6 and 8, was based on low weight and minimum complexity. System 6 weighed less (5 to 325 lb) than any of the five systems studied and was the primary selection. System 8 was selected because of its low degree of complexity and because it would offer a good comparison with System 6 (the only system studied using ambient temperature pressurant storage).

e. Final Screening, Pump-Fed Systems

In the final selection phase, Systems 6 and 8 were compared. System 8 consisted of a container storing helium at ambient temperature and fed both propellant tanks directly. System 6 used a helium container immersed in the liquid hydrogen tank. The helium is used in both propellant tanks after being passed through four heat exchangers immersed in the four lox tanks. A complete analysis was performed on the two systems using the "Propellant, Tankage, and Pressurization System" computer program. The program assumed the use of optimized pressurant storage containers and heat exchangers as determined by auxiliary computer programs. The heat input to the external vehicle skin was calculated by the computer program for Radiation Flux to an Orbiting Satellite.

Table 22 Pressurization System Total System Weights,* Pump-Fed Engine, Vent Scheme 1

System	1	5	6†	6†	6 (modified)	8	10
Helium Used							
LH_2 Tank Residual	55.2	74.58	47.69	47.69	47.1	16.26	47.69
O_2 Tank Residual	20.8	18.76	18.76	18.76	18.8	10.28	18.76
H_2 Tank Vented	10.1	66.9	20.60	20.60	20.5	6.71	20.60
O_2 Tank Vented	31.2	34.8	34.80	34.80	34.8	17.60	34.80
Storage Container	14.20	172.81	107.96	56.05	19.0	8.02	27.7
Storage Container	453.5	193.87	121.11	87.2	141.0	500.23	468.0
Propellant Vapor							
H_2 Tank Residual	98.9	88.74	98.13	98.13	99.41	101.70	98.13
O_2 Tank Residual	56.6	55.48	55.48	55.48	55.48	75.76	55.48
H_2 Tank Vented	154.0	136.0	154.0	154.0	157.0	154.00	154.0
O_2 Tank Vented	284.0	283.6	283.60	283.60	283.6	274.40	283.60
Propellant Tankage							
H_2 Tank	166.0	160.8	168.0	168.0	162.0	206.27	168.0
O_2 Tank	85.3	84.5	84.5	84.5	84.5	84.03	84.5
Insulation							
H_2 Tank	233.0	232.0	232.9	232.9	234.0	233.10	232.9
O_2 Tank	164.4	162.7	162.7	162.7	162.7	162.69	162.7
Heat Exchanger	27.9	20.0	20.0	20.0	30.0		20.0
Total Mass	1854.65	1785.58	1610.27	1524.45	1529.2	1850.87	1876.86

*All values are in lb.
†System 6 used two expansion methods; adiabatic and isothermal.

In System 6, the outlet temperature of the heat exchanger is inversely proportional to the pressurant flow rate. The time required to pressurize the propellant tanks is inversely proportional to the pressurant flow rate and temperature. Since the propellant settling subsystem weight is also a function of pressurization time, a study was conducted to determine the optimum tank inlet temperature that would produce the lowest total system weight including settling system weight, pressurant usage, and heat exchanger performance. As pressurization time decreased, the settling subsystem weight decreased by increasing the flow rate; but by increasing the flow rate, the heat exchanger exit temperature decreased. With a lower propellant tank inlet temperature, more helium was used. This weight study was made to optimize System 6 by accounting for pressurization time and heat exchanger performance. An inlet temperature of about 85°R achieved the lowest system weight as shown in Fig. 46.

The data used for final screening were the same as those used in the previous study phase except as follows:

Items included in the system weight are;

LH_2 tank (spherical),

LO_2 tank (spherical),

H_2 vapor,

O_2 vapor,

Pressurant used in tanks,

Pressurant leakage,

Pressurant in settling subsystem,

Pressurant residual and container,

Heat exchanger,

LH_2 tank insulation,

LO_2 tank insulation,

Pressurant sphere insulation,

Settling propellants,

Settling propellants storage,

Settling propellants boiloff and residual,

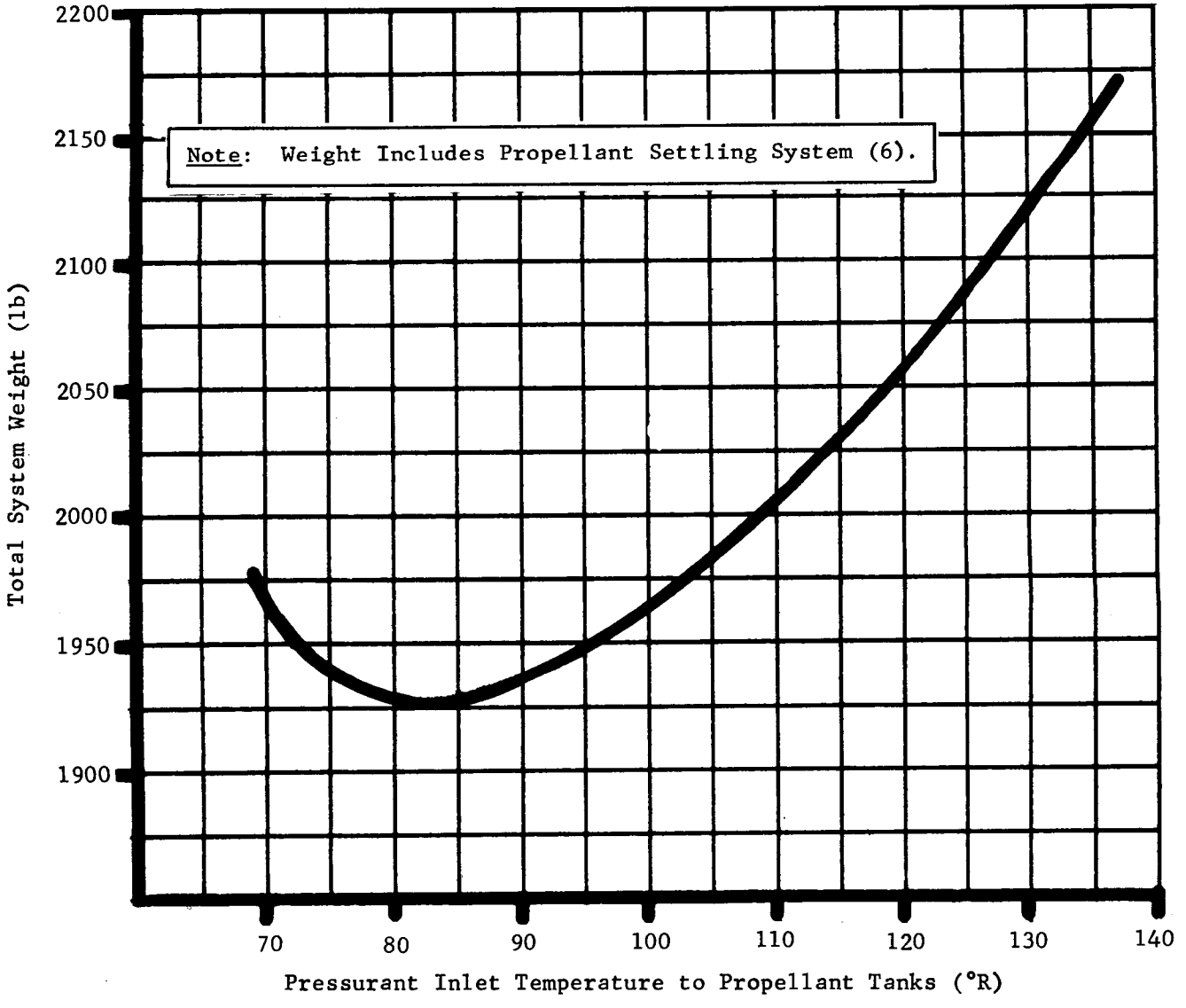

Fig. 46 Optimization of Pressurant Inlet Temperature to Propellant Tanks

The structural heat analysis was included in the Propellant Tankage Pressurization System computer program.

Pressurant expansion processes were also calculated by this computer program using optimum storage pressures as determined from 1620 computer programs;

The sizing of the propellant tanks was based on usable propellants of 25,000 and 5,000 lb for the liquid oxygen and liquid hydrogen tanks, respectively;

The working stress for the propellant tanks is shown by Fig. 37. The working stress for each system was determined by the maximum temperature to which the tank was exposed;

The propellant settling subsystem used the following criteria;

The structural weight of the vehicle was 24,000 lb,

The settling propellants were liquid hydrogen and liquid oxygen,

The specific impulse of the settling rockets was 430 sec,

A minimum settling time of 15 sec was used,

Storage of propellants was in spheres using expulsion diaphragms,

The propellant spheres were pressurized to 180 psia using helium from the main helium storage system,

The helium attained the same temperature as the propellants,

Ninety percent of the stored propellants were usable,

The data used for the vehicle thermal analysis were those listed in Chapter III.C.4;

Assumed acceleration during prepressurization periods was 0.01g. During burn periods, the acceleration was calculated by the Propellant, Tankage, and Pressurization System computer program.

The times (in sec) listed in the following tabulation include both pressurization and propellant settling requirements. It was assumed that pressurization and propellant settling were initiated at the same time. The tabulation lists the higher of the pressurization-settling times.

Event	System 6	System 8
1st Pressurization	15	15
2nd Pressurization	15	15
3rd Pressurization	15	15
4th Pressurization	51	15
5th Pressurization	70	15
6th Pressurization	96	15
Total	262	90

The analytical model used in this screening was the "Propellant, Tankage, and Pressurization System" computer program. This analytical model was set up to use an orifice-limiting, solenoid (bang bang) valve type flow for pressurizing the propellant tanks. During coast periods, continuous venting and equilibrium conditions were used. A computation was done for each 200 sec of coast with heat addition, venting, and equilibrium computations being performed for each time interval.

Pressurant storage for System 8 was provided by four spheres equally spaced between the liquid hydrogen tank and the liquid oxygen tanks. The pressurant tanks were covered with 1/2 in. of super insulation and used structural supports of 6Aℓ-4V titanium 0.785 sq in. in cross section and 20 in. long.

The uninsulated pressurant sphere in System 6 was immersed in the liquid hydrogen tank allowing heat transfer between the pressurant and the liquid hydrogen.

The actual expansion for both the ambient and immersed liquid hydrogen storage system was calculated by the analytical program. The correct heat leak into or away from the pressurant storage sphere was calculated with vehicle structure heat transfer analysis. The optimum initial pressures of the pressurant were determined from IBM 1620 expansion programs. A reasonable change in the heat leak into the container changed the expansion ratio but not the optimum initial storage pressure. The optimum pressure of System 6 was for an isothermal expansion, and that of System 8 was for an adiabatic expansion.

The conditions of the pressurant storage spheres are summarized below.

	System 6	System 8
Number of Spheres	1	4
Initial Pressure (psia)	1100	2700
Initial Temperature (°R)	37.4	520.0
Volume (ft^3)	36.08	36.6
Sphere Weight (lb)	147.9	577.6

The optimized configuration of the liquid oxygen tank heat exchanger determined by IBM 1620 studies was input into the analytical model. Since the equation in both programs was the same, the calculated results were the same. The analytical model calculated all transient conditions of the heat exchanger with the effects due from the total vehicle.

The total system weights for Systems 6 and 8 are shown in Table 23. Note that a substantial weight increase resulted compared to the analysis made during the secondary screening. This weight increase is due to the addition of the propellant settling subsystem. In System 6, an increase in weight was also due to the gas inlet temperature being lowered from an assumed 160°R to a value of about 85°R.

Table 23 Total System Weights (lb) Final Analysis

	System 6	System 8
Helium Used		
LH_2 Tank Residual	87.21	22.09
LO_2 Tank Residual	27.13	8.97
LH_2 Tank Vented	32.64	5.76
LO_2 Tank Vented	43.86	15.13
Settling Subsystem	14.69	5.61
Leakage	4.00	0.40
Residual	96.39	5.85
Storage Container	149.92	577.62
Propellant Vapor		
LH_2 Tank Residual	96.61	112.82
LO_2 Tank Residual	39.58	74.80
LH_2 Tank Vented	220.81	206.05
LO_2 Tank Vented	351.06	349.50
Propellant Tanks		
LH_2 Tank	206.90	221.26
LO_2 Tank	86.52	86.15
Insulation		
LH_2 Tank	243.11	239.13
LO_2 Tank	166.32	165.61
Pressurant Storage		35.29
Heat Exchanger	120.90	
Settling Subsystem		
Propellants	186.40	63.90
Storage	12.50	7.85
Boiloff and Residual	18.63	6.39
Total Weight	2205.18	2210.24

f. Conclusions

To optimize pressurization system weight, it is necessary to consider all items affected by the pressurization system. Some items can be optimized separately, i.e., heat exchanger and pressurant expansion ratio. To determine the combined effects of the total system, a large analytical model is essential.

If an active heat source is used, such as, a gas generator, the expansion ratio of the pressurant sphere is a reasonable guide to the total system weight. In both the pressure-fed and pump-fed studies, the systems with combined expansion methods were low in weight. Those combined expansions with a terminal isobaric process resulted in the lowest system weight.

Note from the primary screening of the pump-fed system that the lower the initial temperature, the lower the system weight. It can also be concluded that any expansion method that reduces the residual gas weight is desirable, i.e., recirculation and cascade expansions.

Pressure-fed systems were low in weight when a vaporized propellant was used as a pressurant. The lightest pressure-fed system incorporates helium stored at 37°R for the liquid oxygen tank and vaporized hydrogen propellant as a self-pressurant.

Use of a hydrogen gas bleed from the engine lowers the system weight.

Without an active heat source, increasing the pressurant gas temperature entering the tank eliminates the advantage of low-temperature storage. Insufficient heat can be added to the storage container to reduce the gas residual weight. With no active heat source, ambient pressurant storage is the most desirable system.

6. Reliability

The reliability studies carried on during the program were intended to meet two basic needs. They were:

1) To provide a designers guide to the selection of subsystem configurations;

2) To provide a method of predicting the reliability of total systems resulting from other optimization studies.

To meet the first requirement, studies were made of general types of subsystems, and parametric data were generated. Figures 47 thru 50 indicate the reliability predictions for pressurant storage, heat source, pressure control, and pressurant line heat exchanger subsystems, respectively. Reliabilities were computed using:

$$\text{Reliability} = e^{-\left(\sum F_r K_{op} K_a T\right)} \qquad [82]$$

where

F_r = component failure rate,

K_{op} = environmental modifying factor,

K_a = application modifying factor,

T = time.

Reliabilities indicated by the figures at zero time are actually computed for 1 hr, since at zero time the theoretical reliability would be 1.00. The K_{op} values used were those that were derived for the Titan III Stage III mission and, therefore, may be somewhat conservative for this program if used as absolute values. However, since only a comparison of one subsystem with respect to another was desired, the magnitude of the K_{op} does not significantly degrade the value of the analysis. Values used for F_r and K_a were obtained from Ref 14, and the times used were for the mission studied.

In predicting the reliability of specific total systems, the same approach would be used except that a more detailed analysis would be made of the system. Where the subsystem predictions considered major components only, the overall systems predictions would consider not only major components but details such as line joints, wiring connectors, insulation, and flexible tubing requirements.

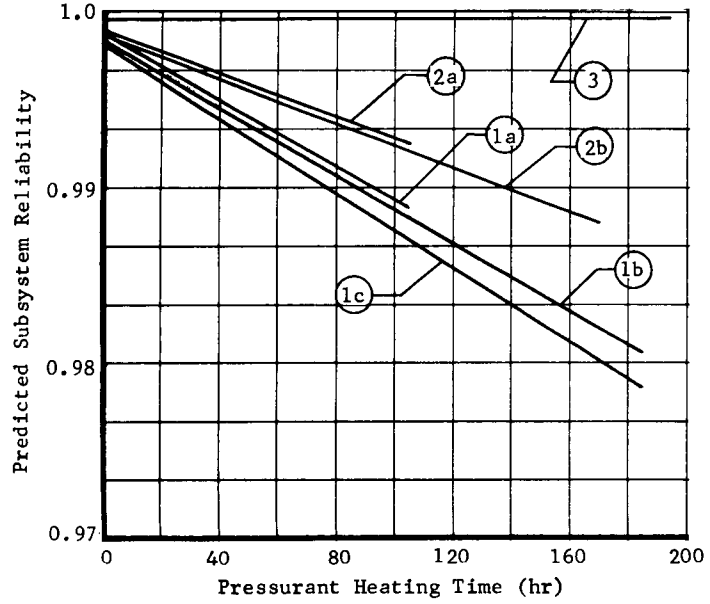

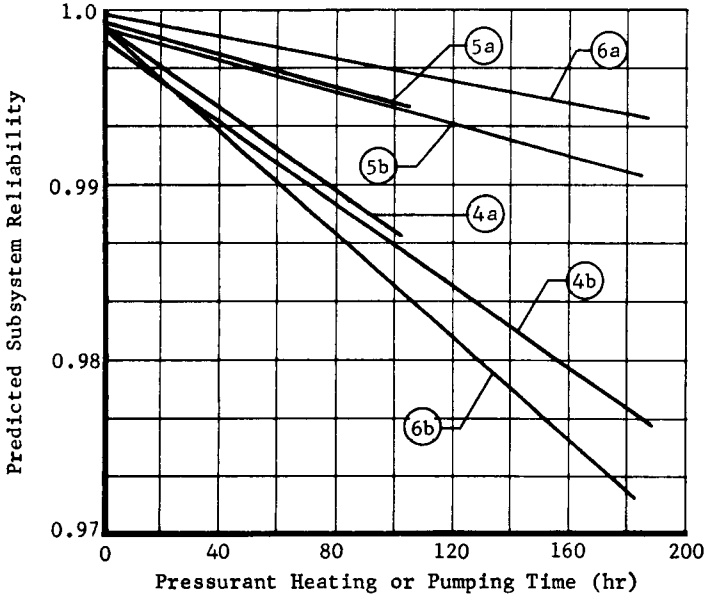

Legend:

(1) Auxiliary Tank, Internal Heating
- (1a) Gaseous Pressurant, Low Pressure Heat Control
- (1b) Gaseous Pressurant, High Pressure Heat Control
- (1c) Liquid Pressurant, High Pressure Heat Control

(2) Auxiliary Tank, Hot Gas Expulsion Gas Generator Products
- (2a) Gaseous Pressurant, Low Pressure Heat Control
- (2b) Gaseous or Liquid Pressurant, High Pressure Heat Control

(3) Auxiliary Tank, External Heating Free Convection

(4) Auxiliary Tank Hot Gas Expulsion Cascade
- (4a) Gaseous Pressurant, Low Pressure Heat Control
- (4b) Gaseous or Liquid Pressurant, High Pressure Heat Control

(5) Auxiliary Tank, External Heating Forced Convection
- (5a) Gaseous Pressurant, Low Pressure Heat Control
- (5b) Gaseous or Liquid Pressurant, High Pressure Heat Control

(6) Main Tank, Pump System
- (6a) Centrifugal Pump and Series Check Valves
- (6b) Axial Pump and Series Check Valves

Fig. 47 Predicted Reliability, Pressurant Storage Subsystem

Legend:

(1) Storable Bipropellant Gas Generator Heat Source

- (1a) Ullage Pressure Maintained Constantly.
- (1b) Ullage Pressure Maintained During Gas Generator Burning and for 10 sec Prior to Each Start.
- (1c) Same as 1 but with Common Pressure Regulator for Both Tanks
- (1d) Same as 2 but with Common Pressure Regulator for Both Tanks.

(2) Electric Heat Source

(3) Mono-propellant Gas Generator Heat Source

(4) Cryogenic Bipropellant Gas Generator Heat Source with Centrifugal Pump

(5) Cryogenic Bipropellant Gas Generator Heat Source with Axial Pump

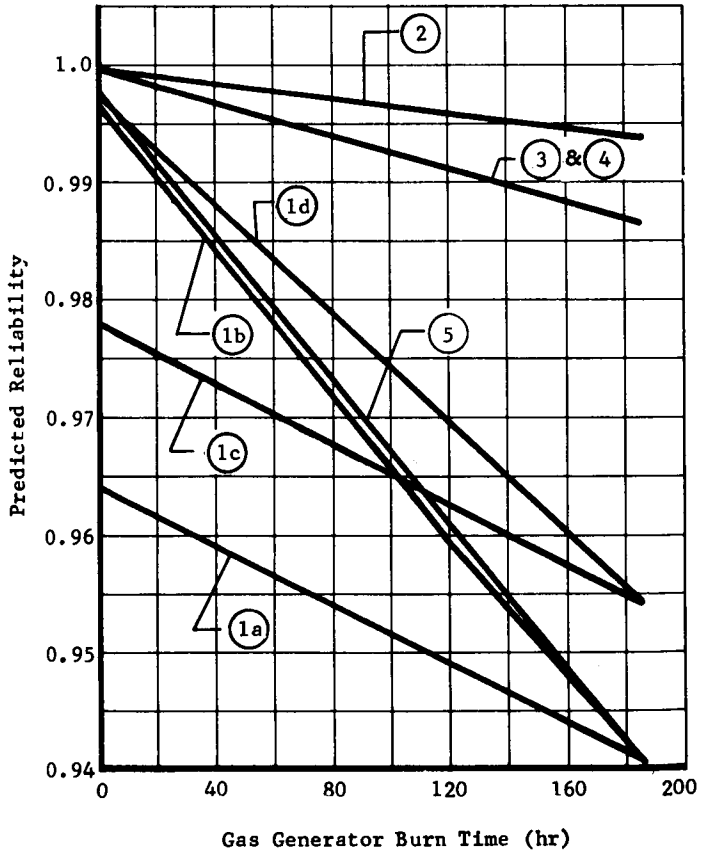

Fig. 48 Predicted Gas Generator Reliability

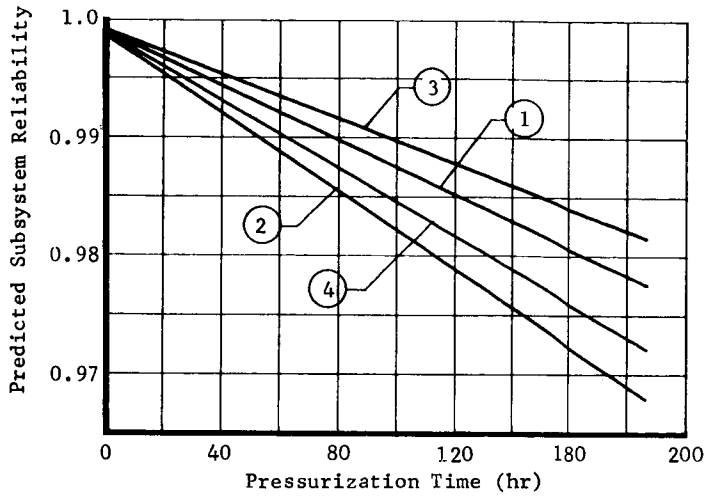

(a) Separate Tank - Hot Gas Regulation

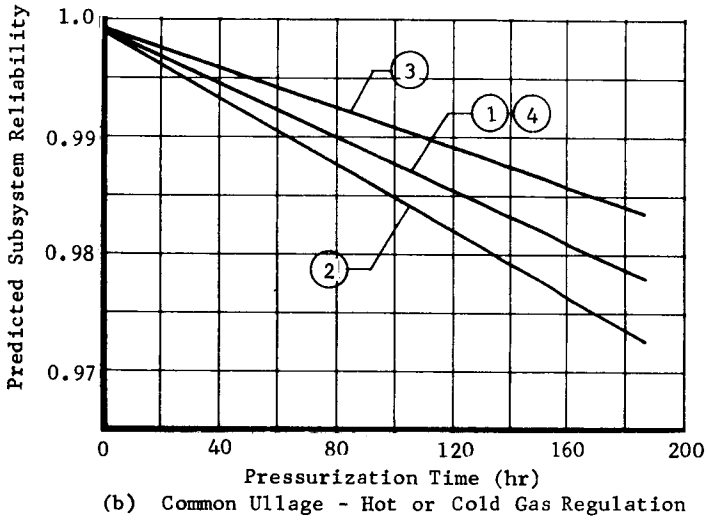

(b) Common Ullage - Hot or Cold Gas Regulation

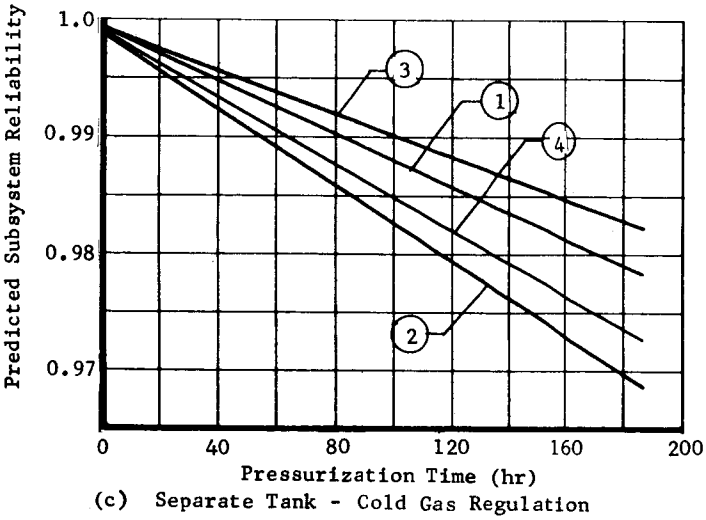

(c) Separate Tank - Cold Gas Regulation

Legend:

1. Regulator
2. Solenoid Valve and Pressure Switch
3. Regulator and Series Check Valve
4. Solenoid Valve, Pressure Switch, and Series Check Valve

Fig. 49 Predicted Reliability, Pressure Control Subsystem

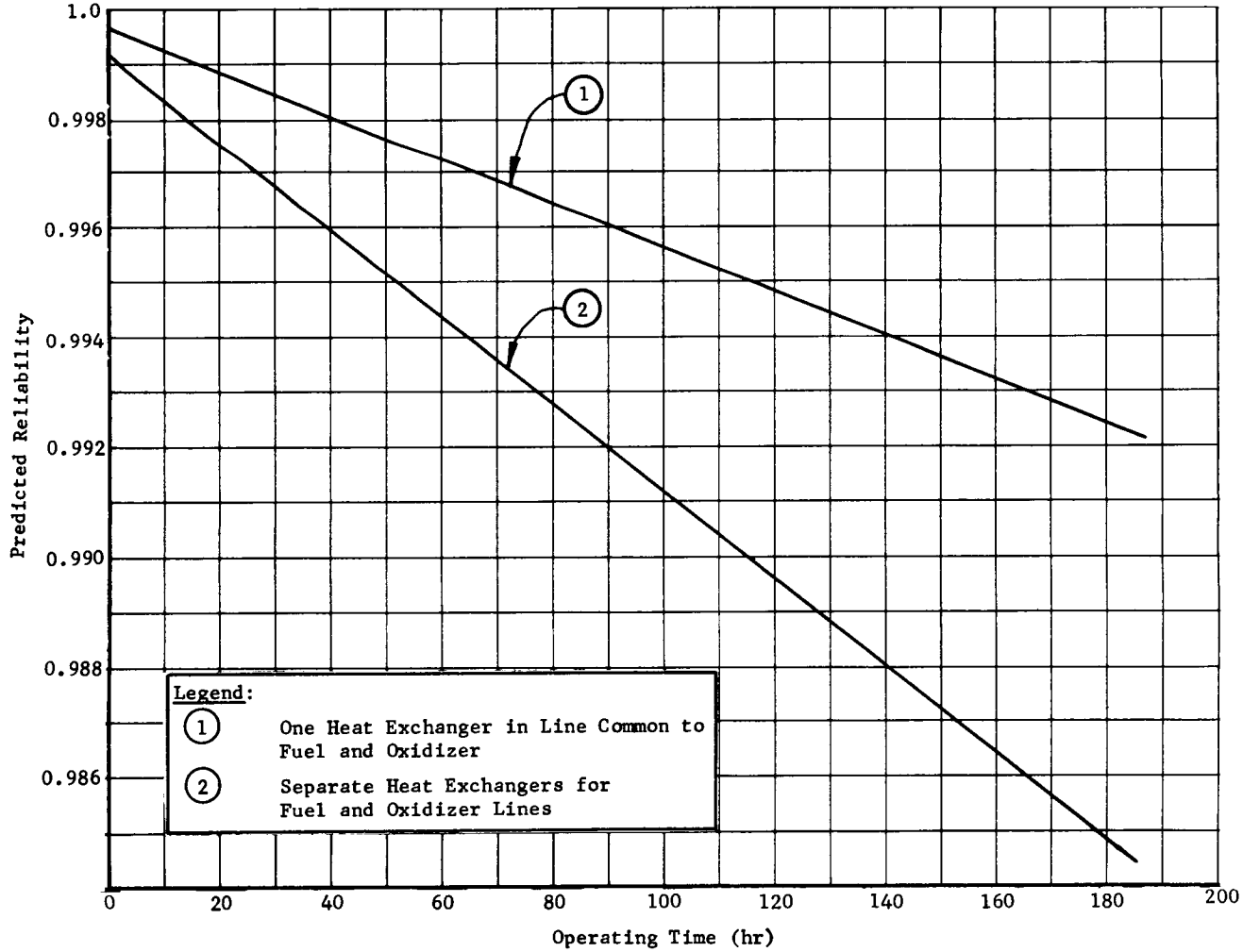

Fig. 50 Heat Exchanger Reliability, Pressurant Line Heat Exchanger in Gas Generator

The reliability predictions of the selected pump-fed system (System 8) are shown in Table 24. This prediction was based on the failure rates shown in Table 25 and the system schematic in Fig. 42.

Table 24 Reliability Prediction for System 8

Function	System Failure Rate x 10^{-6} GFR	Application Modifying Factor, K_a	Environmental Modifier, K_{op}	Time, t (hr)	$x = GFR \cdot K_a \cdot K_{op} \cdot t$ and Reliability
P	115.83	1	3	0.0333	0.000012
P and E	115.83	1	55	0.2328	0.001483
C	11.58	1	3	158.0	0.000550
					0.002045
					R = 0.9980

Note:
1. P = pressurization system operating.
2. P and E = pressurization system and engine operation.
3. C = coast.
4. x = failure rate.
5. $R = e^{-x}$.
6. GFR = system failure rate.

Table 25 Component Failure Rates

Nomenclature	Usage	Failure Mode	Failure Rate for Functional Requirements ($N \times 10^{-6}$)		
			Operative*	Containment† Only	Non-Operative‡
Accumulator	Zero-Gravity Propellant Supply	Propellant Starvation	3.6	0.036	0.036
		Internal Leakage	1.8	0.180	0.018
		External Leakage	1.8	0.018	0.018
		Total	7.2	0.234	0.072
Check Valve	Pressure Containment on One-Side	Failure to Open	2.1	0.0210	0.0210
		Failure to Close	0.6	0.0060	0.0060
		Internal Leakage	2.1	0.2100	0.0210
		External Leakage	0.2	0.0200	0.0020
		Total	5.0	0.2570	0.0500
Hard Lines with Fittings	Fluid Flow Path and Pressure Containment	External Leakage	0.2	0.02	0.002
Heat Exchanger	Heat Transfer	Insufficient Restricted Flow	0.83	0.0083	0.0083
		Heat Transfer	0.83	0.0083	0.0083
		Internal Leakage	1.67	0.1670	0.0167
		External Leakage	1.67	0.1670	0.0167
		Total	5.00	0.3506	0.0500
Orifice	Flow Control	Excessively Restricted Flow	0.07	0.0007	0.0007
		Increased Flow	0.01	0.0001	0.0001
		External Leakage	0.07	0.0070	0.0007
		Total	0.15	0.0078	0.0015
Pressure Switch	Pressure Relief from Propellant Tank to Atmosphere	Regulates High	1.7	0.017	0.017
		Regulates Low	1.8	0.018	0.018
		External Leakage	1.0	0.100	0.010
		Total	4.5	0.135	0.045
Pressure Switch	Pressure Regulation from Storage to Propellant Tank	Regulates High	1.7	0.017	0.017
		Regulates Low	1.8	0.018	0.018
		External Leakage	1.0	0.100	0.010
		Total	4.5	0.135	0.045

*Pressurization system operating and engine operating
†System pressurized and engine off
‡Coast

Table 25 (concl)

Nomenclature	Usage	Failure Mode	Failure Rate for Functional Requirements ($N \times 10^{-6}$)		
			Operative*	Containment† Only	Non-Operative‡
Pressure or Temperature Actuated Switch	Control of Pressure Generating Device	Regulates High	1.7	0.017	0.017
		Regulates Low	1.8	0.018	0.018
		External Leakage	1.0	0.100	0.010
		Total	4.5	0.135	0.045
Solenoid Valve	Pressure Relief to Atmosphere with Pressure Containment on One Side	Failure to Open	2.50	0.0250	0.0250
		Failure to Close	2.50	0.0250	0.0250
		Internal Leakage	2.50	0.2500	2.0250
		External Leakage	1.25	0.1250	0.0125
		Total	8.75	0.4250	0.0875
Solenoid Valve	Pressure Control with Pressure Containment on One Side	Failure to Open	2.5	0.0250	0.0250
		Failure to Close	2.5	0.0250	0.0250
		Internal Leakage	2.5	0.2500	0.0250
		External Leakage	2.5	0.1375	0.0250
		Total	10.5	0.4375	0.1000
Solenoid Valve (for usage on the ground, refer to data in the preceding item)	Fill and Drain with Pressure Containment on One Side	Failure to Open			
		Failure to Close			
		Internal Leakage	2.50	0.2500	0.0250
		External Leakage	1.25	0.1250	0.0125
		Total	3.75	0.3750	0.0375
Solenoid Valve	Pressure Regulation with Pressure Containment on Both Sides	Failure to Open	2.5	0.0250	0.0250
		Failure to Close	2.5	0.0250	0.0250
		Internal Leakage	2.5	0.2500	0.0250
		External Leakage	2.5	0.2500	0.0250
		Total	10.0	0.550	0.1000
Storage Tanks Less Insulation Device	Pressure Containment	External Leakage	0.18	0.018	0.0018
Motor Pump, Centrifugal	Propellant Pump	Pump Inoperative	0.62		0.006
		Leakage Excessive	0.48	0.048	0.005
		Power Consumption	0.08		
		Total	1.18	0.048	0.011

D. TESTING

1. Main Tank Injection (MTI)

An experimental program was conducted to determine the feasibility of pressurizing a liquid hydrogen tank by injecting a hypergolic fluid, fluorine, directly into the hydrogen tank.

Initially, the tests were to consist only of attempting to pressurize a small aluminum tank (5.33 cu ft) of liquid hydrogen by injecting liquid fluorine into the tank. If pressurization was accomplished, attempts would be made to maintain pressure while the hydrogen was being outflowed. Secondary objectives were to measure tank pressures and temperatures during the test and to determine how the injections contaminated the hydrogen.

However, while this test program was being run, certain events occurred which could not be explained. It was postulated that a delayed reaction or no reaction may have occurred. To investigate the causes of these events, it was desirable to photograph the injections. Therefore, a series of tests were conducted using a clear glass dewar to hold the liquid hydrogen. These tests were photographed with high speed motion picture cameras.

For clarity, the tests conducted in the aluminum tank are hereafter referred to as the main tank injection (MTI) tests and the tests conducted in the clear glass dewar are referred to as the liquid-hydrogen-liquid fluorine reaction tests.

a. Main Tank Injection Test Equipment

1) Fluorine Supply System

Since liquid fluorine storage and handling equipment was not readily available and only a small quantity of liquid was needed, the fluorine was stored and handled as a gas. The liquid fluorine for injection was produced in a condenser coil which was integral with the injector. A schematic of the fluorine supply system is included in the overall MTI Test Equipment Schematic (Fig. 51). The fluorine supply system consisted of a cylinder of fluorine gas, remote operating valves, fluorine accumulator, connecting lines, helium purge system, and connections to the vapor disposal system.

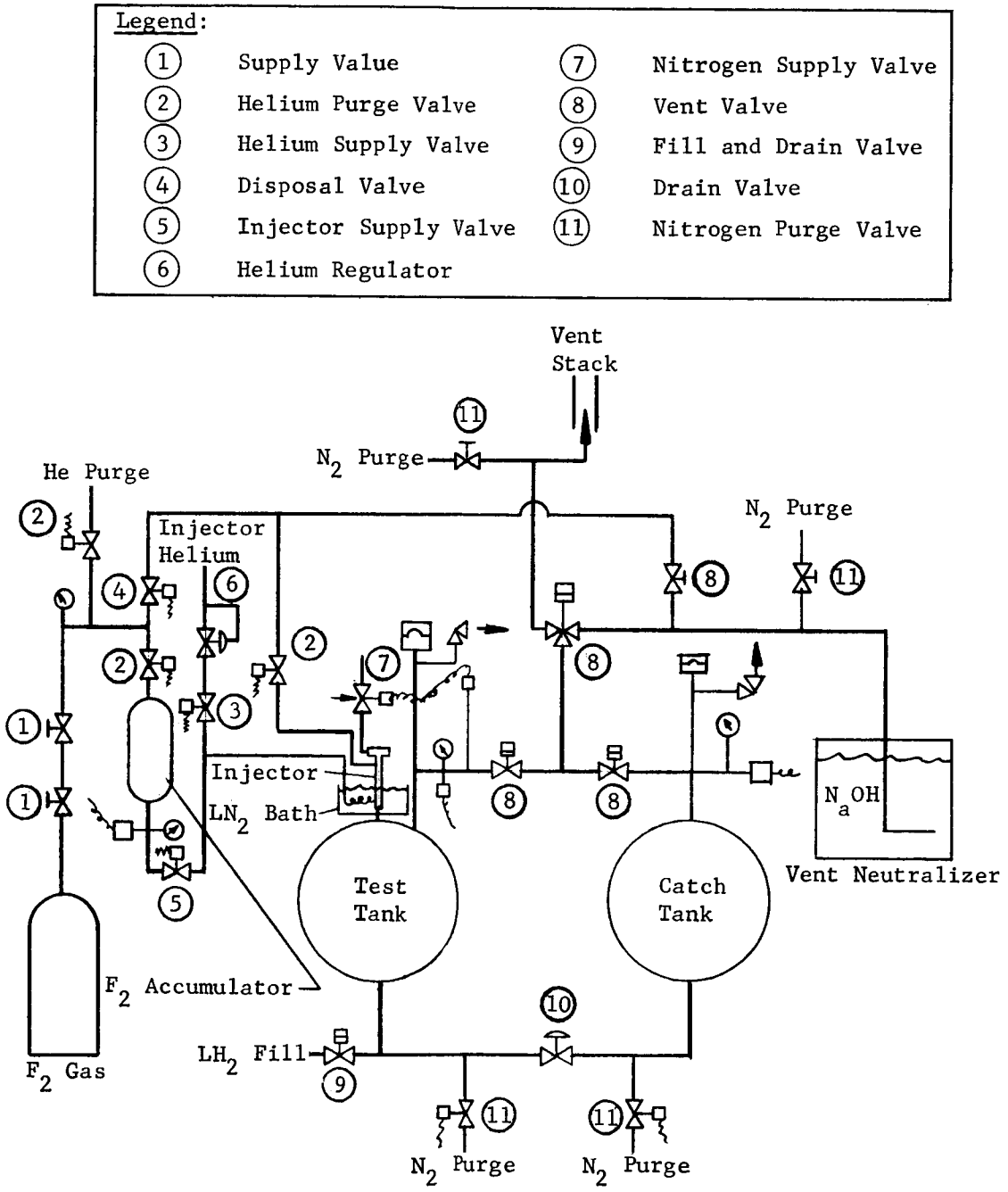

Fig. 51 Test System Schematic, Liquid Fluorine Injection into Liquid Hydrogen

The fluorine gas cylinder was provided by the fluorine manufacturer. It is a high pressure returnable cylinder with a capacity of 6 lb of gas at 400-psig pressure. The cylinder is equipped with a Chlorine Institute valve. A "T" wrench and gearing arrangement was attached to the cylinder valve so that it could be operated from behind a concrete wall.

Valves 1 and 2 were Hoke, 1/4-in, hand operated, bellows seal valves. Valve 1 (upper) served as a backup shutoff valve for the fluorine cylinder. Valve 2 was used as a positive shutoff valve to prevent water from entering the fluorine system from the vapor disposal system. All other valves in the fluorine system were Hoke 1/4-in. solenoid valves with 1/32-in. orifices. The valve bodies and poppets were stainless steel. The valves are supplied with teflon seats. These seats were removed and replaced with lead. To increase reliability, two valves were mounted in series whatever zero leak shutoff capability was needed.

All lines in the system were 1/4-in. copper tubing with flared fittings. A stainless steel accumulator was used in the fluorine system. The accumulator had sufficient volume to supply fluorine for one test run. Therefore, the accumulator could be filled from the fluorine "K" bottle and the "K" bottle could be closed before the test. This gave the system an added safety feature by limiting the amount of fluorine in the system during a test.

2) Vapor Disposal System

Vented gases which might contain F_2 or HF had to be neutralized. As the maximum amount of fluorine which was present in the test cell at any time was only 6 lb, a relatively simple disposal system was used. The vent lines from the fluorine supply system vent and the test equipment vent were connected to a 2-in. copper line. The 2-in. line was led into and across the bottom of a 55-gal. drum. The end of the 2-in. line was plugged and the horizonal section of the tube was perforated to disperse the gas into the tank. The tank contained a 10% solution of NaOH. This system diluted the vent gases with the nitrogen purge than neutralized them as they bubbled through the solution.

Vent gases from the test tank were not vented through the disposal system when the tank contained liquid hydrogen. The low temperature of the hydrogen would condense any fluorine and hydrogen fluoride which might be present. Therefore, the only hazardous material which had to be disposed of was the hydrogen itself. This was accomplished by venting the tank to an atmospheric vent stack which was under continuous nitrogen purge. The outflow catch tank was vented in the same manner as the test tank.

3) Injector System

Figure 52 is a schematic of the injector. The shutoff rod actuator is a pneumatic piston with a spring to return it to the closed position. A chemical spray gun operator was modified for this use. Pneumatic pressure for the actuator was supplied by a 1/2 in., solenoid operated, three-way valve. The three-way valve was controlled by a pressure switch in the test tank or a manual switch on the control console.

The actuator controlled the injector shutoff rod. This shutoff rod ran the length of the injector body and seated in the orifice spray tip. The shutoff rod, injector body, and orifice tip were constructed of stainless steel. The annular clearance between the rod and the body was kept to a minimum and sealed with teflon. The long injector body allowed liquid fluorine to be maintained above the orifice, but caused the liquid to be vaporized in the long annular space. The teflon seal is thus protected from the liquid by a buffer zone of gas.

A condensing coil of 1/4-in. copper tubing was connected to the injector. The coil length of 110 in. allowed approximately 0.15 lb of fluorine to be condensed. The condensing coils and the lower end of the injector were immersed in a liquid nitrogen bath. The liquid nitrogen not only condensed the fluorine, but also prevented the fluorine from solidifying due to the liquid hydrogen environment of the tank.

The injector could be controlled either manually or automatically. A selector switch on the control console determined the mode of control. In manual, a switch on the console controlled the injector. In automatic, the injector was controlled by a pressure switch in the test tank.

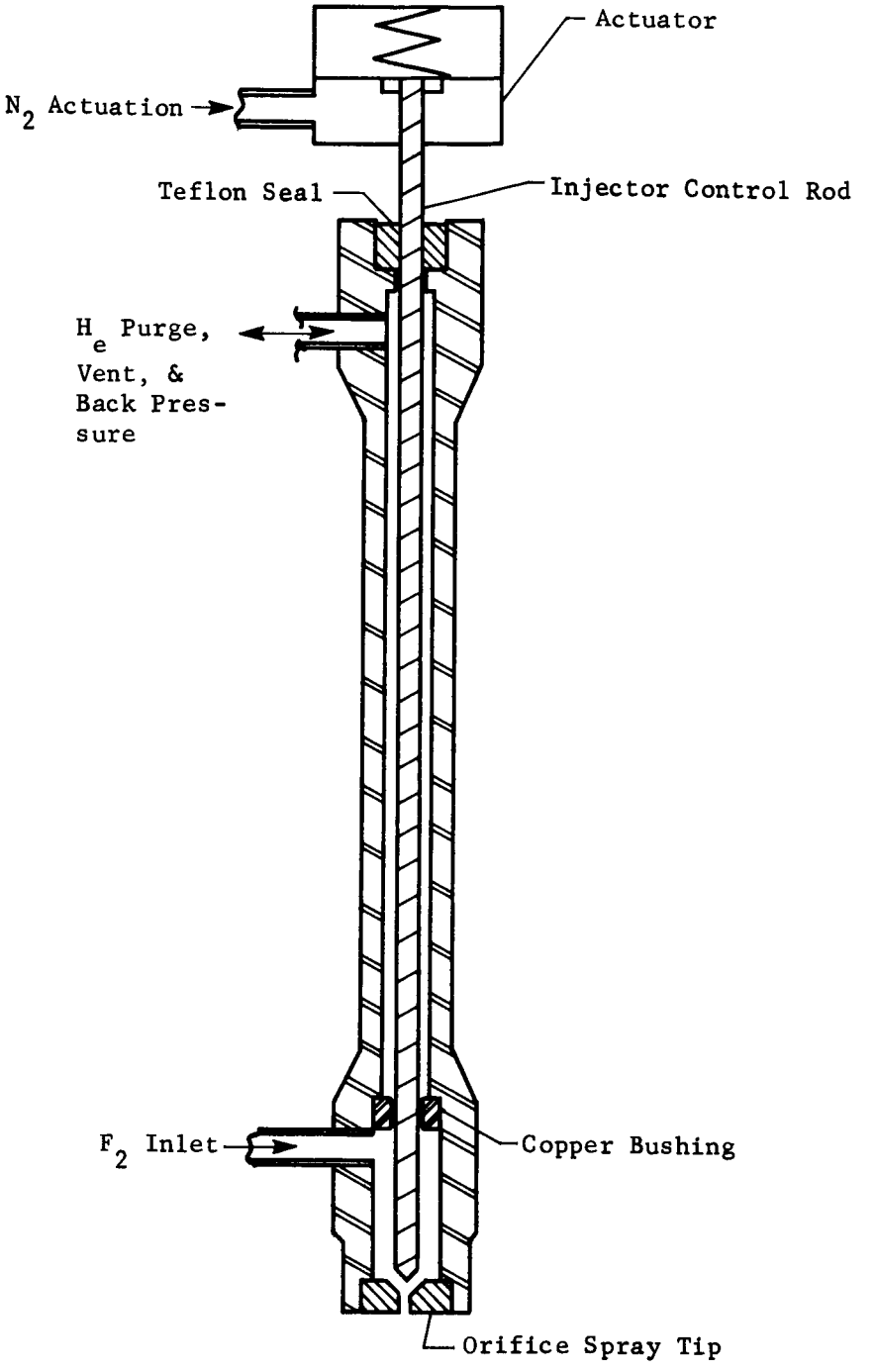

Fig. 52 F_2 Injector Detail

4) Tank System

The tanks used for the MTI test were 5.33-cu-ft aluminum (6061-0) spheres with a 5/8-in. wall thickness. One sphere was used as a test tank and one was used as an outflow catch tank. The test tank was equipped with ports for the injector, instrumentation, vents, and fill lines. A standoff pipe was used to isolate pressure transducer, pressure switches, relief valves, and burst discs from the liquid hydrogen environment. The instrumentation rake entered the tank through the vent port.

A single line entering the bottom of the test sphere served as a fill and outflow line. The line was teed with one line connected to the liquid hydrogen fill valve and the other line connected through the outflow control valve to the catch tank.

The catch tank had an inlet line at the bottom which was connected to the outflow control valve. A single port in the top of the catch tank was used to connect the tank to the vent system and to a standoff pipe. The standoff pipe was used for mounting a pressure gage, a relief valve, and a burst disc.

The test tank was insulated with 1/4-in. granulated cork board cut in "orange peel" sections and bonded to the tank with Narmco adhesive. The outflow line and outflow control valve were insulated by wrapping them with polystyrene foam. The catch sphere was left uninsulated.

After the fifth test, the test tank was modified to improve the liquid hydrogen loading operation. The pressure transducer, pressure switch, and pressure relief valve were mounted on the vent line. The standoff pipe was removed and replaced with a liquid hydrogen fill line and valve. The teed fill and outflow line in the bottom of the tank was replaced with an elbow connection to the outflow control valve. Figure 53 shows the final tank configuration.

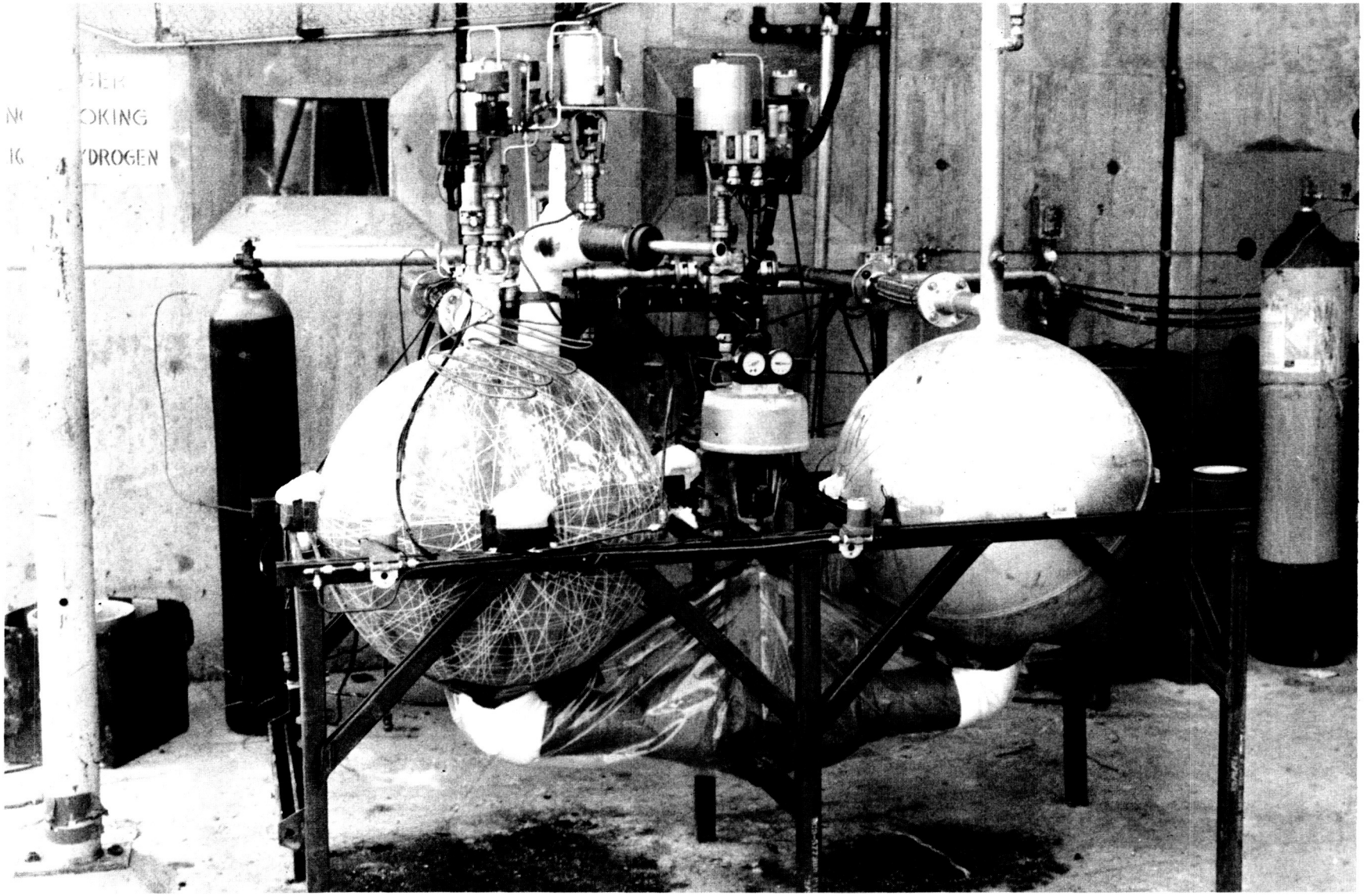

Fig. 53 Final Tank Configuration

5) Instrumentation

The following instrumentation was used to monitor the tests:

a) Pressure

Accumulator and test tank pressures were recorded for all tests. Statham pressure transducers which had been calibrated on a dead weight tester were used for these pressure measurements. In addition, visual read out gages were installed in the fluorine system downstream of the fluorine bottle shutoff valve and at the accumulator. Helium purge and pressure bottles were equipped with standard bottle regulators and pressure gages. A visual read out pressure gage was used to observe the catch tank pressure.

b) Temperature

No temperatures were recorded during the first five tests since these tests were to establish feasibility only. In the remaining tests a thermocouple rake was installed in the test tank. Copper-constantan thermocouples were used with an ice reference bath.

c) Liquid Level

Initially, two thermistors were used to measure liquid level. The thermistors used were Keystone Carbon Company midget discs. These thermistors were calibrated by measuring their resistance at saturated liquid hydrogen temperatures. After the fifth test, three thermistors were used.

d) Television

Two remote television cameras were used to monitor the test visually.

6) Test Area

The test equipment was installed in the service cell of the Liquid Hydrogen Test Facility. This provided ready access to instrumentation and control equipment. No cell modifications were necessary because the quantities of fluorine handled were small.

b. Liquid Fluorine-Liquid Hydrogen Reaction Test Equipment

1) Fluorine Supply System

The fluorine system of the MTI equipment was used for the LF_2 - LH_2 reaction test.

2) Vapor Disposal System

The vapor disposal system of the MTI equipment was used for the LF_2 - LH_2 reaction test.

3) Injector System

The injector system of the MTI equipment was used for the LF_2 - LH_2 reaction test. However, a smaller liquid nitrogen bath and condensing coil was used for the LF_2 - LH_2 reaction test.

4) Test Vessel

The LF_2 - LH_2 reaction tests were conducted in a clear glass dewar with a 120-mm inside diameter and a 300-mm depth. A metal cover with a neoprene gasket was bolted to the support stand to seal the dewar. The injector, fill line, and vent line entered the dewar through and were supported by the cover. Figure 54 shows the test dewar and associated equipment.

5) Solid Fluorine Equipment

A glass fluorine condenser was used to condense and freeze fluorine inside the dewar for one test. The condenser consisted of a glass tube with a small side tube attached to it. The neck of the tube passed through the dewar cover and was connected to the fluorine system. The side tube of the condenser was placed against a fixed rod extending down from the cover of the dewar. A loop of wire attached to a movable rod was then fitted around the side tube. The movable rod was actuated by a pneumatic cylinder. When actuated, the movable rod would move up shearing off the side tube against the fixed rod.

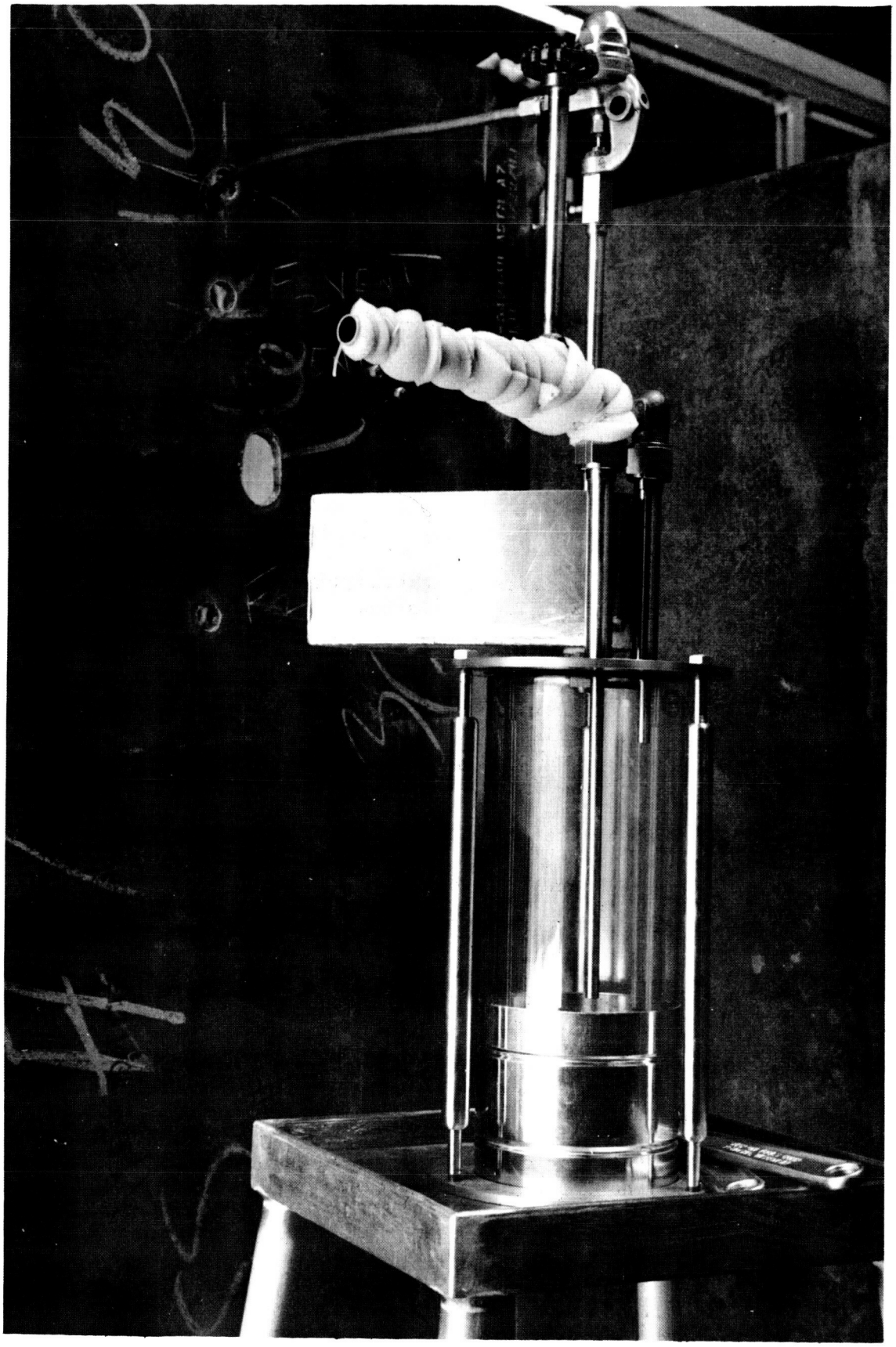

Fig. 54 Test Dewar and Associated Equipment

6) Instrumentation

The following instrumentation was used to monitor the tests.

a) Pressure

Only the pressures in the fluorine supply system were monitored. These were monitored with the visual gages described previously.

b) Temperature

No temperatures were measured.

c) Television and Photographic Coverage

Two remote television cameras were used to monitor the test. Two high speed motion picture cameras were used to record the results of the test. One camera running at approximately 2000 frames/sec. was mounted 3 ft away from the test dewar to take closeup pictures of the experiments. The second camera was mounted approximately 20 ft away to get overall pictures of the test equipment at speeds of 200 frames/sec.

7) Test Area

The test equipment for the LF_2-LH_2 reaction tests was also installed in the service cell of the Liquid Hydrogen Laboratory. This permitted maximum use of the equipment previously used in the MTI tests. The test and catch tank from the MTI tests were removed and the LF_2-LH_2 reaction test dewar was installed in their place. A blast shield of 3/8-in. steel was placed around the test dewar to prevent damage to the equipment in the test cell.

The MTI equipment control console was used for controlling the LF_2-LH_2 reaction test.

c. Test Procedure

1) Main Tank Injection Tests

The test tank ullage pressure switch would be set to the desired pressure before each test. If the fluorine was to be injected as a liquid, the liquid nitrogen bath would be filled just prior to loading liquid hydrogen. After purging the tank with gaseous hydrogen the tank would be filled with hydrogen from a portable dewar. The dewar would then be removed from the cell and all personnel cleared from the area.

When the test area was clear, the fluorine bottle would be opened from behind the cell wall by means of the extension handle. Fluorine gas would be purged through the system and out the vent to remove the residual helium in the system. The vents would then be closed and the accumulator charged with fluorine. When the proper accumulator pressure was reached, the fluorine supply bottle would be closed and the operator would return to the control room.

For liquid injections, the fluorine would be admitted to the condensing coils and liquefied. The injection pressure would then be adjusted by venting or pressurizing the accumulator with helium gas. Injection pressure for gaseous injections was supplied by the fluorine gas pressure in the accumulator.

The basic procedure for pressurizing and outflowing the liquid hydrogen was as follows:

The test tank vent would be closed;

A single short injection would be made;

If a pressure increase was obtained the injector was placed in automatic and the tank allowed to pressurize to the pressure switch setting;

If the proper pressure was obtained the outflow control valve would be opened and the liquid hydrogen outflowed to the catch tank where it would boil off through the vent. The injector would remain in automatic control throughout the outflow tests;

When the test tank was empty, the injector would be returned to manual control and the test tank would be vented;

Hydrogen outflow rate was approximately 0.44 cu ft/sec.

If at any time the proper pressure response was not obtained, the injection would be stopped and the test tank vents opened.

After a test, any liquid hydrogen remaining in the test tank would be emptied into the catch tank and allowed to boil off through the vent. After the liquid hydrogen had boiled off the test tank and catch tank would be purged with warm nitrogen. Residual fluorine would be vented through the scrubber bath and the system purged with helium.

2) Liquid Fluorine-Liquid Hydrogen Reaction Tests

The procedure for loading hydrogen and fluorine for the reaction tests was the same as that used for the MTI tests. The injection tests were made as follows:

When the fluorine and hydrogen were ready, the cameras and lights would be turned on;

One or two short injections would be made with the vents open;

The camera and lights would be turned off;

If the dewar was still intact, the hydrogen would be removed by purging the dewar with helium;

Residual fluorine would be vented through the scrubber bath and the system purged with helium.

The solid fluorine tests were made as follows:

The fluorine system would be thoroughly purged with helium to remove all residual fluorine;

The dewar would be filled with liquid hydrogen;

The accumulator would be pressurized with fluorine to about 10 psig;

The fluorine would be admitted to the condenser and a small amount of fluorine condensed and solidified;

The fluorine system would then be vented and the system purged to remove residual fluorine from the condenser;

The cameras and lights would be turned on;

The movable arm would be actuated and the side tube of the condenser broken so that the liquid hydrogen could flow onto the fluorine;

When the reaction has ceased, the camera and lights would be turned off;

If the dewar was still intact, the hydrogen would be purged out of it with helium.

d. Results

1) Main Tank Injection Tests

Initial attempts to pressurize the liquid hydrogen tank by injecting fluorine directly into the hydrogen were stymied by the fluorine freezing in the injector orifice. This problem was solved by (a) mounting the injector in a "stand-off" fitting to insure that the orifice was maintained at liquid nitrogen temperature or higher and (b) increasing the orifice size from 0.013- to 0.026-in. diameter. Following these corrections, the tank was successfully pressurized by using liquid fluorine (Test No. 4).

Test No. 5, however, resulted in explositon inside the hydrogen tank. This explosion was attributed to a delayed reaction. Following repair of the equipment, the remainder of the MTI tests were successfully conducted with gaseous fluorine (although injector tip burning did occur).

Results of all MTI tests are listed in Table 26.

Table 26 Fluorine Injection Feasibility Test Summary

Test No.	Injector Orifice Diameter (in.)	Injector Pressure (psig)	Fluorine Injected as:	Hydrogen Tank Ullage (%)	Remarks
1	0.013	150	Liquid	25	Several injections were made with both open and closed vents. No pressure rise obtained. Orifice apparently frozen closed.
2	0.013	150	Liquid	15	One injection was made with no rise in tank pressure noted. Injector again apparently frozen closed.
3	0.026	150	Liquid	25	Three injections caused tank pressure rise, then orifice froze closed. The orifice was increased in hopes of eliminating the freezing problem.
4	0.026	150	Liquid	30	Injector mounted in standoff fitting to protect tip from liquid hydrogen temperatures in tank. Manual injections caused pressure rise. Automatic control was attempted with tank outflow. Tank pressure was controlled over a band of 46 to 50 psig during outflow.
5	0.026	150	Liquid	10	Full automatic system checkout, vents were closed, and run was started. No pressure rise was noted. Three normal injections were made with no pressure rise. A sudden explosion occurred in the tank. Review of test data indicated 0.15 lb of fluorine was injected prior to a reaction.
6	0.026	225 to 60	Gas	30	Two outflow runs were made with no problems. Tank pressures varied from 46 to 50 psig. Maximum ullage temperature was 60°K.
7	0.026	210 to 100	Gas	25	Twenty sec were required to build tank pressure from ambient to 150 psig with the injector wide open. Outflow occurred at an excessive rate causing injector to remain open. Tank pressure decayed during run.
8	0.026	210 to 195	Gas	30	Thirty sec were required to build tank pressure from ambient to 175 psig. Outflow was started, but due to rapid tank pressure drop, it was stopped. Tank pressure would not build up above 150 psig with injector open.
9	0.026	375 to 320	Gas	30	Tank pressures were maintained between 172 and 175 psig during outflow. Maximum ullage temperature was below 70°K.
10	0.026	340 to 305	Gas	15	

Note: % ullage is an estimate based on loading conditions.

2) Liquid Fluorine-Liquid Hydrogen Reaction Tests

The liquid fluorine-liquid hydrogen reaction tests were initiated to further investigate the delayed reactions. Photographic proof of the delayed reaction was obtained during these tests. Although ignition was instantaneous for most injections, several-millisecond delays were noted in some injections and a few injections were made in which no ignition was obtained.

A summary of individual tests is presented in Table 27.

Figure 55 shows a series of high speed photographs from Tests 2 and 5. Reaction occurred in one test but not in the other, even though test conditions were the same.

e. Conclusions

This test program demonstrated that it is possible under some conditions to pressurize a liquid hydrogen tank by main tank injection. However, the tests also showed there are several problems which would have to be solved in order to produce a reliable MTI pressurization system for liquid hydrogen tanks. These problems are:

Hydrogen and fluorine are not always reactive;

Local hot spots in the ullage can melt the injector when using gaseous injection;

Freezing of fluorine within the injector is possible.

2. Storage Container Testing

A test program to verify analytical data for expansion of helium from a spherical container was performed in the liquid hydrogen laboratory.

The test hardware consisted of a shrouded 5.33-cu ft helium storage sphere mounted inside an insulated cylindrical tank. Figure 56 presents schematically the entire test installation. During helium loading, both the shroud and the cylindrical tank were filled with liquid hydrogen. Two types of tests were performed. During Test 1, liquid hydrogen was maintained in both the shroud and the cylindrical tank to simulate isothermal conditions. For Test 2, however the liquid hydrogen in the shroud was expelled by helium gas prior to initiation of helium outflow from the container. The helium gas in the shroud, because of its low thermal conductivity, provided an insulation barrier which simulates adiabatic conditions in the container.

Table 27 Fluorine Hydrogen Reaction Test Summary

Test No.	Injector Orifice Diameter (in.)	Injection Pressure (psig)	Fluorine Injected as:	Remarks
1	0.013	50	Liquid	One injection was made. Ignition occurred as soon as stream entered hydrogen atmosphere.
2	0.013	50	Liquid	Two injections of different duration were made. Same results occurred as in Test 1.
3			Solid	Fluorine was condensed and solidified in a glass tube within the hydrogen dewar. The condenser tube was then opened to the liquid hydrogen. Ignition occurred at the moment of contact of the liquid hydrogen and solid fluorine.
4	0.013	50	Gas	Gaseous fluorine was injected into the hydrogen gas ullage above liquid hydrogen. No reaction was observed.
5	0.013	50	Liquid	Liquid fluorine was injected into the hydrogen gas ullage above liquid hydrogen. No reaction was observed.
6	0.013	50	Gas	Gaseous fluorine was injected into the hydrogen gas ullage above liquid hydrogen. No reaction was observed; however, the ullage space became cloudy indicating the presence of a condensible vapor.
7	0.013	50	Gas	
8	0.013	110	Gas	Gaseous fluorine was again injected. No reaction was noted, although the ullage again became cloudy.
9	0.013	100	Liquid	Liquid fluorine was injected into liquid hydrogen. One short injection was made with no reaction. A second long injection was made which was followed by detonations. Photographic results indicated the fluorine from the second injection was frozen and dropped to the bottom of the liquid hydrogen container prior to detonation.

Reaction Test No. 2, Liquid Injection (Reaction Occurred)

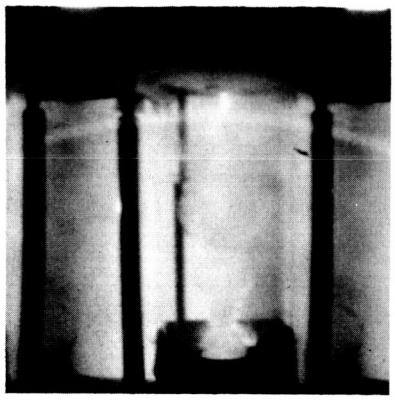

0.025 second

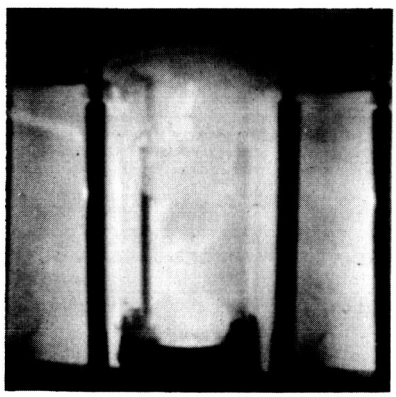

0.035 second

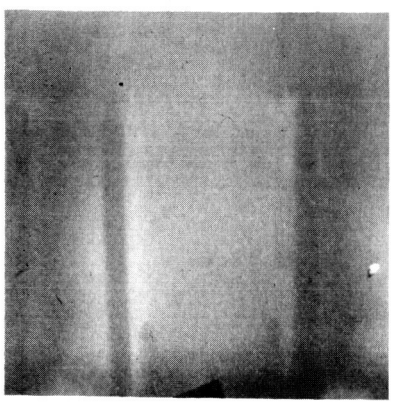

0.50 second

Reaction Test No. 5, Liquid Injection (No Reaction Occurred)

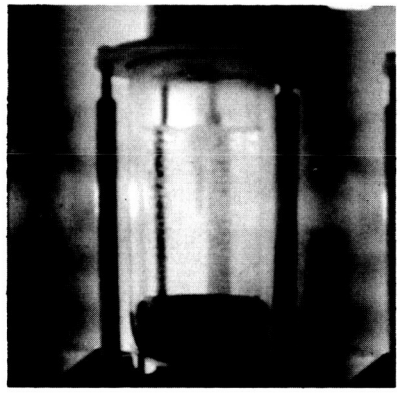

0.025 second

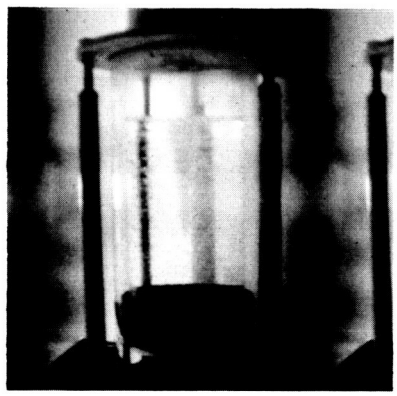

0.035 second

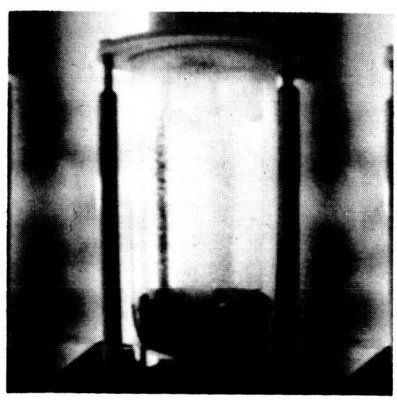

0.50 second

Fig. 55 Reaction Test, Fluorine and Hydrogen, Test 2 and 5

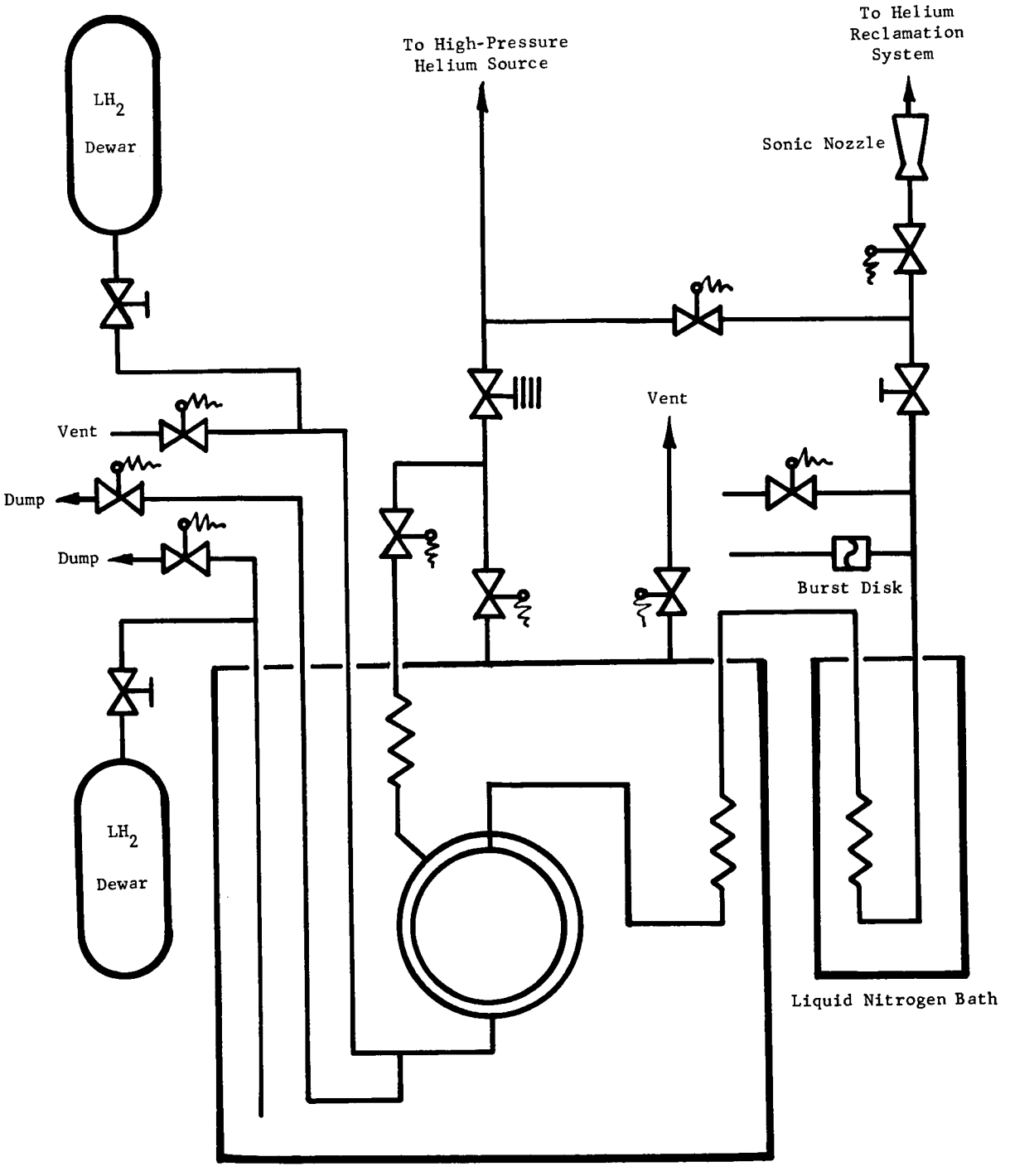

Fig. 56 Plumbing Schematic, Pressurant Storage Test Facility

During container outflow, the helium passed through a heat exchanger in an external liquid nitrogen bath and then to a measuring and flow control device. The flow control device consisted of a 0.15-in. diameter sonic nozzle mounted in a standard flowmeter section. Flow rate through the nozzle was controlled by varying the nozzle inlet pressure with a hand valve upstream of the nozzle. Helium container gas pressure and temperatures, container wall temperature, shroud gas temperature, and the nozzle inlet pressures and temperatures were recorded. The accuracy of the instrumentation used is shown in Table 28. The accuracy value quoted includes, in addition to the basic instrumention calibration accuracy, such items as power supply stability, recorder drift, and data reduction. The use of chromel-alumel thermocouples at cryogenic temperatures is not desirable as indicated by the extremely poor accuracy quoted in Table 28. The chromel-alumel thermocouples were originally installed to investigate heating of the pressurant storage container by passing hot gas generator exhaust through the shroud. When this phase of the test plan was discontinued, the decision was made not to change the thermocouples to a more applicable copper-constantan type because the test fixture has been assembled with the lid on the cylindrical tank welded closed. The actual thermocouple readings were approximately 40°R above the thermistors measuring the helium gas temperature in the container. A correction factor consisting of the initial difference between the thermocouple and thermistor readings was applied to the thermocouple readings throughout the entire outflow period.

Table 28 Instrumentation Accuracy

Measurement	Type of Instrument	Accuracy
Container Gas Temperature	Thermistor	± 0.8°R
Container Gas Pressure	Pressure Transducer	± 1.5%
Shroud Gas and Container Wall Temperature	Chromel-alumel Thermocouples	±43.0°R

The container mass outflow was calculated assuming a choked flow condition. However, it was found that when the calculated mass flow rate history was integrated, the resulting expelled gas weight was much less than that calculated from the initial and final container pressures and temperatures. This difference in expelled weight was attributed to a leak in the region of the flowmeter section flanges. To obtain a realistic flow rate, the

container gas mass history was calculated using the equation-of-state from Ref 3 and the container pressure and temperature histories. The flow rates were then obtained by differentiating the weight history. Table 29 summarizes the test conditions for each of the two tests performed.

Table 29 Initial Test Conditions

Condition	Test No.	
	1	2
Simulated Expansion	Isothermal	Adiabatic
Initial Pressure (psia)	2910	3052
Initial Temperature (°R)	35.9	35.4
Initial Helium Mass (lb_m)	64.4	65.8
Storage Container Volume (ft^3)	5.33	5.33
Nozzle Diameter (in.)	0.15	0.15

Following the tests, it was desirable to compare the experimental data with data generated by the analytical models used in the study. Therefore, the experimental values of initial gas pressure and temperature, container volume, wall temperature, and container mass outflow rate were supplied as inputs to a computer program based on the energy balance equation derived in Appendix B.

Figures 57 thru 59 present data for Test No. 1, and Fig. 60 thru 62 present Test No. 2 data. The experimental pressure, temperature, and mass histories are plotted in the figures as dashed lines. The computer-program-generated data are shown as solid lines. As indicated in the figures, the computer run was not started at time zero but at a point where the outflow was stabilized. Prior to this time, the test technician experienced difficulty in adjusting the hand valve to regulate nozzle inlet pressure.

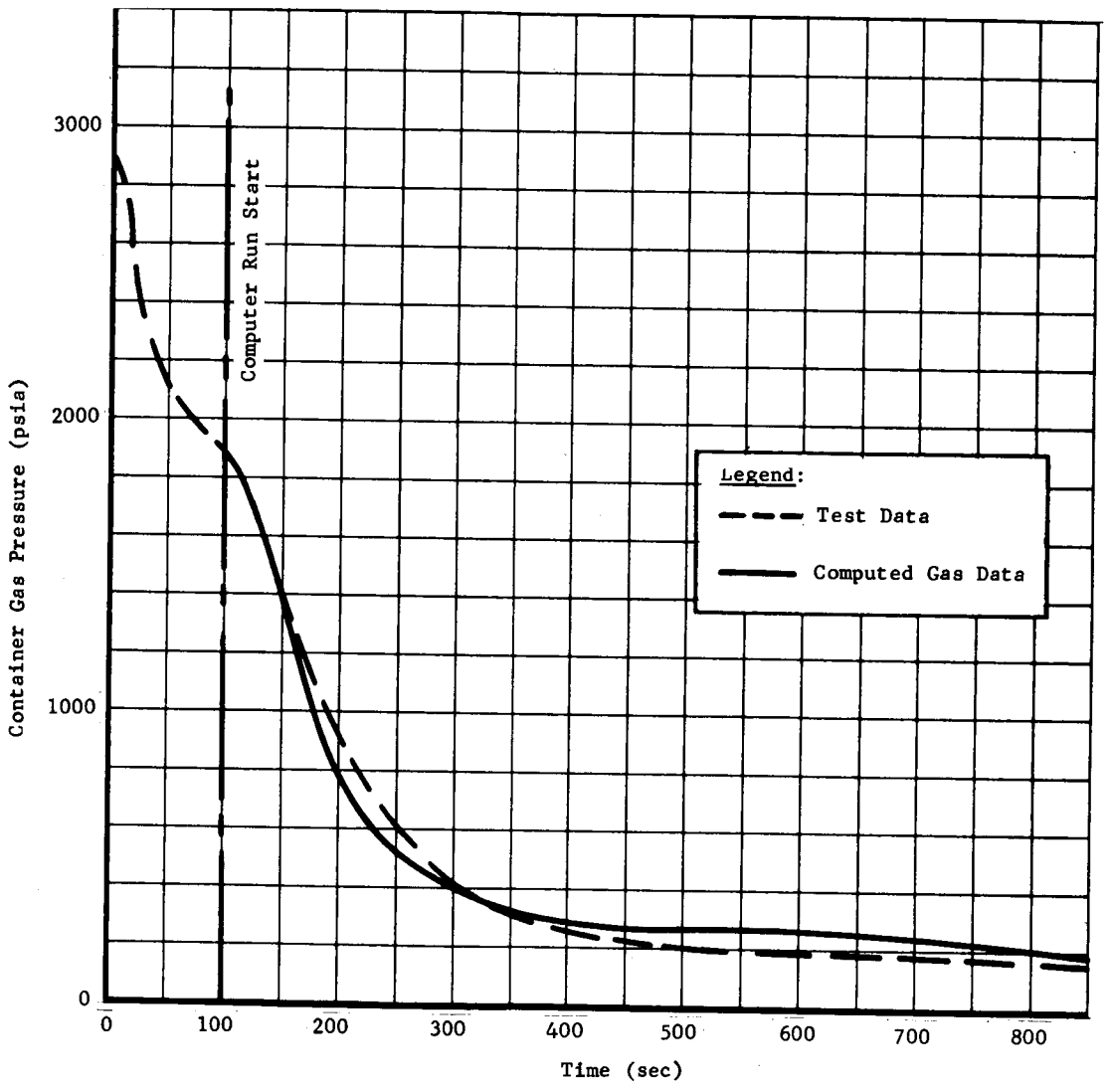

Fig. 57 Helium Container Expansion Test Data, Test No. 1 (Pressure)

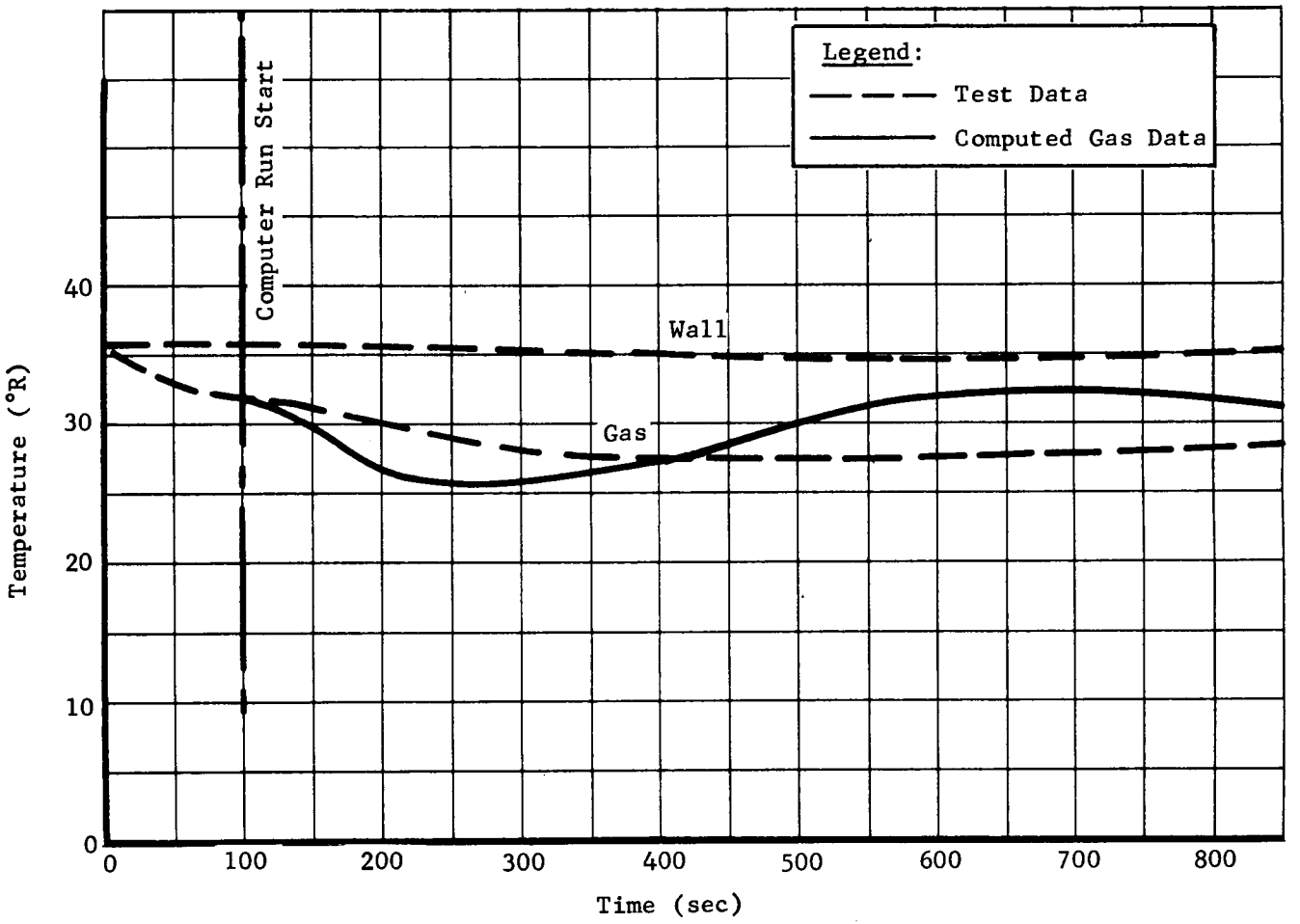

Fig. 58 Helium Container Expansion Test Data, Test No. 1 (Temperature)

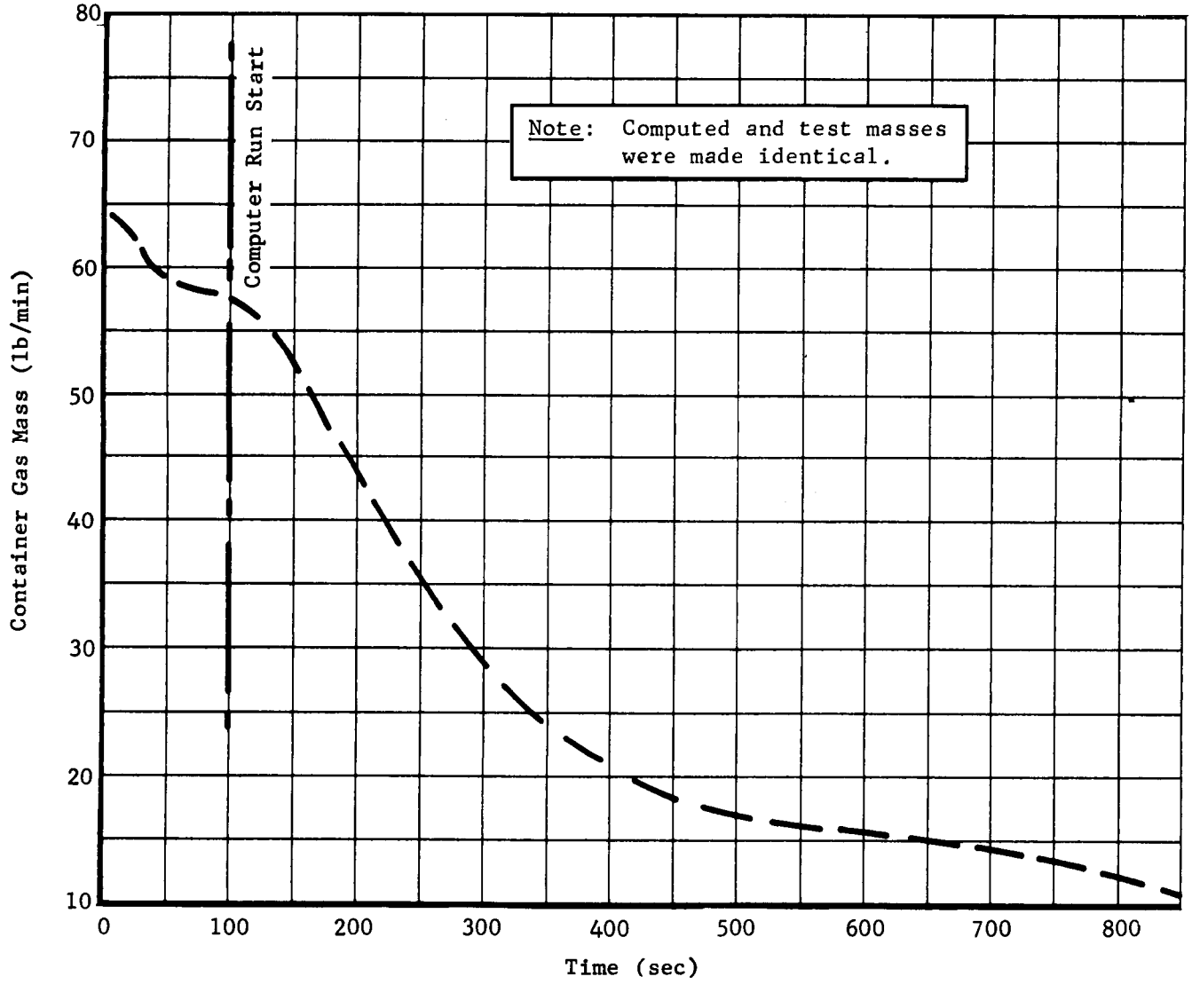

Fig. 59 Helium Container Expansion Test Data, Test No. 1 (Mass)

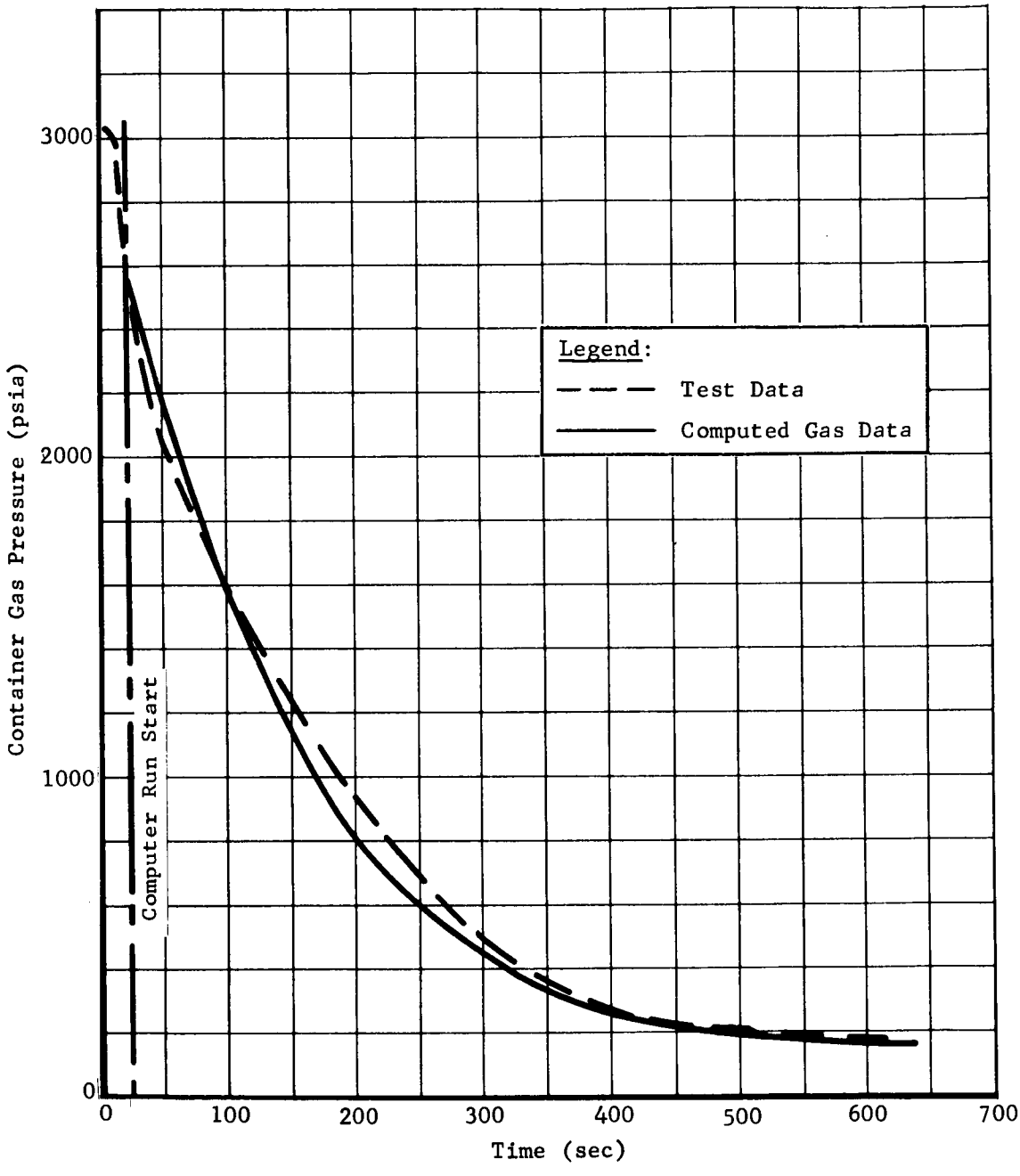

Fig. 60 Helium Container Expansion Test Data, Test No. 2 (Pressure)

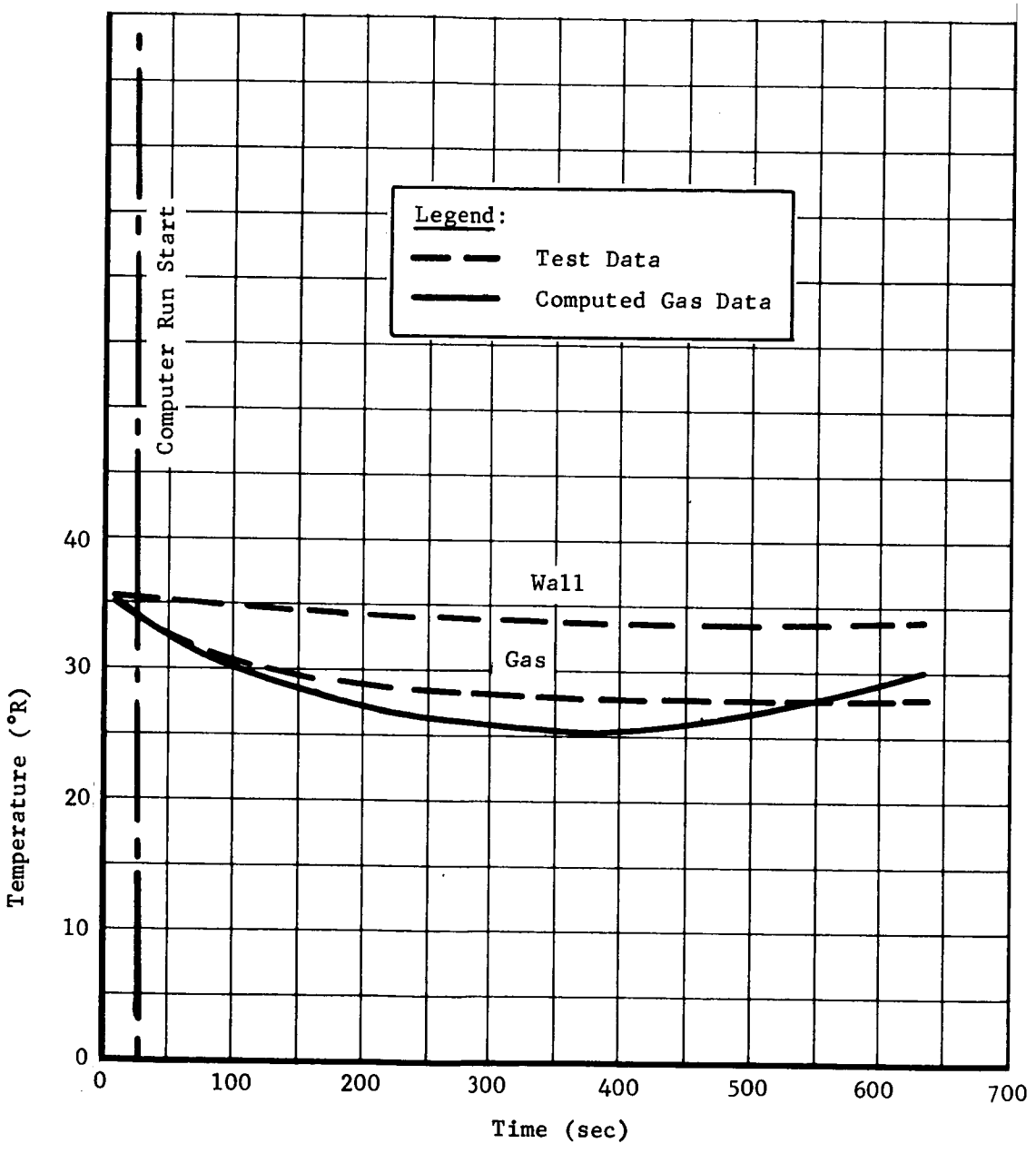

Fig. 61 Helium Container Expansion Test Data, Test No. 2 (Temperature)

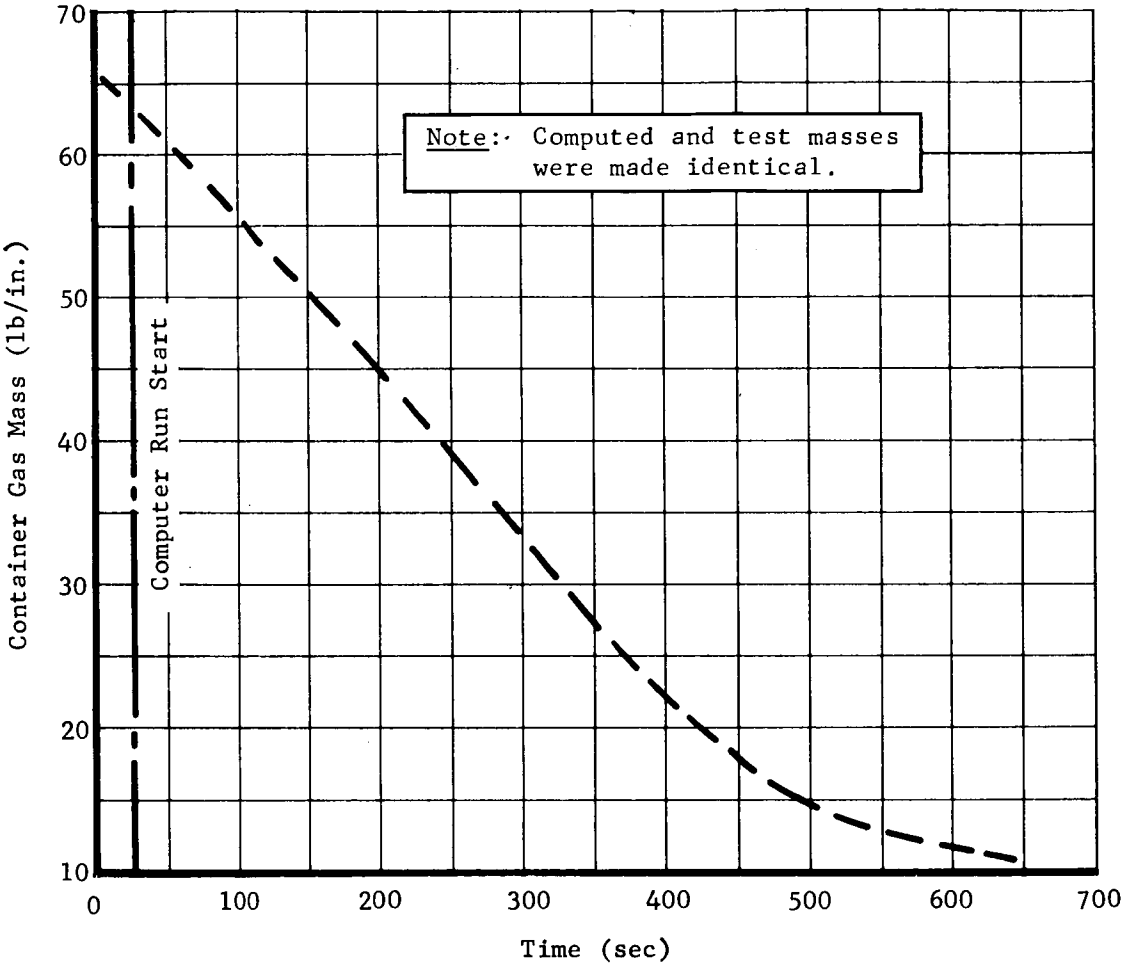

Fig. 62 Helium Container Expansion Test Data, Test No. 2 (Mass)

Since the mass outflow rate was fixed for these tests, the final gas temperature and pressure should have been higher for Test No. 1 (isothermal) than for Test No. 2 (adiabatic). Failure to obtain a significant difference in the experimental results probably reflects (a) instrumentation inaccuracies, (b) high heat transfer to the pressure vessel from the helium gas in the shroud or from extraneous heat leaks, and (c) transient effects caused by difficulty in adjusting nozzle inlet pressure. However the correlation between experimental and computer data was reasonable. Test No. 1 showed the widest variation in temperature and pressure. Maximum deviation in temperature was approximately 4°R for Test No. 1 and 2.5°R for Test No. 2. When the computed temperature history is below the experimental value, the computed pressure also below its corresponding experimental value. Thus, if better temperature correlation was obtained, the pressure correlation would also be improved. The container gas temperature, as generated by the computer program, is based on an energy balance considering both the energy dissipated by the container mass outflow and the heat transfer into the container gas from the wall. Since the mass outflow has been fixed by the experimental mass outflow, the heat transfer rate is the only factor affecting the temperature history that can be readily modified in the program. In the program, the heat transfer rate is calculated by employing the following heat transfer coefficient equation (Ref 4):

$$h_f = 0.13K_f \left[\frac{\rho_f^{\,2} C_p g \Delta T \beta_f}{\mu_f K_f} \right]^{1/3}, \qquad [83]$$

where

h_f = heat transfer coefficient $(\text{Btu/sec ft}^2\text{-°R})$,

K_f = thermal conductivity (Btu/sec ft °R),

ρ_f = density $\left(\text{lb}_m/\text{ft}^3\right)$,

C_p = specific heat at constant pressure $(\text{Btu}/\text{lb}_m\text{-°R})$,

g = acceleration (ft/sec^2),

ΔT = temperature difference (°R),

β_f = coefficient of thermal expansion $(°\text{R}^{-1})$,

μ_f = viscosity $(\text{lb}_m/\text{ft-sec})$.

This heat transfer equation was developed for turbulent flow on vertical surfaces. Since the container was spherical, the equation is not strictly applicable, although, no better equation was available for a spherical surface. However, no further improvement of the analytical data was attempted, since the variation of experimental and analytical data was within instrumentation accuracy.

By modification of either or both the constant 0.13 and the exponent 1/3 in the heat transfer equation, better correlation between analytical and experimental data might be obtained. However, considering the uncertainty in wall temperature measurement, these additional refinements in the analytical model could not be justified. Even with the uncertainty, the correlation between analytical and experimental data was considered adequate to verify that the analytical model could supply reasonable data for design purposes.

3. Component Testing

Testing was accomplished on pressurization control (bang bang) solenoid valves, gas generators, pressure switches, check valves, solenoid temperature compensators, mechanical couplings, seals, and fittings. These tests were performed to determine which design types or design modes of various components would be most suitable for application to the cryogenic systems under investigation. Only those parameters in each component were checked that would best signify a trend or change in performance from normal ambient to the anticipated cryogenic temperatures. For example, in solenoid valves, leakage and response time were measured.

For the purpose of evaluation, certain limits were specified for each tested parameter. Solenoid valve internal leakage in excess of 1000 sccm/hr of helium at 3000 psig was considered to be out of limits. Response time was set at a maximum of 50 msec. Static seals, couplings, and fittings were expected to have no measurable leakage utilizing a pressure decay or bubble displacement method of leak check.

Vendors of the components tested were contacted to determine if suitable designs for the stated parameters were available and if sample units were available for loan during the test period. Also, vendors of pressurization control devices were asked to submit either pressure regulator and/or solenoid valve designs that they deemed best for this application. B. H. Hadley, Inc, was the only vendor to submit a pressure regulator in preference to a solenoid valve. This regulator is a part of the Apollo system, but after approximately six months of flight certification and development tests, the unit had not met all design parameters. For this reason, only the solenoid valve/pressure switch combination was considered.

Only W. M. Lanagan Company and Calmec Manufacturing Corporation submitted solenoid valves for test. The Lanagan valve was stated as being noncryogenic; however, it was decided to test it along with a Martin valve, also noncryogenic, to observe the effects of the lower temperatures.

Of the cryogenic solenoid valve designs submitted, only the designs by the Sterer Engineering and Manufacturing Company and the Calmec Manufacturing Corporation were evaluated as suitable for this application. This conclusion was based on the following information.

In the size requested, a pilot-operated valve would be required for minimum weight. Pilot-operated valves require a controlled bleed from upstream pressure past the main poppet to make use of this pressure in closing the poppet. Also, this bleed must be less than the flow through the pilot orifice when the pilot is opened to ensure a pressure differential across the main poppet causing the poppet to open. All other pilot-operated valve designs employed an elastomer type seal around the main poppet in conjunction with an orifice. With the difference in the expansion/contraction rate between the metal and seal at cryogenic temperatures, it is possible that cold flow would occur in the seal and change the controlled bleed rate past the poppet. This would affect the opening/closing time because of the time difference in creating a required pressure differential across the main poppet. Further, if this bleed should equal the bleed through the pilot orifice, the valve would not open.

The Sterer, P/N 28370 and Calmec, P/N 400-503 valve designs employed a metal piston ring around the poppet; therefore, bleed rates can be predetermined and held constant.

The Sterer valve was available in "hard seat" and stainless-on-stainless only. The Calmec valve was available in either hard seat; stainless-on-stainless; or "soft seat," Kel-F on stainless design. For extended usage, the hard-seat valve may be desirable but leak rates (internal) may be higher. The soft-seat valves would probably indicate lower leakage initially, but extended usage may cause cold flow on the seat and increased leakage.

The Sterer valve, even though evaluated as suitable for this application, was not obtained in time to be included in the tests.

In the pressure switch designs, two parameters, (dead band and temperature compensation) were considered most important. Other parameters such as vibration and shock loading were also considered, but in many cases, these parameters could be compensated for by proper packaging; therefore, they were not considered as limiting parameters. Hydra-Electric was the only vendor to submit switch units (Serial No. 14377 and Serial No. 14402) for test. The internal design was not made available.

The Frebank Company submitted a design (P/N 8212-1) that illustrated the use of bimetallics for temperature compensation to avoid shifting of switch point with temperature change. They stated that this switch design was being used for the Saturn IV and had been qualified at liquid hydrogen temperatures. This switch was ordered for test but was not delivered on the contracted date and could not be included in the tests.

The check valve designs were evaluated on the basis of good poppet guidance, large length-to-diameter ratio at the guidance surface (to ensure reseating to the same point), and good flow characteristics (as near axial flow as possible with a minimum of reentry angles). Consolidated Controls Corporation submitted one valve for test. This was a hard-seat type, vendor P/N 189W63. Two valves were purchased from the Sterer Company, vendor P/N 28270 (hard seat) and P/N 28270-1 (soft seat). These two valves were similar to design except for the seat material.

The mechanical couplings, seals, and fittings selection was limited to new or unusual designs because it was felt that sufficient information is available on the common O-ring and spring-loaded elastomer types of seals.

Results of the tests on components are as follows:

a. Solenoid Valves

The three valves tested were the Lanagan solenoid valve, vendor P/N 90059 (Kel-F seat), the Calmec solenoid valve, vendor P/N 400-503 (Kel-F seat) and the Martin solenoid valve, P/N LAB6002065 (tungsten carbide on stainless-steel seat).

The Lanagan valve showed zero leakage, both internal and external, using gaseous nitrogen at room temperature. When cooled down to liquid nitrogen temperature, the leakage rate using helium was excessive -- greater than 1000 sccm/minute. The leakage remained high when ambient temperature was restored. There was apparent permanent damage to the valve, so all further testing was discontinued. Measured leak rates are shown in Table 30.

The Calmec valve showed essentially zero leakage, internal or external, at all the temperatures tested, i.e., at ambient and liquid nitrogen temperatures, using gaseous nitrogen at room temperature and helium at cryogenic temperatures as pressurants. The valve was cycled ON/OFF 1000 times at room temperature, and the temperature was cycled between LN_2 temperature and room temperature with no significant leakage occurring in the 5- to 10-minute measurement time (see Table 30).

Table 30 Solenoid Valve Leakage

Temperature (°F)	Pressure (psig)	Leakage (std cc/min)	Pressurant	Actuated during Test	Remarks
Lanagan Solenoid Valve					
39	2700	0	N_2	no	
200	2700	0	N_2	no	After liquid nitrogen immersion, the valve leakage rate was excessive.
-320	2700	Leakage Rate Excessive	He	no	
52	2700	9060	N_2	no	
Calmec Solenoid Valve					
44	2750	1755	N_2	yes	After actuation of the valve.
46	2700	0	N_2	no	
46	2600	0	N_2	yes	
62	2800	0	He	no	
62	2800	0	He	yes	
-320	2750	0	He	yes	
-320	2750	6.0	He	yes	
53	2775	0	He	yes	
53	2800	0	N_2	yes	
Martin Solenoid Valve					
-320	2275	16.4	He	yes	
52	2400	5.7	He	yes	
66	2800	5.5	He	yes	After a 1000-actuation cycle test of the valve.
-320	2800	1450	He	yes	
-320	2800	1370	He	yes	

The leak rate for the Martin valve was within limits at room temperature. However, the rate became excessive (over 1000 sccm/minute) at liquid nitrogen temperature. Therefore, no further testing was attempted at liquid hydrogen temperature. On reheating to room temperature, the valve again demonstrated satisfactory leakage operation indicating no permanent damage had occurred in the temperature cycle. The poppet of this valve was made of tungsten carbide and the valve seat of stainless steel. Due to the large difference in expansion coefficients between these two materials, it is probable that the increase in leakage at lower temperatures was caused by the differential in contraction causing a different seating point within the valve. Since the poppet was lapped-in at room temperatures, at temperatures other than ambient an unlapped portion of the seat would be in contact with the poppet. This condition existed even after 1000 ON/OFF cycles. Therefore, it is recommended that the materials selected for poppet and poppet seat be identical or nearly identical in contraction or expansion coefficients in applications where a hard-seat valve is used. A good combination would be "300" series and A-286 stainless steels.

The Lanagan valve was not tested for response because the apparent damage that occurred during initial testing prevented any further valve investigations.

The Calmec valve response time was within the 50-msec limit for opening and closing at room temperature, but the closing time increased approximately two and one-half times at liquid nitrogen temperature and approximately nine times at liquid hydrogen temperature. The response time was measured as the difference between the electrical actuation (or deactuation) time and the full-open (or closed) time. Opening response decreased slightly with a decrease in temperature due to an increase in current flow because of the lowered solenoid coil resistance (see Table 31).

The response time for the Martin valve was within the required limits for opening at both room and cryogenic temperatures and within limits for closing at room temperature. The closing time did increase at liquid nitrogen temperature to approximately three times the room temperature value, however, and was out of limits (see Table 31).

Table 31 Solenoid Valve Response

Upstream Pressure (psig)	Temp. (°F)	Pressur-ant	Time to Start Opening (msec)	Time for Full Flow* (msec)	Time to Start to Close (msec)	Time for No Flow† (msec)
Martin Solenoid Valve						
2100	55	He	7.9	33.75	5.7	30.6
2000	55	He	7.6	38.75	5.9	25.25
2750	-320	He	8.0	18.75	19.5	71.25
2750	-320	He	8.0	18.00	20.0	91.25
Calmec Solenoid Valve						
1700	55	He	31.25	37.87	48.8	77.1
1600	55	He	28.75	35.00	47.5	75.0
2800	-320	He	10.5	28.00	153	185
2800	-320	He	12.5	30.2	168	192
2100	-423	He	12.5	36.25	-	-
1500	-423	He	12.5	36.25	630	681

*Time to open is measured from the time electrical power is applied to the full-flow condition.

†Time to close is measured from the time electrical power is removed to the no-flow condition.

In all tests, response was determined from initiation and discontinuance of electrical current to the pressure rise or decay downstream from the valve. Note that this method of testing, in effect, represents a system response and is not truly indicative of the actual valve response. The valve response would, in all cases, be lower than the indicated values.

b. Gas Generator

To establish the performance of an oxygen-hydrogen fueled gas generator, an investigation was made of the availability of an off-the-shelf design of the size desired. Since the investigation produced negative results, a gas generator was designed and built as shown by the assembly drawing in Fig. 63. Gaseous hydrogen and gaseous oxygen were supplied into two plenums in the injector back plate. The hydrogen plenum was annular in shape. From this plenum, eight 0.185-in. diameter holds led to a second plenum on the inner injector plate from which the hydrogen gas issued through a diffuser plate into the combustion chamber. Flow was sonic at the injector face. The oxygen plenum was of circular cross section, feeding into a converging nozzle and thence to the chamber. Oxygen flow was sonic at the nozzle exit. The development test of the gas generator was conducted in two phases. Phase I testing consisted of establishing line pressure requirements as a function of flow rate and the degree of flow control and response of the system. The second phase consisted of firing of the generator at a single flow rate and mixture ratio.

For the Phase I tests, the generator was installed in a test cell according to the flow schematic (Fig. 64). Hydrogen and oxygen, at ambient temperature, were supplied to remotely controlled dome-loaded regulators, then to pneumatic-operated shutoff valves just upstream of the generator. Flow rates in each gas system were measured by orifice meters. The fuel flow section used a 0.5-in. diameter orifice to cover the desired flow range of 0.118 to 0.244 lb/sec, while a 0.25-in. diameter orifice was used on the oxidizer side to cover a range of 0.2- to 0.35- lb/sec flow rate. An initial mixture ratio of 0.35 was used to produce a chamber temperature of approximately 1200°R. A throttling valve was installed at the outlet of the gas generator to maintain the desired chamber pressure of 120 psig. The primary purpose of the Phase I testing was to establish a mass flow versus orifice upstream pressure plot for both gases to be used during the Phase II firing tests.

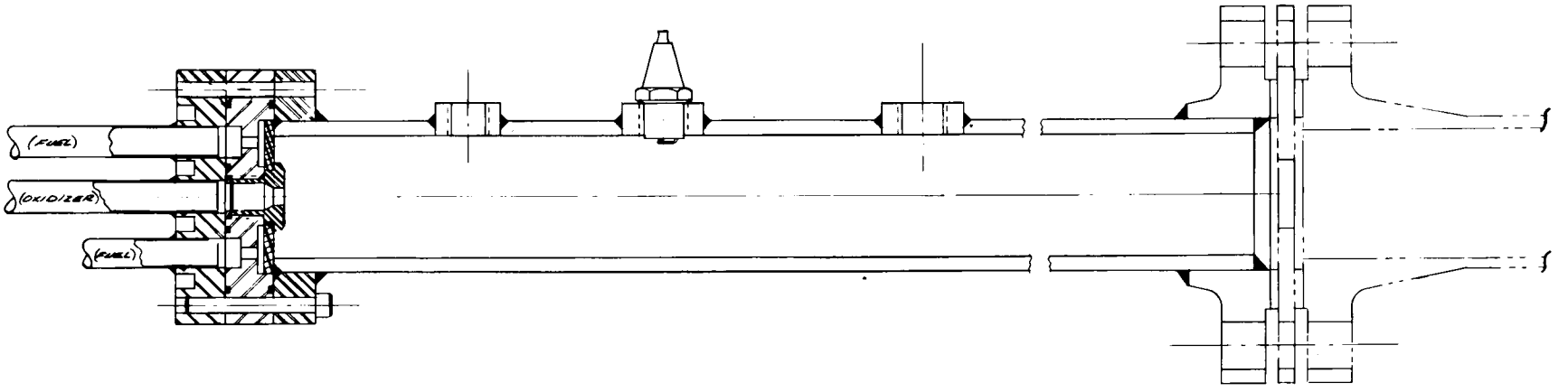

Fig. 63 Gas Generator Assembly

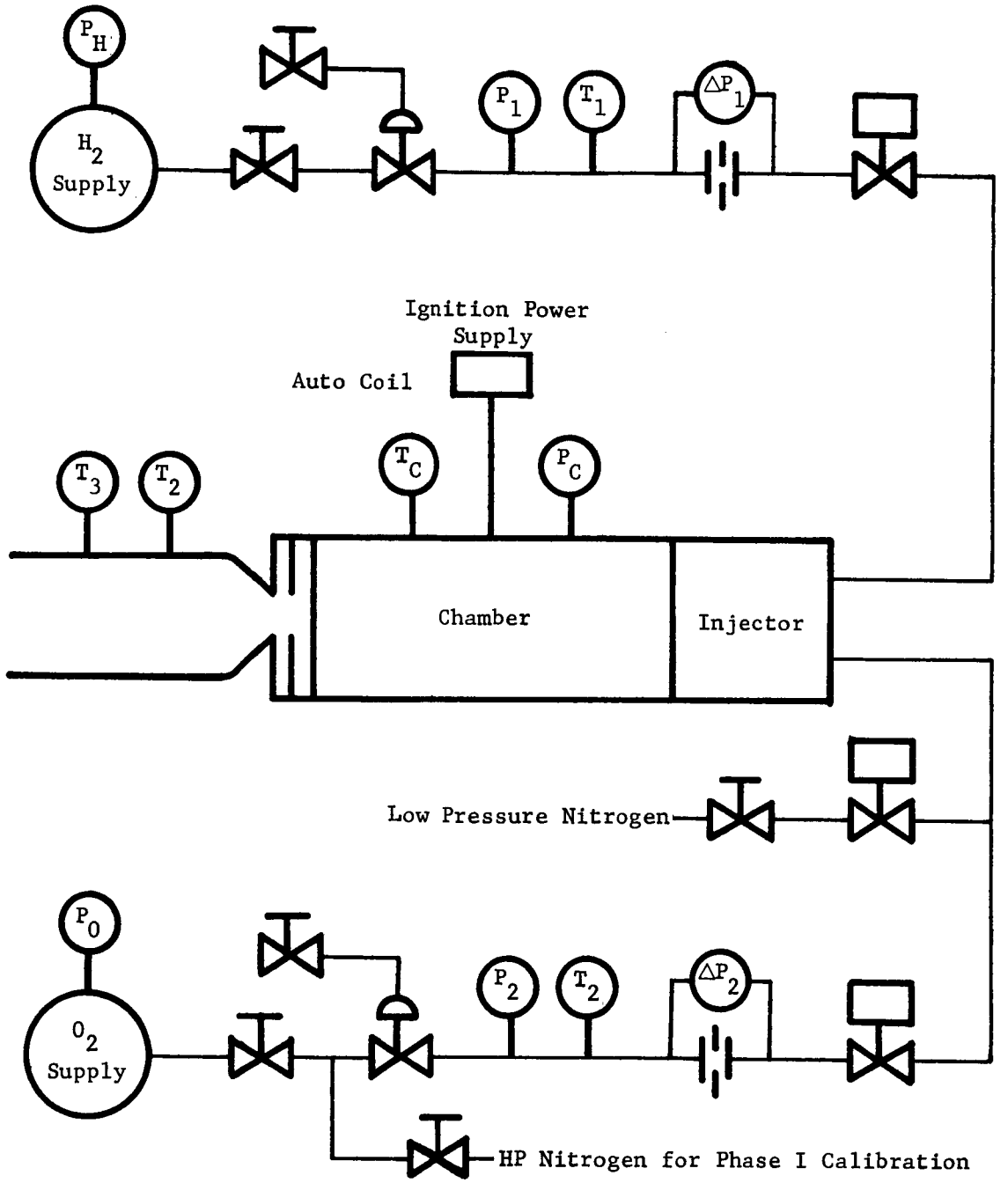

Fig. 64 Test Schematic, Hydrogen-Oxygen Gas Generator

Nitrogen gas was substituted for oxygen during Phase I testing with the following conversion factor used to predict required oxygen upstream pressure:

$$\frac{P_{N_2}}{P_{O_2}} = \sqrt{\frac{\text{molecular wt } O_2}{\text{molecular wt } N_2}} \qquad [84]$$

The results of the calibration runs which completed the Phase I testing are shown in Fig. 65.

For Phase II testing, the throttling valve on the chamber outlet was replaced with a 1/2-in. diameter orifice. During an initial checkout firing, it was found that the glow plug used was not adequate, even though a 10-sec run was accomplished. The glow plug was replaced with a spark plug for the second run. The second run which lasted for 6 minutes and 14 sec was terminated as the result of a metal gasket failure at the chamber exit. The fuel and oxidizer regulators were adjusted after ignition as shown in the variation of the upstream pressure in Table 32.

Table 32 Gas Generator Firing, Run 2

	Fuel*			Oxidizer*			Chamber			
Time (min)	ΔP (psi)	Upstream Pressure (psig)	Upstream Temperature (°F)	ΔP (psi)	Upstream Pressure (psig)	Upstream Temperature (°F)	Pressure (psig)	T_c (°F)	T2 (°F)	T3 (°F)
0	0.5	7.5	76.5	4.5	7.5	76	0	--	--	--
1	8.1	97.5	83.8	6.8	37.5	76	27	1190	950	1000
2	7.6	135.0	83.0	16.7	87.5	76	58	1520	1130	1285
3	7.6	134.0	81.5	14.6	80.0	76	53	1490	1135	1300
4	8.5	134.0	80.2	14.2	75.5	76	53	1470	1122	1280
5	6.0	134.0	79.0	14.2	75.5	76	52	1455	1100	1200
6	2.5	95.0	77.5	7.5	23.5	76	38	1080	870	980

Note: 1. ΔP = differential pressure.
2. T_c = inside chamber temperature.
3. T2 = first outside chamber temperature from nozzle.
4. T3 = last outside chamber temperature from nozzle.
5. Atmospheric pressure = 23.91 in. Hg.

*See Fig. 64 for location of pressure and temperature taps.

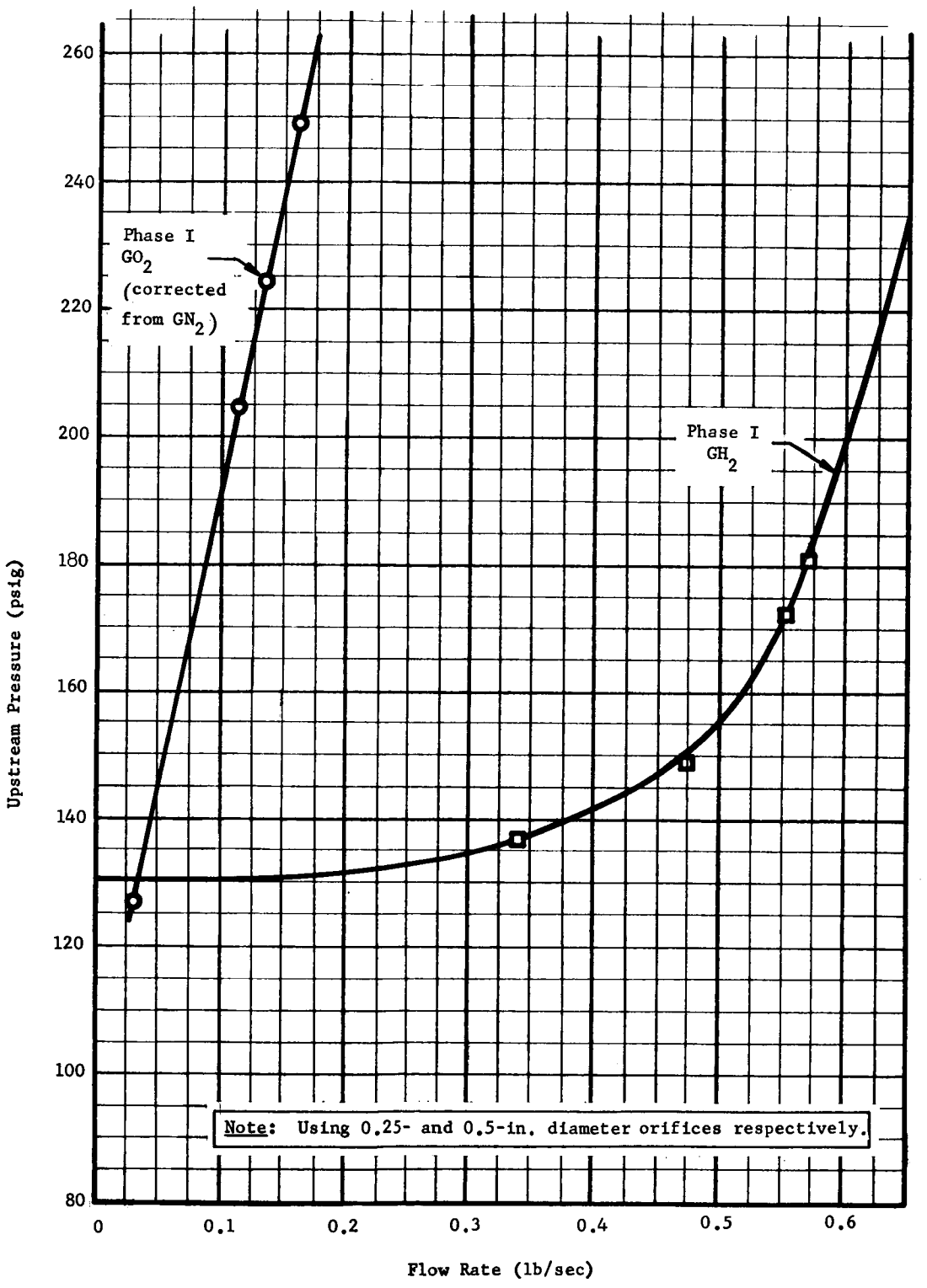

Fig. 65 GO_2 and GH_2 Flow Rate Comparisons for the Gas Generator

In the Phase II run, it was determined that either a discrepancy existed in the calculated flow rate that was due to instrumentation, or the oxygen flow was different than that predicted. Since primary pump-fed engine systems only were considered from this point on, no further analysis of the gas generator was necessary.

c. Pressure Switches

Two 165-psig pressure switch cells were tested both of which were built by Hydra-Electric (Fig. 66). One switch showed a set point shift of up to 1.5 psi due to intentional overpressurization to 200 psig. The other switch did not exhibit this same characteristic when exposed to the same test. The set points for both switches were constant from room temperature to liquid nitrogen temperature but showed a decrease of approximately 1 psi at liquid hydrogen temperature. The dead band for both switches was 5 psi at ambient temperature and 7 psi at cryogenic temperature (see Table 33).

d. Check Valves

The check valves tested consisted of one Consolidated Controls check valve, vendor P/N 189W63, and two configurations of Sterer check valves (P/N 28270 and P/N 28270-1).

The Consolidated Controls check valve uses a conical stainless steel poppet against a soft copper seat. During initial room temperature installation, the leakage was greater than the allowable limit of 1000 sccm/minute using a back pressure of 100 psig gaseous nitrogen. Subsequent cycling of the valve decreased the leakage considerably, but it was still above the limit. Total cycles of the valve exceeded 1500. Cracking pressure was approximately 1.4 psid (See Table 34).

The Sterer check valves (both hard seat and soft seat) showed excessive leakage -- more than the stated 10 sccm/hr of helium at room temperature. At liquid nitrogem temperature, the leakage was beyond the range of the instrumentation (1000 sccm/sec). After cleaning of the valves, to ensure no contamination existed, tests were repeated, but the leakage rate did not improve. A solenoid operative valve may be necessary for this application. The test results are listed in Table 34.

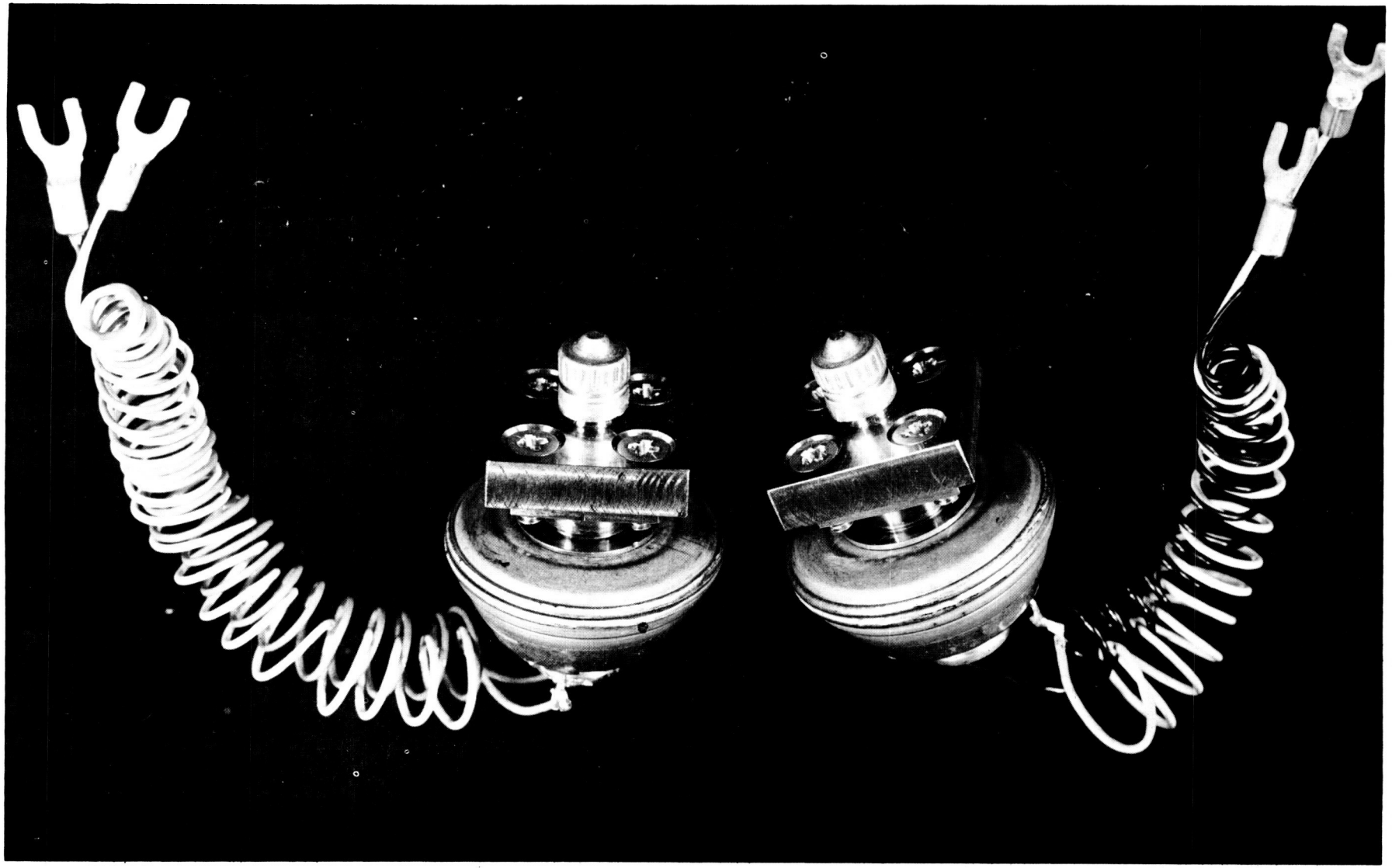

Fig. 66 Hydra-Electric Pressure Switches

Table 33 Hydra-Electric Pressure Switch Test Results

Actuation, Switch 14377			Actuation, Switch 14402		
Temperature (°F)	Pressure Rising Switch Opened (psig)	Pressure Decaying Switch Closed (psig)	Temperature (°F)	Pressure Rising Switch Opened (psig)	Pressure Decaying Switch Closed (psig)
70	165.3	160.2	70	165.1	159.5
70	165.3	160.1	70	165.1	159.5
70	165.25	160.0			
	Pressure was increased to 200 psig before decreasing pressure.			Pressure was increased to 200 psig before decreasing pressure.	
			70	165.1	159.5
70	164.7	158.5	70	165.1	159.5
70	164.8	159.0			
-320	165.0	159.3	-320	165.0	159.7
-320	165.0	159.3	-320	165.0	159.7
-320	165.0		-320	165.0	
	Pressure was increased to 200 psig.			Pressure was increased to 200 psig.	
		159.1			159.6
-320	164.9	159.2	-320	164.8	159.8
-320	164.9	159.2	-320	164.8	159.8
-320	164.8		-320	164.8	
	Pressure was increased to 200 psig.			Pressure was increased to 200 psig.	
		159.0			159.6
-320	164.8	159.1	-320	164.8	159.8
-320	164.8	159.1	-320	164.8	159.8
	Pressure was released to zero.			Pressure was released to zero.	
-320	165.6	159.2	-320	165.6	159.8
-320	164.9	159.2	-320	164.8	159.8
-423	163.8	157.3	-423	163.6	159.7
-423	163.8	157.3	-423	163.6	159.6
-423	163.8		-423	163.6	
	Pressure was increased to 200 psig.			to 200 psig	
		157.2			159.2
-423	163.9	157.3	-423	163.6	159.5
-423	163.9	157.3	-423	163.6	159.5
-423	163.9	157.3	-423	163.5	159.4
-423	163.9		-423	163.5	159.1
	Pressure was increased to 200 psig.			to 200 psig	
		157.3	-423	163.5	159.3
-423	163.9	157.3	-423	163.5	159.3
-423	163.9	157.4		Pressure was released to zero.	
-423	163.9	157.4	-423	164.1	159.3
	Pressure was released to zero.		-423	164.1	159.3
-423	164.8	157.8	-423	164.1	159.1
-423	164.2	157.7	-423	to 200 psig.	
-423	164.2			164.1	159.3
	Pressure was increased to 200 psig.				
		157.4	-423	164.0	159.2
-423	164.1	157.5			

Table 34 Leak Test Data

Temperature (°F)	Reverse Pressure (psig)	Leakage (std cc)	Time (sec)	Leakage Rate (sccm)	Remarks
Consolidated Controls Check Valve					
70	20	37.5	80	28	Pressurant nitrogen gas. After at least 500 actuations.
70	100	56	50	67	Cracking pressure, 1.4 psig. Full-flow pressure, 1.7 psig. Pressurant nitrogen gas.
70	20	30	180	10	Actuated 500 times again (total 1000).
70	100	14	180	5	Cracking pressure, 1.4 psig. Full flow, 1.7 psig.
-320	20	51	50	61	Pressurant helium gas. 500 actuations (total 1500).
-320	100	94	20	282	Pressurant helium gas.
70	20	26	180	9	Pressurant nitrogen.
70	100	60	180	20	Pressurant nitrogen.
Sterer Check Valve No. 28270-1					
70	5 1000	28.5 0	180 360	9.5	Check valve at ambient temperature with dry nitrogen gas as pressurant.
70	5 1000	12.8 0	360 360	2.177	Recheck Sterer check valve after cleaning.
Sterer Check Valve No. 28270					
70	5 1000	32.5 8.2	360 360	5.44 1.36	Check valve at ambient temperature with dry nitrogen gas as pressurant.
70	5 1000	57.2 37.5	120 120	28.6 18.77	Recheck Sterer check valve after cleaning.

e. Solenoid Temperature Compensator

A device was constructed to compensate for the usual decrease in electrical resistance of the copper wire solenoid coil as the temperature approached very low values. This was done to prevent excessive current drain on the electrical power supply. A configuration employing a shunted thermistor and resistor combination, supplied by the General Electric Company, performed very well showing an increase in solenoid current of only 0.1 amp (at 28 vdc) from room temperature to liquid nitrogen temperature and an additional 0.1 amp (at 28 vdc) from liquid nitrogen temperature to liquid hydrogen temperature. The decrease in normal room temperature solenoid current flow, caused by the compensator, is less than 0.25 amp which can be easily accounted for in coil design if the current is critical (see Fig. 67).

f. Couplings, Fittings, and Seals

Testing was completed on the Harrison Astro-Weight coupling and "K" seal, the Flexible Metal Hose Manufacturing Company AN-type fitting, and the Parker V-type metal seal with Teflon coating. The Harrison coupling and seal were tested at room temperature with 2800-psig helium gas with no detectable leakage using the Consolidated Electrodynamics Corporation leak detector. When submerged in liquid nitrogen, no leakage (bubbles) was visible. In liquid hydrogen, the leakage rate was more than expected but proved to be the least of the three types of seals tested. Results are shown in Table 35 and Fig. 68.

The Flexible Metal Hose coupling and seal showed no leakage at room temperature and liquid nitrogen temperature but showed an excessive leak at liquid hydrogen temperature. On teardown, a flake of plating (electroless nickel) separated from the sealing surface. Another unit was not available for check. Test results are shown in Table 35 and Fig. 69.

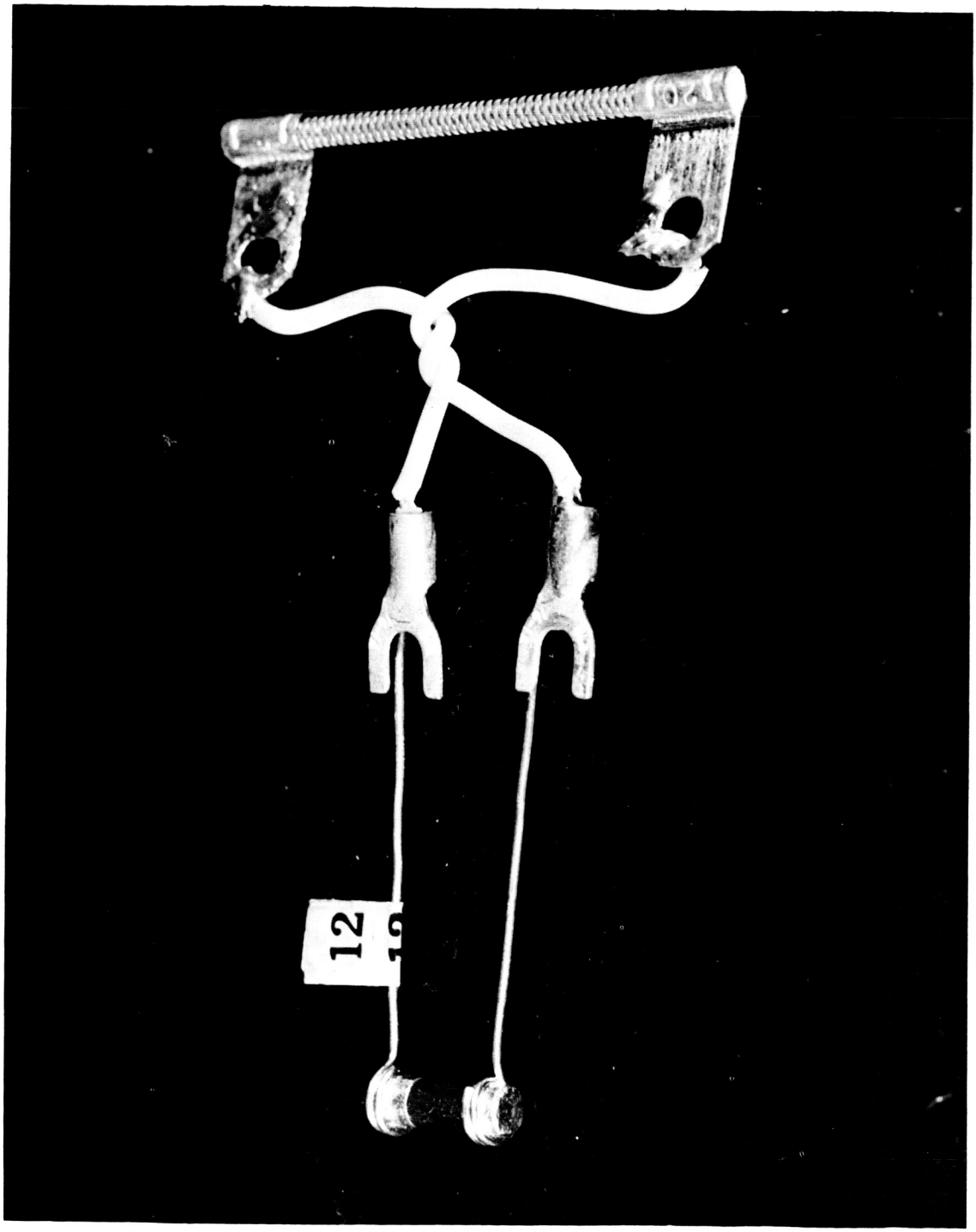

Fig. 67 Temperature-Resistance Compensator for Solenoid Coil

Table 35 Seals, Couplings and Fittings Leak Tests

Pressurization Temperature (°F)	Seal No.	Elapsed Time (min)	1st Test Pressure Decay (psig)	2nd Test Pressure Decay (psig)	Leakage (sccm/hr)
Harrison Seal and Coupling Leak Test					
-423	1	10	2325 to 2115	2325 to 2220	94.2
-423	2	10	2190 to 2135	2190 to 2175	13.6
-423	3	10	2260 to 2245	2260 to 2252	7.17
-320	4	10	2800 to 2800	--	0
62	4	10	2800 to 2800	--	0
Flexible Metal Hose Manufacturing Company Fitting (AN-Type)					
-423		10	2340 to 2215	2340 to 2240	79.7
-320		10	2875 to 2875	--	0
70		10	2875 to 2875	--	0
Parker V-Seal Leak Test					
70	1	10	2045 to 2045	2045 to 2045	None
70	2	10	2060 to 2060	2060 to 2060	None
70	3	10	2060 to 2060	2060 to 2060	None
-320	1	10	2040 to 1125	2040 to 1195	718
-320	2	10	2035 to 680	2035 to 730	1110
-320	3	10	2210 to 695	2210 to 995	1034
-423	1	10	2190 to 1215	2190 to 1300	757
-423	2	10	2255 to 445	2250 to 505	1485
-423	3	10	2110 to 1210	2100 to 1390	603

Note: Helium was used as the pressurant in all cases.

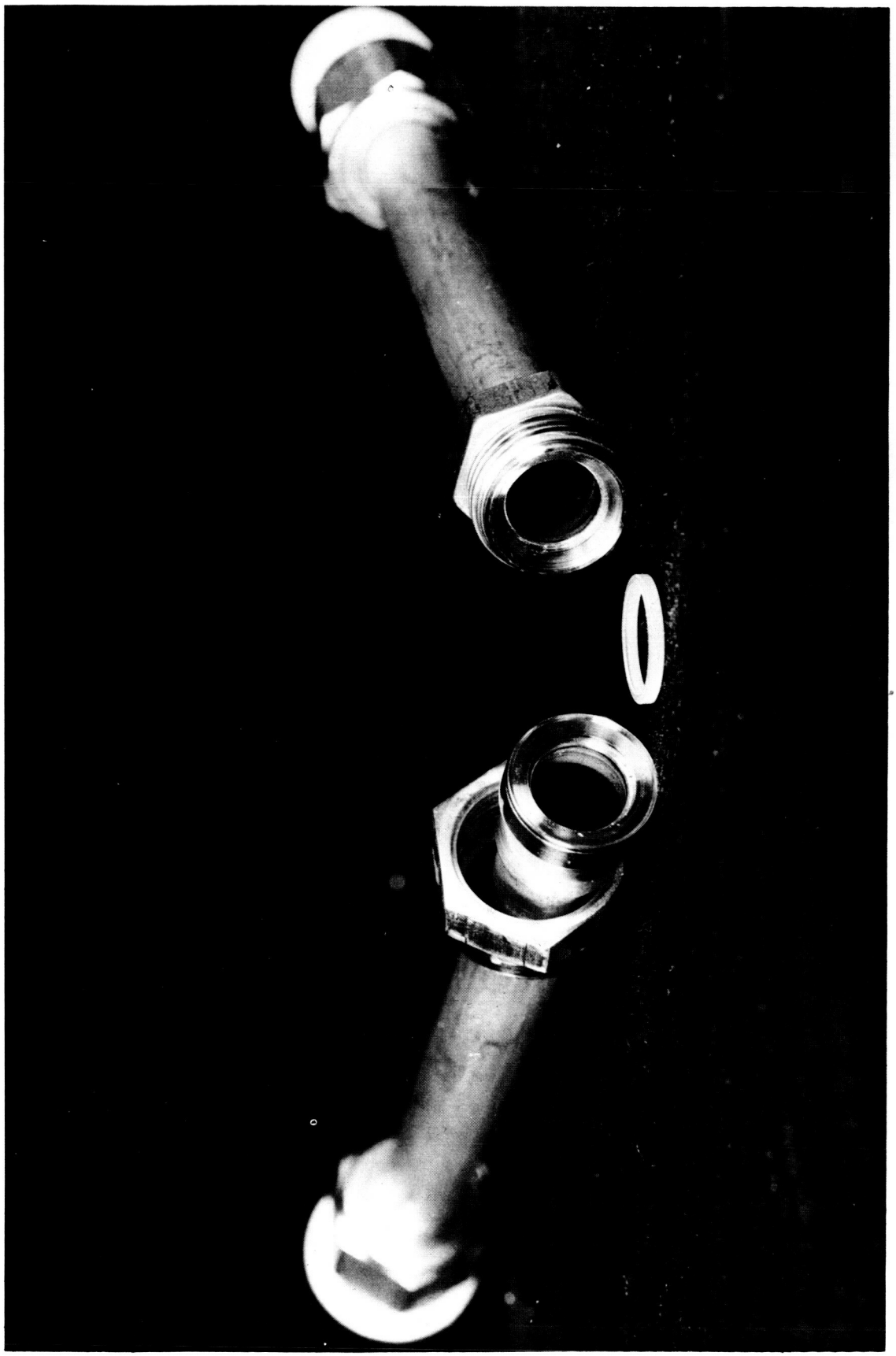

Fig. 68 Harrison Astro-Weight Coupling and Seal

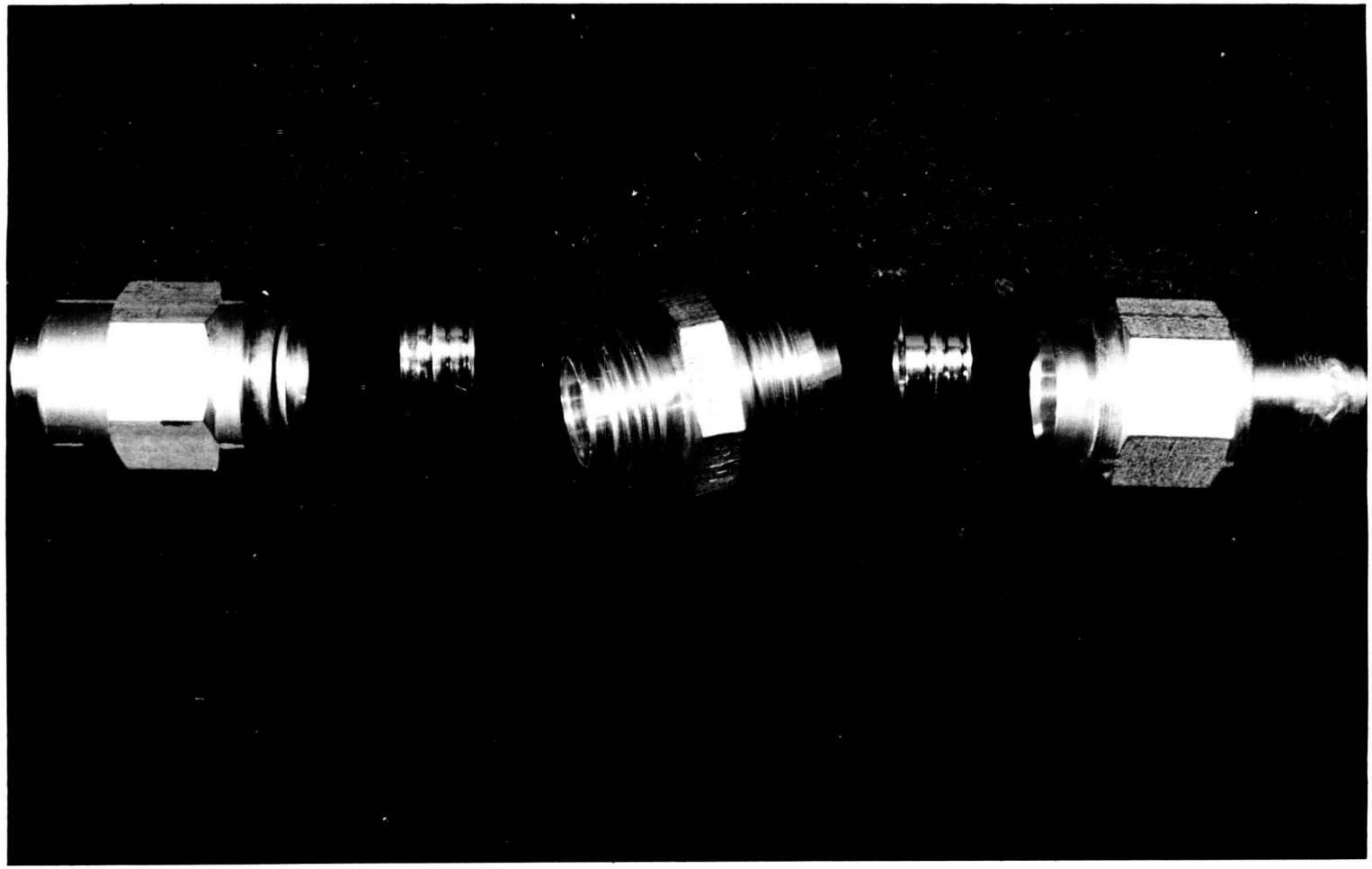

Fig. 69 Flexible Metal Hose Coupling and Seal, "AN" Type

The Parker V-section seal of inconel "X" coated with Teflon showed no leakage at room temperature but leaked excessively at liquid nitrogen and liquid hydrogen temperature. Three seals were tested and approximately the same results were obtained. This seal is three times as large in diameter as the first two seals tested, but this difference in size cannot account for the difference in leakage. Results are shown in Table 35 and Fig. 70.

It is apparent from the tests to date that sealing helium gas at liquid nitrogen temperature poses no serious problems. However, in attempting to seal helium at liquid hydrogen temperature, more research will be necessary if reducing leakage to undetectable limits is required.

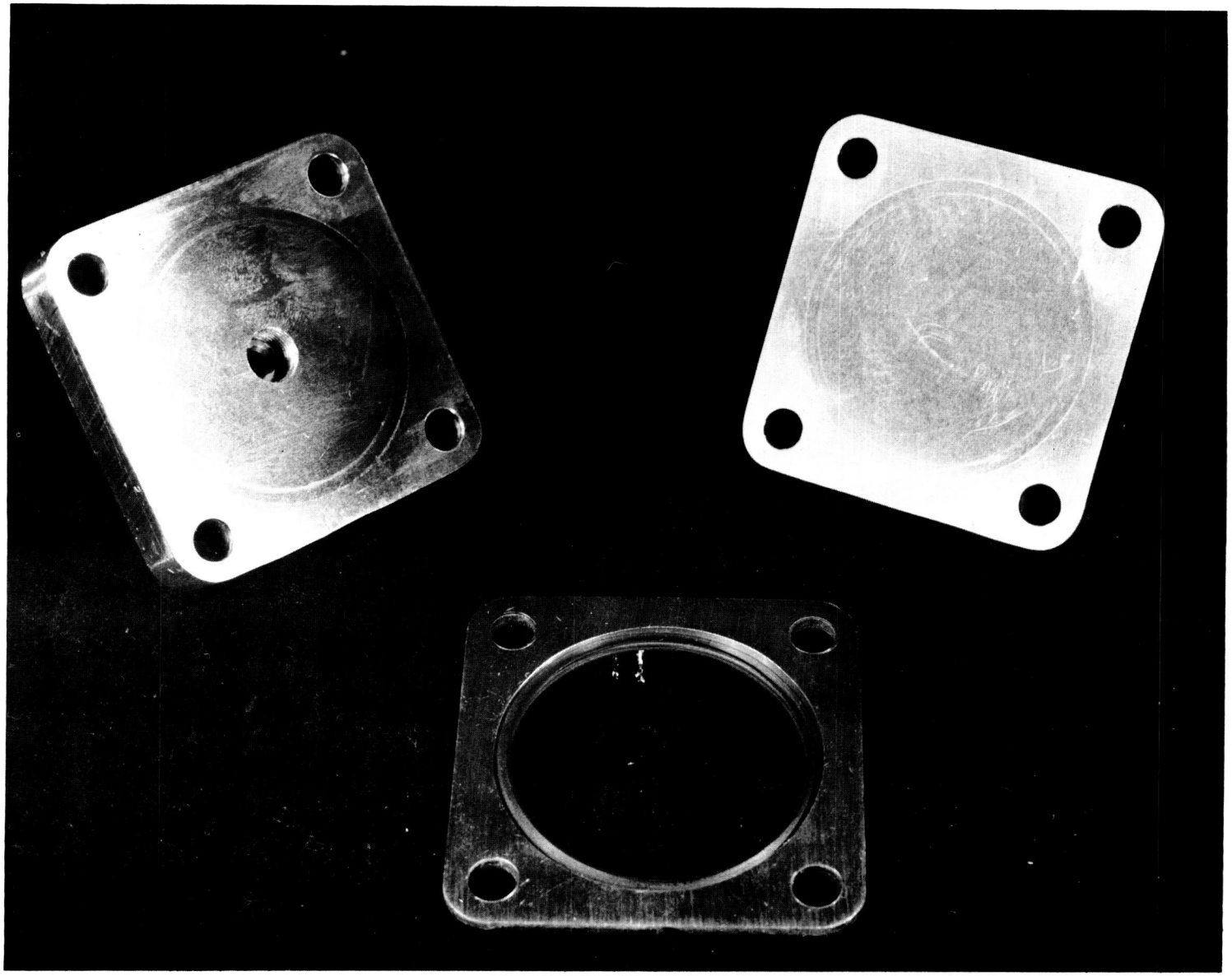

Fig. 70 Parker "V" Section Metal Seal and Test Fixture

E. CONTROL SYSTEMS

Another major area of effort involves the selection of components and operating logic to best match the analytical design. In reality, the theoretical operation cannot be exactly duplicated, since real components operate over ranges rather than at discrete points and do not attain perfect repeatability.

1. Component Selection

Figure 71 indicates the options available for the selections of a control system and the general types of components that may be used. The areas of system definition are listed in the right-hand column of the chart, with the possible options to the left.

For the purpose of demonstrating the use of the chart, the system using ambient-stored helium previously discussed will be used. Since the system considered was designed to meet the requirements of a specific mission, some of the selections are mandatory. Under Operating Phases and Restart, the mission requires command starts and stops with a multiple-burn capability. Again, due to the mission, an active closed-loop control system must be used. An example of a system that might use passive open-loop control would be for a booster stage requiring a single burn to produce a preprogramed and gross total impulse.

The remaining selection categories involve the specific hardware to be used to operate and control the system. In the case of the system considered, the sensing of tank gas pressure and operating time during burn periods will provide an accurate determination of both specific and total impulse during the burn.

Since tank gas pressure must be sensed and controlled, the location of the pressure sensor would be in the ullage space or in the outflow line of each propellant tank. In the case of pressurant feed control, several approaches may be taken: continuous feed through an orifice, proportional feed through a regulator, or intermittent feed through a solenoid valve. Due to the wide variations in gas flow rate requirements, from initial prepressurization with low ullage to prepressurization prior to the final burn phase with a large ullage, a single orifice could not be used. Multiple orifices would require additional valving, making this system more complex than either a regulator or solenoid valve system. Considering the regulator approach versus a solenoid valve and pressure switch, either system will provide the necessary control.

At this point, the selection is based on such things as cost, availability, reliability, and technical risk if the component must be developed.

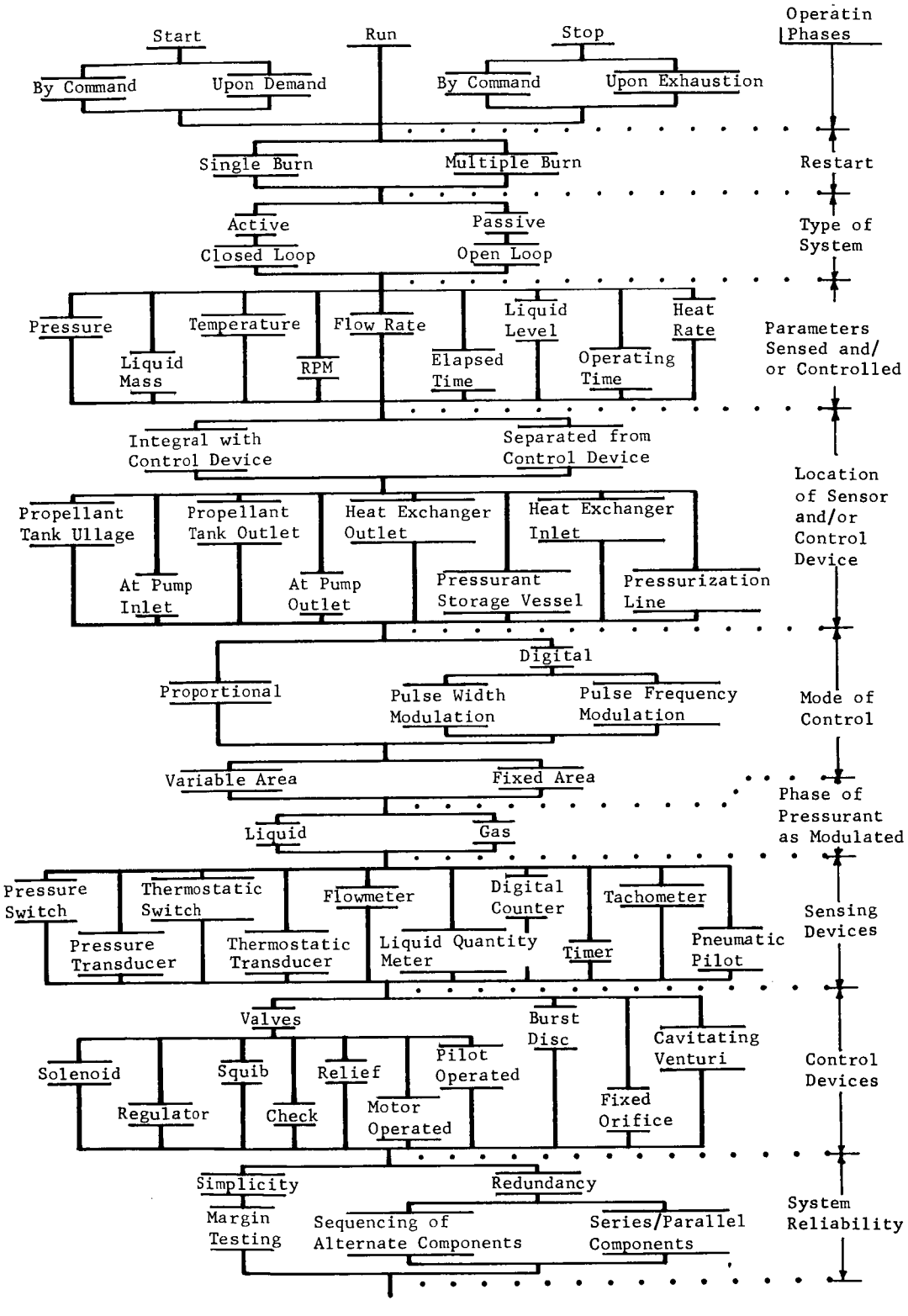

Fig. 71 Possibilities of a Control System

Since the phase of the pressurant in this case is always a gas, no consideration need be given to flow control of liquids.

The sensing device may be the pneumatic pilot section, of a regulator, or, in the case of a solenoid valve, a pressure switch or a pressure transducer. In any event, the sensor must sense ullage gas pressure.

2. Operating Logic

With a mission defined and the selection of the major components of the control system completed, operating logic of the system may be established. Operating logic is the sequencing of operations required to make the vehicle perform as desired; i.e., opening valves to start propellant flow at desired engine fire time. In a multiple-burn mission, the vehicle is required to go through several operations of coast, pressurization, and burn.

To ensure the accomplishment of a successful space mission, the operating logic was designed so that a single component failure would not cause a failure of the mission. This requires redundancy of component parts. The valve configuration was designed so that a valve failure, either failed open or failed closed, would not affect system operation.

In the design of the pressurization system for the six-burn mission of the pump-fed systems it was necessary to have variable orifice areas for the pressurant inlet valve to the propellant tanks. This was accomplished by using values of different flow areas at different times of the mission.

To accomplish a mission of coast, vent, prepressurization, and burn periods and to include redundancy and various valve flow areas, the control system shown in Fig. 72 was devised. Table 36 describes the operation of this system logic including the redundancy. Figure 73 illustrates a typical cycle of operation of the system covering coast, prepressurization, burn, and return to coast condition.

Although a detailed description of the electrical sequences is not given, their internal design concept would follow the same principles used in the design of the mechanical portions of the system. Redundancy would be provided, so that no single component malfunction would cause a failure of the mission.

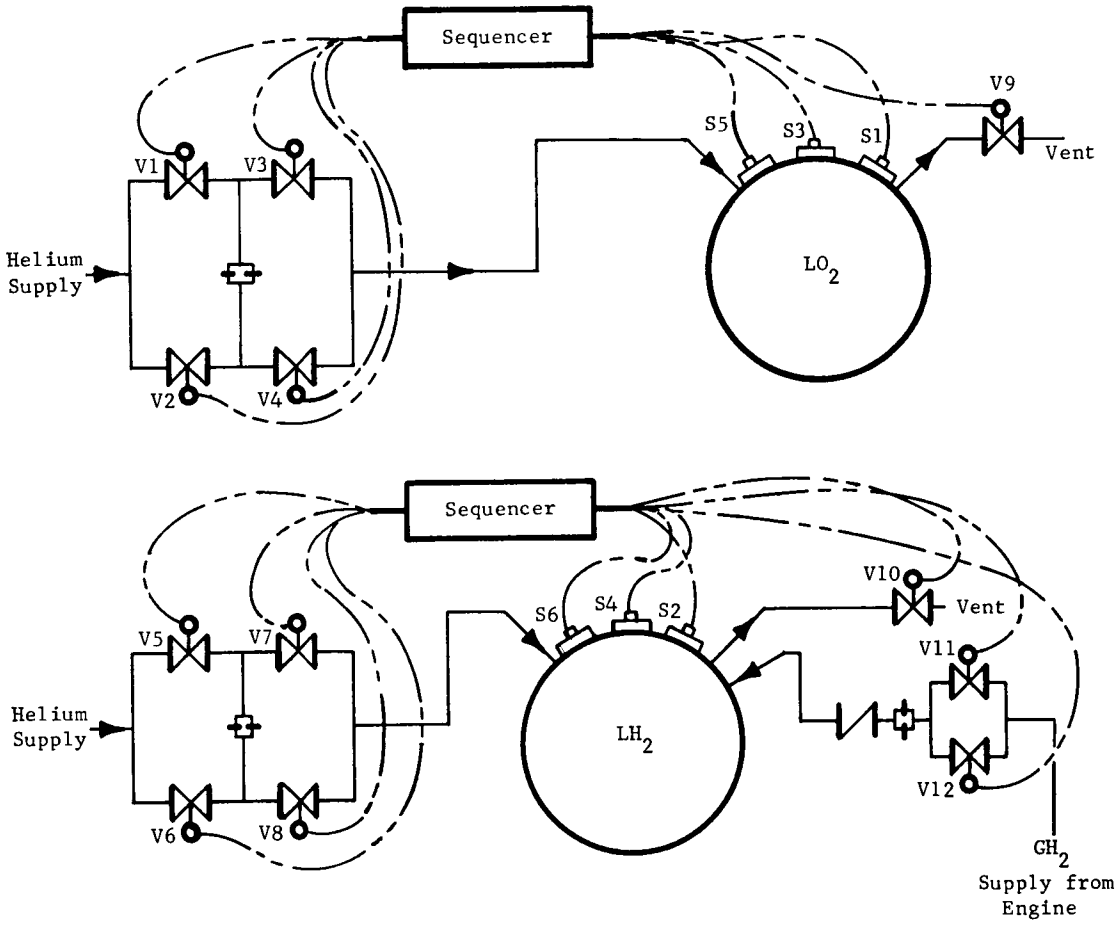

Legend:

S1	LO_2 Tank Pressure Switch, Normally Closed, 33.0 to 34.6 psia
S2	LH_2 Tank Pressure Switch, Normally Closed, 28.0 to 29.6 psia
S3	LO_2 Tank Underpressure Switch, Normally Closed, 31.9 to 33.5 psia
S4	LH_2 Tank Underpressure Switch, Normally Closed, 26.9 to 28.5 psia
S5	LO_2 Tank Vent Switch, Normally Closed, 16.3 to 17.7 psia
S6	LH_2 Tank Vent Switch, Normally Closed, 16.3 to 17.7 psia
V1 thru V4	LO_2 Tank Helium Pressurization Valves, Normally Closed
V5 thru V8	LH_2 Tank Helium Pressurization Valves, Normally Closed
V9	LO_2 Tank Vent Valve, Normally Open
V10	LH_2 Tank Vent Valve, Normally Open
V11 and V12	LH_2 Tank Gaseous Hydrogen Pressurization Valves, Normally Closed

Fig. 72 Control System Schematic

Table 36 System Logic Description

Operational Step	System Condition	System Logic	Switches Used		Valves Used	
			LO_2	LH_2	LO_2	LH_2
1. Coast	Normal	Coast prior to first burn. Vent valve switch and vent valve circuits energized. LO_2 and LH_2 tanks at 17 ± 0.7 psia.	S5	S6	V9	V10
	Switch cell failed open or closed	No change in operation since quad, series-parallel switch cells are used. (Vent valve failures are not considered since they are a part of the tank system.)	S5	S6	V9	V10
2. Prepressurization prior to 1st Burn	Normal	Power is removed from vent switches but remains on vent valve. Power is applied to tank pressure switches and valves. Two valves in each tank quad system will open, and tank pressures will rise until switches open.	S1	S2	V1 and V4	V5 and V8
	Valve failed open	No action since valves operate in series.	S1	S2	V1 and V4	V5 and V8
	Switch cell failed open or closed	No action since quad, series-parallel cells are used in each tank pressure switch.	S1	S2	V1 and V4	V5 and V8
	Check for valve failed closed	A timer was initiated at the start of Step 2. When timer reaches 10 sec, power is applied to tank underpressure switch circuit. If S3 and S4 switch contacts are open, no further action occurs.	S1 and S3	S2 and S4	V1 and V4	V5 and V8

Table 36 (cont)

Operational Step	System Condition	System Logic	Switches Used		Valves Used	
			LO_2	LH_2	LO_2	LH_2
	Valve Failed Closed, V1 and V4 and V5 or V8	At 10-sec timeout, closing of S3 or S4 contacts (indicating tank underpressure) will cause power removal from valves in use and power application to the remaining pair. This will occur only in the tank indicating underpressure. (Subsequent prepressurizations or burns, using the diagonal valve arrangement, will not attempt to use the failed diagonal pair as the switchover will be locked in.)	S1 and S3	S2 and S4	V1 and V4 or V2 and V3	V5 and V8 or V6 and V7
3. 1st Burn	Normal	Operation continues per Step 2 for the LO_2 tank. At engine start, the active valves in the LH_2 tank pressurization system (V5 and V8 or V6 and V7) are deenergized, and valve V11 is energized. Tank pressure switch S2 is still active and now operates valve V11.	S1 and S3	S2 and S4	V1 and V4	V11
	Valve Failed Open, V1 or V4	No action	S1 and S3	S2 and S4	V1 and V4	V11
	Switch Cell Failed Open or Closed	No action				
	Valve Failed Closed, V1 or V4 (LO_2)	Same as Step 2 except timer is not used, and, any time the underpressure switch contacts close, a switchover is made.	S1 and S3	S2 and S4	V1 and V4	V11

Table 36 (concl)

Operational Step	System Condition	System Logic	Switches Used		Valves Used	
			LO_2	LH_2	LO_2	LH_2
	Valve Failed Closed, V11	If V11 fails closed, tank pressure will drop until S4 contacts close, at which time power is removed from V11 and is applied to V12. In addition, a lockup is made that prevents V11 from being energized on subsequent burns.	S1 and S3	S2 and S4	V1 and V4	V11 or V12
	Valve Failed Open, V11	No action. The line orifice is sized so that, although some tank overpressure occurs, tank limit pressure is not reached during the longest burn requirement.	S1 and S3	S2 and S4	V1 and V4	V11
4. Coast After 1st Burn	Normal	At the completion of the programed burn time, power is removed from switches S1, S3, S2, and S4 and valves V1, V4, and V11. At the same time, power is applied to vent switches, S5 and S6.	S1 and S3; then S5	S2 and S4; then S6	V1 and V4; then V9	V11; then V10

Note: Steps 1 through 4 are repeated for 2nd and 3rd burns. However, at the initiation of prepressurization for the 4th burn, valves V1 and V3 and V5, and V7 are used instead of valves V1 and V4 and V5 and V8. This takes the orifice out of the system allowing higher helium flow rates which are required due to large ullage. Lockups, which occurred during the first three burns in the LO_2 and LH_2 helium pressurization system due to valve malfunction, are removed. Malfunction switchover is then made to valves V2 and V4 or V6 and V7, if required. The operation of the GH_2 system is not changed at this time.

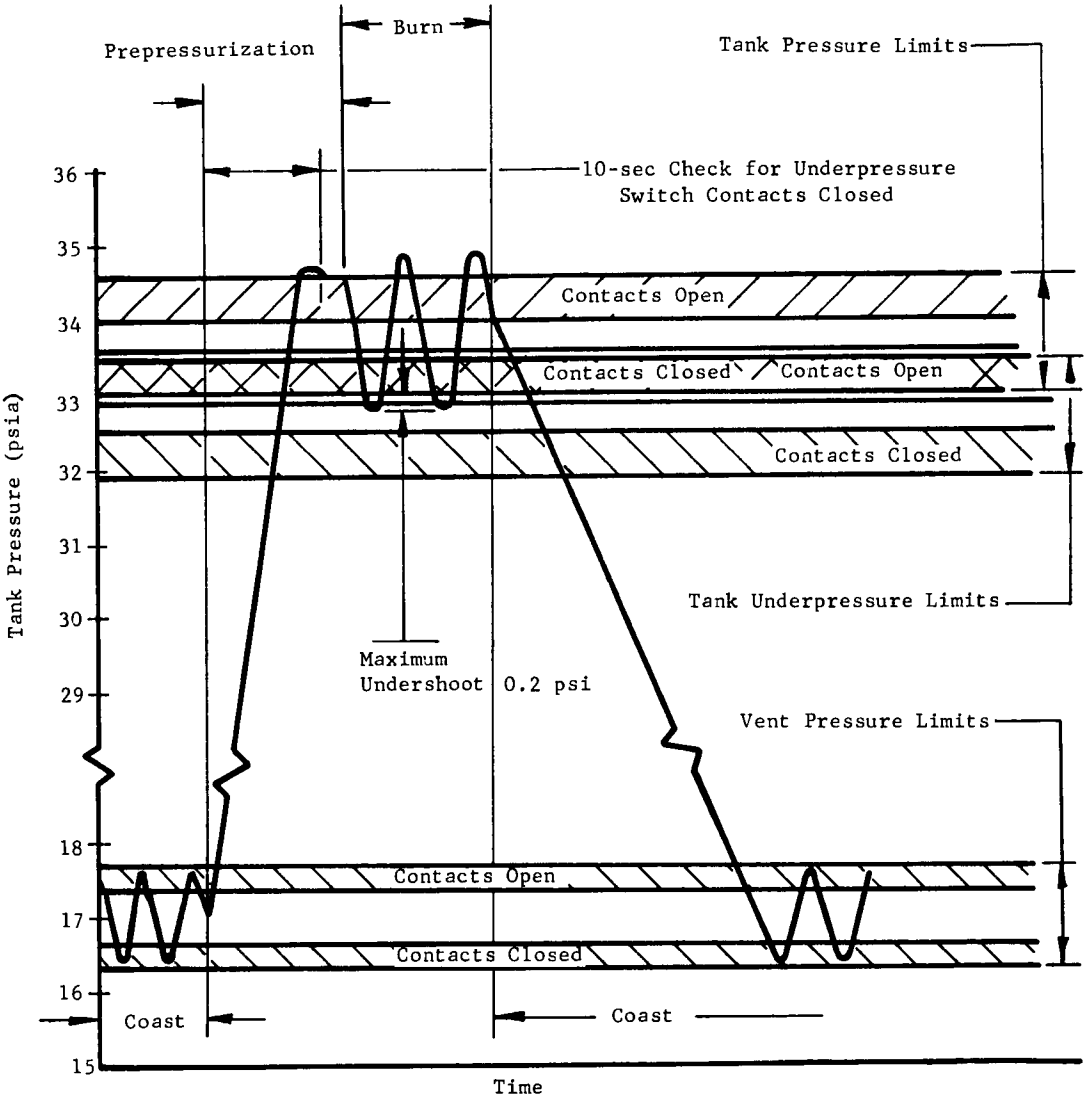

Fig. 73 Liquid Oxygen Tank, Typical Operation

IV. SYSTEM SELECTION

Selection of a final or best system for the pump-fed vehicle was based on a number of factors. System weight, complexity, and zero-gravity operating capability were considered to be the major factors of comparison with leakage, minimization of pressurization time, cost, and 20-day storage capability -- the lesser factors of comparison. Each item considered for the system comparison was studied separately with summarized results presented in Table 37. Considerable emphasis was placed on the system weight. This selection process was accomplished for System 8 (Fig. 42) and System 6 (Fig. 40).

Table 37 System Comparison

Item	Weighting (%)	Category Comparison		System Comparison	
		System 8	System 6	System 8	System 6
Weight	25	10	10	250	250
Complexity	25	10	10	250	250
Zero-Gravity Capability	20	10	5	200	100
Leakage	10	10	8	100	80
Minimization of Pressurization Time	10	10	6	100	60
Cost	5	10	6	50	30
20-Day Storage	5	9	10	45	50
Total				995	820

A. GENERAL

1. Weight

The weight comparison of the two final systems studied was explained in detail in Section III.C. Weights of the two systems differed by only 5 lb for total system weights of 2200 lb or about 0.3%. With this insignificant difference, the two systems were rated as equal in the comparison of Table 37.

2. Complexity

This comparison considered the actual components that would be used in each system and the complexity of one component with respect to another. A complexity grading system was used that assigned a numerical rating to each component. Two general classes of components were considered: active and passive. Active components were defined as those having moving parts while passive components were those having no moving parts. The range of values assigned to passive components was from 1 to 10, with 10 being the most complex. Active components were rated using a range of assigned values from 30 to 50 with 50 being the most complex. Table 38 indicates the value assigned to each component and the total point comparison for the two systems considered. With a difference of only 4 in 800 or 0.5%, the systems were considered equal in complexity.

3. Zero-Gravity Capability

In the case of zero-gravity operating capability, both systems were similar except for the heat exchanger of System 6. Section III.C.3. covers the analytical design of the exchanger and indicates that prediction of the performance of a simple finned tube exchanger under low- or zero-gravity conditions is extremely difficult. The heat exchanger design, therefore, represents a major technical risk, since exact performance cannot be determined until actual flight test of the system. Since the vehicle is in orbit during prepressurization periods, essentially no forces exist on the system, and even in powered flight, only a force of 0.2g is available to provide the free-convection flow necessary to permit this type of exchanger to perform properly.

4. Leakage

Considering the two systems from the standpoint of potential leakage and its consequences, System 8 is superior to System 6. System 6 has more connecting joints and operates at a lower temperature than System 8. Since it is virtually impossible to build a zero-leak system, and since leaks occur at joints rather than in continuous systems such as tube runs or tank walls, leakage is considered to be a direct function of the number and size of system joints. In addition, any given leak will pass a greater mass flow rate of fluid as temperature of the fluid decreases or the pressure increases due to the increase in density of the fluid. The physical size of the leakage path can either increase or decrease with a decrease in temperature, although the net effect of decreasing the system temperature usually produces a greater mass leak rate.

Table 38 Complexity Comparison

Item	Active or Passive	Assigned Value	System Points	
			8	6
Storage Containers				
Liquid Propellant	Passive	3	6	6
Pressurant	Passive	3	12	3
Coolant	Passive	3		
Heat Exchangers	Passive	5		5
Orifices, Venturis and Screens	Passive	1	3	3
Insulation	Passive	10	10	10
Seals, Lines, and Couplings	Passive	10	10	10
Valves				
Check	Active	30	30	30
Regulating or Control	Active	42	420	420
Fill and Drain	Active	35	70	70
Prevalve				
Pressure Switches	Active	42	252	252
Total			813	809

Potential leakage of the two final systems studied was based on an estimate of the number and size of the joints in each system and the temperature and pressure of the fluids in the system. The total leakage mass was obtained by integration of the leakage rates under average pressure and temperature conditions over the mission profile. Each system was broken down into subsystems or segments of different line sizes. Computed leakage of the two systems considered is tabulated as follows.

	Leakage (sccm/ft) Average	Number of Joints
System 8		
Storage to Supply Manifold	10	24
Supply Manifold to Liquid Hydrogen Tank	30	16
Supply Manifold to Liquid Oxygen Tank	10	24
Integrated Total Leakage for Mission -- 0.4 lb		
System 6		
Storage to Heat Exchanger	100	8
Heat Exchanger	300	26
Heat Exchanger to Supply Manifold	50	4
Supply Manifold to Liquid Hydrogen Tank	50	26
Supply Manifold to Liquid Oxygen Tank	10	9
Integrated Total Leakage for Mission -- 4.0 lb		

5. Minimization of Pressurization Time

During the coast phases of orbital flight, the propellant tanks are vented and maintained at a relatively low pressure to maintain the required tank liquid bulk temperature. (An increase in bulk liquid temperature causes a proportional decrease in suction head available to the engine pump.) Prior to each engine burn phase, the propellants must be returned to the tank bottoms and the tanks pressurized to provide the required net pump suction head (NPSH). Fifteen sec was arbitrarily selected for the propellant settling period, and since settling and pressurization may occur simultaneously, pressurization within the 15-sec period is preferred.

In System 8, the pressurization time required prior to each of the six burn periods is less than 15 sec. For System 6, the pressurization time prior to the first three burn periods is less than 15 sec; however, pressurization times for the final three burns are 51, 70, and 79 sec. The additional times required for System 6 pressurization prior to the final three burns is due primarily

to large propellant tank ullages and cold pressurant gas. In System 8, the pressurant gas temperature at the tank inlets is higher, and, therefore, the gas is less dense giving a higher tank pressure rise rate for a given mass flow rate in the systems.

6. Costs

Several cost factors were considered for the two final systems studied. The cost of an ultimate flight system based upon quantity production could be considerably different from a one-of-a-kind test system. For this program, the one-of-a-kind test systems were costed and compared, since the next logical step in the program would be to build a system to prove feasibility and obtain performance data. In addition, components for the final systems studied had been selected and cost data obtained (Table 39).

The difference in cost between the stored-at-ambient-temperature system and the system stored at cryogenic temperature was primarily the cost of the heat exchanger for the cryogenic system. One additional cost allowed for the cryogenic system over the ambient system was a valve contingency expense to cover the costs of modifying the solenoid controlled valves to enable them to operate properly at cryogenic temperatures.

7. 20-Day Storage Capability

This item of comparison involves the effect on each system of adding 20 days to the existing mission time. Considering the main propellant tanks, additional boiloff would occur equally for both systems, since the heat leak to the two systems is almost identical. This would require equal enlargement of the tanks for each system.

Additional leakage would occur from each system in the proportions previously indicated in this chapter. This leakage will require a proportional enlargement of the storage sphere adding weight to System 6.

Table 39 Component Cost Estimate of Systems 6 and 8

Detail No.	Quantity	Unit Cost	System 8 Total	System 6 Total	Description
1	1	--			Tank, LH_2
2	3	10,000	30,000	30,000	Tank, He
3	1				Tank, LO_2
4	2*	350	2,800	2,800	Filter, He
5	7	75	525	525	Orifice, He
6	10	2,000	20,000	20,000	Valve, Pressurization, Solenoid
7	2	150	300	300	Valve, Manual, He
8	1	1,300	1,300	1,300	Valve, Vent, Solenoid, LH_2
9	1	1,300	1,300	1,300	Valve, Vent, Solenoid, LO_2
10	6 (Quad)	1,200	7,200	7,200	Switch, Pressurization, Continuity, He
11	1	2,000	2,000	2,000	Electrical Sequencer
12			10,000	10,000	Miscellaneous Plumbing, Fittings
13			8,250	8,250	Spares
14				10,000	Heat Exchanger
15				6,000†	Additional Valve Costs
Total			$83,675	$99,675	

*Eight units, the size of Titan III filters, are required that flow at the rate of 1.3 lb/sec at 600 psia; $350 each = $2,800.

†Additional cost of valves for use at cryogenic temperatures.

Note: This comparison is based on preliminary estimates of component costs which may, in a final analysis, vary for a given component but should not affect the overall comparison.

To reduce the heat leak into the propellant tanks, the vehicle was constructed to provide the lowest heat transfer possible from space radiation into the propellant tanks. As a result, the average temperature of the vehicle is less than that of the ambient sphere which will result in a heat loss from the storage container to the vehicle structure. This decrease in storage temperature will cause a decrease in pressure in the container which requires an increase in container size. On the other hand, the System 6 storage container is mounted in the liquid hydrogen tank; consequently, it will not lose heat during extended storage periods.

The combined effect of the leakage of both systems and the pressure loss of System 8 will result in a greater required increase in the pressurant storage subsystem of System 8 for an additional 20-day storage period.

B. CONCLUSIONS

Each system was compared by items (Table 37) with a range of values from 10 to 1. The value of 10 was assigned to the most desirable system, and the other system was compared to it. The weighting column multiplied by the comparison resulted in a system comparison in which the higher number identified the most desirable system.

Both systems are comparable in weight with each having a value of 250. The major disadvantage of System 6 is the uncertainty of the heat exchangers, immersed in liquid oxygen, operating in a low-gravity field as reflected by the value of 100 compared to 200 for System 8.

From Table 37, it was determined that System 8 was more desirable than System 6. System 8 had a value of 995 out of a possible 1000, while System 6 had a value of 820.

V. GENERAL CONCLUSIONS AND RESULTS

During this study, a wide variety of problem areas associated with the design of cryogenic pressurization systems was investigated.

A study of various pressurizing gases led to the conclusion that the gas that has more applications as a pressurant was helium. Hydrogen, being the lightest, was most desirable for use in the liquid hydrogen propellant tank but could not be used in the oxidizer tank because of the explosive hazard.

Considerable effort was devoted to evaluating pressurant storage conditions and expansion processes. For simple expansions (i.e., isobaric, isothermal, and isentropic), it was found that the isobaric process provided the lightest combined weight of initial gas and storage container. It was found that the addition of heat reduced the weight of the initial gas and storage container. Furthermore, it was found that by combining the simple expansions (i.e., initial isobaric; terminal isentropic), even lower weights could be achieved. It was concluded that in a combined expansion it was most desirable to use the isobaric as the terminal process.

An isentropic expansion process used to estimate the weight of the gas and container gave a larger weight than an adiabatic expansion which included the container wall with its heat capacity. Thus an ideal expansion process was conservative.

An isothermal expansion was 25% lighter in gas and container weight than an adiabatic process which included the wall heat capacity. Engine-bleed hydrogen used to heat the storage gas results in approximately the same weight as an isothermal process, since the heat is applied intermittently. However, additional complexity in storage container design is required to install the heat exchanger.

The investigation of cascade and recirculation helium storage concepts indicated both methods offered significant reduction in pressurant storage system weights over the simple expansion. The cascade system appears most desirable of the two systems although more analysis of both is required.

Passive heat exchangers employed in the oxidizer tank to heat the helium flowing from the storage container required large tubes to prevent the lox from freezing. Series flow of helium through the four oxidizer tank heat exchangers was more desirable than parallel flow design. Fin spacing in the heat exchanger is critically affected by the vehicle acceleration.

Several attempts were made to pressurize a liquid hydrogen tank by injecting liquid or gaseous fluorine directly into the hydrogen. It was concluded that this system is not feasible at the current state of the art.

By considering the effect of the pressurization system on the total vehicle weight, the following conclusions can be drawn. If an active heat source is used (e.g., a gas generator), the weight of the initial pressurant gas and container is a reasonable guide to the total system weight. This was true except for the isobaric expansion in which the high heat rate required in the gas produced a very large heating system. In both the pressure-fed and pump-fed engine studies, the systems with combined expansion methods were low in weight, especially those with terminal isobaric expansions. It was also noted during the primary screening of pump-fed systems, using an active heat source, that lower initial storage temperatures produced lower total system weights. It can also be concluded that any expansion method, i.e., recirculation and cascade expansions, that reduces the residual gas weight is desirable.

Pressure-fed systems were low in weight when a vaporized propellant was used as a pressurant. The lightest pressure-fed system used helium stored at 37°R for the lox tank and vaporized hydrogen propellant as a self-pressurant.

Hydrogen gas-bleed from the engine, if used, lowers the pump-fed system weight. Without an active heat source, increasing the pressurant gas temperature entering the propellant tanks eliminated the advantage of low-temperature storage. The pressurant required at low tank-inlet temperatures offsets the advantage of low-temperature storage. Insufficient heat is added to the storage gas to reduce the gas residual. Without an active heat source, ambient temperature pressurant storage is the most desirable system. Similarly, with no active heat source, propellants cannot be vaporized and used as a pressurant.

Since the final system selection was based on the unavailability of an active heat source, the ambient temperature storage system was the most desirable. This system was also the least complex.

Table 40 summarizes the total system weight of the selected systems at various points in the program. Comparable analyses of the primary and advanced pressure-fed systems have been made so they can be compared with each other. Analyses of the secondary and final screening of pump-fed systems were not comparable. It was determined that the systems had different weights when a more complete analysis was performed.

Table 40 Optimum System Characteristics

System Description	Helium Storage		Optimum	
	Temperature (°R)	Pressure (psia)	Weight*	Tank Inlet Temperature
Primary Pressure-Fed				
Combined Expansion (Isobaric-Isentropic)	37	1000	2860	420
Combined Expansion (Isobaric-Isothermal)	37	1000	2815	410
Combined Expansion (Isentropic-Isobaric)	37	1000	2790	410
Combined Expansion (Isothermal-Isobaric)	37	1000	2755	415
Advanced Pressure-Fed				
System 2; Vaporizing Propellants			2930	200
System 7; Vaporized LH_2, Isothermal He	37	1000	2300	200
System 7; Vaporized LH_2, Isentropic He	37	1000	2500	200
System 8; Vaporized LH_2, Isothermal He	37	1000	2660	400
System 12; Cascade Expansion				
Primary	37	1000	2790	400
Cascade	37	2500		
Secondary Screening Pump-Fed				
System 1; Engine H_2 Bleed Heat of Storage	165	1800	1855	
System 5; Passive Heating by LO_2	37	1200	1785	
System 6; Passive Heating by LO_2, GH_2 Bleed	37	1200	1610	
System 6; Passive Heating by LO_2, GH_2 Bleed	37	1200	1525	
System 6 (Mod); Passive Heating by LO_2, GH_2 Bleed Heating	37	1100	1530	
System 8; Ambient Storage, GH_2 Bleed	520	2700	1850	
System 10; Passive Heating by LO_2, GH_2 Bleed	165	1500	1877	
Final Screening Pump-Fed				
System 6; Passive Heating by LO_2, GH_2 Bleed	37	1200	2205	
System 8; Ambient Storage, GH_2 Bleed	520	2700	2210	

*Includes, as necessary:

1) Pressure-fed systems,
   a) Propellant tanks,
   b) Propellant vapors,
   c) Usable pressurant
   d) Pressurant container and residual pressurant,
   e) Gas generator and its propellants,
   f) Heat exchangers,
   g) Pumps;

2) Secondary screening, pump-fed systems,
   a) Propellant tanks and insulation,
   b) Propellant vapors,
   c) Usable pressurant,
   d) Pressurant container and residual pressurants,
   e) Heat exchangers;

3) Final screening pump-fed systems,
   a) Propellant tanks and insulation,
   b) Propellant vapors,
   c) Pressurant required and leakage,
   d) Pressurant container and residual pressurant,
   e) Pressurant-container insulation,
   f) Heat exchangers,
   g) Propellant settling subsystem.

REFERENCES

1. J. A. Clark: Advances in Cryogenic Engineering. Volume 10, Plenum Press, New York, New York, 1965.

2. D. V. Sallis, E. R. Boogar: Transient Heating Digital Analysis for Structural Design. RM 63, Martin Company, Baltimore, Maryland, December 1960.

3. D. B. Mann: The Thermodynamic Properties of Helium from 6 to 540°R Between 10 and 1500 psia. National Bureau of Standards Technical Note 154, U. S. Government Printing Office, Washington, D. C., 1962.

4. Kreith: Principles of Heat Transfer. International Textbook Company, Scranton, Pennsylvania, 1958.

5. Schneider: Conduction Heat Transfer. Addison - Wesley, Reading, Massachusetts, 1957.

6. W. M. Kays, A. L. London: Compact Heat Exchangers. McGraw-Hill Book Company, Inc., 1958.

7. W. J. Masica, D. A. Petrash, E. W. Otto: Hydrostatic Stability of the Liquid-Vapor Interface in a Gravitational Field. NASA Technical Note D-2267, May 1964.

8. Helium Heater Subsystem for a Cryogenic Tankage Pressurization System. Sundstrand Aviation Proposal No. 5656, 6 March 1964.

9. Air Weapons Materials Application Handbook Metals and Alloys. ARDC TR59-66, Air Research and Development Command, 1st Edition, U. S. Air Force, December 1959.

10. Cryogenic Materials Data Handbook. (Prepared under Contract AF33(657)-9161 by Martin Company, Denver, Colorado), September 1963.

11. R. J. Roark: Formulas for Stress and Strain. Third Edition, McGraw-Hill Book Company, Inc., 1954.

12. Pneumatic Systems, Design Installation and Testing in Aircraft. MIL-P-5518B.

13. General Specification for Liquid Propellant Rocket Propulsion Subsystems. FTC-CR-63-1.

14. Reliability Policy Procedures Manual. M-63-3, Martin Company, Denver, Colorado, January 1963.

15. B. F. Dodge: Chemical Engineering Thermodynamics. McGraw-Hill Book Company, Inc., 1944.

APPENDIX A

DERIVATION OF THE STORAGE CONTAINER WEIGHT RATIO EQUATION FOR A SPHERICAL CONTAINER

The spherical storage container weight ratio is defined as the ratio of the loaded container weight to the expelled gas weight. The loaded container weight includes the container weight and the initial gas weight. Mathematically, the container weight ratio is stated as follows:

$$\frac{W_L}{W_{GE}} = \frac{W_C + W_{GI}}{W_{GI} - W_{GF}}, \qquad [85]$$

where

W_L = loaded container weight,

W_{GE} = expelled gas weight,

W_C = container weight,

W_{GI} = initial gas weight,

W_{GF} = final or residual gas weight.

The container wall thickness is assumed to be small compared to the container radius so that the container material volume is approximately equal to the surface area times the wall thickness. The container weight is

$$W_C = \rho_M A_C t_C, \qquad [86]$$

where

ρ_M = container material density,

A_C = container surface area,

t_C = container wall thickness.

To determine the wall thickness, t_C, it is assumed that the hoop stress is applicable, so that

$$t_C = \frac{P_c R_c}{2S_W}, \qquad [87]$$

where

P_c = container design pressure,

R_c = container radius,

S_W = container material working stress.

Substituting [87] in [86],

$$W_C = \frac{\rho_M A_C R_c P_c}{2 S_W}. \qquad [88]$$

For a sphere,

$$A_C = 4\pi R_c^2. \qquad [89]$$

Substituting [89] in [88],

$$W_C = \frac{2\pi \rho_M P_c R_c^3}{S_W}. \qquad [90]$$

The weight of gas, W_G, is calculated as follows:

$$W_G = \frac{P_G V_G}{Z_G R_G T_G} = \frac{4}{3} \frac{\pi R_c^3}{R_G} \left(\frac{P_G}{Z_G T_G} \right), \qquad [91]$$

where

P_G = gas pressure,

V_G = gas volume,

Z_G = gas compressibility,

R_G = gas constant,

T_G = gas temperature.

Applying the subscripts I for initial and F for final to Equation [91] and substituting the resulting equations together with Equation [90] in Equation [85], results in the following:

$$\frac{W_L}{W_{GE}} = \frac{\frac{2\pi\rho_M P_c R_c^3}{S_W} + \frac{4}{3}\frac{\pi R_c^3}{R_G}\left(\frac{P_{GI}}{Z_{GI}T_{GI}}\right)}{\frac{4}{3}\frac{\pi R_c^3}{R_G}\left(\frac{P_{GI}}{Z_{GI}T_{GI}}\right) - \frac{4}{3}\frac{\pi R_c^3}{R_G}\left(\frac{P_{GF}}{Z_{GF}T_{GF}}\right)}. \qquad [92]$$

Simplifying,

$$\frac{W_L}{W_{GE}} = \frac{\frac{1.5\rho_M P_c R_G Z_{GI} T_{GI}}{P_{GI} S_W} + 1}{1 - \frac{Z_{GI}}{Z_{GF}}\frac{T_{GI}}{T_{GF}}\frac{P_{GF}}{P_{GI}}}.$$

APPENDIX B

DERIVATION OF ENERGY BALANCE EQUATION FOR PREDICTING TEMPERATURE CHANGE DURING OUTFLOW OF A GAS STORAGE CONTAINER

A particle of gas leaving a fixed volume container possesses an instantaneous specific heat content equal to the specific enthalpy of the container gas. The total heat energy leaving the container, then, is equal to the product of the mass leaving the container and the specific enthalpy. If there is heat transfer from the container wall to the gas, the total internal energy change in the container is equal to the difference between the heat transferred into and heat energy leaving the gas. Mathematically stated,

$$dE = dQ - hdm, \qquad [93]$$

where

dE = change in total internal energy of the gas,

dQ = heat transfer to the gas,

h = specific enthalpy of container gas,

dm = differential mass leaving the container.

Now,

$$E = me, \qquad [94]$$

where

E = total internal energy,

m = mass,

e = specific internal energy.

Differentiating [94], $dE = mde + edm$, and noting that dm is leaving the container so that it is a negative quantity,

$$dE = mde - edm. \qquad [95]$$

Substituting [95] in [93],

$$mde - edm = dQ - hdm. \qquad [96]$$

Rearranging,

$$mde = dQ - (h - e)dm, \qquad [97]$$

Enthalpy is defined as

$$h = e + pv, \qquad [98]$$

where

p = container gas pressure,

v = container gas specific volume.

Substitution of [98] in [97] and simplifying,

$$mde = dQ - pvdm. \qquad [99]$$

An expression for de whose derivation may be obtained from any standard thermodynamics text (e.g., Ref 15) is

$$de = C_v dT + \left[T\left(\frac{\partial P}{\partial T}\right)_v - p \right] dv. \qquad [100]$$

Substituting [100] in [99],

$$mC_v dT + m\left[T\left(\frac{\partial P}{\partial T}\right)_v - p \right] dv = dQ - pvdm. \qquad [101]$$

The specific volume, v, is defined as

$$v = \frac{V}{m}, \qquad [102]$$

where

V = container total volume.

Differentiating [102], noting again that dm is a negative quantity,

$$dv = \frac{Vdm}{m^2}. \qquad [103]$$

Substituting [102] and [103] in [101],

$$mC_v dT + \left[T\left(\frac{\partial P}{\partial T}\right)_v - p \right] \frac{Vdm}{m} = dQ - \frac{pVdm}{m}. \qquad [104]$$

Simplifying,

$$mC_v dT + \left(\frac{\partial P}{\partial T}\right)_v \frac{VTdm}{m} = dQ. \qquad [105]$$

Dividing Equation [105] by the time infinitesimal, $d\theta$, and rearranging,

$$\frac{dT}{d\theta} = \frac{\frac{dQ}{d\theta} - \left(\frac{\partial P}{\partial T}\right)_v \frac{VT}{m} \frac{dm}{d\theta}}{mC_v},$$

or

$$\dot{T} = \frac{\dot{Q} - \left(\frac{\partial P}{\partial T}\right)_v \frac{VT}{m} \dot{m}}{mC_v} \qquad [106]$$

where

$\dot{T}$ = time rate of change of container temperature,

$\dot{Q}$ = heat transfer into gas,

$\dot{m}$ = mass outflow rate.

APPENDIX C

DERIVATION OF THE FIN SPACING LIMITATION FOR A FINNED TUBE HEAT EXCHANGER

The Bond Number, Bo, is defined as the ratio of gravity force to capillary force as follows:

$$Bo = \frac{F_g}{F_c} = \frac{\rho V g}{\sigma Le} \qquad [107]$$

where

F_g = gravity force $\left(lb_f\right)$,

F_c = capillary force $\left(lb_f\right)$,

ρ = liquid density $\left(lb_m/ft^3\right)$

V = liquid volume $\left(ft^3\right)$,

g = acceleration (g),

σ = surface tension $\left(lb_f/ft\right)$,

Le = characteristic length (ft).

The volume, V, is defined as the volume occupied by the liquid between the fins as follows:

$$V = \frac{\pi}{4}\left[D_F^2 - D_T^2\right] b, \qquad [108]$$

where

V = volume $\left(in.^3\right)$,

D_F = fin diameter (in.),

D_T = tube diameter (in.),

b = fin spacing (in.).

If V is in cubic feet,

$$V = \frac{\pi}{6912}\left[D_F^2 - D_T^2\right] b. \qquad [109]$$

The characteristic length, Le, is defined as the two-dimensional perimeter between the fins which would be wetted by the liquid. This definition is strictly arbitrary and has, at this time, no experimental confirmation.

For Le in inches,

$$Le = b + 2\left[\frac{D_F - D_T}{2}\right] = b + D_F - D_T. \qquad [110]$$

For Le in feet,

$$Le = \frac{b + D_F - D_T}{12}. \qquad [111]$$

Substitution of [109] and [111] in [107],

$$\left.\begin{aligned} Bo &= \frac{\frac{\pi\rho g}{6912}\left[D_F^2 - D_T^2\right] b}{\sigma\left[\frac{b + D_F - D_T}{12}\right]}, \\ Bo &= \frac{\pi 12\rho g\left[D_F^2 - D_T^2\right] b}{6912\sigma\left[b + D_F - D_T\right]}, \\ Bo &= 0.00545\left(\frac{\rho}{\sigma}\right)\frac{g\left(D_F^2 - D_T^2\right) b}{\left(b + D_F - D_T\right)}. \end{aligned}\right\} \qquad [112]$$

Solving for b, the fin spacing,

$$b = \frac{Bo\left(D_F - D_T\right)}{0.00545\ (\rho/\sigma)\ g\left(D_F^2 - D_T^2\right) - Bo}, \qquad [113]$$

where the dimensions are

b, D_F, D_T (in.),

ρ $\left(lb_m/ft^3\right)$,

σ $\left(lb_f/ft\right)$,

g = acceleration (g).

APPENDIX D

VEHICLE THERMAL ANALYSIS DATA

This appendix contains tables of values and figures (Tables 41 thru 46) used in the vehicle thermal analysis, Section III.C.4. Three vehicle configurations were considered during the study. The first configuration shown in Fig. 30 was used for all systems studied during the secondary screening of pump-fed systems. The vehicle configuration shown in Fig. 31 and 32 were used in the final screening of pump-fed systems.

To determine the internal radiation heat transfer, the geometric view factors and equivalent conductances had to be evaluated. A geometric view factor is equal to the fraction of the total radiation emitted from one surface that is intercepted by another.

Equivalent conductance is used in obtaining the radiation heat transfer between surfaces. It accounts for multiple reflection from other surfaces and for the fact that not all of the radiation is absorbed by the surfaces. The total heat transferred between surfaces is equal to the equivalent conductance multiplied by the difference in emissive power of the two surfaces.

To evaluate the radiation and conduction heat transfer in the vehicle, a nodal (lumped) system was used. During the secondary screening, a nodal system shown in Fig. 74 and 75 and Table 47 was used. In the final screening, the nodal system used is shown in Fig. 76 and Table 48.

Table 41 Geometric View Factors for Fig. 30

Zone I

	1	2	3	4
1	0	0.365	0.581	0.054
2	0.3824	0	0.5191	0.0985
3	0.3435	0.2930	0.2165	0.1470
4	0.1362	0.237	0.6268	0

Zone II

	1	2	3	4
4	0	0.487	0.44	0.073
5	0.156	0	0.728	0.116
6	0.121	0.625	0.109	0.145
7	0.075	0.375	0.55	0

Zone III

	7	8	9	10	11	12	13	14
7	0	0.0908	0.0447	0.0447	0.0447	0.0447	0.651	0.0793
8	0.022	0	0.0464	0.0464	0.0464	0.0464	0.611	0.1814
9	0.071	0.304	0	0.055	0.014	0.055	0.399	0.102
10	0.071	0.304	0.055	0	0.055	0.014	0.399	0.102
11	0.071	0.304	0.014	0.055	0	0.055	0.399	0.102
12	0.071	0.304	0.055	0.014	0.055	0	0.319	0.102
13	0.1042	0.4032	0.0402	0.0402	0.0402	0.0402	0.2199	0.1119
14	0.0355	0.4234	0.03635	0.03635	0.03635	0.03635	0.3957	0

Table 42 Equivalent Conductances for Fig. 30

Zone I (ft^2)

	1L	1D	2L	2D	3L	3D	4L	4D
1L		0.0	1.0304	0.0	1.6706	0.0	0.39408	0.0
1D	0.0		0.0	1.0311	0.0	1.6682	0.0	0.39406
2L	1.0304	0.0		0.0	1.8214	0.0	0.45105	0.0
2D	0.0	1.0311	0.0		0.0	1.8217	0.0	0.45101
3L	1.6706	0.0	1.8214	0.0		1.9212	6.77342	0.0
3D	0.0	1.6682	0.0	1.8217	1.9212		0.0	0.77388
4L	0.39408	0.0	0.45105	0.0	6.77342	0.0		0.0
4D	0.0	0.39406	0.0	0.45101	0.0	0.77388	0.0	

Zone II (ft^2)

	4L	4D	5L	5D	6L	6D	7L	7D
4L		0.0	0.6877	0.0	0.86005	0.0	0.23596	0.0
4D	0.0		0.0	0.68801	0.0	0.85945	0.0	0.23595
5L	0.6877	0.0		0.0	2.4696	0.0	0.67613	0.0
5D	0.0	0.68801	0.0		0.0	0.24675	0.0	0.67617
6L	0.86005	0.0	2.4696	0.0		1.2782	0.87763	0.0
6D	0.0	0.85945	0.0	0.24675	1.2782		0.0	0.87811
7L	0.23596	0.0	0.67613	0.0	0.87763	0.0		0.0
7D	0.0	0.23595	0.0	0.67617	0.0	0.87811	0.0	

Zone III (ft^2)

	7L	7D	8L	8D	9	10L	10D	11	12L	12D	13L	13D	14L	14D
7L		0.0	0.39214	0.0	0.11935	6.0021	0.0	0.0	6.0021	0.0	0.83131	0.0	0.2004	0.0
7D	0.0		0.0	0.37615	0.0	0.0	6.5176	0.12989	0.0	6.5176	0.0	0.68872	0.0	0.20108
8L	0.39214	0.0		0.0	0.41081	0.20688	0.0	0.0	0.20688	0.0	2.8183	0.0	0.77318	0.0
8D	0.0	0.37615	0.0		0.0	0.0	6.20546	0.40655	0.0	0.20546	0.0	2.8408	0.0	0.76746
9	0.11935	0.0	0.41081	0.0		6.1211	0.0	5.0915	6.1211	0.0	0.76024	0.0	0.20465	0.0
10L	6.0021	0.0	0.20688	0.0	6.1211		0.0	0.0	2.7124	0.0	0.38216	0.0	0.10433	0.0
10D	0.0	6.5176	0.0	6.20546	0.0	0.0		5.6129	0.0	2.8342	0.0	0.38026	0.0	0.10288
11	0.0	0.12989	0.0	0.40655	5.0915	0.0	5.6129		0.0	5.6129	0.0	0.75435	0.0	0.19388
12L	6.0021	0.0	0.20688	0.0	6.1211	2.7124	0.0	0.0		0.0	0.38216	0.0	0.10433	0.0
12D	0.0	6.5176	0.0	0.20546	0.0	0.0	2.8342	5.6129	0.0		0.0	0.38026	0.0	0.10288
13L	0.83131	0.0	2.8183	0.0	0.76024	0.38216	0.0	0.0	0.38216	0.0		0.0	1.3725	0.0
13D	0.0	0.68872	0.0	2.8408	0.0	0.0	0.38026	0.75435	0.0	0.38026	0.0		0.0	1.3722
14L	0.2004	0.0	0.77318	0.0	0.20465	0.10433	0.0	0.0	0.10433	0.0	1.3725	0.0		0.0
14D	0.0	0.20108	0.0	0.76746	0.0	0.0	0.10288	0.19388	0.0	0.10288	0.0	1.3722	0.0	

Table 43 Geometric View Factors for Fig. 32

Zone I

i \ j	1	2	3	4	17	18	19	20
1	0	0.205	0.398	0.219	0.063	0.026	0.026	0.063
2	0.400	0	0.40	0.008	0.073	0.03	0.03	0.073
3	0.517	0.28	0.07	0.05	0.027	0.016	0.016	0.027
4	0.645	0.005	0.024	0.284	0.015	0.006	0.006	0.015
17	0.442	0.256	0.136	0.035	0.0866	0.0202	0.0067	0.017
18	0.442	0.256	0.199	0.035	0.04	0	0.0025	0.0163
19	0.442	0.256	0.199	0.035	0.0163	0.0025	0	0.0493
20	0.442	0.256	0.136	0.035	0.017	0.0067	0.0202	0.0866

Zone II

	4	5	6	7	11	12
4	0	0.032	0.946	0.003	0.013	0.014
5	0.011	0	0.690	0.133	0.099	0.069
6	0.181	0.389	0.102	0.121	0.094	0.113
7	0.003	0.264	0.424	0.124	0.100	0.085
11	0.012	0.279	0.471	0.142	0	0.096
12	0.013	0.164	0.562	0.120	0.095	0.046

Table 44 Equivalent Conductances for Fig. 32

Zone I ($in.^2$)

	1	2	3	4	17	18	19	20
1		536.75	750.91	805.43	156.52	64.07	64.07	156.56
2	536.75		392.48	347.31	82.29	33.66	33.66	82.29
3	750.91	392.48		499.06	104.81	43.85	43.85	104.81
4	805.43	347.31	499.06		103.34	42.27	42.27	103.34
17	156.52	82.29	104.81	103.34		9.47	8.81	21.56
18	64.07	33.66	43.85	42.27	9.47		3.53	9.29
19	64.07	33.66	43.85	42.27	8.81	3.53		8.81
20	156.52	82.29	104.81	103.34	21.56	9.29	8.81	

Zone II ($in.^2$)

	4	5	6	7	11	12
4		589.25	899.89	223.68	229.15	179.24
5	589.25		1173.5	344.3	346.85	261.62
6	899.89	1173.5		447.03	452.64	353.89
7	223.68	344.3	447.03		144.58	105.48
11	229.15	346.85	452.64	144.58		110.98
12	179.24	261.62	353.89	105.48	110.98	

Table 45 Geometric View Factors for Fig. 31

Zone I

i \ j	1	2	3	4	17	18	19	20
1	0	0.205	0.398	0.219	0.063	0.026	0.026	0.063
2	0.400	0	0.40	0.008	0.073	0.03	0.03	0.073
3	0.517	0.28	0.07	0.05	0.027	0.016	0.016	0.027
4	0.645	0.005	0.024	0.284	0.015	0.006	0.006	0.015
17	0.442	0.256	0.136	0.035	0.0866	0.0202	0.0067	0.017
18	0.442	0.256	0.199	0.035	0.04	0	0.0025	0.0163
19	0.442	0.256	0.199	0.035	0.0163	0.0025	0	0.0493
20	0.442	0.256	0.136	0.035	0.017	0.0067	0.0202	0.0866

Zone II

i \ j	4	5	6	7	8	9	10	11
4	0	0.032	0.947	0.0008	0.0008	0.0008	0.0008	0.01735
5	0.011	0	0.762	0.021	0.021	0.021	0.021	0.058
6	0.181	0.42	0.210	0.040	0.040	0.040	0.040	0.130
7	0.0021	0.166	0.606	0	0.055	0.014	0.055	0.102
8	0.0021	0.166	0.606	0.055	0	0.055	0.014	0.102
9	0.0021	0.166	0.606	0.014	0.055	0	0.055	0.102
10	0.0021	0.166	0.606	0.055	0.014	0.055	0	0.102
11	0.0167	0.164	0.677	0.0356	0.0356	0.0356	0.0365	0

Table 46 Equivalent Conductances for Fig. 31

Zone I $(in.^2)$

	1	2	3	4	17	18	19	20
1		536.75	750.91	805.43	156.52	64.07	64.07	156.56
2	536.75		392.48	347.31	82.29	33.66	33.66	82.29
3	750.91	392.48		499.06	104.81	43.85	43.85	104.81
4	805.43	347.31	499.06		103.34	42.27	42.27	103.34
17	156.52	82.29	104.81	103.34		9.47	8.81	21.56
18	64.07	33.66	43.85	42.27	9.47		3.53	9.29
19	64.07	33.66	43.85	42.27	8.81	3.53		8.81
20	156.52	82.29	104.81	103.34	21.56	9.29	8.81	

Zone II $(in.^2)$

	4	5	6	7	8	9	10	11
4		636.0	953.67	62.62	62.62	62.62	62.62	250.17
5	636.0		1269.5	91.92	91.92	91.92	91.92	358.07
6	953.67	1269.5		125.59	125.59	125.59	125.59	494.03
7	62.62	91.92	125.59		10.45	9.27	10.45	39.93
8	62.62	91.92	125.59	10.45		10.45	9.27	39.93
9	62.62	91.92	125.59	9.27	10.45		10.45	39.93
10	62.62	91.92	125.59	10.45	9.27	10.45		39.93
11	250.17	358.07	494.03	39.93	39.93	39.93	39.93	

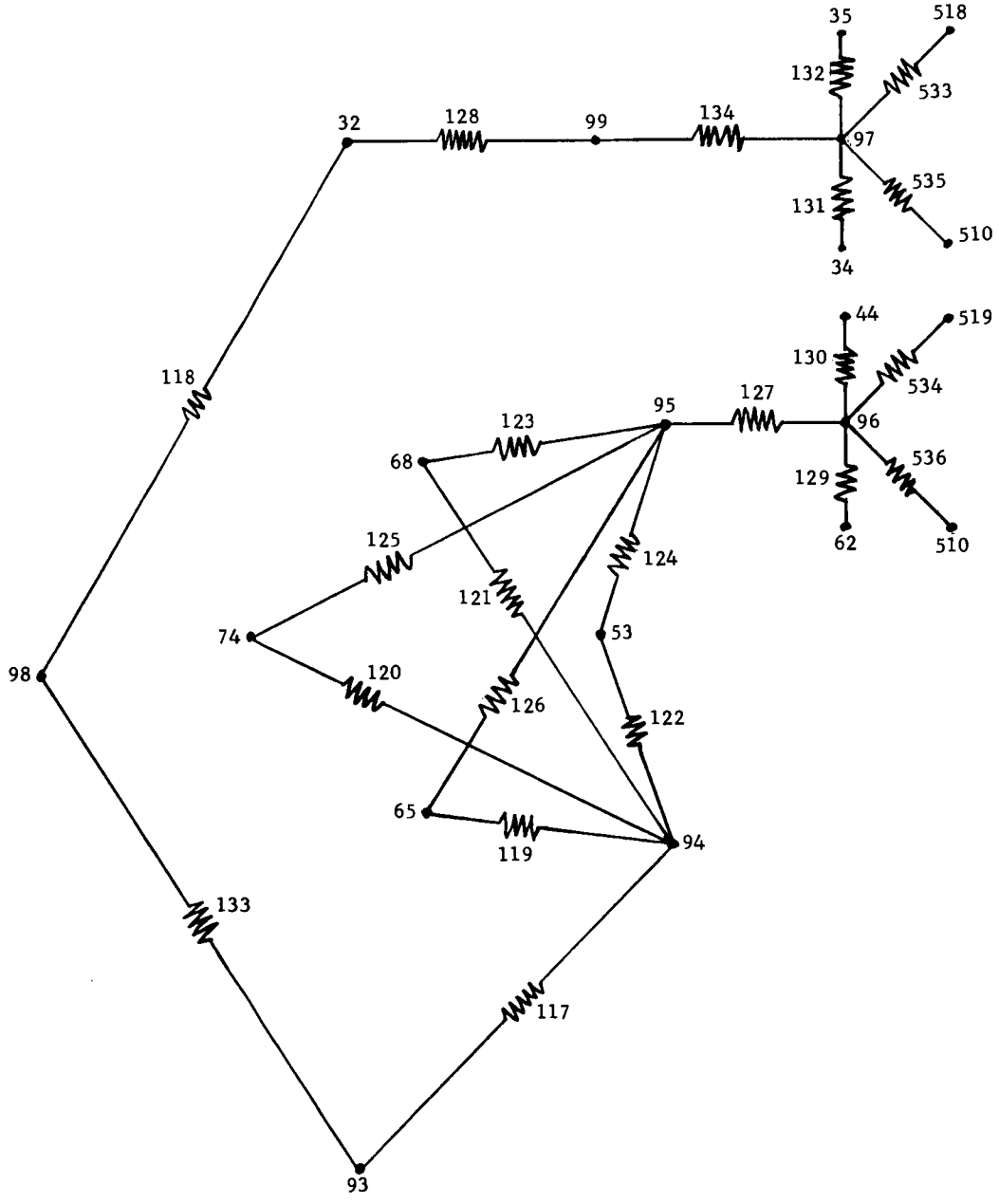

Fig. 74 Suction Line and Vent Line Heat Transfer Network Model-FD-018

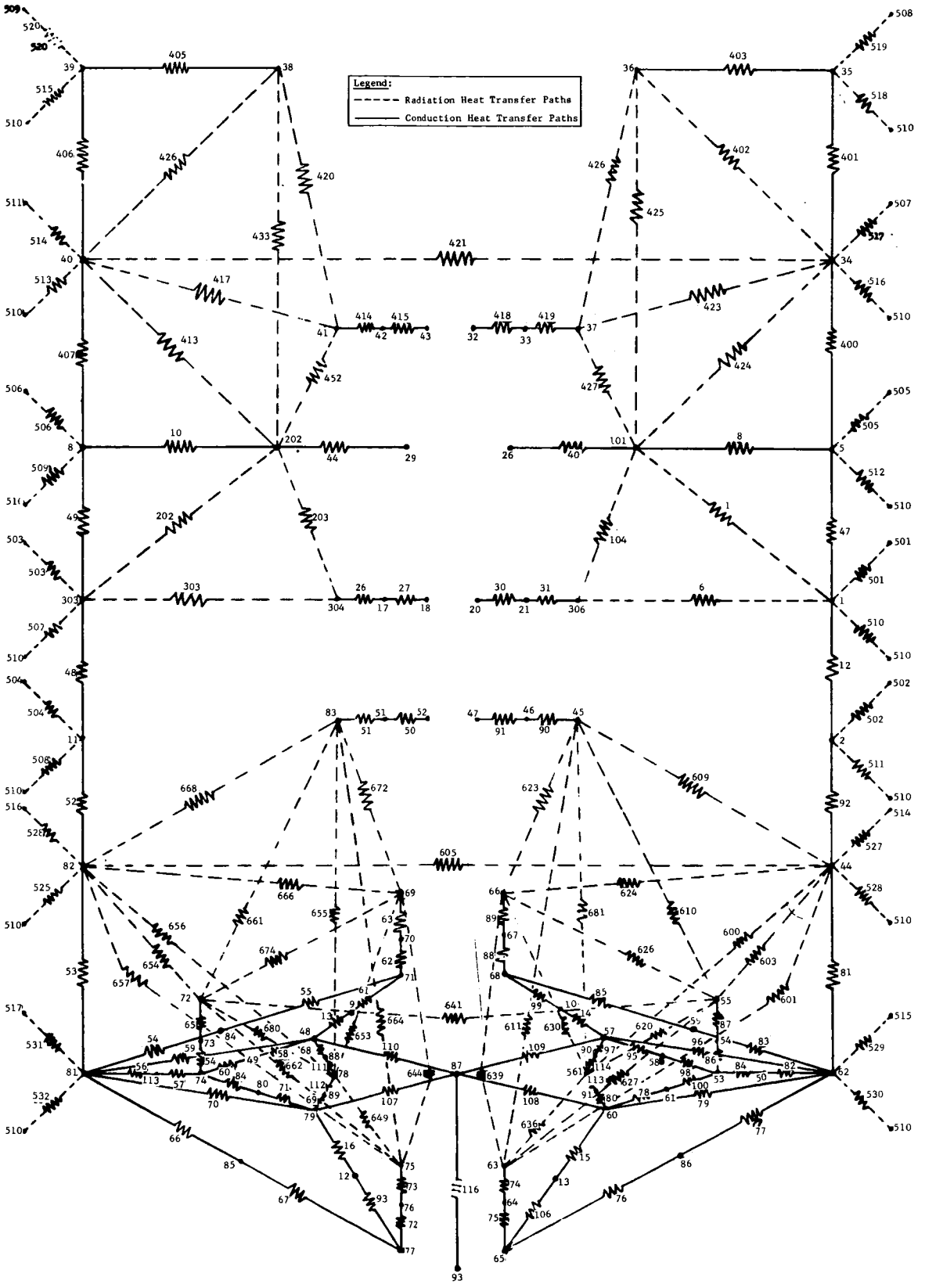

Fig. 75 Vehicle Heat Transfer Network FD-18, Heat Transfer Model for Secondary Screening of Pump-Fed Systems

Table 47 Node Description for Heat Transfer Network

Node Number	Node Location
1	Vehicle skin on sun side, Station 159
2	Vehicle skin on sun side, Station 133
5	Vehicle skin on sun side, Station 186
8	Vehicle skin on dark side, Station 186
9	1/3 tank support ring for No. 12 lox tank on dark side
10	1/3 tank support ring for No. 12 lox tank on sun side
11	Vehicle skin on dark side, Station 133
12	1/3 tank support ring for No. 10 lox tank on dark side
13	1/3 tank support ring for No. 10 lox tank on sun side
17	Midpoint on liquid hydrogen tank, super insulation, dark side, Station 159
18	Liquid hydrogen tank wall, dark side, Station 159
20	Liquid hydrogen tank wall, sun side, Station 159
21	Midpoint on liquid hydrogen tank, super insulation, sun side, Station 159
26	Liquid hydrogen tank wall on sun side, Station 186
27	Liquid hydrogen tank wall on dark side, Station 186
32	Liquid hydrogen tank wall on sun side, Station 207
33	Midpoint on liquid hydrogen tank, super insulation, sun side, Station 207
34	Vehicle skin on sun side, Station 220
35	Vehicle skin on sun side, Station 253
36	1/2 forward end on sun side, Station 253
37	Liquid hydrogen tank, insulation surface on sun side, Station 207
38	1/2 forward end on dark side, Station 253
39	Vehicle skin on dark side, Station 253
40	Vehicle skin on dark side, Station 220
41	Liquid hydrogen tank, insulation surface on dark side, Station 207
42	Midpoint on liquid hydrogen tank, insulation on dark side, Station 207
43	Liquid hydrogen tank wall on dark side, Station 207
44	Vehicle skin on sun side, Station 90
45	Liquid hydrogen tank, insulation surface on sun side, Station 100
46	Midpoint on liquid hydrogen tank, super insulation on sun side, Station 100
47	Liquid hydrogen tank wall on sun side, Station 100
48	Midpoint on spider beam on dark side
49	1/3 tank support ring for No. 11 lox tank
50	1/3 tank support ring for No. 9 lox tank

Table 47 (cont)

51	Midpoint on liquid hydrogen tank, insulation on dark side, Station 100
52	Liquid hydrogen tank wall on dark side, Station 100
53	No. 9 lox tank
54	Midpoint on super insulation for top of No. 9 lox tank
55	Insulation surface for top of No. 9 lox tank
56	Insulation surface for area between lox tanks on sun side
57	Midpoint on spider beam on sun side
58	1/3 tank support ring for No. 9 lox tank
59	1/6 tank support ring for No. 12 lox tank
60	Midpoint on spider beam on sun side
61	1/3 tank support ring for No. 9 lox tank
62	Vehicle skin on sun side, Station 48
63	Insulation surface for top of No. 10 lox tank on sun side
64	Midpoint on insulation for top of No. 10 lox tank on sun side
65	No. 10 lox tank on sun side
66	Insulation surface for top of No. 12 lox tank on sun side
67	Midpoint on insulation for top of No. 12 lox tank on sun side
68	No. 12 lox tank on sun side
69	Insulation surface for top of No. 12 lox tank on dark side
70	Midpoint on insulation for top of No. 12 lox tank on dark side
71	No. 12 lox tank on dark side
72	Insulation surface for top of No. 11 lox tank
73	Midpoint on insulation for top of No. 11 lox tank
74	No. 11 lox tank
75	Insulation surface for top of No. 10 lox tank on dark side
76	Midpoint on insulation for top of No. 10 lox tank on dark side
77	No. 10 lox tank on dark side
78	Insulation surface for area between lox tanks on dark side
79	Midpoint on spider beam on dark side
80	1/3 tank support ring for No. 11 lox tank
81	Vehicle skin on dark side, Station 48
82	Vehicle skin on dark side, Station 90
83	Insulation surface for liquid hydrogen tank, Station 100

Table 47 (concl)

84	1/6 tank support ring for No. 12 lox tank on dark side
85	1/6 tank support ring for No. 10 lox tank on dark side
86	1/6 tank support ring for No. 10 lox tank on sun side
87	Intersection of spider beams and engine support point
88	Midpoint of insulation for area between lox tanks on dark side
89	Midpoint of insulation for area between lox tanks on dark side
90	Midpoint of insulation for area between lox tanks on sun side
91	Midpoint of insulation for area between lox tanks on sun side
93	Engine
94	Lox suction line manifold
95	Lox vent line manifold
96	Vehicle skin location for lox vent line on sun side
97	Vehicle skin location for liquid hydrogen vent line on sun side
98	Midpoint of liquid hydrogen suction line
99	Midpoint of liquid hydrogen vent line
101	Midpoint of liquid hydrogen tank support on sun side, Station 186
113	1/3 tank support ring for No. 11 lox tank
202	Midpoint of liquid hydrogen tank support on dark side, Station 186
303	Vehicle skin on dark side, Station 159
304	Insulation surface for lox tank on dark side, Station 159
306	Insulation surface for lox tank on sun side, Station 159
501-509	Space nodes for radiation to vehicle
510	Space nodes for radiation from vehicle
511-519	Space nodes for radiation to vehicle

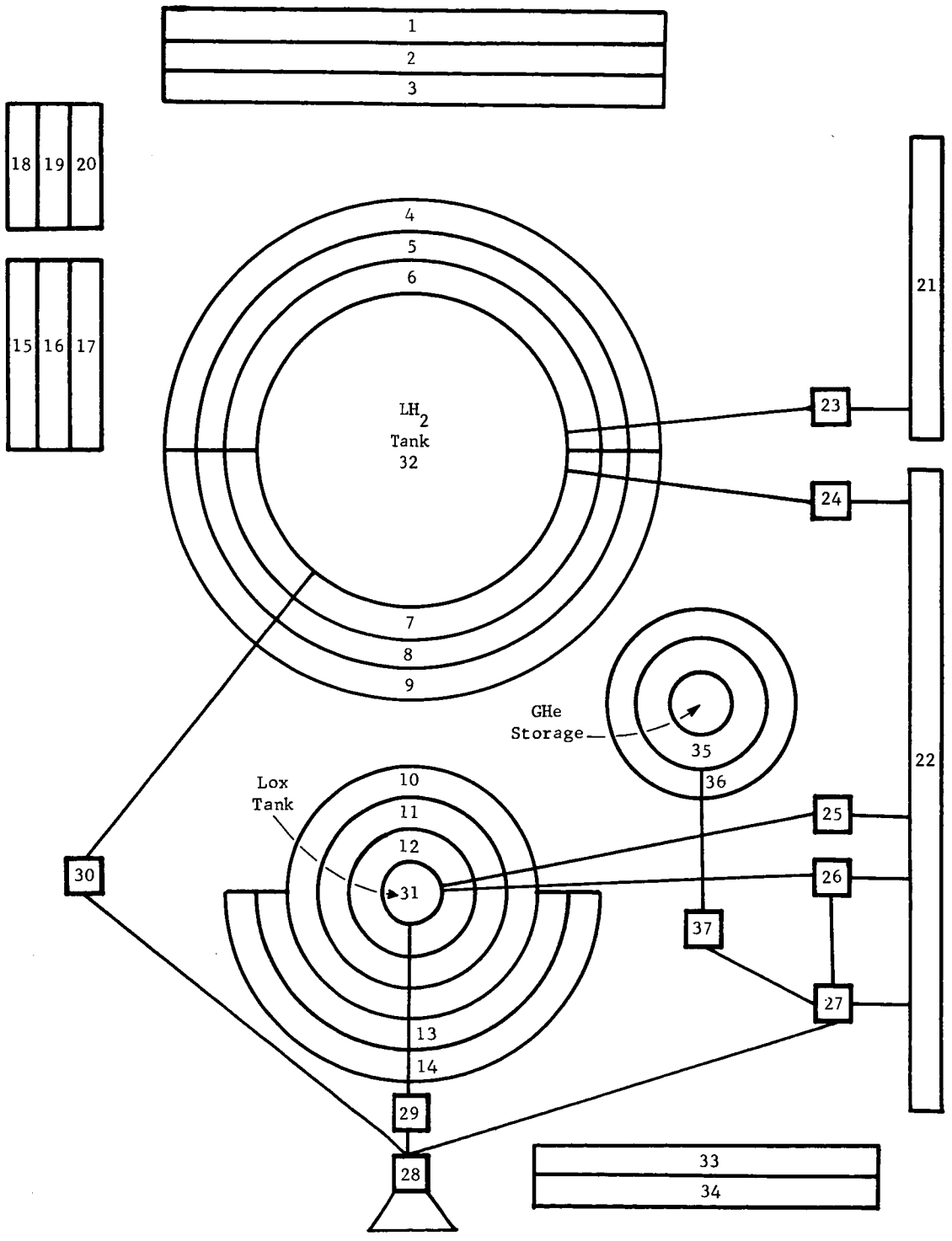

Fig. 76 Nodal System Schematic, System 6 and 8, for Final Screening of Pump-Fed Systems

Table 48 Description of ØB014 Nodal System for Systems 6 and 8

Node Number	Description of Node
1	Cabin node constant temperature of 520°R
2	1/2 of forward end insulation
3	1/2 of forward end insulation
4	1/3 of top half of liquid hydrogen tank insulation
5	1/3 of top half of liquid hydrogen tank insulation
6	1/3 of top half of liquid hydrogen tank insulation
7	1/3 of bottom half of liquid hydrogen tank insulation
8	1/3 of bottom half of liquid hydrogen tank insulation
9	1/3 of bottom half of liquid hydrogen tank insulation
10	1/3 of liquid oxygen tank insulation
11	1/3 of liquid oxygen tank insulation
12	1/3 of liquid oxygen tank insulation
13	1/2 of aft insulation for lox tank
14	1/2 of aft insulation for lox tank
15	Fuel cell radiator
16	1/2 of fuel cell insulation
17	1/2 of fuel cell insulation
18	Environmental radiator
19	1/2 of environmental insulation
20	1/2 of environmental insulation
21	Top portion of vehicle skin
22	Bottom portion of vehicle skin
23	Liquid hydrogen tank support
24	Liquid hydrogen tank vent line
25	Lox tank vent line
26	Lox tank support
27	Spider beam
28	Engine
29	Lox tank suction line
30	Liquid hydrogen tank suction line
31	Liquid oxygen liquid
32	Liquid hydrogen liquid
33	1/2 of aft end insulation between lox tanks
34	1/2 of aft end insulation between lox tanks
35	Storage sphere wall
36	Insulation on storage sphere
37	Storage sphere supports

Note: Two environmental radiators are lumped as one as were the fuel cell radiators. Four liquid oxygen lox tanks are lumped as one.